



HAL
open science

Regulation of Human T Helper Cell Diversity : From In Vitro Dendritic Cell-Based Mechanisms to Candidate Biomarkers in Atopic Dermatitis

Coline Trichot

► **To cite this version:**

Coline Trichot. Regulation of Human T Helper Cell Diversity : From In Vitro Dendritic Cell-Based Mechanisms to Candidate Biomarkers in Atopic Dermatitis. Immunology. Université Paris Saclay (COmUE), 2019. English. NNT : 2019SACLS423 . tel-03092309

HAL Id: tel-03092309

<https://theses.hal.science/tel-03092309>

Submitted on 2 Jan 2021

HAL is a multi-disciplinary open access archive for the deposit and dissemination of scientific research documents, whether they are published or not. The documents may come from teaching and research institutions in France or abroad, or from public or private research centers.

L'archive ouverte pluridisciplinaire **HAL**, est destinée au dépôt et à la diffusion de documents scientifiques de niveau recherche, publiés ou non, émanant des établissements d'enseignement et de recherche français ou étrangers, des laboratoires publics ou privés.

Regulation of human T helper cell diversity: from in vitro dendritic cell-based mechanisms to candidate biomarkers in atopic dermatitis

Thèse de doctorat de l'Université Paris-Saclay
préparée à l'Institut Curie et à Sanofi

École doctorale n°582
Cancérologie : biologie - médecine - santé (CBMS)
Spécialité de doctorat : Aspects moléculaires et cellulaires de la biologie

Thèse présentée et soutenue à Paris, le 22 Novembre 2019, par

Coline Trichot

Composition du Jury :

Jean-David Bouaziz PUPH, Hôpital Saint-Louis	Président
Jenny Valladeau-Guilemond CR1, Centre de recherche en Cancérologie de Lyon (– UMR INSERM 1052)	Rapporteur
Stéphanie Graff-Dubois Enseignant-Chercheur, Laboratoire Immunologie, Immunopathologie, Immunothérapie (– UMRS 959)	Rapporteur
Géraldine Schlecht-Louf MCU, Université Paris-Sud (– UMR-S 996)	Examineur
Vassili Soumelis PUPH, Hôpital Saint-Louis (– UMR INSERM 976)	Directeur de thèse
Benoit Pasquier Chef d'équipe Checkpoint Immunology, Sanofi	Co-encadrant

ACKNOWLEDGMENTS

First, I would like to thank the members of my thesis jury: Dr Jenny Valladeau-Guilemond, Dr Stéphanie Graff-Dubois, Dr Géraldine Schlecht-Louf and Pr Jean-David Bouaziz for accepting to evaluate my PhD work.

I wish to deeply thank Vassili Soumelis for welcoming me in his team 6 years ago, first as an engineer and then for these 3 years of PhD. Thank you for your trust, advices, guidance and the freedom you gave me to test my ideas.

I am greatly thankful for the sponsorship from the ARNT (Association Nationale Recherche Technologie) and Sanofi for my 3 years of Cifre PhD (Industrial Agreements for Training through Research). My project was followed not only by Benoit Pasquier, my Sanofi supervisor, but also by Joe Blois first, and then Hamid Mattoo, both in Sanofi Cambridge. The three of them advised me along the 3 years of my PhD project. I am deeply grateful for their supervision. In addition, working at Sanofi has been a huge opportunity to discover the industry world. I had the chance to attend and participate to Benoit's team meetings, follow projects and learn their problematics. I was able to spend a few months doing experiments in Benoit's lab and benefit from Sanofi's tools and expertise, which was a great experience. Besides, I had the great chance to visit Sanofi Cambridge for a few days, and this would not have happened without Hamid, who planned a great trip for me. I met many people there, had great discussions and lots of feedback on my project. Thank you so much, it was a great experience and a real pleasure to meet everyone. Also, I would like to thank the entire Sanofi team: Solana, Carolina, Charlotte, Erwan, Ellen, Delphine, Sandrine, Eve, Tsing-Lee and Laure. In the end I am very thankful, I have learnt a lot and had many great opportunities thanks to this Cifre program.

I would also like to thank Sebastian Amigorena for welcoming me in his unit and being part of my thesis committee. Thank you for your advices and helpful scientific critics. Thanks as well to all PI and all people from U932. This unit is an amazing scientific environment to work and learn. I feel particularly lucky to have had the chance to perform my PhD in such a place.

I would like to thank the entire Soumelis team, past and current members: Irit, Alix, Carolina, Paula, Solana, Salvatore, Mahé, Marine, Gérome, Antonio, Marie, Ares, FX,

Omar, Rabie, Lilith, Charlotte, Caroline, Camille, Philémon, Sarantis, Elise, Floriane, Maude, Arturo, Faezeh, Justine, Alain, Lucile, Jasna, Alba, Iris, Mélissa, Sara and Fanny. Thanks for the great atmosphere, the evening apero and all the fun. It has been awesome to work with you all during these 6 years.

My biggest thanks to Max for helping me during my entire PhD. Thanks for all the scientific discussions, advices and expert proof-reading of this manuscript.

My sincere thanks to Lucia, it has been such a pleasure to work with you. And my PhD project would not have been created if it was not for you. I had so many great opportunities thanks to this Cifre PhD and it is thanks to you.

My special thanks to Léa for the psychological and experimental support, even during long and hard revisions, the hummus shared, the haircut, the mutual complaints and all the laughter!

I wish to thank the Institut Curie Cytometry platform: Zosia and even more Sophie and Annick for all the cell sorts they performed for me, struggling with the Astrios. My project would have been a nightmare without you girls!

I would like to express my sincere gratitude to Pr Jean-David Bouaziz, Dr Marie Jachiet, Dr Anne Saussine and all people working at the Dermatology Service in Saint-Louis Hospital who helped me receiving patient samples for my study on atopic dermatitis.

I would like to thank all the people from CrossFit XIII, my second home. Thank you to the 7am team and all my CrossFit partners, and above all Emilie and Leslie. My morning WODs are probably the one reason I did not entirely go insane those last 3 years.

Finally, many thanks to my friends, especially Catherine, Claire, Tiffany, and of course my family: my parents, grand-parents and my two sisters, who supported me from the beginning.

TABLE OF CONTENT

ACKNOWLEDGMENTS	1
PREAMBLE	5
LIST OF ABBREVIATIONS	7
LIST OF FIGURES	9
INTRODUCTION	11
1. T helper cell subset diversity and functional impact	13
1.1. T helper cell subsets, phenotypes and functions	13
1.1.1. Th1/Th2 paradigm.....	13
1.1.2. Additional T helper subsets	14
1.2. T follicular helper cells: A T helper cell subset specialized in B cell help	16
1.2.1. General features of T follicular helper cells.....	16
1.2.2. Peripheral blood Tfh cell subsets partially mirror Th cell subsets.....	17
1.2.1. Additional T follicular helper cell phenotypes	19
1.3. Limits of the current T helper cell classification	20
1.3.1. Th cell heterogeneity and plasticity.....	20
1.3.2. Extensive diversity of the Th cell subsets	22
2. Dendritic cells: the main drivers of T helper differentiation	24
2.1. Role of the different dendritic cell subsets in the T helper cell diversity generation	25
2.1.1. Human dendritic cell subsets.....	25
2.1.2. T helper cell polarization induced by each subset	28
2.2. Role of the dendritic cell activating signal	29
2.2.1. Immune sensing by dendritic cells.....	29
2.2.2. DC induce different Th profiles depending on their activating signal.....	35
2.3. Role of the diversity of communication molecules expressed by dendritic cells	36
2.3.1. Primary view: One signal induces one T helper cell profile	36
2.3.2. A more complex system: combinatorial of dendritic cell communication molecules....	38
3. T helper cell contribution to diseases, example of Atopic Dermatitis	41
3.1. General characteristics of Atopic Dermatitis.....	42
3.2. T helper cell role in Atopic Dermatitis pathogenesis.....	43
3.3. Atopic Dermatitis treatments	45
3.3.1. Traditional treatments	45
3.3.2. New immunotherapies for Atopic Dermatitis treatment.....	46

3.3.2.1.	Th2 pathway as therapeutic target	46
3.3.2.2.	Other T helper pathways as therapeutic targets	47
3.3.2.3.	Additional therapeutic strategies	48
3.3.2.4.	Dupilumab specific case.....	48
4.	Objectives	51
	RESULTS	53
1.	Publication n°1	55
	TSLP-activated dendritic cells induce human T follicular helper cell differentiation through OX40-ligand	
2.	Publication n°2	79
	A quantitative multivariate model of human dendritic cell-T helper cell communication	
3.	Publication n°3	145
	Th17 cells decrease correlated with EASI improvement in atopic dermatitis patients during Dupilumab treatment	
	GENERAL DISCUSSION AND PERSPECTIVES	157
1.	TSLP-activated DC induced Tfh cell polarization.....	159
2.	Mathematical modeling of DC/T cell communication	162
3.	Monitoring of Th cell populations in AD patients treated with Dupilumab	164
	APPENDICES.....	167
1.	Appendix 1.....	169
	TSLP-DC-activated T cells express OX40 and OX40L and self-maintain their cytokine production	
1.1.	Results	169
1.2.	Material and Methods	177
2.	Appendix 2.....	181
	A model for the integration of conflicting exogenous and endogenous signals by dendritic cells	
3.	Appendix 3.....	195
	TLR1/2 orchestrate human plasmacytoid pre-dendritic cell response to Gram+ bacteria	
4.	Appendix 4.....	219
	Synthèse en français des travaux de thèse	
	REFERENCES	231

PREAMBLE

The human immune system is constituted of a sophisticated network of cells communicating through molecules expressed at their surface, or secreted in their microenvironment. When the organism is invaded by a pathogen, a complex response is set up, which is specific of the threat encountered. In this process, dendritic cells, which are located in the skin, will be one of the first cells to sense the pathogen. They will capture antigens in their microenvironment and get activated. Then, they will migrate to secondary lymphoid organs and present the antigens to naive CD4 T cells. Naive T cells able to recognize specific antigens will in turn get activated and adopt the proper T helper phenotype specific of the pathogen. T helper cells are characterized by their production of cytokines, which allow the recruitment and activation of many other cell types of both innate and adaptive immune system, in order to mount the appropriate immune response. If this complex process is not controlled correctly, unregulated T helper responses will arise and possibly become pathogenic. Indeed, T helper cells have been described to be involved in many diseases, which shows the necessity of regulating T helper responses, but also suggests the potential for therapies targeting specifically T helper pathways.

I focused my PhD work on studying T helper cell subset diversity and specific regulation: first in the context of TSLP-activated dendritic cells, then, with the purpose of understanding dendritic cell impact on T helper cell differentiation and finally in a pathologic setting, by monitoring T helper cell populations in atopic dermatitis patients.

In the introduction, I start by presenting T helper cells, the different subsets that have been identified as well as their features and functions. Then, I continue by describing dendritic cells, which are the main drivers of T helper cell polarization, and how their different characteristics influence Th cell differentiation. Finally, I present the link between T helper cells and diseases, with the specific example of atopic dermatitis.

My results are divided in three projects. The first results are in the form of a publication, demonstrating TSLP-activated dendritic cells ability to induce T follicular helper cells through OX40L. The second results are in the form of an accepted manuscript, showing a mathematical model able to predict the behavior of 18 T helper cell parameters in response to 36 dendritic cell-derived signals. This model allowed us to identify a context-dependent role for IL-12p70 in the presence of IL-1 in the differential induction of IL-17F without IL-17A. The last results are in the form of a manuscript in preparation describing the evolution of eight T helper and T follicular helper cell populations in peripheral blood from atopic

dermatitis patients along the course of their treatment with Dupilumab, an immunotherapy targeting the IL-4 receptor alpha subunit. This study led us to show that decrease of the Th17 cell percentage measured during Dupilumab treatment correlated with improvement of the EASI clinical score.

In the general discussion and perspectives, I review these three projects in light of the current literature, discuss their limitations and potential perspectives.

In the appendices are included: 1) an ongoing work on OX40L impact on T cell polarization, 2) a publication from a collaboration with biophysicians on signal integration by dendritic cells, 3) a publication I was involved in showing plasmacytoid dendritic cells activation through TLR1/2 and 4) a summary of my PhD work in French.

LIST OF ABBREVIATIONS

AD	Atopic Dermatitis
AHR	Aryl hydrocarbon receptor
CD	Cluster of Differentiation
CLA	cutaneous lymphocyte antigen
CLR	C-type lectin receptors
CytoF	Cytometry by time-of-flight
DC	Dendritic cell
EASI	Eczema Area and Severity Index
FACS	Fluorescence Activated Cell Sorting
FOXP3	Forkhead box P3
GATA3	GATA Binding Protein 3
GM-CSF	Granulocyte Macrophage Colony Stimulating Factor
ICOSL	Inducible costimulator ligand
IFN	Interferon
Ig	Immunoglobulin
IL	Interleukin
ILC	Innate Lymphoid Cell
iTreg	induced regulatory T
LPS	Lipopolysaccharides
MDC	Macrophage-derived chemokine
MHC	Major Histocompatibility Complex
MoDC	Monocyte-derived dendritic cell
ODN	Oligodeoxynucleotides
PAMP	Pathogen Associated Molecular Patterns
PBMC	Peripheral blood mononuclear cells
PD1	Programmed Cell Death 1
pDC	plasmacytoid dendritic cell
Poly(I:C)	Polyinosinic-polycytidylic acid
PRR	Pattern Recognition Receptors
RORγT	Retinoic acid-related orphan receptor γ T
SAP	SLAM-Associated Protein
SCORAD	Scoring atopic dermatitis

STAT Signal Transducer and Activator of Transcription
TARC Thymus and activation-regulated chemokine
T-bet T-Box Expressed in T Cells
TCR T cell receptor
Tfh T follicular helper
Tfr T follicular regulatory
TGF- β transforming growth factor β
Th T helper
TLR Toll-like receptors
TNF Tumor Necrosis Factor
TSLP Thymic Stromal Lymphopoietin

LIST OF FIGURES AND TABLES

INTRODUCTION

Figure 1: Human T helper cell subsets	15
Figure 2: Tfh cell differentiation in secondary lymphoid organs	17
Figure 3: Peripheral blood Tfh cell subsets partially mirror Th cell subsets.....	18
Figure 4: Combination of five surface markers identifies nine subsets of memory Tfh cells in human peripheral blood	19
Figure 5: Th17 cell heterogeneity and plasticity	21
Figure 6: Antigen-specific T cell response initiation	24
Figure 7: Human dendritic cell subsets	25
Table 1: Table recapitulating some of the human PRRs, their location, ligands and expression according to human DC subsets.....	34
Figure 8: T helper polarization by dendritic cells depends on the type of pathogen they encounter ...	35
Figure 9: T helper polarization towards Th1 or Th2 subset by dendritic cell requires 3 signals.....	37
Figure 10: Dendritic cell/T cell communication molecules.....	39
Figure 11: Atopic Dermatitis pathogenesis in Acute (A) and Chronic (B) phases	44
Figure 12: Dupilumab mechanism of action	49

RESULTS

Figure 13: TSLP-activated DC induce human Tfh cell differentiation through OX40L	56
--	----

APPENDICES

Figure 14: OX40L blocking decreases IL-21 and increases IL-4 production in TSLP-DC/T coculture	171
Figure 15: rhOX40L increases IL-21 and decreases IL-4 and IFN- γ in a DC-free Th polarization system	172
Figure 16: OX40L ⁺ DC induce more IL-21 and less IL-4 producing cells than OX40L ⁻ DC	174
Figure 17: TSLP-DC-activated T cells express OX40L, and its blocking increases IL-4 production	176

INTRODUCTION

1. T helper cell subset diversity and functional impact

CD4 T helper (Th) cells play a major role in the adaptive immune response which allows host defense against a wide variety of pathogens. Through the secretion of specific sets of cytokines, Th cells instruct other cell types to set up the proper immune response, specific of the pathogen encountered, allowing its clearance.

1.1. T helper cell subsets, phenotypes and functions

1.1.1. Th1/Th2 paradigm

In 1986, was published the first report describing two in vitro-derived Th clones: Th1 and Th2, obtained after mice immunization with a protein antigen [1]. In 1989, Mosmann and Coffmann summarized the latest advances on T helper cells and reported that Th1 cells were characterized by production of IL-2, IFN- γ , TNF- α and TNF- β , while Th2 cells produced IL-4, IL-5, IL-6 and IL-13 [2].

Later, identification of master regulators associated to each cytokine profile and responsible for their setup introduced the notion of lineages. The transcription factors identified in Th1 cells are T-bet [3], STAT1 and STAT4 [4], while Th2 cell development involved GATA3, STAT5 and STAT6 [5].

Additionally, a mutual exclusion between the two subsets has been described: GATA3 represses STAT4, thus inhibiting Th1 features [6] and T-bet and Runx3 activate IFN- γ gene and silence GATA3 and IL-4 [7, 8]. Additionally, a positive feedback loop occurs, GATA3 will induce IL-4, which in turn will instruct non-IL-4 producer-cells to produce IL-4, but also enhance IL-4 production from IL-4 producer-cells [5]. Conversely, the IFN- γ -STAT1-T-bet pathway strongly amplifies Th1 differentiation [9].

Further characterization of the two subsets lead to the identification of specific chemokine receptors, homing receptors which will lead Th cells to different location. Th1 specifically express CCR5, receptor for MIP-1 α , MIP-1 β and RANTES, and CXCR3, receptor for IP-10 and MIG, which will direct them to inflamed tissues [9, 10]. On the other hand, Th2 exhibit CCR3, an eotaxin receptor, CCR4, receptor for MDC and TARC, and CCR8, receptor for TARC and I-309 (Figure 1). MDC, TARC, I-309 and eotaxin will not only attract Th2 to the inflammation site, but also eosinophils, basophils and monocytes. IL-4 and IL-5 production by Th2 will activate these different cell types and ensure their survival [10, 11]. Besides, Th2 express specifically CRTH2, a receptor for Prostaglandin D₂ [12].

Moreover, respective functional roles have been identified for each Th subset. For instance, Th1 are necessary for the clearance of intracellular viruses and bacteria. IFN- γ activates phagocytosis on macrophages increasing their ability to kill intracellular pathogens. Th1 also secrete IL-2, TNF- α and TNF- β which participate in antimicrobial responses [13]. On the opposite, Th2 have been linked to the control of extracellular parasites such as helminths. Th2 production of IL-4 induces isotype switching on B cells which produce IgG1 and IgE [2]. By producing IL-4 and IL-13, Th2 are also able to activate macrophages [14]. And through their production of IL-5, Th2 recruit eosinophils as well [15].

1.1.2. Additional T helper subsets

For more than two decades, the Th1/Th2 paradigm prevailed, with the idea that T cells could only adopt one of two fates, until the discovery of several additional Th cell subsets.

First, Th17 cells were described as Th cells producing IL-17A and developing through a different lineage than Th1 and Th2 cells [16]. Additional characterization of Th17 cells demonstrated that they also produce the cytokines IL-17F, IL-21, IL-22 and IL-26, as well as the chemokines CCL20 and CXCL8, express the transcription factors ROR γ T, ROR α and STAT3, exhibit the specific surface marker CD161 and the chemokine receptor CCR6 [17] (Figure 1). Th17 cells play an important role in inducing protective immunity against bacteria and fungi at mucosal sites [18]. IL-17A, IL-17F and IL-22 produced by Th17 cells are strongly pro-inflammatory and will induce expression of antimicrobial peptides from epithelial cells and keratinocytes but also their permeability, proliferation and survival [19]. CCL20 and CXCL8 produced by Th17 cells will attract more Th17 cells, but also neutrophils on the site of infection [18].

IL-22 was first described as a Th17 cytokine, until a skin homing memory Th cell population secreting IL-22 but neither IL-17 nor IFN- γ was identified and named Th22 [20]. Th22 specific transcription factor has been identified as well: AHR [21]. Th22 express the chemokine receptor CCR6 and the skin homing receptors CCR4 and CCR10 indicating their crucial roles in skin inflammation [22] (Figure 1). And just as for Th17 cells, IL-22 secreted by Th22 induces production of antimicrobial peptides by epithelial cells and keratinocytes.

Similarly, IL-9 was originally described as a Th2 cytokine [23], secreted in combination with IL-4, but later, Th cells secreting IL-9 independently of IL-4 were identified, and labelled Th9 [24]. Th9 cell specific transcription factor is PU.1, but like Th2 cells, Th9 cell differentiation also involves GATA3 and STAT6 [25]. Th9 cells express the major skin homing receptor cutaneous lymphocyte antigen (CLA), suggesting their role in skin immunity and cutaneous defense against extracellular pathogens [26] (Figure 1). IL-9

has been shown to be important for mast cell recruitment and activation in tissues. Activated mast cells will in turn produce proinflammatory cytokines such as TNF- α and IL-6, which are involved in anti-fungal response. IL-9 can also attract neutrophils, on the infection site, which will have an important role in eliminating fungi as well [26].

In parallel to these Th cell subsets, induced regulatory T (iTreg) cells have been described arising from naive CD4 T cells in secondary lymphoid organs or inflamed tissues. iTreg are a particular subset characterized by the production of IL-10 and TGF- β , expression of the surface markers CD25 (IL-2 receptor), GITR and CTLA4 and the transcription factor FoxP3 [27, 28] (Figure 1). Treg cells are critical for the prevention of autoimmune diseases by inhibiting activation and proliferation of T and B cells specific for self-antigens [29]. IL-10 is important for keeping a state of immune tolerance, while CTLA4 binding to CD80/CD86 expressed by dendritic cells will lead to decreased naive CD4 T cell activation [27].

All these new subsets significantly complexified the view of the T helper cells (Figure 1).

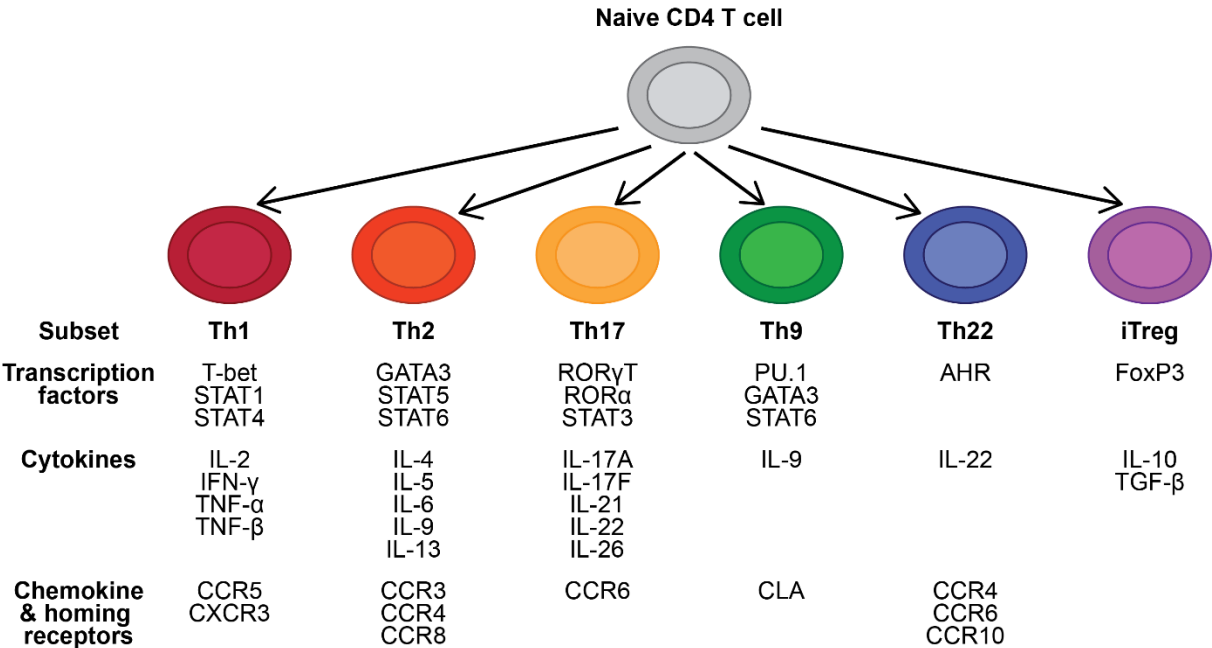


Figure 1: Human T helper cell subsets
Schematic of known human Th cell subsets: Th1, Th2, Th17, Th9, Th22 and iTreg with their respective transcription factors, cytokines and chemokine/homing receptors

1.2. T follicular helper cells: A T helper cell subset specialized in B cell help

1.2.1. General features of T follicular helper cells

In addition to the six T helper cell subsets, particular T follicular helper (Tfh) cells were described. Initially named “follicular B helper T cells” based on their characteristic localization in secondary lymphoid organs, Tfh cells were identified in 2000. Several groups observed a large proportion of CD4 T cells expressing high levels of the chemokine receptor CXCR5 in tonsils, and discovered they were able to support immunoglobulin (Ig) production from B cells [30-32].

Since then a lot of work has been done to fully characterize them. Tfh cells express high levels of several effector molecules, including the surface markers ICOS, CD40L, OX40, PD1, BTLA, the cytoplasmic adaptor protein SAP and produce large amounts of the cytokine IL-21 and of the chemokine CXCL13, which is CXCR5 ligand [33]. Tfh cell differentiation depends on the transcriptional repressor Bcl-6, antagonist of Blimp-1 which is a strong inhibitor of Tfh polarization [34].

Tfh cells main function is to provide help to B cells by delivering signals that enable B cell proliferation, differentiation and isotype switching. Tfh cells are also necessary for the proper formation of germinal centers, particular structures forming inside B cell zone of secondary lymphoid organs [35].

Tfh cell differentiation happens in the secondary lymphoid organs and requires 3 steps (Figure 2). First, in the T cell zone, DC activate antigen-specific naive CD4 T cells expressing CCR7, the T cell zone homing receptor. Activated pre-Tfh will downregulate CCR7 and upregulate CXCR5, homing receptor to the B cell follicle, positioning them to the T-B border. Then, pre-Tfh cells will encounter activated antigen-primed B cells. This interaction will lead either: 1) to the B cell differentiation into short-lived extrafollicular plasmablasts, contributing to early production of specific antibodies, or 2) to the migration of pre-Tfh cells and B cells to form the germinal centers. Finally, further interaction with antigen-specific B cells will drive the complete differentiation of germinal center Tfh cells. Once in the germinal center, B cells will go through the processes of affinity maturation and isotype switching, and differentiate either into high-affinity long-lived plasma cells or long-lived memory B cells [33, 36, 37].

Even if the majority of Tfh cells reside in germinal centers, in human a small subset of memory Tfh cells have been identified in peripheral blood [32]. They express CXCR5 but low levels of other prototypical Tfh markers: PD1, ICOS, OX40 and even do not express Bcl-6 protein [38].

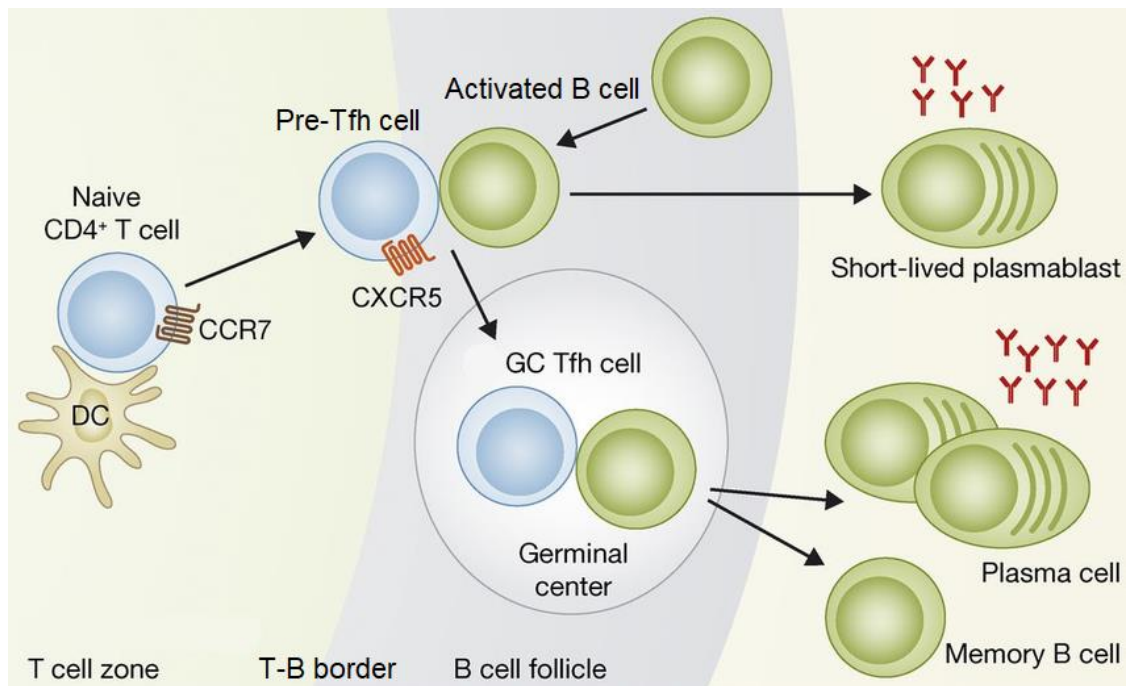


Figure 2: Tfh cell differentiation in secondary lymphoid organs

Schema from Ma, Deenick, Batten and Tangye [33]

DC activate antigen-specific naive CD4 T cells, which will migrate from the T cell zone towards the B cell follicle. At the T-B border, activated pre-Tfh cells will interact with activated antigen-specific B cells. This interaction will lead to B cell differentiation into short-lived plasmablasts or to the migration of the pre-Tfh cells and B cells and formation of germinal centers. Further interaction between B cells and pre-Tfh cells will enable full differentiation of germinal center Tfh cells. Germinal center B cells will differentiate into long-lived plasma cells or long-lived memory B cells.

Additionally, T follicular regulatory (Tfr) cells have been described, controlling germinal center responses by inhibiting Tfh and B cells. Tfr cells exhibit the same markers than Tfh cells, they express CXCR5, PD1, ICOS, Bcl-6, but they also possess specific Treg markers such as FoxP3, CD25, CTLA4, GITR [39]. Besides, they produce large amounts of inhibitory cytokines such as IL-10 and TGF- β . Similar to Tfh cells, Tfr differentiation is a multistep process requiring interaction with DC and B cells. Tfh and Tfr cells are necessary for the balance between immune activation and tolerance [40].

1.2.2. Peripheral blood Tfh cell subsets partially mirror Th cell subsets

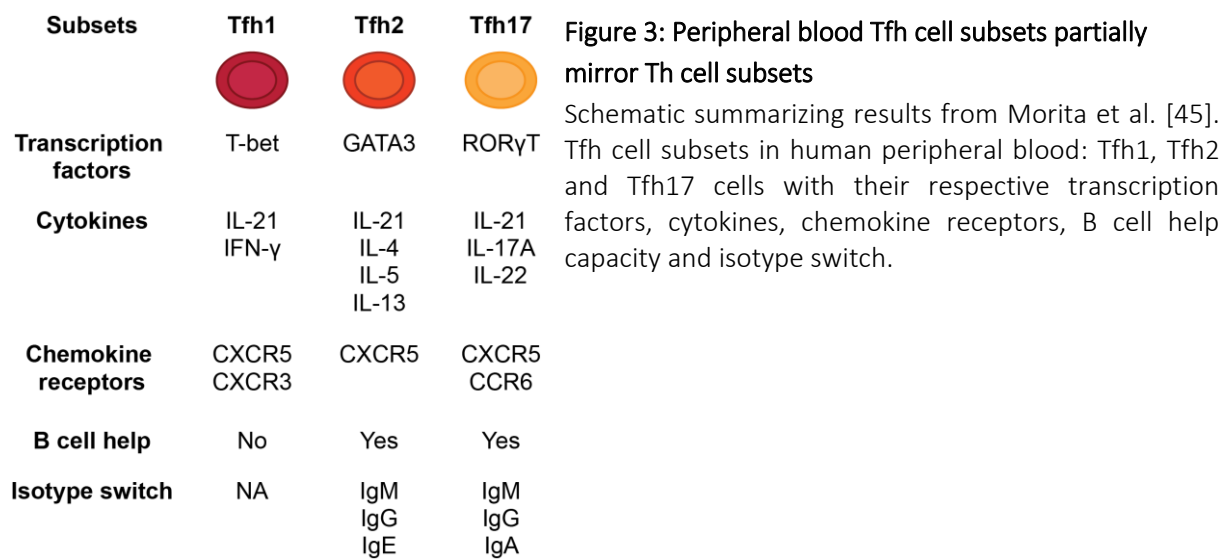
After the discovery of Tfh cells as a new Th cell subset, Tfh producing not only IL-21 but also other Th signature cytokines, have been described first in mice.

Three different teams, using the same IL-4 reporter mice infected with different parasites, discovered IL-4 producing cells exhibiting all Tfh specific markers in the lymph nodes [41-43].

Additionally, Bauquet et al. identified IL-17 producing Tfh in mice draining lymph nodes [44].

Later, Morita et al. demonstrated that Tfh cells from human peripheral blood mirror Th cells, and can also be subdivided into distinct subsets. Looking at the expression of CXCR5, CCR6 and CXCR3 in the CD4 memory cell compartment, they could identify three functionally distinct Tfh cell subsets mirroring the three Th cell subsets: Th1, Th2 and Th17. Tfh1 cells characterized by expression of CXCR5 and CXCR3, expressed T-bet, produced IFN- γ in addition to IL-21 and were not able of B cell help. Tfh2 cells were identified as CXCR5⁺CXCR3⁻CCR6⁻, expressed GATA3, produced IL-21, IL-4, IL-5 and IL-13 and induced high levels of IgG and IgE and low levels of IgM and IgA from B cells. Finally, Tfh17 cells identified as CXCR5⁺CCR6⁺, expressed ROR γ T, produced IL-21, IL-17 and IL-22 and induced high levels of IgA, IgM and IgG production by B cells [45] (Figure 3).

This demonstrates a partial mirror between peripheral blood Tfh cell subsets and Th cell subsets. We can wonder if, as well as for Th1, Th2 and Th17, we could identify a mirror for Th9 and Th22 subsets in the CXCR5⁺ memory compartment of peripheral blood, maybe using more markers.



Looking at the expression of ICOS, PD1 and CCR7, three subsets of memory Tfh cells have been identified in human peripheral blood. ICOS⁺PD1⁺ subsets have been described as activated Tfh cells, while the ICOS⁻PD1⁺ and PD1⁻ subsets do not exhibit activation markers and have been defined quiescent. [46-48]. Added to the three subsets identified by Morita et al. [45], memory Tfh cell diversity reaches a total of nine distinct subsets [49] which strongly increases Tfh cell subset complexity (Figure 4).

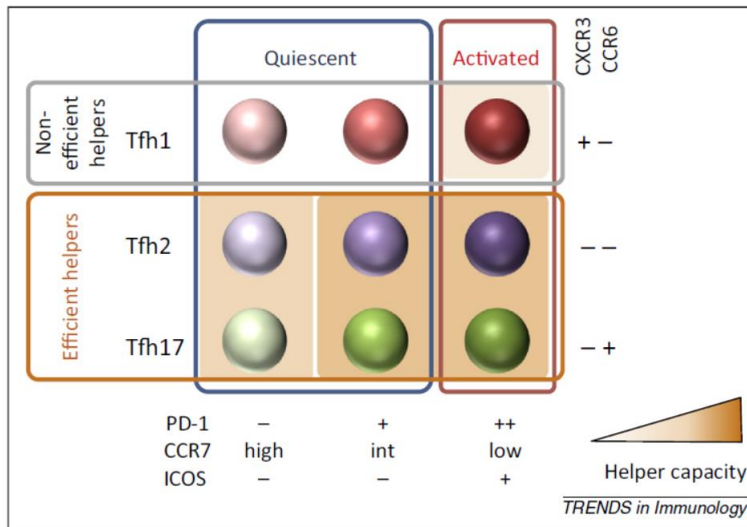


Figure 4: Combination of five surface markers identifies nine subsets of memory Tfh cells in human peripheral blood

Figure from Schmitt, Bentebibel and Ueno [49]

The nine memory Tfh cell subsets identified in human peripheral blood. CXCR3 and CCR6 identify Tfh1, Tfh2 and Tfh17 cells and separate non-B cell helpers (Tfh1) from efficient B cell helpers (Tfh2 and Tfh17). ICOS expression delineate activation in each subset. Helper capacity is indicated by a color gradient.

1.2.1. Additional T follicular helper cell phenotypes

For a long time, B cell help function was attributed to Th2 cells because of their IL-4 production. Initially, IL-4 has been described as “B cell differentiation factor γ ”, “B cell growth factor” or “B cell stimulatory factor-1” and it was known for inducing IgG1 and IgE switch from B cells [2].

However, the discovery of the T follicular helper cells questioned that view. Since then, Tfh cells have been described as the specialized B cell help providers through production of IL-21 and IL-4 and their capacity to enter the germinal center of secondary lymphoid organs [35]. Nevertheless, B cell helper capacities have been demonstrated from cells that do not display the prototypical Tfh phenotype.

First, in 2017 PD1^{hi}CXCR5⁺CD4⁺T cells were identified at very high frequency in synovial fluid and synovial tissue of rheumatoid arthritis patients. Those T cells produced high levels of IL-21 and CXCL13 and when cocultured with memory B cells, they were capable of inducing B cell differentiation into plasma cells producing IgG [50].

In 2018, T cells from systemic lupus erythematosus exhibiting CD4⁺CXCR5⁺CXCR3⁺PD1^{hi} were shown to help B cells through the production of IL-10 and succinate (an intermediate of the tricarboxylic acid cycle), independently of IL-21 [51].

This demonstrated that there is not just one possible phenotype capable of providing B cell help. On the contrary multiple Th cell profiles seem to potentiate isotype switch and Ig production from B cells.

1.3. Limits of the current T helper cell classification

1.3.1. Th cell heterogeneity and plasticity

In the current Th cell classification, each subset is defined by a specific and strict set of cytokines associated to transcription factors. Th1 cells are known for their secretion of IFN- γ , TNF- α and IL-2 under control of T-bet, STAT1 and STAT4, Th2 cells produce IL-4, IL-5 and IL-13 regulated by GATA3, STAT5 and STAT6, etc. However, the system seems to be a lot more complex than that, and Th cells might be characterized by further plasticity than what was originally defined.

One example is the description of Th1/Th17 cells, in patients with Crohn's disease, producing both IL-17 and IFN- γ and expressing at the same time ROR γ t and T-bet. In this study Th17 clones cultured with IL-12 started producing IFN- γ in addition to IL-17 [52]. This shows that IL-17 and IFN- γ production are not exclusive.

Additionally, Cosmi et al. demonstrated that both Th17 and Th1/Th17 cells, if cultured with IL-12, could differentiate into "non-classic Th1", downregulating ROR γ t expression and IL-17 production [53]. Th17, Th1/Th17 and non-classic Th1 cells were characterized by the expression of the CD161 marker, as opposed to classical Th1 which do not express it [54].

An additional intermediate profile of Th17/Th2 cells was described in peripheral blood of chronic asthma patients. These Th17/Th2 cells produced the Th17 cytokines IL-8, IL-17, IL-21 and IL-22, as well as Th2 cytokines IL-4, IL-5, IL-9, and IL-13. Th17/Th2 cells could be derived from Th17 cells cultured with IL-4 [55].

Furthermore, IL-9 production could be induced on memory Th17 cells, extracted from peripheral blood, when cultured with a cocktail of TGF- β , IL-1 β , IL-6, IL-21 and IL-23 [56].

Additionally, Treg/Th17 co-expressing FoxP3, RORC and IL-17 have been described in human. And induction of IL-10 production by Th17 cells in response to IL-21 has been shown, promoting regulatory Th17 [57].

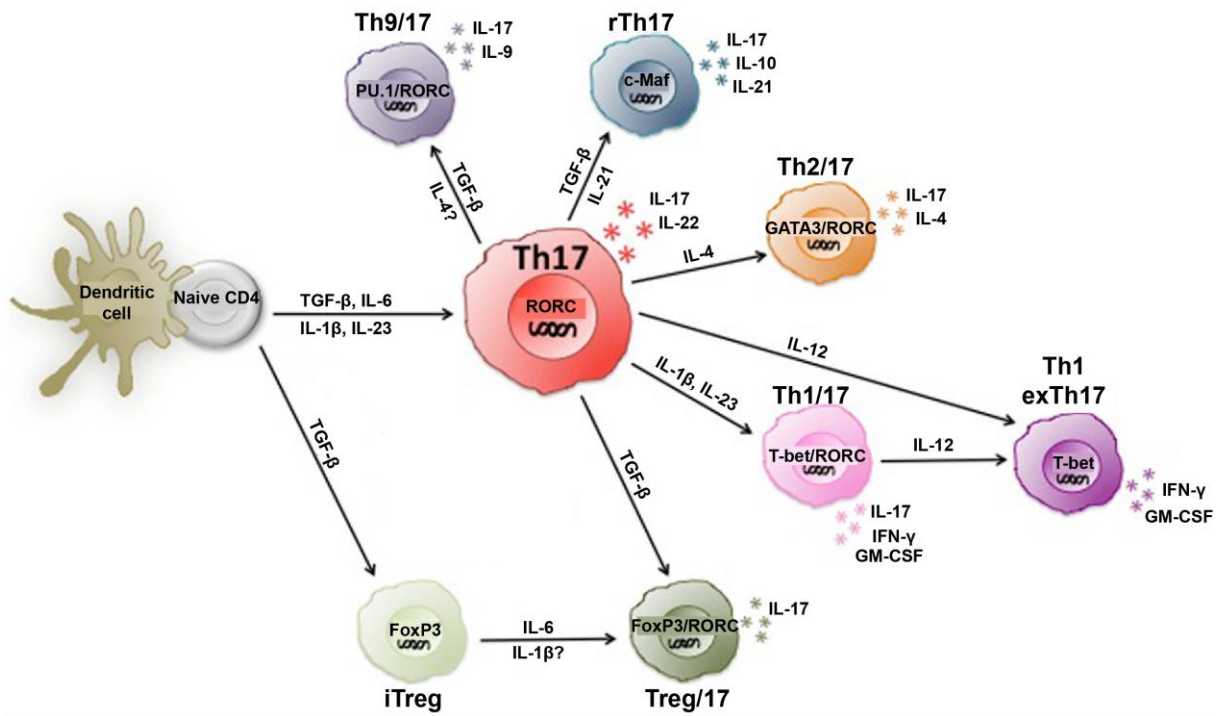


Figure 5: Th17 cell heterogeneity and plasticity

Schema from Geginat [57]

Th17 cells can be induced to differentiate into Th17/Th9, regulatory Th17 (rTh17), Treg/Th17, Th17/Th2, Th1/17 or even non-conventional Th1.

These studies demonstrated the heterogeneity and plasticity of the Th17 cells (Figure 5). Similarly, few studies tend to prove that other Th cells might not be terminally differentiated either.

In atopic asthma patients, memory/effector Th2 cells producing the Th17 cytokines: IL-17A and IL-22, in combination with Th2 cytokines: IL-4, IL-5 and IL-13 have been identified, they also co-expressed both transcription factors ROR γ T and GATA3. This study further demonstrated, using a mouse model, that classical Th2 cells treated with IL-1 β , IL-6, and IL-21 started producing IL-17 [58].

Moreover, Hegazy et al. described Th2/Th1 cells. They demonstrated both in vivo, in lymphocytic choriomeningitis virus infected mice, and in vitro, using type I and II interferon and IL-12, that Th2 cells could produce both IL-4 and IFN- γ and express both GATA3 and T-bet [59].

In a mouse model of house dust mite sensitization, Ballesteros-Tato et al. demonstrated that the first sensitization induced IL-4 committed Tfh cells, but no Th2 cells. Besides, they showed that following re-challenge with house dust mite, these IL-4 committed Tfh cells would differentiate into Th2 cells [60].

These studies question the relevance of the notion of Th lineages and their strict phenotypes. The Th cell polarization process seems substantially more flexible and plastic than what was initially described. Indeed, reprogramming of committed Th cells has been demonstrated in these studies, but also existence of mixed profiles showing combination of usually exclusive Th cell phenotypes. Therefore, we could imagine that all Th cytokine combinations are virtually possible. Polarized Th cells just need the proper stimulation from unique microenvironments to either change entirely their polarization or acquire an intermediate Th profile, in order to finely tune the immune response to specific threats.

1.3.2. Extensive diversity of the Th cell subsets

Recent studies essentially using mass cytometry, also known as cytometry by time-of-flight (CyTOF) and analyzing increasing number of parameters identified a lot more Th cell subsets than what was initially described.

Duhen et al. studied the expression of four chemokine receptors: CCR6, CXCR3, CCR4 and CCR10 on memory CD4⁺CD45RO⁺CD25^{hi}CD127^{lo}FoxP3⁺ Treg cells sorted from human peripheral blood. They were able to identify 4 distinct subsets: Th1-like Treg cells producing IFN- γ and expressing CXCR3, CCR6⁺CCR4⁺ Th17-like Treg cells producing IL-17, Th22-like cells secreting IL-22 and expressing CLA, CCR6, CCR4 and CCR10 and IL-4 producing Th2-like Treg cells expressing CCR4. Even though all populations possessed inhibitory functions, this suggests a mirror between human peripheral blood Th cells and Treg cells [61].

Mason et al. sorted CD4⁺CD25^{high}CD127^{low} Treg cells from peripheral blood mononuclear cells (PBMC) from four healthy donors and analyzed them by CyTOF including 25 surface markers. They were able to identify 22 different subsets, among which they detected the five previously established Treg subsets [62]. This demonstrates an important phenotypical complexity and heterogeneity of the human peripheral blood Treg compartment.

Kunicki et al. used 23 markers, including surface markers and transcription factors, to study Th cells and Treg in PBMC from eight healthy donors by CyTOF. They analyzed their data by unsupervised clustering and visualized 15 Th cell subsets: three different populations in the Th1 subset, three populations among Th2 cells, one Th17 population, three Treg populations and five populations inside the Tfh subset. Moreover, many populations overlapped between subsets, for example Th1 and Tfh, Tfh and Th17, Th1 and Th17 or Th2 and Treg [63].

Additionally, Barcenilla et al. analyzed PBMC from nine healthy donors compared to nine patients with high risk of developing a type-1 diabetes. They used 33 markers, including transcription factors, chemokine receptors and activation markers, to study Th and Treg subsets by CyTOF. They identified 11 clusters of naive CD4 T cells, four clusters among the central memory CD4 T cells and five clusters in the effector memory CD4 T cells [64].

These new studies demonstrate an important heterogeneity among the Th cell subsets but also bring a lot more questions. As the original number of subsets defined appears obsolete, how many are they in vivo? Also, is it really relevant to consider Th cells as stringent subsets? Otherwise, since several populations seem to overlap, would it be more accurate to view Th cells as a continuum of profiles? Depending on the threat, particular combination of cytokines might arise to efficiently neutralize it. However, these last three studies only looked at surface markers and transcription factors, they do not analyze cytokines or functional properties of the different subsets they identified.

Wong et al. studied T cells in eight different human tissues: blood but also lymphoid and non-lymphoid tissues, by CyTOF using a panel of 41 markers including surface markers, chemokine receptors and cytokines. Using unsupervised clustering, they identified 75 clusters, indicating a wide heterogeneity, but they also identified tissue-specific profiles in particular when looking at the expression of chemokine receptors, which are not homogeneously expressed among tissues. They also analyzed all possible combinations of five Th specific cytokines: IFN- γ for Th1, IL-4 for Th2, IL-10 for Treg, IL-17A for Th17 and IL-22 for Th22, and calculated their frequencies within each tissue. Only 12 out of the 32 possible combinations were detectable among tissues. Within the 12 combinations, five corresponded to each cytokine produced alone, six corresponded to two cytokines co-produced and only one subset co-producing three cytokines: IFN- γ , IL17A and IL-22 was identified [65].

This study only includes five cytokines but it surprisingly demonstrates that not all cytokine combinations are relevant and that only specific ones are secreted by Th cells depending on the tissue considered. This same analysis would be very interesting to conduct including all Th cytokines. Especially, it would be informative to see if cytokines of a same subset are always co-produced together or if there is a tissue-specific signature for cytokine production. For example, are Th2 cytokines: IL-4, IL-5 and IL-13 always co-produced together by the same cells? Or are they produced by distinct cells present in the same microenvironment? In the end, an important work remains to be done to entirely capture Th cell diversity and complexity, as well as their relative physiopathological relevance.

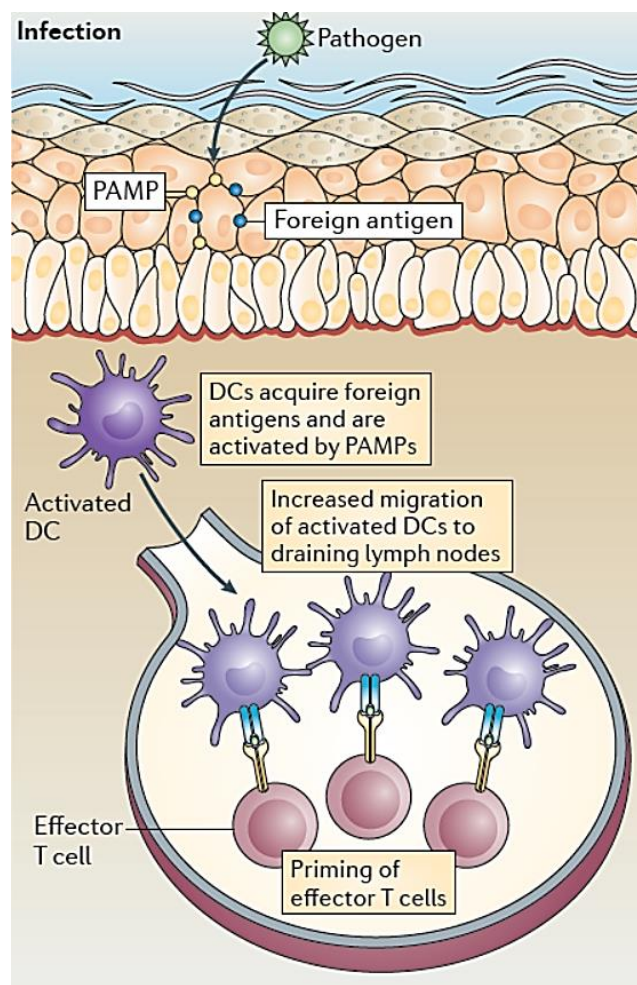
2. Dendritic cells: the main drivers of T helper differentiation

Dendritic cells (DC) are responsible for the initiation of immune responses. Indeed, DC are professional antigen-presenting cells, thanks to their high expression of class II Major Histocompatibility Complex (MHC-II) molecules. At steady state, immature DC are resting in peripheral tissues and will get activated in case of infection through all the pattern recognition receptors (PRR) they express, which allow them to recognize Pathogen Associated Molecular Patterns (PAMP) from pathogens surrounding them. DC capture antigens from their microenvironment and process them into peptides in order to present them on their MHC-II molecules. Once activated, DC will migrate to secondary lymphoid organs in order to activate antigen-specific naive CD4 T cells. DC-T cell interaction involves recognition of the antigen-MHC-II complex by the T cell receptor (TCR) on the T cell. If a T cell recognizes its specific antigen, it will become activated and proliferate in order to launch the appropriate immune response [66-68] (Figure 6).

Figure 6: Antigen-specific T cell response initiation

Illustration from Summers deLuca and Gommerman [69]

At steady state, DC are resting in peripheral tissues. In case of infection, they uptake foreign antigens and get activated by PAMPs present in the microenvironment. As a consequence, they migrate to secondary lymphoid organs. Once there, they will present the antigens as processed peptides on their MHC-II molecules to antigen-specific naive CD4 T cells, which are able to recognize antigen-MHC-II complexes via their TCR. When activated, T cells will differentiate into effector T cells able to mount a proper adaptive immune response.



2.1. Role of the different dendritic cell subsets in the T helper cell diversity generation

2.1.1. Human dendritic cell subsets

Several DC subsets have been identified, deriving from a common bone-marrow DC progenitor [70]. In addition to non-lymphoid tissue DC, which migrate from peripheral tissues to lymph nodes after antigen uptake and activation, some DC can be resident in lymphoid tissues in which they capture antigens from blood stream and lymph to present them directly to nearby T cells [71].









Subset	DC progenitors								
	early pre-DC	pre-cDC1	pre-cDC2	cDC1	cDC2	pDC	Langerhans cells	MoDC	
Surface markers	 HLA-DR CD123 CD33 CD45RA	 HLA-DR CD33 CD45RA CADM1	 HLA-DR CD33 CD45RA CD1c	 HLA-DR CD11c CD141 Clec9A XCR1 CADM1	 HLA-DR CD11c CD11b CD1c	 HLA-DR CD123 BDCA2 BDCA4	 HLA-DR CD11c CD1a Langerin EpCAM	 HLA-DR CD11c CD11b CD1c CD206 CD14	
Anatomical location	Blood Lymphoid organs	Blood Lymphoid organs	Blood Lymphoid organs	Blood Lymphoid organs Skin Peripheral tissue	Blood Lymphoid organs Skin Peripheral tissue	Blood Lymphoid organs	Skin	Skin Peripheral tissue	

Figure 7: Human dendritic cell subsets

Human DC subset classification, including new findings from See et al. [70] and Dutertre et al. [72]. Under each DC subset, some of their specific surface markers and their anatomical location.

In human, depending on the location, several DC subsets have been described. First, plasmacytoid DC (pDC) are characterized by expression of BDCA-2, BDCA-4, CD123 and their major capacity to produce IFN- α upon activation and can be found in the blood and lymphoid organs [71]. Additionally, two subtypes of myeloid or conventional DC have been described, expressing CD11c: 1) cDC1 characterized by the surface markers CD141, CLEC9A, CADM1 and XCR1, 2) cDC2 expressing CD1c and CD11b, both subsets can be identified in the skin, the blood, lymphoid organs and peripheral tissues [73]. In the skin, one specific DC subset populate the epidermis: Langerhans cells expressing CD1a, Langerin and EpCAM [74] (Figure 7).

In addition, DC deriving from monocytes have been described first in the skin and referred to as dermal DC [74]. Then, a population of Inflammatory Dendritic Epidermal Cell distinct from Langerhans cells and phenotyped as HLA-DR⁺CD1a⁺CD1b⁺CD36⁺ were identified in the skin of atopic dermatitis patients [75].

Additionally, in a *Leishmania* infection model in mice, monocyte-derived DC (MoDC) were identified and originally termed inflammatory DC because of their involvement in inflammation [76]. Inflammatory DC were also identified in ascites from patients with breast tumors and described as deriving from monocytes [77]. Later, MoDC were further identified in peripheral tissue samples from healthy patients, strengthening their *in vivo* relevance [78]. Furthermore, due to the difficulties of studying human primary DC from blood or tissues, *in vitro* protocols to generate DC from blood monocytes have been created, using granulocyte macrophage colony stimulating factor (GM-CSF) and IL-4 and are widely utilized across the scientific community [79] (Figure 7).

New technologies, in particular single-cell RNA sequencing and CyTOF, brought new insights into the study of DC subsets.

Villani et al. revised DC classification by sequencing human blood cells from healthy donors. First, they demonstrated that cDC2 are actually constituted of two subsets with similar phenotypes: CD1c⁺_A which are non-inflammatory and CD1c⁺_B displaying an inflammatory gene signature. Additionally, they identified a cluster of CD141⁻CD1c⁻ DC related to CD16 monocytes. These cells had previously been described in the blood by MacDonald et al. as CD16⁺CD11c⁺CD14^{lo}HLA-DR^o DC [80], but they had been poorly characterized since then. Finally, Villani et al. identified a new subset named "AS-DC" forming a continuum between cDC1c⁺ DC and pDC and sharing phenotypic markers with both subsets [81]. However, the results of the flow cytometry analysis to retrieve CD1c⁺_A and CD1c⁺_B cells at the protein level are confusing, the two subtypes actually partly overlap. Plus, they did not observe real functional differences between the two subsets except when looking at cytokine production, CD1c⁺_A secreted slightly higher levels of a few cytokines. If this slightly higher level of cytokines produced by the CD1c⁺_A subset has any relevance in functional specialization remains to be determined.

Furthermore, another team also identified two subsets among cDC2 from blood and lymphoid organs based on CD5 expression by flow cytometry. They fully characterized CD5^{high} and CD5^{low} DC by looking at their respective gene expression and functional properties [82]. These two populations were not identified by single-cell RNA sequencing and directly contradict results from Villani et al. [81].

Alcantara-Hernandez et al. used a CyTOF panel of 38 markers combined with unbiased analysis to characterize DC subsets from blood, skin, spleen and tonsils from 18 healthy donors. They retrieved cDC1 and cDC2 in all tissues, while pDC were present in the blood and lymphoid organs but not in the skin. They found Langerhans cells specifically in the skin. And also identified the AXL⁺ DC described by Villani et al. [81] in the blood and lymphoid organs. However, they retrieved neither the CD1c⁺_A and

CD1c⁺_B subsets identified by Villani et al. [81], nor the CD5^{high} and CD5^{low} subsets identified by Yin et al. [82]. Furthermore, they identified 3 clusters among cDC2, based on the markers CD163 and CD172a, but they observed that their frequencies were dramatically variable between tissues, but also between individuals and also that the expression of the surface markers identifying them varied among the clusters. They concluded that rather than conserved subpopulations of cDC2, these clusters were an important interindividual heterogeneity of the cDC2 population [83]. As highlighted in the publication, there is a bias in the study by Villani et al. in the number of donors analyzed and the use of only one tissue. They do not discuss the results from Yin et al., however, CD5 is among the 38 surface markers used for their CyTOF analysis and is not retained as defining different cDC2 subsets. Another discrepancy appears between Alcantara-Hernandez et al. and Villani et al. studies. Alcantara-Hernandez et al. did not retrieve the CD16⁺ DC subset identified originally by MacDonald et al. [80] and described by Villani et al. [81]. Besides, they did not identify the CD14⁺ DC which have been described, among other location, in the skin [74]. However, they compared in vitro generated MoDC to the other DC subsets. MoDC clustered separately not only from DC but also from monocytes, which lead them to conclude that they are not representative of any DC subsets present in healthy individuals. However, the fact that they cluster away from other DC subsets is not surprising since they arise from different progenitors. Also, since in vitro derived, they are probably influenced during culture, which alter their phenotype compared to ex vivo. Nevertheless, in vitro derived-MoDC remain a good model to study DC functions and Th polarization.

Using combination of single-cell RNA-sequencing and CyTOF to study human DC in blood, spleen and bone marrow, See et al. described a continuous process of differentiation within the human DC lineage. A common DC progenitor CD34⁺ in the bone marrow give rise to pDC and pre-DC, sharing phenotypic markers with pDC. Pre-DC can further differentiate into early-pre-DC and then give rise to pre-cDC1 and pre-cDC2. Pre-cDC1 and pre-cDC2 differentiate exclusively in cDC1 and cDC2 respectively. They also described how to specifically discriminate pre-DC from pDC: using CD33, CD2 and CX3CR1 specifically expressed on pre-DC compared to pDC [70]. Since the markers and gating strategies are different, it is hard to formally conclude, but the AXL⁺ DC/AS-DC identified by Alcantara-Hernandez et al. [83] and Villani et al. [81] might at least partially overlap with the pre-DC described by See et al. [70].

Very recently, Dutertre et al. confronted the results from Villani et al. [81]. Using Infinity Flow, RNA sequencing, single-cell RNA sequencing and CyTOF they analyzed each subset defined by Villani et al. [81] and contradicted some of their results. First, they demonstrated that the DC4 subset defined as CD141⁻CD1c⁻ DC were not DC, but CD16⁺ non-conventional monocytes. Then, they showed that the AS-DC defined by Villani et al. [81] and retrieved by Alcantara-Hernandez et al. [83] comprised pre-DC but

also pre-cDC2. Finally, they demonstrated that cDC2 heterogeneity was greater than the two CD1c⁺_A and CD1c⁺_B subsets identified by Villani et al. [81]. Among the cDC2 they identified a subset of CD5⁺ DC with a gene signature corresponding to the CD1c⁺_A subset described by Villani et al. [81]. Corresponding to the CD1c⁺_B subset they actually found three distinct subsets: one CD5⁻CD163⁻CD14⁻ subset, one CD5⁻CD163⁺CD14⁻ subset and one CD5⁻CD163⁺CD14⁺ subset. Dutertre et al. demonstrated that all cDC2 subsets were functionally capable of inducing T cell proliferation and they showed an increasing capacity to induce IL-4 and IL-17 production from CD5⁺ cells and CD5⁻CD163⁻CD14⁻ cells to CD5⁻CD163⁺CD14⁻ cells and finally CD5⁻CD163⁺CD14⁺ cells [72] (Figure 7). The top markers to differentiate cDC2 subsets identified by Dutertre et al. were CD5, CD14, CD163 [72], while Alcantara-Hernandez et al. showed high variance in the expression of CD32, CD163, CD172a and BDCA1 between individuals and clusters [83]. Also, the number of cDC2 clusters is not the same between the two studies: four subsets for Dutertre et al. [72] compared to three clusters for Alcantara-Hernandez et al. [83].

In the end, much work remains to be done to harmonize these recent discoveries and fully comprehend the human DC system. In particular, in depth studies will be needed to understand cDC2 heterogeneity, and determine if they can be separated into distinct populations, if the different clusters are just interindividual heterogeneity as described by Alcantara-Hernandez et al. [83] or if they have to be considered as subsets with functional differences as suggested by Dutertre et al. [72].

2.1.2. T helper cell polarization induced by each subset

An important concept in the field of DC, is that DC subsets would intrinsically possess specific capacities to activate T cells and induce differential Th responses. This concept still remains to be fully demonstrated, but some studies already tried to demonstrate this point.

For instance, Klechevsky et al. showed that ex vivo human Langerhans cells induced more Th2 cytokines production from allogeneic naive CD4 T cells than dermal cDC2 and CD14⁺ DC [84]. Furio et al. confirmed that human Langerhans cells were more potent than dermal cDC2 at inducing not only IL-4 but also IFN- γ production from allogeneic naive CD4 T cells, while dermal cDC2 induced more IL-10 producing-T cells [85].

Fujita et al. demonstrated that human Langerhans cells were more efficient than dermal cDC2 at polarizing naive CD4 T cells to produce IL-22, without IL-17, characteristic of Th22 cells [86]. Penel-Sotirakis et al. confirmed that Langerhans cells were the strongest inducers of IL-22 production without

IL-17 by T cells, compared to dermal cDC2 and CD14⁺ DC, but they also induced a higher production of IL-21 [87].

Segura et al. studied human DC isolated from non-invaded lymph nodes or blood and compared their Th polarizing capacities. They demonstrated that Langerhans cells induced preferentially IL-5 and IL-13 production by allogeneic naive CD4 T cells. When comparing cDC1 and cDC2 from lymph nodes to cDC1 and cDC2 from blood they observed that all DC induced both Th1 and Th2 profiles from T cells, but blood DC induced more IFN- γ , while lymph nodes DC induced more IL-5 and IL-13 production [88]. This could demonstrate a functional specialization due to DC original location and microenvironment.

Furthermore, Durand et al. showed that ex vivo cDC2 from human tonsils are the most efficient to induce Tfh polarization, compared to cDC1 and pDC. Indeed, cDC2 induced significantly higher proportion of CXCR5⁺PD1⁺ cells and production of IL-21 and CXCL13 from allogeneic naive CD4 T cells, compared to cDC1 and pDC [89]. This shows a functional specialization for tonsillar cDC2 to induce Tfh cell differentiation.

Yu et al. compared the Th polarization capacity of human blood cDC1 and cDC2 cocultured with allogeneic naive CD4 T cells. They demonstrated that cDC1 were more potent than cDC2 to induce a Th2 profile, characterized by IL-4 and IL-13 producing T cells, while cDC2 induced more IFN- γ producer-cells than cDC1 [90].

Nonetheless, despite these different studies, proving that freshly isolated human DC have intrinsic properties which give them capacities to induce specific Th cytokine patterns is a complicated task. Especially, since they are extracted from a specific microenvironment which could influence their Th polarization capacities. Also, since in vivo DC will migrate and activate T cells only when activated by external pathogens, studying their Th polarization capacities while immature and non-activated is not the most relevant.

2.2. Role of the dendritic cell activating signal

2.2.1. Immune sensing by dendritic cells

In order to recognize both exogenous and endogenous danger signals from their microenvironment, DC display a large repertoire of receptors.

Pattern recognition receptors (PRRs) allow them to recognize Pathogen-Associated Molecular Patterns (PAMPs) which are conserved pathogen motifs ranging from glycoproteins and polysaccharides, to double-stranded DNA and RNA and single-stranded RNA, but also Damage-Associated Molecular Patterns (DAMPs) which are endogenous danger signals released upon cellular stress or tissue damage such as histones, heat-shock proteins, ATP, actin for example [91, 92]. PRR binding to its specific PAMP or DAMP leads to the activation of an intracellular signaling cascade, resulting in DC activation, increase of maturation markers and production of proinflammatory cytokines and chemokines.

Toll-like receptors (TLRs) are membrane-bound PRRs. In human, the TLR family counts 10 members, from TLR1 to TLR10. TLR1, TLR2, TLR4, TLR5, TLR6 and TLR10 are expressed at the plasma membrane, where they directly encounter their ligands: bacterial and fungal PAMPs, while TLR3, TLR7, TLR8 and TLR9 are localized on the membrane of the endosomal compartment, where they detect nucleic acids from bacteria and viruses. Binding with their ligand facilitates TLRs dimerization. TLR2 has been shown to heterodimerize with TLR1, TLR6 and possibly TLR10, while the other members of the family are thought to homodimerize. TLR dimerization triggers activation of the intracellular signaling cascade, leading to DC activation [91, 93]. Human TLR ligands, locations and specific expression according to DC subsets are described in Table 1.

C-type lectin receptors (CLRs) are also membrane-bound proteins. The CLR superfamily includes more than 1000 proteins, which are divided into 17 subgroups according to their structures and domain composition. CLR play a role in the host defense against fungal infections by recognizing a wide range of carbohydrate structures, such as mannose, fucose, sialic acid and β -glucan [94, 95]. Details of the main CLR that have been described on human DC subsets with their ligands and locations are listed in Table 1.

Retinoic acid-inducible gene-I-like receptors (RLR) are cytosolic proteins and essential intracellular viral sensors which detect pathogens that bypassed detection in the extracellular and endosomal compartment. RLR are a family of RNA helicases which counts 3 members: RIG-I which senses ssRNA, MDA5 which recognizes dsRNA, and LGP2 which lacks the necessary domains to induce downstream signaling pathways and is thought to act as a cofactor of RLR signaling. RIG-I and MDA5 induce type-I IFN and proinflammatory cytokines production in response to viral infection [96, 97]. RLR expression on human DC subsets is listed in Table 1.

Nucleotide-binding oligomerization domain-like receptors (NLRs) are cytosolic sensors. The human NLR family contains 22 molecules which are structurally conserved and are able to recognize a wide range

of PAMPs from fungal zymosan to viral RNA and DAMPs such as products of cell death. NOD1 and NOD2 function as TLR, after recognition of their ligand and dimerization they lead to proinflammatory cytokines and chemokines production by DC. On the other hand, following ligand binding, the other NLR proteins form multi-protein oligomers, identified as “inflammasomes”, and responsible for proinflammatory responses [98, 99].

AIM2-like receptors (ALRs) are cytosolic proteins responding to bacterial- or viral-derived cytoplasmic double-stranded DNA. In human, the ALR family contains four members: AIM2, IFI16, PYHIN1 and MDA5. AIM2 and IFI16 have been shown to have the potential, like NLR proteins, to form inflammasomes. Ligand binding leads to proinflammatory cytokine production [100, 101]. AIM2 expression has been demonstrated in human pDC [102] and MoDC [103].

Formyl peptide receptors (FPRs) are seven transmembrane domains, Gi-protein-coupled receptors (GPCRs). The human family of FPRs contains three members: FPR1, FPR2 and FPR3. They recognize bacterial and mitochondrial peptides containing N-formylated methionine as well as endogenous non-formylated peptides and even lipids [104]. Recognition of their ligand leads to DC activation and production of reactive oxygen species [105]. FPR expression on human DC subsets is listed in Table 1.

Overall, not all DC subsets are able to recognize all pathogens, but across DC, all PRR are represented allowing recognition of every existing pathogen.

Class of PRR	PRR	Location	Ligand	PRR expression on human DC subsets					
				cDC1	cDC2	mDC (cDC1+cDC2)	pDC	Langerhans cells	MoDC
TLR	TLR1/2 Heterodimer	Plasma membrane	Triacyl lipopeptides, PAM3CSK4	+ [106]	+ [106-108]	+ [109]	+ [106-110]	+ [108]	+ [111-113]
	TLR2	Plasma membrane	Peptidoglycan, Lipoproteins, Lipoteichoic acids, PAM2CSK4, HKLM, HKSA, HKSP, HKCA	+ [106] - [114]	+ [106-108, 114, 115]	+ [109]	- [106-109, 114, 115] + Upon PAM3 stimulation [110]	+ [108]	+ [111-113, 115]
	TLR3	Endosomal membrane	Double-stranded RNA, Poly(I:C)	+ [106, 114]	+ [106-108, 114, 115]	+ [109]	- [106-110, 114, 115]	+ [108]	+ [111-113, 115]
	TLR4	Plasma membrane	Lipopolysaccharide (LPS), Mannan	- [106, 114]	+ [106-108, 114, 115]	+ [109, 116]	- [106-110, 115, 114, 116]	- [108]	+ [111-113, 115]
	TLR5	Plasma membrane	Flagellin	- [106, 114]	+ [106, 107, 114]	+ [109]	- [106, 107, 109, 110, 114]	Weak [108]	+ [111-113]
	TLR2/6 Heterodimer	Plasma membrane	Diacyl lipopeptides, Zymosan	+ [106]	+ [106-108]	+ [109]	+ [106-110]	+ [108]	+ [112, 113]
	TLR7	Endosomal membrane	Single-stranded RNA, Imiquimod, R848	- [106, 114]	- [106, 114] + [107, 108]	- [109] + [116]	+ [106-110, 114, 116]	- [108]	+ [112, 113]
	TLR8	Endosomal membrane	Single-stranded RNA, R848	+ [106] - [114]	+ [106-108, 114]	+ [109]	- [106-110, 114]	- [108]	+ [112, 113]
	TLR9	Endosomal membrane	DNA with unmethylated CpG	- [106, 114]	- [106-108, 114]	- [109, 116]	+ [106-110, 114, 116]	- [108]	- [112, 113]
	TLR10	Plasma membrane	Unknown	+ [106]	+ [106, 108]	+ [109]	+ [106, 108-110]	+ [108]	+ [113] - [112]

Class of PRR	PRR	Location	Ligand	PRR expression on human DC subsets					
				cDC1	cDC2	mDC (cDC1+cDC2)	pDC	Langerhans cells	MoDC
CLR	Dectin-1/CLEC7A	Plasma membrane	β -glucans, curdlan	+ [117]	+ [117, 118]		weak [117]		+ [119]
	Dectin-2/CLEC6A	Plasma membrane	High mannose, α -mannans	+ [117]	+ [117]		+ [117]		
	Dectin-3/MCL/CLEC4D	Plasma membrane	mycobacterial Trehalose-6,6-dimycolate				+ [120]		
	BDCA2/CLEC4C	Plasma membrane	Carbohydrates	- [121]	- [121]		+ [121]		
	DC-SIGN/CLEC4L	Plasma membrane	High mannose, fucose	+ [117]	+ [117]		weak [117]		+ [119]
	Langerin/CD207	Plasma membrane	β -glucan	+ [117]	+ [117]		+ [117]	+ [122]	
	MRC1/CD206	Plasma membrane	mannose, fucose, or N-acetyl glucosamine from microbial carbohydrates	+ [117]	+ [117]		+ [117]		
	MRC2/CD280	Plasma membrane	collagen ligands	+ [117]	+ [117]		weak [117]		
	DEC-205/CD205	Plasma membrane	Unknown	+ [117]	+ [117]		+ [117]		
	DCIR/CLEC4A	Plasma membrane	Plasma membrane	+ [117]	+ [117]		+ [117]		
	MGL/CLEC10A/CD301	Plasma membrane	terminal GalNAc structures	+ [117] - [123]	+ [117, 123]		weak [117] - [123]		
	CLEC9A/CD370	Plasma membrane	actin filaments	+ [117]	- [117]		- [117]		
	Mincle/CLEC4E	Plasma membrane	α -mannose, mycobacterial Trehalose-6,6-dimycolate						+ [119]
	MICL/CLEC12A	Plasma membrane	Uric acid crystals	+ [124]	+ [124]		+ [124]		

Class of PRR	PRR	Location	Ligand	PRR expression on human DC subsets					
				cDC1	cDC2	mDC (cDC1+cDC2)	pDC	Langerhans cells	MoDC
RLR	RIG-1	Cytosol	Single-stranded RNA			+ Upon stimulation with poly(I:C) [125]	+ Upon stimulation with CpG-A [126, 127]		+ [128, 129]
	MDA5	Cytosol	Double-stranded RNA			+ Upon stimulation with poly(I:C) [125]	+ Upon stimulation with CpG-A [126]		+ [129]
	LGP2	Cytosol	Unknown						
FPR	FPR1	Plasma membrane	N-formyl-methionyl peptides		+ [105]		+ [105]		
	FPR2	Plasma membrane	N-formyl-methionyl peptides		+ [105]		+ [105]		
	FPR3	Plasma membrane	N-formyl-methionyl peptides		+ [105]		+ [105]		

Table 1: Table recapitulating some of the human PRRs, their location, ligands and expression according to human DC subsets

Level of expression is annotated as + for positive constitutive expression, weak for weak constitutive expression, – for no expression detected and detailed if expression happens upon stimulation.

2.2.2. DC induce different Th profiles depending on their activating signal

The purpose of this variety of receptors expressed across DC subsets, is that DC will be able to detect any pathogen that will invade the organism. Nevertheless, different pathogens will lead to different Th cell polarization from the same DC (Figure 8).

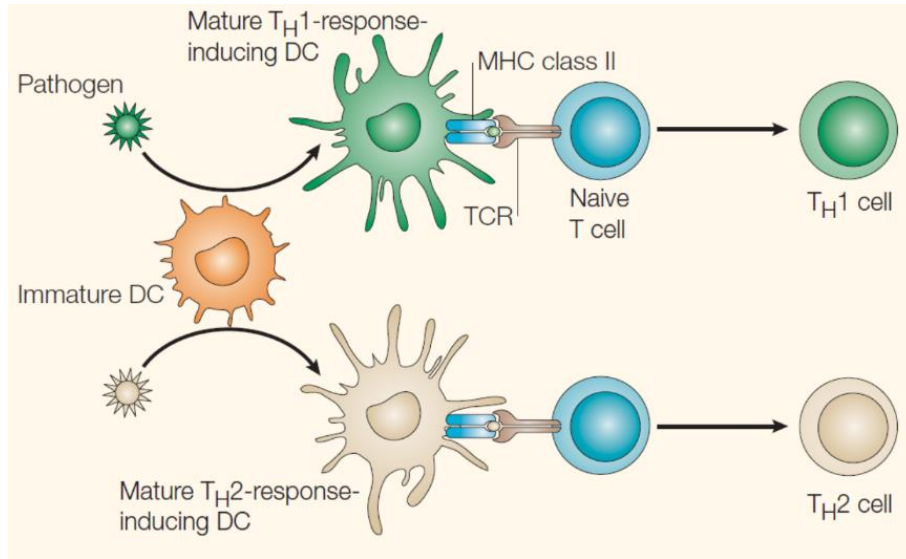


Figure 8: T helper polarization by dendritic cells depends on the type of pathogen they encounter

Illustration adapted from Kalinski and Moser [130]

Simplistic view of the Th polarization induced by DC in response to different pathogens. Depending on the pathogen immature DC will detect through their specific receptors, they will mature in a way to induce the most appropriate Th profile, in this example either Th1 or Th2.

For example, Agrawal et al. demonstrated that human MoDC stimulated with *Escherichia coli* LPS or flagellin, triggering TLR4 and TLR5 respectively, induced a Th1 response from allogeneic naive CD4 T cells, which highly produced IFN- γ . On the other hand, Pam3cys, TLR2 agonist, activated MoDC to induce Th2 polarization from T cells, with production of IL-5 and IL-13 [131]. In another study, they showed that human MoDC stimulated with Curdlan, a Dectin-1 (CLR family) agonist, or zymosan, a Dectin-1 and TLR2 agonist, induced IL-17 production by allogeneic naive CD4 T cells [132].

Thymic stromal lymphopoietin (TSLP) is a cytokine from the IL-7 family produced by keratinocytes in different allergic pathologies, like atopic dermatitis [133]. It has been demonstrated that human CD11c⁺ myeloid DC (pooled cDC1 and cDC2), stimulated with TSLP, polarized allogeneic naive CD4 T cells to produce the Th2 cytokines IL-4, IL-5 and IL-13 in combination with high levels of TNF- α , while LPS-

activated DC induced T cell production of IL-10 and IFN- γ [134]. Ito et al. confirmed the Th2 polarization induced by TSLP-activated DC in comparison to Poly(I:C), a TLR3 agonist, stimulated-DC which induced production of TNF- α , IL-10 and IFN- γ from naive CD4 T cells [135].

Also, human Langerhans cells stimulated with poly(I:C) polarized allogeneic naive CD4 T cells to produce IFN- γ in combination with IL-10 [136].

When stimulated with type B CpG oligodeoxynucleotides (ODN), a TLR9 agonist, human blood pDC were able to polarize allogeneic naive CD4 T cells into FoxP3⁺CD25⁺ T regs producing IL-6, IL-10, IFN- γ and TGF- β [137]. On the other hand, when activated with curdlan, human blood pDC induced a Th2 profile on allogeneic naive CD4 T cells, with production of IL-4, IL-5 and IL-13 [138].

These different studies demonstrate that a same DC subset, activated via distinct PRR or cytokine receptor signaling, can induce different Th cell profiles, thus shaping the appropriate immune response to a specific pathogen.

2.3. Role of the diversity of communication molecules expressed by dendritic cells

2.3.1. Primary view: One signal induces one T helper cell profile

After antigen capture, DC process those antigens into peptides in order to load them onto their MHC class II molecules. They migrate to the secondary lymphoid organs, and present these peptides to antigen-specific T cells that recognize them through their TCR. This MHC-II/TCR interaction represents the first activating signal for T cells.

Once activated by antigens, DC upregulate their expression of costimulatory molecules CD80 and CD86, which bind to the CD28 molecules expressed by T cells. This is the second signal needed for Th polarization. In absence of this secondary signal, T cells become anergic, leading to tolerance.

Depending on the danger signal: pathogen or cytokine that activated DC, they will produce specific cytokines in order to launch an appropriate Th response. This is the third Th polarizing signal and this one really determines the Th polarization that will arise [139] (Figure 9).

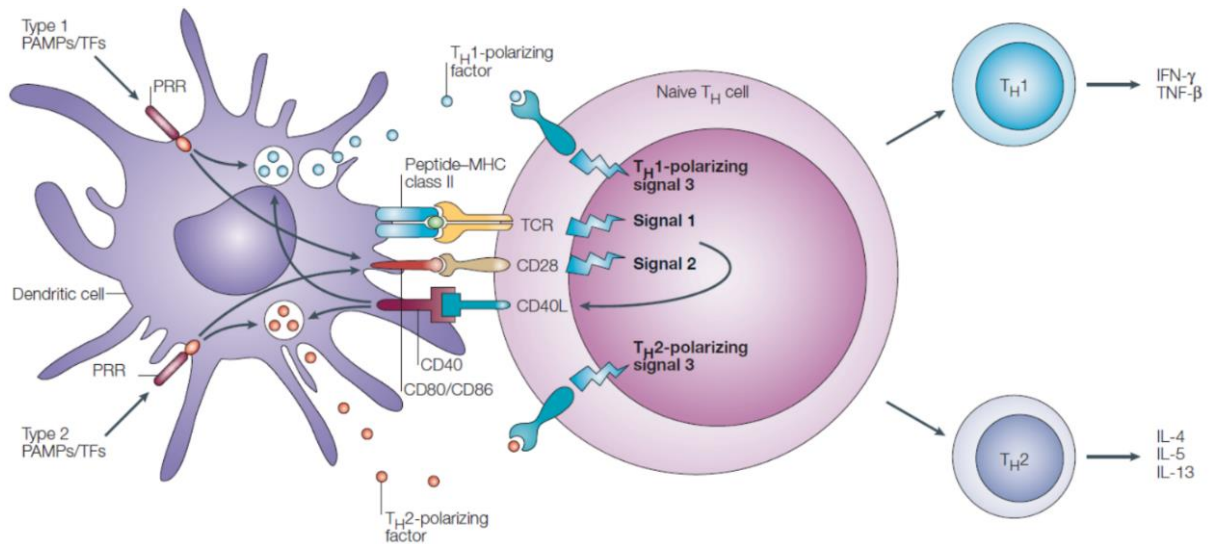


Figure 9: T helper polarization towards Th1 or Th2 subset by dendritic cell requires 3 signals

Illustration from Kapsenberg [139]

Signal 1 is the recognition by the T cell antigen-specific TCR of peptides loaded on the DC MHC-II molecules. Signal 2 comes from the binding of the co-stimulatory molecules CD80 and CD86 expressed at the surface of the DC with the CD28 molecules expressed at the surface of the T cell. Signal 3 is given by specific polarizing cytokines produced by the DC and signaling through corresponding receptors expressed by T cells, e.g. IL-12 induces Th1 polarization, while IL-4 promotes Th2 polarization.

Several DC molecules have been characterized as able to dictate a specific Th profile. For instance, IL-12 has been extensively described as a potent inducer of IFN- γ and Th1-polarization [140]. Nevertheless, the third signal can also be another DC surface molecule, rather than a cytokine.

TSLP-activated-DC are known for producing very few cytokines except TARC and CCL22 [134]. It has been demonstrated that in the context of TSLP-activated-DC, OX40L was responsible for the Th2 polarization, its blocking leading to a decrease of the IL-4, IL-5 and IL-13 production [135].

OX40L blocking during a coculture between influenza virus-activated cDC1 and allogeneic naive CD4 T cells also lead to significant decrease in IL-4 and IL-13 production [90]. These results confirmed OX40L role in Th2 polarization.

OX40L has also been linked to Tfh polarization. Addition of soluble recombinant human OX40L protein to a DC-free system of naive or memory CD4 T cell culture lead to the upregulation of multiple Tfh associated genes [141]. Furthermore, we established that blocking OX40L in a coculture between TSLP-activated DC and allogeneic naive CD4 T cells inhibited IL-21 and CXCL13 production [142], thus Tfh polarization, which confirmed results from Jacquemin et al. [141].

Ito et al. demonstrated that human blood pDC activated with CpG ODN induced IL-10-producing cells through ICOSL. When blocking ICOSL during coculture between CpG-activated pDC and allogeneic naive CD4 T cells, IL-10 production significantly decreased [143].

Yu et al. showed that blocking CD40L during coculture between human blood cDC2 activated with influenza virus and allogeneic naive CD4 T cells induced significant IL-13 production by T cells while decreasing IFN- γ production [90]. This demonstrated the role of CD40 in Th1 polarization.

These studies demonstrated the role of different molecules as third signal in the Th polarization process, such as IL-12 and CD40 linked with Th1 polarization, OX40L associated to Th2 profile, OX40L also responsible for Tfh polarization and ICOSL related to IL-10 production.

2.3.2. A more complex system: combinatorial of dendritic cell communication molecules

Nevertheless, this view of the three signals responsible for Th polarization is a bit simplistic. Indeed, more than 75 molecules have been described produced or expressed by DC: Interleukins and Chemokines, as well as B7, TNF, SLAM, Notch, Nectin, Galectin, Semaphorin, Integrin, immunoglobulin-like transcripts and TIM family of molecules (Figure 10).

This means that a considerable number of molecule combinations can emerge after DC activation, depending on the activating signal. These molecules will act collectively on T cells and one specific molecule will not have the same effect depending on the other molecules that are co-expressed.

This implies the notion of the context-dependency of each molecule. To illustrate this concept, we can take the example of Ito et al. who showed that OX40L expressed by TSLP-activated DC induced IL-4 production by naive CD4 T cells. They further demonstrated that naive CD4 T cells cultured with anti-CD3/CD28 monoclonal antibodies and a human OX40L recombinant protein produced IL-4, IL-5 and IL-13, and this production, was increased if IL-4 was added to the culture. On the contrary, if IL-12 was combined to OX40L, Th2 cytokines production by T cells was inhibited and they started producing IFN- γ instead [135]. This demonstrates the importance of the context-dependency in which each DC communication molecule is placed. One molecule can have a totally different impact depending on the context it is placed in.

Since a huge diversity of communication molecules can be expressed by DC (Figure 10), it means that countless numbers of contexts can arise and influence each molecule effects. Several teams have looked into the impact of signal combination and its integration by T cells, on Th polarization.

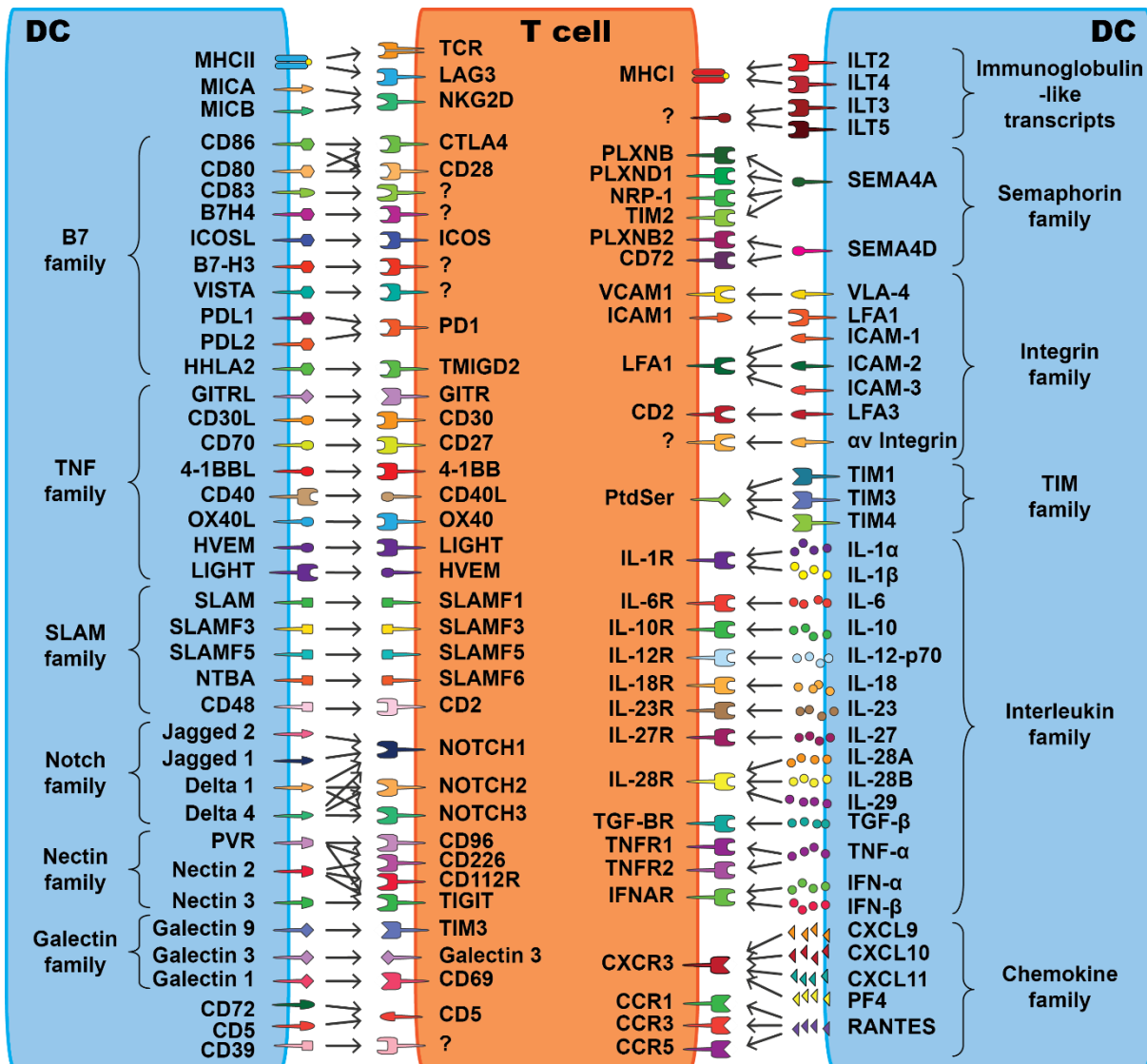


Figure 10: Dendritic cell/T cell communication molecules

Schema recapitulating 75 communication molecules, surface or secreted, that can be expressed by dendritic cells and interact with its ligand or receptor expressed at the surface of a T cell.

Volpe et al. studied the combination of the five cytokines IL-1 β , IL-6, TNF, TGF- β and IL-23 on Th17 polarization in a DC-free human T cell culture system using anti-CD3/anti-CD28 Dynabeads. They showed that each cytokine alone, or combination of only two or three would not induce IL-17

production, or at low levels, and that only the combination of the four cytokines IL-1 β , IL-6, TGF- β and IL-23 would induce high levels of IL-17 production from T cells [144].

Later, Schmitt et al. took a systematic approach to study the combination of signals responsible for Tfh polarization in human, again in a DC-free human T cell culture system using anti-CD3/anti-CD28 antibodies. They combined 12 cytokines for a total of 48 conditions and ranked them for their induction of Tfh markers such as CXCR5, ICOS and IL-21. In the end, they demonstrated that IL-12 and IL-23 contributed to Tfh polarization with TGF- β acting as an important cofactor [145].

Eizenberg-Magar et al. went a bit further and used mathematical modelling to map the Th response to a large number of cytokine combinations. They cultured T cells from spleens of C57BL/6 mice with anti-CD3/anti-CD28 antibodies and six cytokines (IFN- γ , IL-12, TGF- β , IL-6, IL-4, and IL-2) combined systematically for a total of 64 conditions. They found out that in response to most combinations, Th cells would adopt intermediate profiles in terms of cytokines produced and transcription factors expressed rather than committing to a specific polarization fate [146].

But those studies were using DC-free T cell culture systems, with a limited number of communication molecules involved and only cytokines as inputs. This greatly simplifies the number of molecules acting on T cells. No study was conducted to really understand the complexity of the DC/T communication process and the impact of the combination of DC molecules on the Th profile induced as a response. In this context, there was a real need to try to comprehend what specific Th cell differentiation is induced depending on the combination of signals expressed by the DC.

3. T helper cell contribution to diseases, example of Atopic Dermatitis

Numerous studies have shown that T helper cells can have a pathogenic role and be involved in many pathologies, when they are not properly regulated.

After description of the Th1/Th2 paradigm by Mosmann and Coffman [2], evidence accumulated to show that the balance between Th1 and Th2 cytokines is the determinant between protection and immunopathology. Indeed, it was shown that upregulation of the Th1 cytokines would be responsible for autoimmunity, while upregulated Th2 cytokines would lead to allergic diseases [147].

First, evidence described multiple sclerosis, type 1 insulin-dependent diabetes mellitus, and posterior uveitis as Th1-mediated autoimmune diseases [148].

Then, excess of Th2 cells have been described in numerous allergic diseases: asthma, chronic rhinosinusitis, Atopic Dermatitis (AD), eosinophilic gastrointestinal disorders, allergic rhinitis, anaphylaxis [149, 150].

Afterwards, Th17 cells have been extensively described in the pathogenesis of psoriasis [151], but they have also been associated to ankylosing spondylitis, rheumatoid arthritis [152], systemic lupus erythematosus [153], multiple sclerosis [154], inflammatory bowel's disease [155] and type-2 diabetes [156].

Th9 cells have been described in Asthma and Airway Hyper-Responsiveness, tuberculosis, rheumatoid arthritis, atopic dermatitis, psoriasis [157].

Studies demonstrated that Th22 cells could play a role in skin disorders, such as AD and psoriasis but also in autoimmune diseases like rheumatoid arthritis, systemic lupus erythematosus, systemic sclerosis, inflammatory bowel disease [22].

An altered suppressive capacity of Treg cells has been observed in type-1 diabetes, associated to a higher resistance to suppression of T effector cells, which explain the onset of the disease. Also, in systemic lupus erythematosus, increasing evidence shows that a diminished number and suppressive function of Treg cells play an important role in the disease. In some cancer, studies demonstrated that increased number of Treg cells was associated to poor prognosis, possibly because of decreased anti-tumor responses [27].

Different studies have shown a role for Tfh cells in autoimmune diseases such as Sjogren's syndrome, systemic lupus erythematosus, myasthenia gravis, rheumatoid arthritis, Grave's disease and Hashimoto's disease but also primary immunodeficiency, lymphoma, asthma and other allergic diseases [158]. In HIV infection, germinal centers as well as Tfh cells are altered, preventing proper humoral response and efficient HIV-specific B cell selection [159].

This non-exhaustive list of Th-related pathologies demonstrates the importance of a fine tuning in the Th polarization but also the possibility of targeting Th pathways as therapy. Furthermore, it proves that in most pathologies several Th profiles arise at the same time, worsening the condition and making it more difficult to efficiently treat the disease.

We were particularly interested in studying AD because of the known role of TSLP, which is part of our experimental model, in its pathogenesis [134, 160], for this reason I will specifically focus on AD pathogenesis and treatments in the following parts.

3.1. General characteristics of Atopic Dermatitis

Atopic Dermatitis or atopic eczema is a chronic and inflammatory disease characterized by patches of red and itchy skin. AD is characterized by an IgE sensitization to environmental allergens, driven by both dysfunctions of the epidermal barrier and immune dysregulation.

AD primarily affects infants and young children, 15-25% worldwide, and usually resolves within a few years. But in some cases, it can continue during adulthood and affect up to 10% of adults.

The causes of AD are still not entirely clear, some data suggest that the combination of extrinsic environmental factors, intrinsic immune mechanisms and genetic factors would be the origin [161].

Disease severity is evaluated using several scores, the most commonly used are the Eczema Area and Severity Index (EASI) and the Scoring atopic dermatitis (SCORAD), allowing measurements of AD outcomes [162].

3.2. T helper cell role in Atopic Dermatitis pathogenesis

Atopic dermatitis is characterized by the occurrence of two phases: first an acute phase in which a Th2 and Th22 responses dominate, and a chronic phase in which the Th1 axis gets activated in parallel of enhanced Th2 and Th22 responses [163].

Two contradictory hypotheses compete to explain AD pathogenesis: the “outside in” hypothesis, which sees the altered skin barrier as the cause of AD inflammatory cascade and the “inside out” hypothesis, according to which defective cutaneous immune response and cytokine dysregulation are the origin of the disease [164].

Even though it is not clear which event comes first, one possible scenario of the acute lesion onset is that impaired skin barrier allows entry of allergens and microbial products. As a consequence, keratinocytes start secreting innate cytokines IL-1, IL-6 and IL-18, including pro-Th2 cytokines IL-25, IL-33 and TSLP. Skin DC acquire foreign antigens and in response to cytokines, they get activated and migrate to the draining lymph nodes to polarize naive CD4 T cells into Th2 cells [160, 165] (Figure 11).

Th2 molecules, such as IL-4, downregulate multiple genes regulating epidermal barrier function. IL-4 and IL-13 have been shown to alter filaggrin gene expression during keratinocytes differentiation, as well as loricrin and involucrin. These mechanisms contribute to skin barrier impairments, allowing bacteria and allergens to penetrate the skin, which leads to infections and allergens sensitization. In addition, IL-4 and IL-13 inhibit antimicrobial peptides production by the skin and Th2 responses enable *Staphylococcus aureus* colonization, leading to *Staphylococcus aureus* infection. This increases even more the skin inflammation [163] (Figure 11).

IL-4 is also known to induce IgE switch from B cells. These IgE are directed against allergens but some also react to self-antigens, contributing to disease activity [166] (Figure 11).

Group 2 innate lymphoid cells (ILC2) have also been described to be present at high levels in AD skin compared to healthy donors. ILC2 are induced by IL-25 and IL-33 and are also able to produce Th2 cytokines, thus promoting Th2 responses [163] (Figure 11).

Th22 cells have also been associated to AD with upregulated production of their specific molecules. Particularly, IL-22 is associated to epidermal hyperplasia and can also downregulate filaggrin gene expression. High levels of S100A proteins, which can act as antimicrobial agents and inflammatory molecules, have been detected at high levels in AD patient skin [167, 168] (Figure 11).

In the chronic phase, in parallel of the Th2 and Th22 responses, a Th1 response emerges with increased production of IFN- γ , CXCL9, CXCL10 and CXCL11 [166]. This rise is thought to come from IL-12 produced by infiltrating eosinophils or inflammatory dendritic epidermal cells. IFN- γ participate in the epidermal keratinocyte apoptosis by inducing the expression of Fas at their surface, which contributes to the spongiosis found in acute AD [169] (Figure 11).

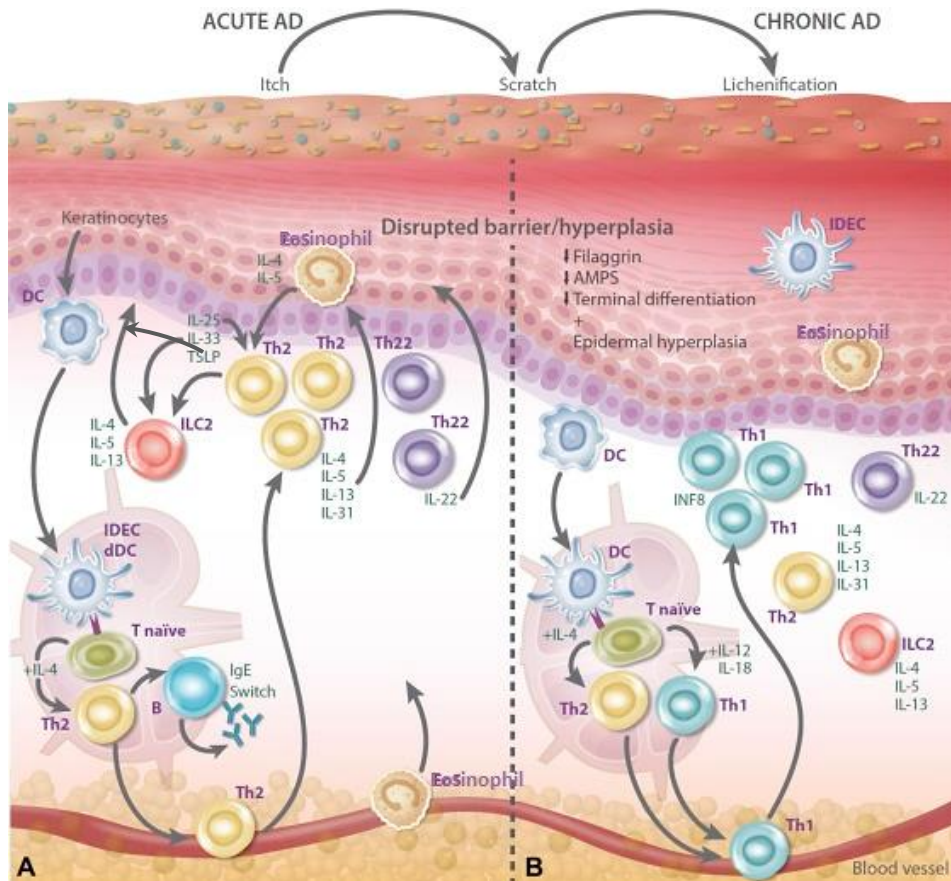


Figure 11: Atopic Dermatitis pathogenesis in Acute (A) and Chronic (B) phases

Illustration from Gooderham et al. [168]

Skin barrier defects lead to the external allergens permeability and induce TSLP, IL-25 and IL-33 secretion from keratinocytes. DC are recruited, acquire antigens and get activated in response to cytokines, they migrate to the draining lymph nodes where they induce T cell polarization towards a Th2/Th22 response. IL-4, IL-13 and IL-22 inhibit filaggrin expression by keratinocytes further worsening the skin impairments. They also downregulate antimicrobial peptides production, which lead to bacterial infections. IL-4 also induces IgE switch on B cells, which produce allergen-specific IgE. Some IgE also target self-antigens, aggravating the disease. In addition, Th1 cells participate in the chronic phase of AD, their production of IFN- γ inducing keratinocyte apoptosis, thus leading to spongiosis and disease chronicity.

In addition to their known role in psoriasis pathogenesis [151], Th17 have also been described in atopic dermatitis. Th17-associated molecules such as IL-17A and CCL20 are upregulated in AD patient skin compared to healthy donors in both acute and chronic phases. IL-17A could upregulate IL-22 and S100A proteins, contributing to the immune dysregulation [163].

The role of Tfh cells in AD pathogenesis has not yet been defined. However, we have described that Tfh cells of type 2 (Tfh2), described as $CD4^+CD45RO^+CXCR5^+CXCR3^-CCR6^-$, are enriched in adult AD patients peripheral blood compared to matching healthy donors [142]. In addition, another study showed a higher proportion of Tfh cells, defined as $CD4^+CXCR5^+PD-1^+IL-21^+$, in children AD patients compared to healthy controls and to adult AD patients [170]. Since the role of Tfh cells, in particular of Tfh2 cells, in inducing IgE switch from B cells has been demonstrated [45], it is highly plausible that Tfh cells have a role in AD pathogenesis.

3.3. Atopic Dermatitis treatments

3.3.1. Traditional treatments

The first treatments offered to AD patients include non-pharmacological interventions such as application of emollients. If this first attempt fails, patients are offered topical therapies such as corticosteroids, calcineurin inhibitors and antibiotics. Those have moderate side-effects like skin atrophy, itching and burning, which limits the frequency of application.

If non-pharmacological interventions and topical therapies both fail, patients with severe and refractory AD are proposed systemic immune suppressant treatments such as cyclosporine, methotrexate or mycophenolate mofetil. But these treatments present an important toxicity with a wide list of serious side-effects [171, 172].

AD represents a real burden for patients and impacts greatly their quality of life. Additionally, due to significant adverse effects carried by systemic treatments, there was a need for more effective and safer long-term treatments, especially for moderate-to-severe AD patients.

3.3.2. New immunotherapies for Atopic Dermatitis treatment

In this context, several immunotherapies were recently developed by pharmacological companies to treat AD. Different strategies have been conceived, aiming at targeting key molecules involved in AD pathogenesis.

3.3.2.1. Th2 pathway as therapeutic target

One common target chosen by pharmaceutical companies is the Th2 pathway, which major role has been extensively described in AD pathogenesis. Many drugs have been developed to target different molecules implicated at different steps in Th2 cell development.

Two anti-IL-13 inhibitors were conceived. First, Lebrikizumab (Roche) completed phase II trial and induced significant improvement in moderate-to-severe AD, but patients were also treated with topical corticosteroids, limiting the understanding of Lebrikizumab as single agent (NCT02340234) [173]. Tralokinumab (AstraZeneca) induced significant improvement of EASI score in treated patients compared to placebo in phase II trial (NCT02347176) and is currently being tested in three phase III trials (NCT03131648, NCT03160885 and NCT03363854).

Two IL-5 antagonists were also created, Benralizumab (AstraZeneca) which is currently in phase II trial (NCT03563066) and Mepolizumab (GlaxoSmithKline) which was terminated after inducing decreased eosinophil levels and showing no efficacy in phase I trial (NCT03055195) [174].

Nemolizumab (Galderma) is an anti-IL-31 receptor A inducing improvement compared to baseline in treated-patients in phase II trial (NCT01986933) [175]. BMS-981164 (Bristol-Myers Squibb), an anti-IL-31 monoclonal antibody, did not go further than phase I trial (NCT01614756).

A TSLP antagonist, Tezepelumab (Amgen) induced non-significant improvements compared to placebo in phase II clinical trial (NCT03809663) [176] and MK-8226 (Merck) TSLP receptor antagonist, was terminated before the end of phase I (NCT01732510). These two cases demonstrate that TSLP might not be the more potent target in AD treatment, since other cytokines have redundant effects on DC activation to induce Th2 polarization and might also be too upstream of the Th2 pathway.

Two OX40 antagonists were developed: GBR830 (Glenmark Pharmaceuticals) which showed great efficacy in phase II trial (NCT02683928), and KHK4083 (Kyowa Hakko Kirin) which completed phase I trial (NCT03096223) in Japan, and for which phase II trial is ongoing (NCT03703102).

ANB020 (AnaptysBio, Inc.), an anti-IL-33 monoclonal antibody, is currently in phase II clinical trial for moderate-to-severe AD (NCT03533751).

Several IgE antagonists were also created: Omalizumab did not show potent effect in AD treatment [177], MEDI4212 (MedImmune) completed phase I trial showing potency (NCT01544348) [178] and Ligelizumab (Novartis) completed phase I and II clinical trials (NCT01596712 and NCT01552629 respectively).

Overall, because of the known dominant role of Th2 cells in AD pathogenesis, targeting one of the molecules closely involved in Th2 development is a promising choice. The risk here is to choose a molecule not directly responsible for the Th2 polarization and for which other molecules could have redundant properties.

3.3.2.2. Other T helper pathways as therapeutic targets

Since Th17 and Th22 cells are also involved in AD pathogenesis, other approaches than Th2 inhibition have been designed.

For example, Fezakinumab (Rockefeller University) an anti-IL-22 antibody, completed phase II trial and showed good results in treated patients with improvement of clinical scores (NCT01941537) [179]. This therapy might be promising for patients with insufficient response to Th2 inhibition.

Ustekinumab (Rockefeller University) which inhibits p40, the shared subunit between IL-12 and IL-23, has opposite effects in two different phase II clinical trials (NCT01806662 and NCT01945086) [180, 181]. Secukinumab (Novartis) an anti-IL-17A monoclonal antibody already used for treatment of psoriasis, has just completed phase II clinical trial for AD treatment (NCT02594098).

MOR106 (Galapagos NV) an IL-17C antagonist completed phase I trial (NCT02739009) with positive results and is currently in phase II clinical trial (NCT03568071) [182].

Tocilizumab (Roche) an anti-IL-6 inhibitor used in rheumatoid arthritis treatment, showed improvement of clinical signs but caused bacterial infection when tested on 3 severe AD patients [183]. Even if the number of patients is really limited, this suggests that IL-6 might not be the best target for AD treatment, because not directly related to disease onset.

No therapy targeting specifically the Tfh pathway has been developed for the treatment of AD yet. But several IL-21 neutralizing antibodies have been patented, such as patent number WO/2010/055366 by Zymogenetics [184] or WO/2003/087320 by Beth Israel Deaconess Medical Center Inc. [185], as well as monoclonal antibodies against IL-21 receptor, for example patent number WO/2004/083249 by Wyeth Corp [186]. IL-21 has a known role on Tfh differentiation and maintenance but also on germinal B cell survival and proliferation [35]. Thus, we could imagine seeing application for these monoclonal antibodies in AD treatment.

3.3.2.3. Additional therapeutic strategies

Several JAK inhibitors were developed to target the JAK-STAT pathways, mediating numerous intracellular immune dysregulations, Baricitinib (Lilly), Upadacitinib (Abbvie) and PF-04965842 (Pfizer) all showed good efficacy in phase II trials (NCT02576938, NCT02925117 and NCT02780167 respectively) and are now undergoing phase III clinical trials [182]. More trials need to be conducted, on larger number of patients, but those therapies seem promising for AD treatment.

Histamine has been shown to induce pruritus but also inhibit keratinocyte terminal differentiation and impair skin barrier in AD. ZPL-3893787 (Ziarco Pharma Ltd), an anti-histamine H4 receptor, completed phase II clinical trial and showed improved inflammatory skin lesions in treated patients (NCT02424253) [187].

Crisaborole (Pfizer) is a small molecule inhibitor of phosphodiesterase 4 (PDE4) approved in 2016 by the American Food and Drug Agency for topical treatment of mild-to-moderate AD in children. It has the advantage of being corticosteroid-free, safe and effective [188], it appears like a good option for children with mild-to-moderate AD unresponsive to other topical treatments.

3.3.2.4. Dupilumab specific case

As described previously, a large number of therapies have been developed or are still under development for treatment of Atopic Dermatitis, but the first immunotherapy approved for treatment

of moderate-to-severe AD in adult patients by both the American Food and Drug Administration and European Medicines Agency is Dupilumab, developed by Regeneron Pharmaceuticals and Sanofi and initially approved for treatment of asthma.

Dupilumab is a fully human monoclonal antagonist antibody targeting IL-4 receptor alpha subunit, therefore inhibiting IL-4 and IL-13 signaling and thus abnormal Th2 responses [182]. By targeting IL-4/IL-13 signaling, Dupilumab blocking acts on three main mechanisms of Atopic Dermatitis: 1) skin barrier defects due to filaggrin protein inhibition, 2) IgE class-switch induced by IL-4 and 3) Th2 differentiation of the immune infiltrate [189] (Figure 12).

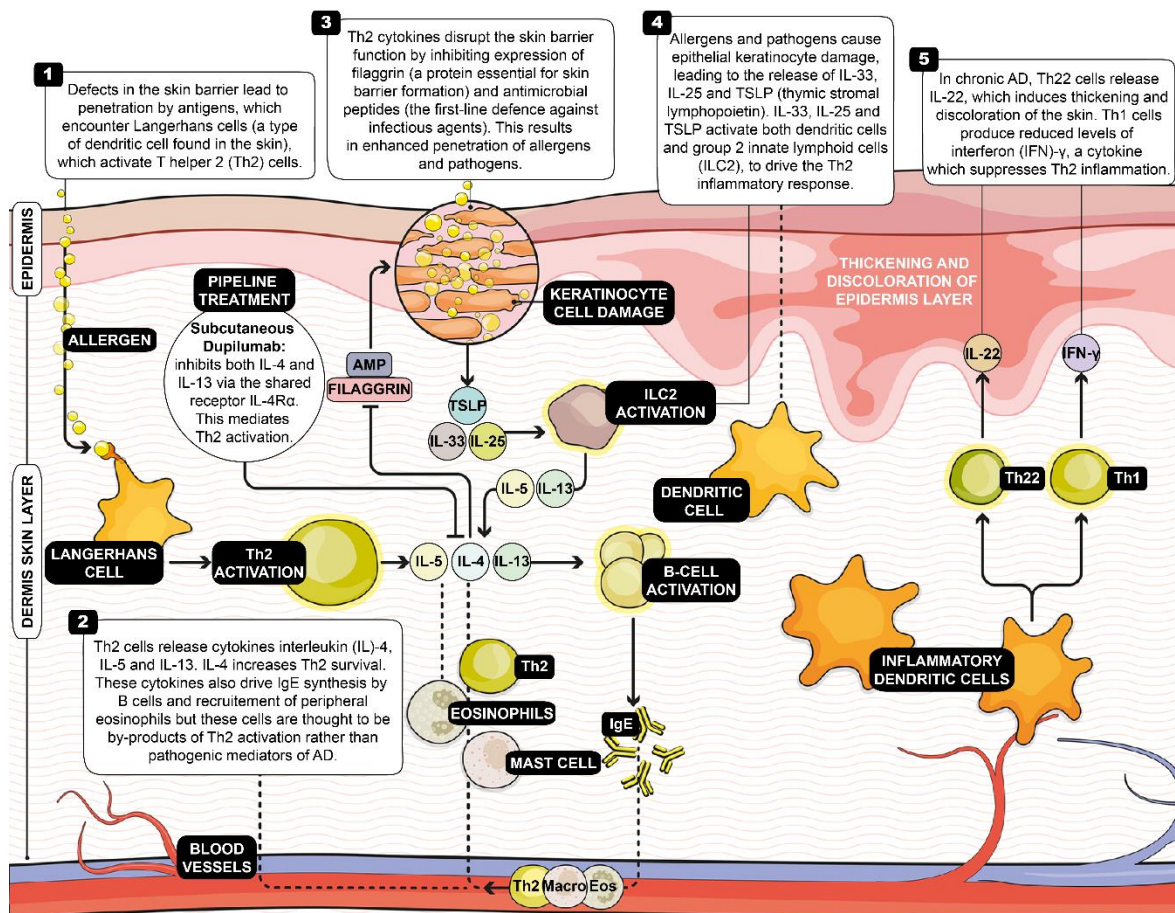


Figure 12: Dupilumab mechanism of action

Illustration from The Pharmaceutical Journal [190]

By targeting IL-4Rα, Dupilumab inhibits IL-4 and IL-13 signaling, thus impacting Th2 survival, B cell activation and IgE production, recruitment of eosinophils, filaggrin and antimicrobial peptides downregulation.

Seven randomized double-blinded, placebo-controlled, clinical trials including a total of 1965 patients with moderate-to-severe AD tested Dupilumab safety and efficacy. The results were that Dupilumab was consistently proven more efficient than placebo, with rare adverse effects such as injection-site reaction, conjunctivitis and eosinophilia [191, 192].

Studies revealed that clinical improvement was associated to significant decrease at the mRNA level of genes related to activation of T cells, DCs, eosinophils, inflammatory pathways and Th2-inducing chemokines, but also keratinocyte proliferation and innate immunity in skin lesions from Dupilumab-treated patients compared to placebo-treated patients [193, 194].

In France, a cohort of 241 adult patients were treated with Dupilumab in a real-life study showing similar effectiveness than clinical trials, but also higher frequency of conjunctivitis and eosinophilia [195].

Long-term effectiveness and safety of the treatment need to be assessed, but so far Dupilumab looks like a potent treatment for adult patients with severe AD unresponsive to traditional modalities.

4. Objectives

In the introduction, I presented the current uncovered T helper cell diversity, starting from the discovery of the Th1 and Th2 subsets, and all the other subsets identified afterwards: Th17, Treg, Th9, Th22 and more recently Tfh cells and their own subsets: Tfh1, Tfh2, Tfh17 and Tfr. Next, I described the different dendritic cell characteristics responsible for inducing this complexity of T helper cell subsets: role of the DC subset, role of the DC activating signal and role of the DC communication molecules. Finally, I demonstrated why the fine regulation of the T helper polarization is very important and how excess of T helper cells can become pathogenic. With the example of Atopic Dermatitis, I also demonstrated how disturbed Th pathways could be triggered by immunotherapies to try to cure the disease.

I focused my PhD work on:

1. Understanding the role of TSLP-activated-DC in the generation of Tfh cells.

Using an in-vitro coculture model of TSLP-activated-DC and naive CD4 T cells we were able to demonstrate that TSLP-DC are able to polarize Tfh-like cells expressing the surface markers CXCR5, ICOS, PD1, as well as the transcriptional repressor Bcl-6, producing the cytokines IL-21, CXCL13, IL-4 and TNF- α and capable of B cell help and inducing IgE production. We further demonstrated that TSLP-DC polarization of Tfh from naive T cells and activation of memory Tfh cells were both going through OX40L. This work is presented as a published article in the first part of the results section.

2. Examining the link between the combination of communication molecules expressed at the surface of dendritic cells and the diversity of T helper profiles induced as a response.

In order to capture the complexity of the DC communication molecules combinatorial and the T helper profile diversity it induces in return, 428 coupled measures on DC and T cells were performed and integrated in an innovative mathematical model. This model allows the prediction of 18 T cell parameters in response to 36 DC-derived signals. This model was extensively validated not only by the existing literature but also experimentally. And it allowed us to discover a new role for IL-12p70 in an IL-1 context in the induction of IL-17F without IL-17A. This work is showed as a published article in the second part of the results section.

3. Studying the evolution of Th/Tfh subsets in Atopic Dermatitis patients treated with Dupilumab. Thanks to a cohort of 29 moderate-to-severe adults AD patients treated with Dupilumab, from whom we received peripheral blood samples at different timepoints, we were able to follow the evolution of

eight Th and Tfh cell populations during their treatment. In parallel of the blood withdrawal, clinicians evaluated clinical scores at each timepoints. Therefore, we were able to demonstrate that decrease of the Th17 cell percentage we measured during patient treatment with Dupilumab, correlated with improvement of the EASI score. This work is depicted as a manuscript in preparation in the third part of the results section.

RESULTS

1. Publication n°1

TSLP-activated dendritic cells induce human T follicular helper cell differentiation through OX40-ligand

J Exp Med. 2017 May 1; 214(5): 1529–1546

In this study, the goal was to understand if and how TSLP-activated-DC were able to polarize naive CD4 T cells into Tfh-like cells capable of B cell help. TSLP-activated-DC are known to induce Th2 polarization [134] and Tfh cells have been described in Th2-dominated environments, such as allergy [196]. However, the prototypical Th2 cytokine IL-4 has been demonstrated to inhibit Tfh polarization [145]. In addition, OX40L has been shown as one key signal triggering IL-21 production by CD4 T cells [141]. And it has been well described that OX40L is highly expressed by TSLP-activated DC [135]. Thus, it was important to study if Tfh polarization was possible in this TSLP-DC context, which is relevant to atopic dermatitis.

For this study, we used an in vitro DC/naive CD4 T cell allogeneic coculture model. We sorted human primary CD11c⁺ DC from peripheral blood, we activated them for 24 hours with TSLP, and cocultured them afterwards with allogeneic human primary naive CD4 T cells. After 6 days of coculture, we analyzed all features of the polarized T cells: cytokines, cell surface molecules and transcription factors. We observed that TSLP-activated-DC induced the polarization of Tfh-like cells which displayed all Tfh features: expression of the surface markers CXCR5, ICOS, PD1, of the transcriptional repressor Bcl-6 and production of the cytokines IL-4, IL-21 and CXCL13.

To definitely assess if those cells were Tfh cells and possessed the Tfh main ability, which is helping B cells, we FACS sorted them and cocultured them with autologous memory B cells. After 14 days of coculture we measured in the culture supernatants the different immunoglobulins produced. We observed an induction of the immunoglobulin switch when CXCR5⁺PD1⁺ TSLP-DC-Tfh were cocultured with memory B cells. This confirmed that these cells were Tfh cells.

To understand if the T cell polarization conducted by TSLP-DC was going through OX40L, we used an OX40L blocking antibody to target it during TSLP-DC/T coculture. We observed that both naive polarization and memory Tfh activation by TSLP-DC were going through OX40L.

Finally, to evaluate the relevance of TSLP-DC-Tfh polarization in human pathology, we studied atopic dermatitis patient peripheral blood samples and compared it with healthy donor peripheral blood samples for the presence of Tfh cells. We were able to detect that the Tfh2 population, described by the production of IL-21 in combination with IL-4 [45], was more represented in AD patients compared to healthy donors. This suggested that TSLP and Tfh cells might have a link with AD pathology.

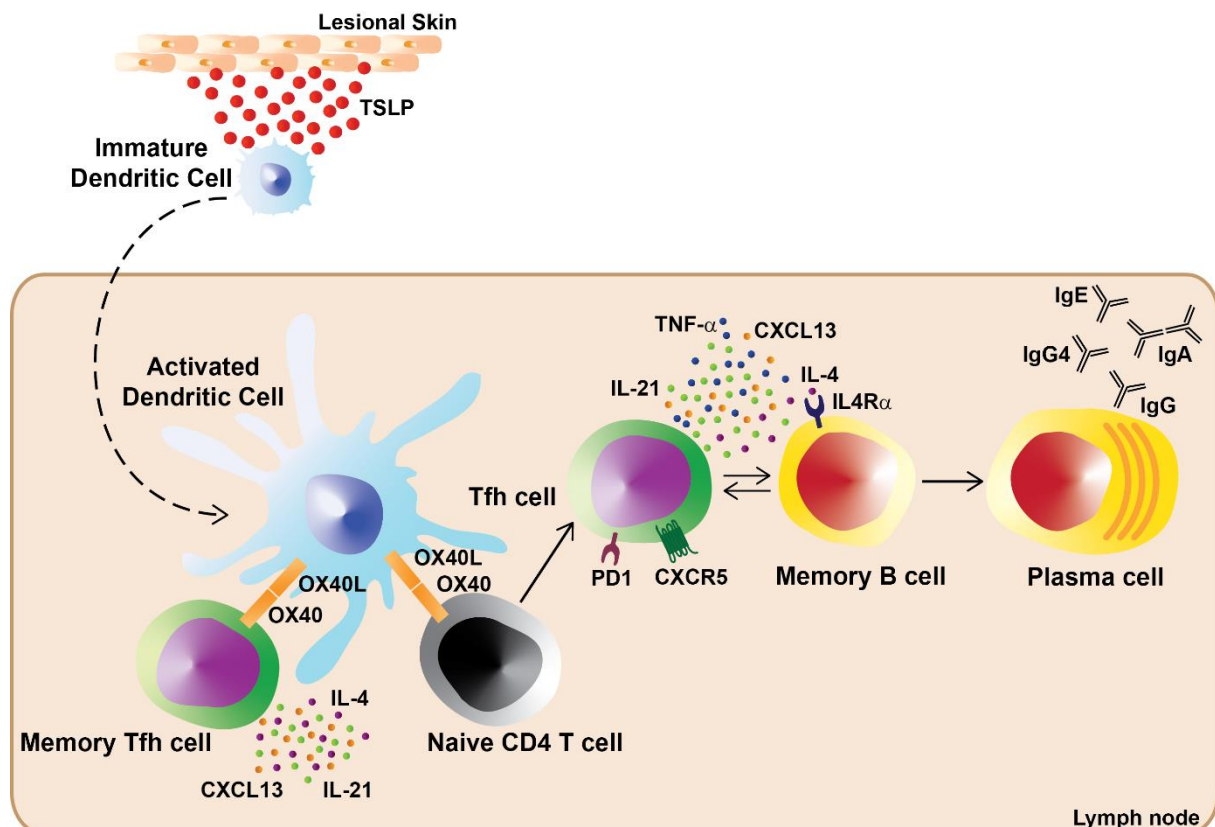


Figure 13: TSLP-activated DC induce human Tfh cell differentiation through OX40L

Schema recapitulating major findings of the publication

TSLP-activated DC were capable of polarizing naive CD4 T cells into Tfh cells expressing CXCR5 and PD1 and producing TNF- α , CXCL13, IL-21 and IL-4. Through their production of IL-4, TSLP-DC-induced Tfh cells were able to induce memory B cell differentiation into plasma cell, as well as isotype switch to IgA, IgG, IgG4 and IgE. TSLP-activated DC were also able to increase production of IL-4, IL-21 and CXCL13 from memory Tfh cells. Mechanistically, both naive CD4 T cell polarization and memory Tfh cells potentialization were going through OX40L expressed by TSLP-activated DC.

TSLP-activated dendritic cells induce human T follicular helper cell differentiation through OX40-ligand

Lucia Pattarini,^{1*} Coline Trichot,^{1*} Sofia Bogiatzi,² Maximilien Grandclaude,¹ Stephan Meller,³ Zela Keuylian,⁴ Melanie Durand,¹ Elisabetta Volpe,⁵ Stefania Madonna,⁶ Andrea Cavani,⁷ Andrea Chiricozzi,⁸ Marco Romanelli,⁸ Toshiyuki Hori,⁹ Alain Hovnanian,⁴ Bernhard Homey,³ and Vassili Soumelis¹

¹Institut Curie, PSL Research University, Institut National de la Santé et de la Recherche Médicale (INSERM), U932, F-75005, Paris, France

²Service de dermatologie et vénéréologie, CHUV University Hospital of Lausanne, 1011 Lausanne, Switzerland

³Department of Dermatology, Heinrich-Heine-University Medical Faculty, 40225 Düsseldorf, Germany

⁴INSERM, UMR 1163, Laboratory of Genetic Skin Diseases, Imagine Institute and Paris Descartes University, F-75015 Paris, France

⁵Laboratory of Neuroimmunology, Fondazione Santa Lucia, 00142 Rome, Italy

⁶Laboratory of Experimental Immunology, Istituto Dermatologico dell'Immacolata-Istituto di Ricovero e Cura a Carattere Scientifico, Fondazione Luigi Maria Monti, 00167 Rome, Italy

⁷National Institute of Health, Migration and Poverty, 00153 Rome, Italy

⁸Department of Dermatology, University of Pisa, 56100 Pisa, Italy

⁹College of Life Sciences, Ritsumeikan University, 1-1-1 Nojihigashi, Kusatsu, Shiga 525-8577, Japan

T follicular helper cells (Tfh) are important regulators of humoral responses. Human Tfh polarization pathways have been thus far associated with Th1 and Th17 polarization pathways. How human Tfh cells differentiate in Th2-skewed environments is unknown. We show that thymic stromal lymphopoietin (TSLP)-activated dendritic cells (DCs) promote human Tfh differentiation from naive CD4 T cells. We identified a novel population, distinct from Th2 cells, expressing IL-21 and TNF, suggestive of inflammatory cells. TSLP-induced T cells expressed CXCR5, CXCL13, ICOS, PD1, BCL6, BTLA, and SAP, among other Tfh markers. Functionally, TSLP-DC-polarized T cells induced IgE secretion by memory B cells, and this depended on IL-4R α . TSLP-activated DCs stimulated circulating memory Tfh cells to produce IL-21 and CXCL13. Mechanistically, TSLP-induced Tfh differentiation depended on OX40-ligand, but not on ICOS-ligand. Our results delineate a pathway of human Tfh differentiation in Th2 environments.

INTRODUCTION

Differentiation of naive CD4 T cells into specialized T helper (Th) lymphocyte subsets is crucial to immune responses (O'Shea and Paul, 2010). Among Th subsets, T follicular helper cells (Tfh) have been characterized for their role in B cell help (Tangye et al., 2013). Tfh cells express specific sets of secreted and surface molecules, comprising IL-21, CXCL13, ICOS, PD1, and CXCR5, which provide important signals for B cell survival and maturation in the germinal centers (GCs; Kim et al., 2004; Crotty, 2014).

The Th1-inducing cytokine IL-12 promotes human Tfh polarization (Trinchieri, 2003; Schmitt et al., 2009). Mutations in the *IL-12R β* downstream pathway affect IL-21 production and Tfh generation in humans (Ma et al., 2012). IL-27, another Th1-inducing factor, can induce human Tfh polarization (Gringhuis et al., 2014). The cytokine cocktail

used to polarize *in vitro* human Th17 cells, and in particular TGF- β , can promote Tfh development as well (Schmitt et al., 2014). Altogether, these data led to the hypothesis that in humans Tfh polarization is preferentially associated with Th1 and Th17 polarizing environments (Ueno et al., 2015).

Tfh cells have been described in Th2-dominated environments, such as allergy (Kemeny, 2012), and in the absence of Th1 and Th17 polarization (Glatman Zaretsky et al., 2009; Liang et al., 2011; Tangye et al., 2013). However, IL-4, the master Th2 cytokine, inhibits human Tfh differentiation (Schmitt et al., 2014). This raises the important question of how Tfh differentiation can occur in Th2-dominated environments in humans.

We hypothesized that the epithelial-derived cytokine thymic stromal lymphopoietin (TSLP) might play a role in Tfh cell polarization. Independent evidences make TSLP a strong candidate for Tfh polarization. First, TSLP is highly expressed in different Th2-dominated environments, such as airways of asthmatic patients, mucosal tissues in helminth

*L. Pattarini and C. Trichot contributed equally to this paper.

Correspondence to Vassili Soumelis: vassili.soumelis@curie.fr; or Lucia Pattarini: lucia.pattarini@curie.fr

Abbreviations used: AD, atopic dermatitis; CBA, cytometric bead array; CD40L, CD40 ligand; GC, germinal center; ICOS, Inducible costimulator; MFI, mean fluorescence intensity; NS, Netherton syndrome; OX40L, OX40 ligand; pDC, plasmacytoid DC; Tfh, T follicular helper; Th, T helper; TSLP, thymic stromal lymphopoietin.

© 2017 Pattarini et al. This article is distributed under the terms of an Attribution-Noncommercial-Share Alike-No Mirror Sites license for the first six months after the publication date (see <http://www.rupress.org/terms/>). After six months it is available under a Creative Commons License (Attribution-Noncommercial-Share Alike 4.0 International license, as described at <https://creativecommons.org/licenses/by-nc-sa/4.0/>).



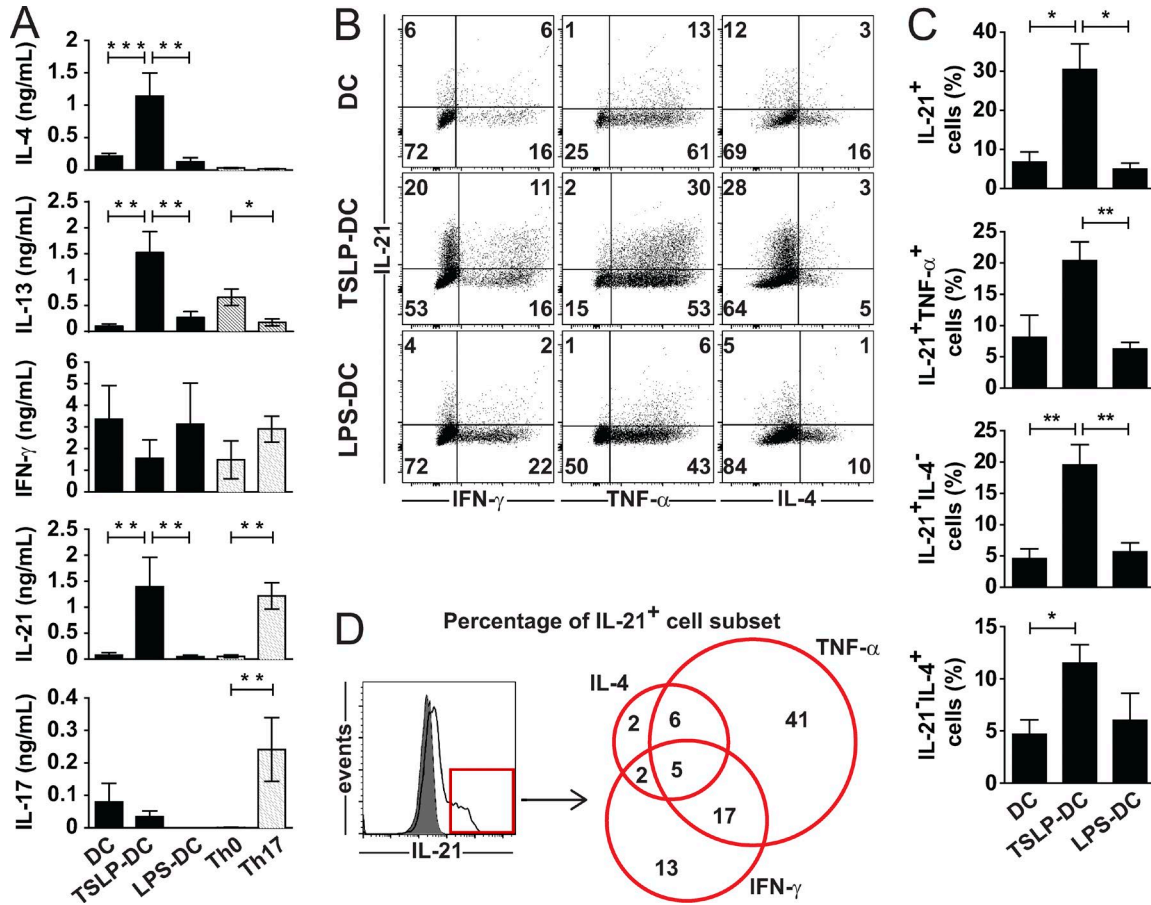


Figure 1. TSLP-activated DCs polarize naive CD4 T cells into IL-21-secreting cells. Untreated DCs, treated with TSLP (TSLP-DC) or LPS (LPS-DC) were cultured with naive CD4 T cells for 6 d. (A) CBA (IL-4, IL-13, IFN- γ , and IL-17A) and ELISA (IL-21) assays after 24 h of restimulation with anti CD3/CD28 beads. Th0, naive T cells cultured for 6 d with anti-CD3/CD28; Th17, Th0 plus Th17 polarizing cytokines (IL1 β , IL-23, TGF- β , and IL-6). Data are mean \pm SEM from nine independent experiments. (B) Intracellular FACS staining for IL-21, IFN- γ , TNF, and IL-4 for one representative donor. Gate is on activated DAPI⁻ CD4 T cells. (C) Quantification of data as in B. Data are mean \pm SEM from six independent experiments. (D) Distribution of IL-21⁺ cells (red square) polarized by TSLP-DC coproducing IL-4, TNF, and IFN- γ . Filled histogram, isotype control; black line, IL-21 staining. Mean of six independent experiments. Single IL-21 producers (16%) are not plotted. *, P < 0.05; **, P < 0.01; ***, P < 0.001, by Wilcoxon or Student's *t* test.

infections, and AD lesional skin (Soumelis et al., 2002; Ying et al., 2005; Ziegler and Artis, 2010). Both AD and allergic patients present deregulated IgE production (Gould et al., 2003). Second, TSLP is expressed in human tonsils, where GC reactions occur (Liu et al., 2007). Third, TSLP contributes to Th2 polarization through DC activation, and induces an inflammatory Th2 response (Soumelis et al., 2002). Fourth, TSLP-activated DCs express OX40 ligand (OX40L), which has been linked to Tfh polarization (Jacquemin et al., 2015).

In this work, we establish a novel Tfh differentiation pathway driven by TSLP. We dissect an axis linking TSLP, DCs, T cells, B cells, and IgE production.

RESULTS

TSLP-activated DCs polarize naive CD4 T cells into IL-21-secreting cells

We used primary DCs from human blood activated with TSLP (TSLP-DC) to differentiate naive CD4 cells into

Th cells in an allogeneic system. As expected, after 6 d of co-culture, TSLP-DC induced Th cells that secreted IL-4 and IL-13, but low levels of IFN- γ , which are features of Th2 polarization (Fig. 1 A; Soumelis et al., 2002; Ziegler and Artis, 2010). To separate the effect of TSLP-induced activation from an intrinsic property of human blood DCs, we used nonactivated DCs as a negative control. As an additional control, we used LPS-activated DCs (LPS-DC), which induced IFN- γ but low IL-4 and IL-13 secretion from T cells (Fig. 1 A), in accordance with Th1 polarization.

Surprisingly, TSLP-DC polarized naive CD4 T cells to produce high amounts of IL-21 (Fig. 1 A). The amount of IL-21 induced by TSLP-DC polarization was similar to that of in vitro polarized Th17 cells. We recently showed that TSLP synergizes with CD40L in DCs to promote the expression of the Th17-polarizing cytokine IL-23 (Volpe et al., 2014). TSLP-DC induced low and inconsistent IL-17A secretion by CD4 T cells in comparison with in vitro-polarized Th17,

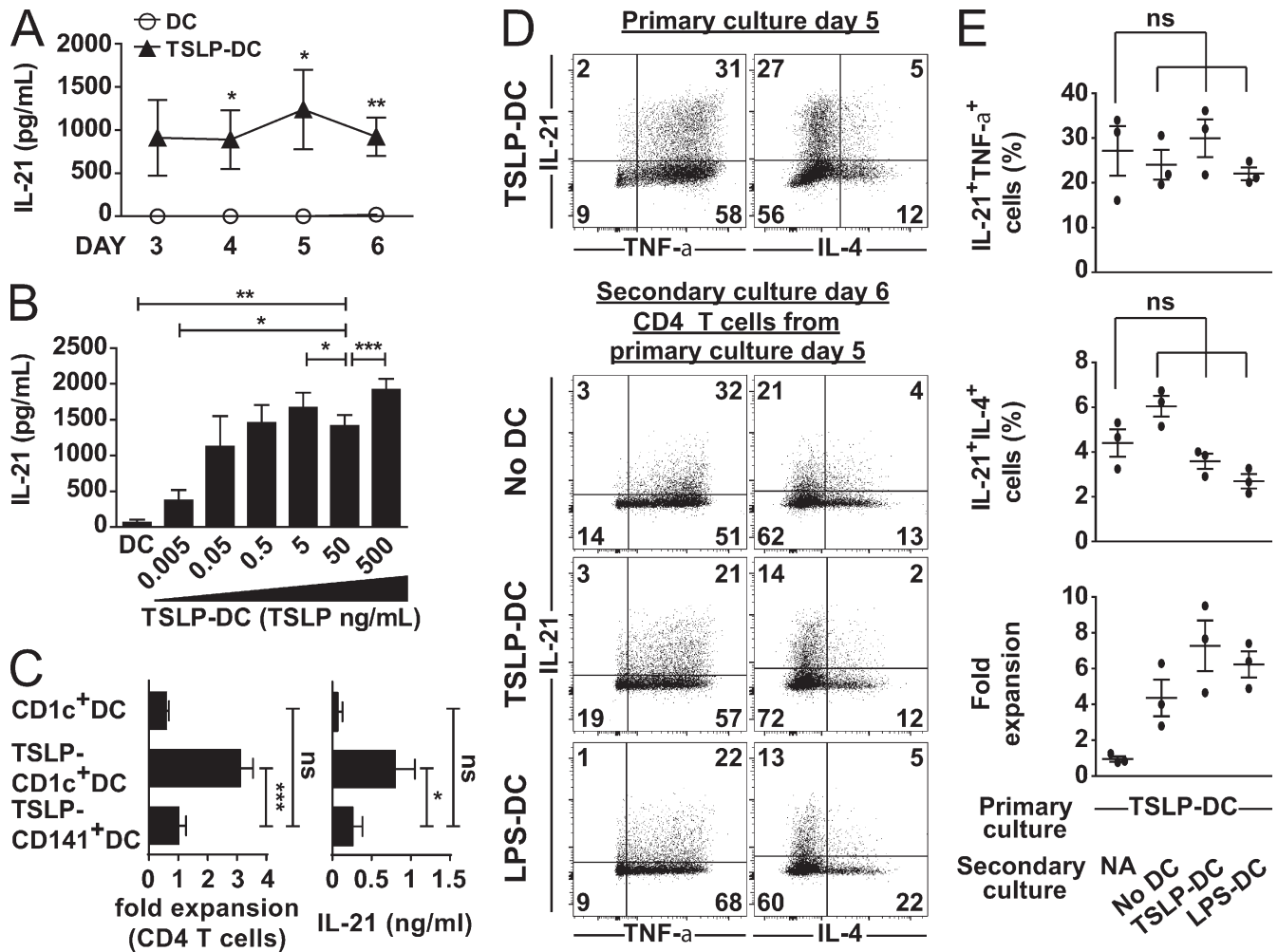


Figure 2. IL-21 production by TSLP-DC-polarized CD4 T cells is stable. (A) DCs were activated with TSLP (50 ng/ml, TSLP-DC, filled triangles) or in control medium (DC, circles). After 24 h, DCs were co-cultured with naive CD4 T cells and stimulated for 24 h with anti-CD3/CD28 beads. IL-21 concentration in the supernatants from seven independent experiments. (B) Quantification of IL-21 secretion by CD4 T cells polarized for 6 d with DCs, previously activated for 24 h with increasing doses of TSLP. SEM for four independent experiments; *, $P < 0.05$; **, $P < 0.01$; ***, $P < 0.001$, paired Student's t test. (C) CD4 T cell fold expansion and IL-21 secretion from co-cultures with untreated CD1c⁺, TSLP-activated CD1c⁺ and TSLP-activated CD141⁺ DCs. SEM for 12 independent experiments; *, $P < 0.05$; ***, $P < 0.001$, paired Student's t test. (D) Intracellular FACS staining of IL-21, TNF, and IL-4 by TSLP-DC-activated CD4 T cells at the indicated days of primary and secondary culture from a representative CD4 T cell donor. In primary culture CD4 T cells were activated by TSLP-DC. In secondary culture, cells from day 5 of primary culture were cultured for 6 d in medium alone (No DC), with TSLP-DC or LPS-DC. (E) Percentage of IL-21⁺TNF- α ⁺ and IL-21⁺IL-4⁺ cells (among activated cells) and fold expansion in primary and secondary culture as indicated, in three independent experiments. NA, not applicable.

excluding a strong Th17 polarization by TSLP-DC. To check whether TSLP could act directly on CD4 T cell, in addition to DCs, we analyzed by FACS the expression of TSLP receptor (R) chains (TSLPR and IL-7R β) in naive CD4 T cells and DCs. DCs expressed high levels of both chains, whereas *ex vivo* or activated (5 d of anti CD3/CD28 beads, Th0 cells) naive CD4 T cells expressed IL7R α but inconsistent levels of TSLPR (Fig. S1 A). We cultured sorted naive CD4 T cells with anti-CD3/CD28 beads and TSLP, in the absence of DCs. After 6 d of culture, we did not detect any induction of IL-21 by Th0 cells cultured either with or without TSLP. As

a control, we detected IL-21 production by *in vitro* polarized Th17 (Fig. S1 B). Therefore, we concluded that TSLP was inducing IL-21 production by CD4 T cells through DCs.

Next, we investigated whether IL-21 was coproduced with other cytokines at the single T cell level. We performed intracellular staining for IL-21, in combination with IFN- γ , IL-4, and TNF as features of inflammatory Th2 differentiation induced by TSLP (Ito et al., 2005). At day 6 of co-culture, ~30% of the CD4 T cells activated by TSLP-DC were positive for IL-21, indicating a strong IL-21 polarization. IL-21 was mainly co-produced with TNF (20% of activated CD4

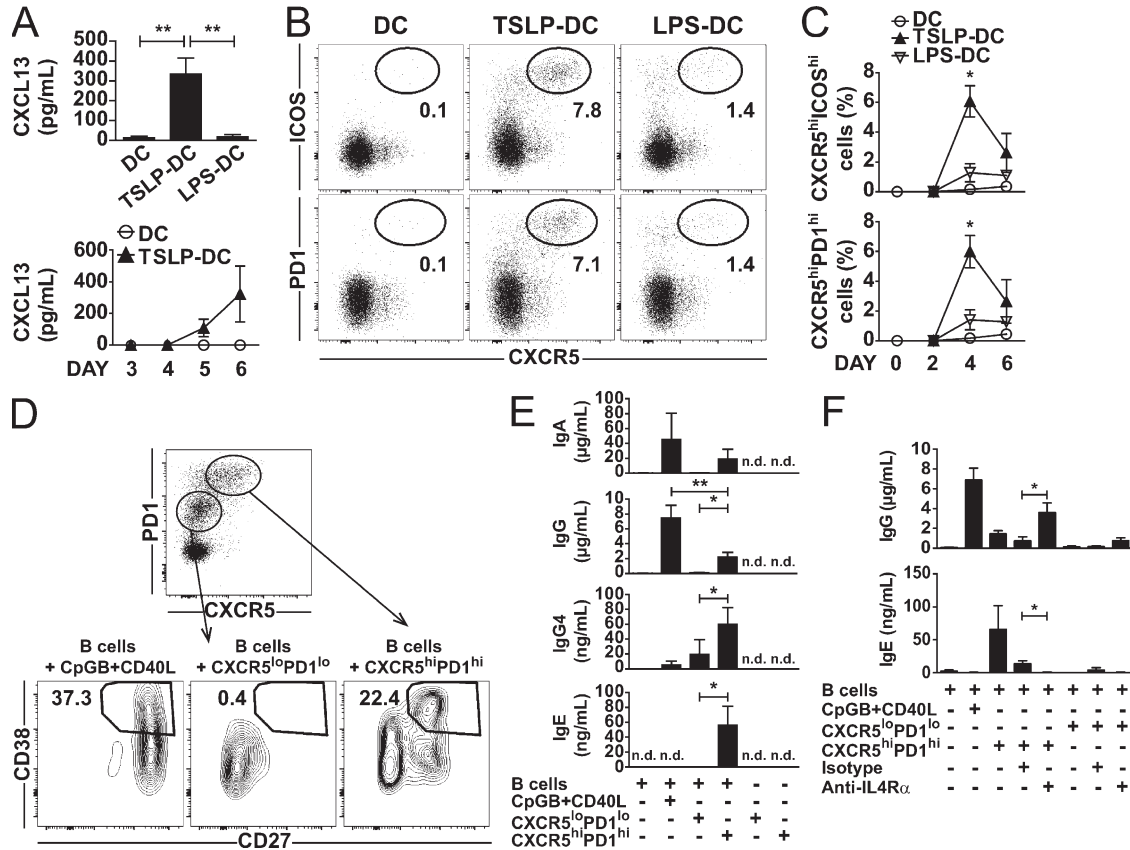


Figure 3. T cells polarized by TSLP-DC possess key features of human Tfh cells. (A) ELISA for CXCL13 production by CD4 T cells differentiated for 6 d in co-culture with DCs, TSLP-DC, or LPS-DC. Cytokines secretion was measured after an additional 24 h of anti-CD3/CD28 bead stimulation. Data are mean \pm SEM from 20 independent experiments. **, $P < 0.01$, paired Student's t test. For the kinetic of CXCL13 expression, CD4 T cells were restimulated for 24 h with anti-CD3/CD28 beads after 3, 4, 5, or 6 d of co-culture with DCs (circles) or TSLP-DC (triangles). SEM for seven independent experiments. (B) FACS staining for ICOS, PD1, and CXCR5 in CD4 T cells after 4 d of co-culture with DCs. CXCR5^{hi}/ICOS^{hi} and CXCR5^{hi}/PD1^{hi} cells within CD4 T DAPI⁻ cells from a representative donor are shown. (C) Quantification of cell populations as indicated in B in naive CD4 T cells after 0, 2, 4, or 6 d of co-culture with DCs (circles), TSLP-DC (filled triangles), or LPS-DC (open triangles). SEM from six independent experiments. (D) CXCR5^{hi}/PD1^{hi} and CXCR5^{lo}/PD1^{lo} CD4 T cells polarized 4 d by TSLP-DC were sorted (top), and co-cultured with autologous memory B cells for 14 d. CD38 and CD27 were measured by FACS on B cells (DAPI⁻/CD3⁻/CD4⁻/CD19⁺). One representative plot is shown. (E) IgA, IgG, IgG4, and IgE were quantified in the supernatants of co-cultures, as in D, in the indicated conditions. Mean \pm SEM for five donors. n.d., not detected. (F) Quantification of IgG and IgE in the supernatants of memory B cells co-cultured as in D, plus IL4R- α blocking or isotype control antibodies. SEM from five independent experiments are plotted. *, $P < 0.05$; **, $P < 0.01$, paired Student's t test.

cells). We identified IL-21⁺IL-4⁻ (20%) and IL-21⁻IL-4⁺ (12%) populations, suggesting that distinct Th subsets arise in the presence of TSLP-DC (Fig. 1, B and C). To better characterize the cytokine expression pattern of IL-21⁺ CD4 T cells after 6 d of co-culture with TSLP-DC, we calculated the percentage of cells coexpressing different combinations of cytokines. Among the IL-21⁺ cells, we detected a small population (5%) of Th cells coexpressing TNF, IL-4, and IFN- γ (Fig. 1 D). The majority (69%) of Th cells expressed IL-21 in combination with TNF (Fig. 1 D).

Next, we examined IL-21 induction by TSLP-DC in CD4 T cells. We detected IL-21 secretion after 3 d of DC/T cell co-culture (Fig. 2 A), using as low as 5 pg/ml TSLP to activate DCs (Fig. 2 B). We separately activated the CD1c⁺ and CD141⁺ DC subsets with TSLP. After co-culture with

naive CD4 T cells, we observed that TSLP CD1c⁺ DCs induced higher CD4 T cell expansion and IL-21 production, as compared with CD141⁺ DCs. We did not measure any significant difference between nontreated CD1c⁺ DCs and TSLP-CD141⁺ DCs with regards to IL-21 production and CD4 T cell expansion (Fig. 2 C).

Next, we investigated the stability of IL-21, TNF, and IL-4 expression by TSLP-DC-activated CD4 T cells. We compared the intracellular expression of these cytokines by CD4 T cells cultured for 5 d in the presence of TSLP-DC (Fig. 2 D, primary culture), with the same CD4 T cells recultured for additional 6 d in medium without DCs (No DC), with TSLP-DC or LPS-DC (Fig. 2 D, secondary culture). The percentages of IL-21⁺TNF⁺ and IL-21⁺IL-4⁺ cells were comparable between the primary and secondary culture (Fig. 2 E), suggesting that the

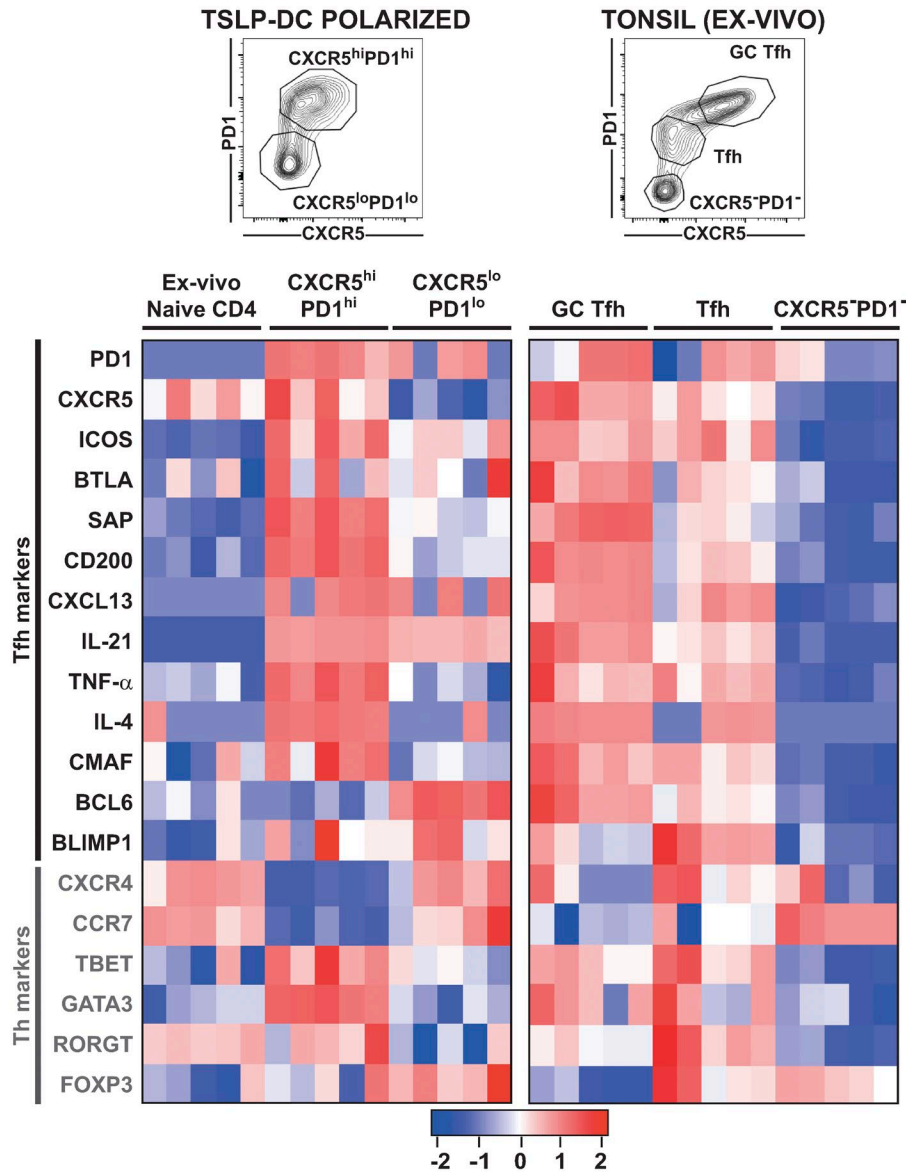


Figure 4. T cells polarized by TSLP-DC show an expression pattern similar to tonsillar Tfh cells. Heat map showing mRNA quantification of Tfh and Th markers in naive CD4 T cells, TSLP-DC-polarized CD4 T cells, and human tonsillar CD4 populations. CD4 T cells differentiated for 4 d with TSLP-DC were sorted as indicated (top left). Three populations of tonsillar CD4 cells were sorted (top right): CXCR5^{hi}/PD1^{hi} (GC Tfh), CXCR5^{int}/PD1^{int} (Tfh), and CXCR5⁻/PD1⁻. mRNA levels normalized on the B2M and RPL34 housekeeping genes and center reduced are displayed on the heat map from five independent donors and two independent experiments.

expression of these cytokines was stable. Additionally, by counting live cells we found that CD4 T cells activated by TSLP-DC expanded, even in the absence of further DC stimulation (Fig. 2 E, bottom). These two results suggested an overall expansion of the IL-21⁺TNF⁺ and IL-21⁺IL-4⁺ cell populations.

Thus, TSLP-DC promoted the generation of a stable, novel Th subset producing IL-21 and TNF, in combination or not with the Th2 cytokine IL-4.

Th cells polarized by TSLP-DC possess features of human Tfh cells

Because IL-21 is highly produced by Tfh cells (Schmitt et al., 2014), we asked whether TSLP-DC-polarized T helper cells had Tfh markers.

We measured the secretion of CXCL13, a chemokine produced by Tfh but not by other Th cell subsets (Kim et al.,

2004), after 6 d of co-culture followed by 24 h of anti-CD3/CD28 stimulation. TSLP-DC, but not unstimulated DCs or LPS-DC, induced the secretion of CXCL13 by CD4 T cells (Fig. 3 A, top), suggesting Tfh polarization. CXCL13 secretion was detectable from day 5 of co-culture (Fig. 3 A, bottom).

A feature of human Tfh cells is the expression of high levels of the CXCL13 receptor CXCR5, in combination with high levels of ICOS and PD1 (Bryant et al., 2007; Crotty, 2014). We identified by FACS CXCR5^{high}ICOS^{hi} and CXCR5^{hi}PD1^{hi} CD4 T cells after 4 d of co-culture with TSLP-DC (Fig. 3 B). TSLP-DC increased the percentage of CXCR5^{hi}ICOS^{hi} and CXCR5^{hi}PD1^{hi} populations at day 4 as compared with day 2 and day 6 of co-culture, and in comparison to nonactivated DC and LPS-DC (Fig. 3 C). The use of naive T cells (CD4⁺CD25⁻CD45RA⁺CD45RO⁻) sorted to 99% purity, without detectable CXCR5⁺ cells (Fig. 3 C),

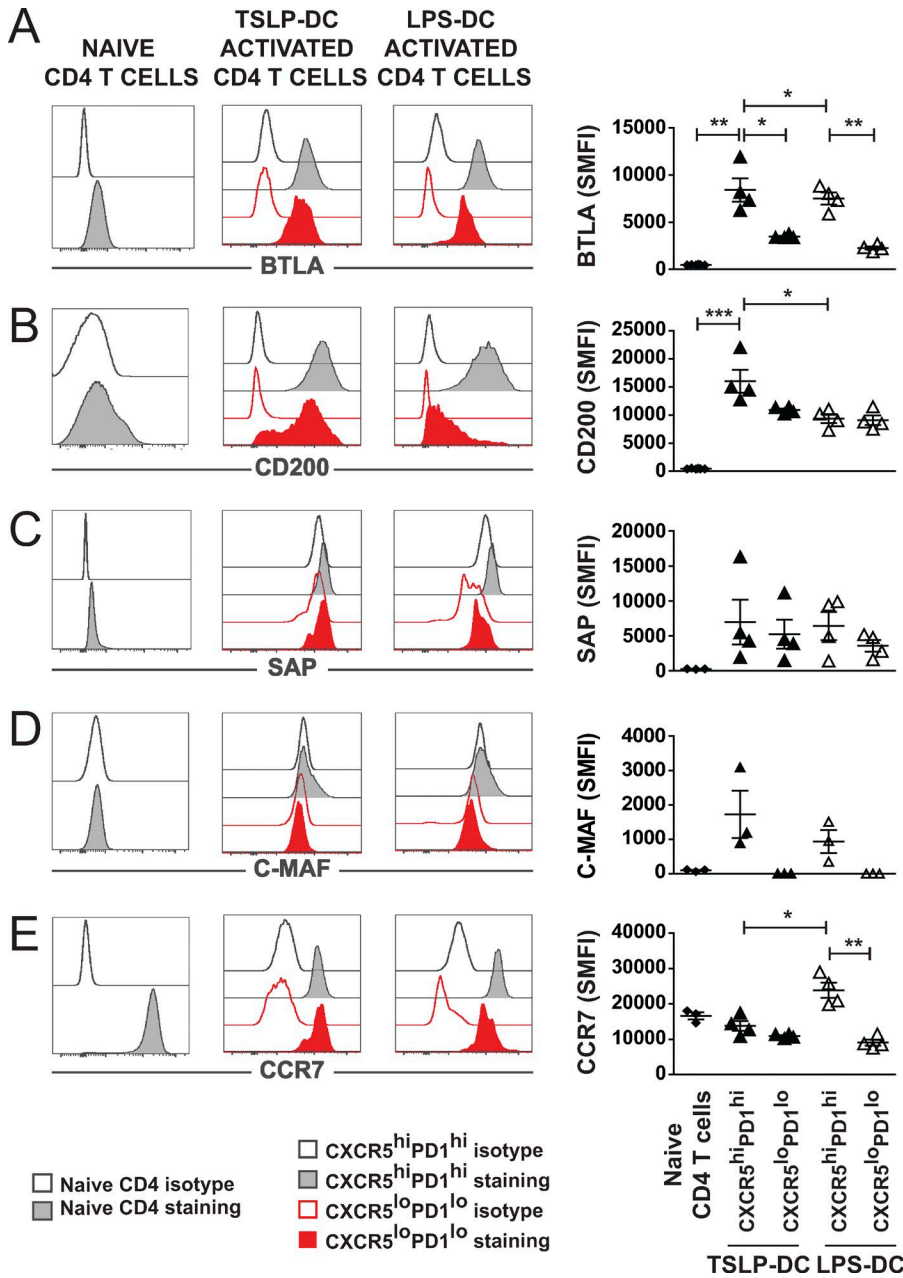


Figure 5. TSLP-induced cells express Tfh markers. FACS analysis of BTLA (A), CD200 (B), SAP (C), C-MAF (D), and CCR7 (E) in naive CD4 T cells and in TSLP-DC and LPS-DC activated cells at day 4 of co-culture with naive CD4 T cells. Isotype and specific staining for naive CD4 T cells and CXCR5^{hi}/PD1^{hi} and CXCR5^{lo}/PD1^{lo} population induced by TSLP-DC and LPS-DC is shown in histogram plot for one representative experiment. Quantification of MFI is plotted for three or four independent experiments. Naive CD4 T cells, filled diamond; TSLP-DC co-culture, filled triangles; LPS-DC co-culture, triangles. *, P < 0.05; **, P < 0.01; ***, P < 0.001, paired Student's t test.

excluded that these cells originated from the rare blood memory Tfh population, characterized by CXCR5 expression (Morita et al., 2011).

One key function of Tfh cells is their ability to help B cells to secrete class-switched Igs (Crotty, 2014). To test whether the CXCR5^{hi}PD1^{hi} cells induced by TSLP-DC were able to help B cells, we sorted CXCR5^{hi}PD1^{hi} and CXCR5^{low(lo)}PD1^{lo} cells after 4 d of co-culture with TSLP-DC, and co-cultured them with autologous memory B cells (Fig. 3 D). We detected CD19⁺CD38^{hi}CD27⁺ B cells after 14 d of co-culture with CXCR5^{hi}PD1^{hi}, but not with CXCR5^{lo}PD1^{lo} T cells polarized by TSLP-DC, similarly to the positive control of memory B cells activated by CD40-Ligand (CD40L) and CpG oligode-

oxynucleotides type B (CpG-B; Fig. 3 D). At the same time point, we measured secretion of class switched Igs in the supernatants. Memory B cells activated with CD40L and CpG-B secreted IgA and IgG, as expected (Bernasconi et al., 2002). TSLP-DC polarized CXCR5^{hi}PD1^{hi} cells specifically induced IgG4 and IgE secretion by memory B cells. In comparison, IgA, IgG, and IgE secretion in the presence of CXCR5^{lo}PD1^{lo} cells was low and inconsistent (Fig. 3 E). We measured lower amounts of IgA and IgG, induced by CXCR5^{hi}/PD1^{hi} cells as compared with memory B cells activated with CD40L and CpG-B (Fig. 3 E), in accordance with selective induction of IgE and IgG4.

Next, we investigated the mechanism by which TSLP-DC-induced CXCR5^{hi}PD1^{hi} cells promoted IgE se-

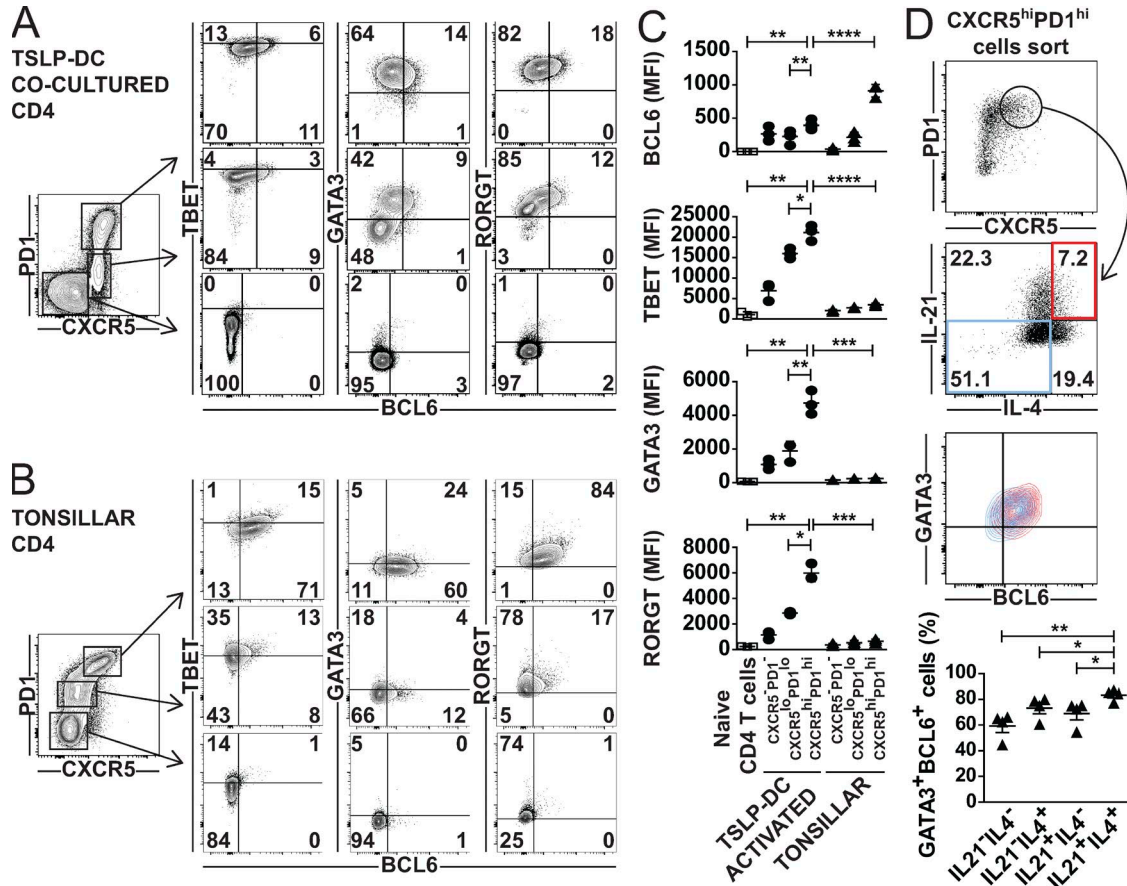


Figure 6. CD4 T cells activated by TSLP-DC coexpress BCL6 and GATA3. (A) FACS staining for BCL6, TBET, GATA3, and RORGT in naive CD4 T cells co-cultured with TSLP-DC for 4 d. (B) Tonsillar CD4 cells analyzed as in A. Gates were set using fluorescence minus one plus isotype, and percentage of cells in each quadrant are shown for one representative donor. (C) Quantification of BCL6, TBET, GATA3, and RORGT MFI in naive CD4 T cells and from data shown in A and B from three or five independent experiments. Empty squares, naive CD4 T cells; dots, TSLP-DC activated CD4; triangles, tonsillar CD4⁺ T cells. *, $P < 0.05$; **, $P < 0.01$; ***, $P < 0.001$; ****, $P < 0.0001$, unpaired Student's *t* test. (D) CD4 T cells sorted as CXCR5^{hi}PD1^{hi} at day 4 of co-culture with TSLP-DC were analyzed for intracellular expression of IL-4, IL-21, GATA3, and BCL6. One representative experiment is shown, and quantification of % of GATA3⁺/BCL6⁺ cells is plotted for four independent experiments. Mean \pm SEM is plotted. *, $P < 0.05$; **, $P < 0.01$, paired Student's *t* test.

cretion by memory B cells. IL-4 mediates IgE production by human B cells (Pène et al., 1988). TSLP-DC-polarized T cells secreted IL-4 (Fig. 1 A). We functionally blocked IL-4 receptor α (IL-4R β) in the co-culture of TSLP-DC-polarized T cells and memory B cells. After targeting of IL-4R β by using a functional blocking antibody, we were unable to detect IgE secretion by memory B cells in the presence of TSLP-DC-polarized CXCR5^{hi}PD1^{hi} cells. In parallel, we detected an increase in IgG production (Fig. 3 F). As a control, we checked that IL-4R β blocking antibody did not decrease B cell viability. Our data are in accordance with previous data showing that IL-4-reduced IgG production by human B cells (Nies et al., 2002).

Altogether, these results show that TSLP-DC induced the polarization of cells expressing Tfh markers such as CXCR5, PD1, and ICOS, and that these cells shared functional features of human Tfh2, comprising the ability to stimulate IgE secretion by B cells. Mechanistically, we showed that IgE induction by TSLP-DC-polarized Tfh cells depended on IL-4R β .

T cells polarized by TSLP-DC show molecular markers similar to tonsillar Tfh

To confirm that TSLP-DC-polarized T cells presented features of Tfh cells, we selected a set of Tfh markers on the basis of transcriptomic analysis of human Tfh cells (Kim et al., 2004). We quantified the expression of these Tfh markers by qPCR on sorted CXCR5^{hi}PD1^{hi} and CXCR5^{lo}PD1^{lo} CD4 T cell populations identified among activated T cells after 4 d of co-culture with TSLP-DC (Fig. 4, top left). As a comparison, we analyzed sorted naive CD4 T cells. CXCR5^{hi}PD1^{hi} cells expressed higher levels of Tfh markers at the mRNA level (BTLA, CXCR5, CXCL13, ICOS, PD1, SAP, CD200, and C-MAF) as compared with CXCR5^{lo}PD1^{lo} cells (Fig. 4 and Fig. S2). Additionally, CXCR5^{hi}/PD1^{hi} cells polarized by TSLP-DC expressed higher mRNA levels of the cytokines IL-21, IL-4, and TNF, as compared with CXCR5^{lo}/PD1^{lo} cells (Fig. 4). As expected, naive CD4 T cells did not express significant levels of Tfh markers.

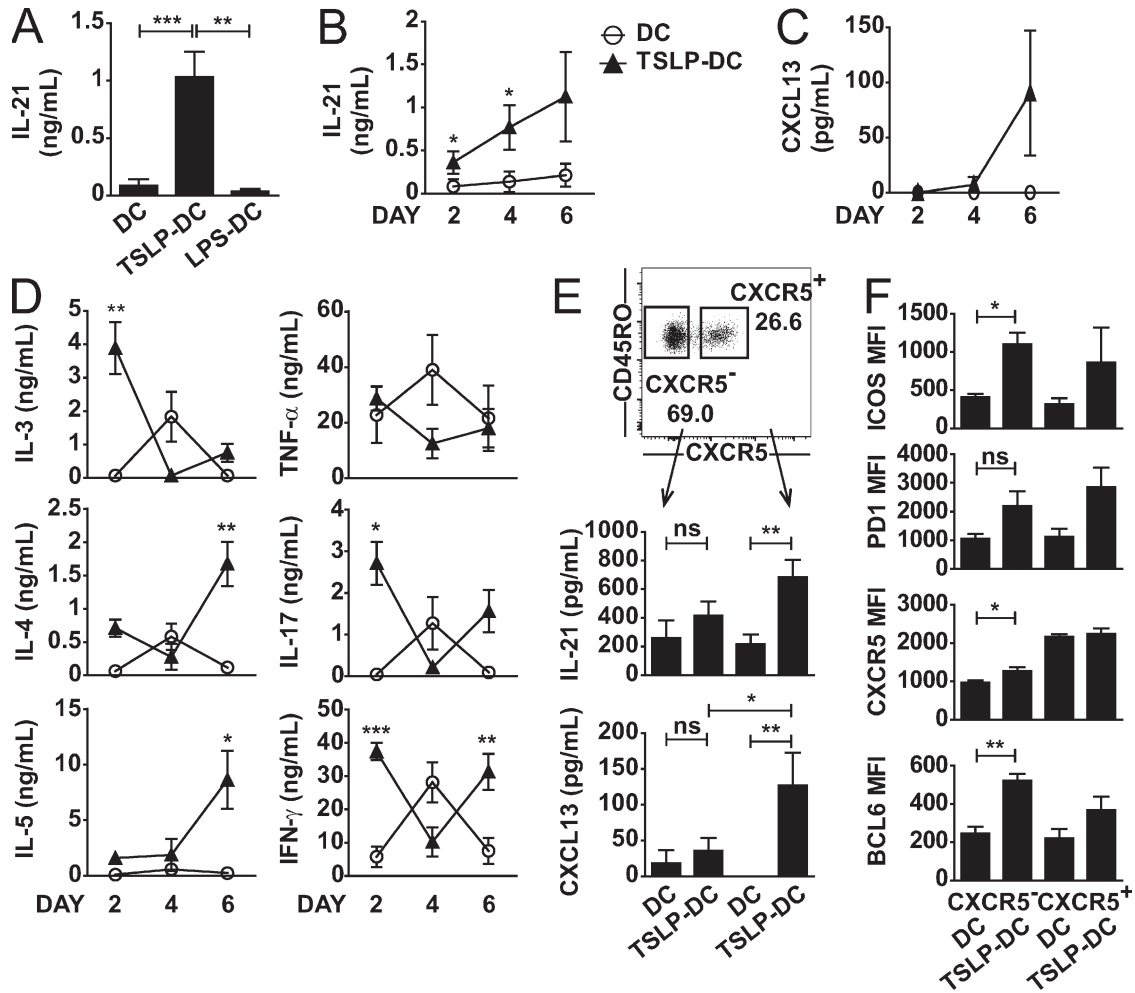


Figure 7. Memory CD4 T cells express Tfh factors after activation by TSLP-DC. CD4 memory T cells were cultured with DCs, TSLP-DC, or LPS-DC, and cytokines were measured at the indicated days after 24 h of restimulation with anti-CD3/CD28 beads. ELISA assay for IL-21 at day 6 of culture in A and at day 2, 4, and 6 in B. Mean \pm SEM for 13 and 5 donors is shown, from four and two independent experiments, respectively. ELISA assay for CXCL13 in C and CBA assay for Th cytokines in D in the same experimental settings as in B. (E and F) Memory CD4 T cells were separated into CXCR5⁺ and CXCR5⁻ cells by FACS sorting, and cultured with DCs or TSLP-DC for 6 d. IL-21 and CXCL13 quantification after 24 h of anti-CD3/CD28 stimulation is shown as mean \pm SEM from nine independent experiments. FACS staining for ICOS, PD1, and CXCR5 at day 6 of co-culture. BCL6 was quantified on the CXCR5^{hi}/PD1^{hi} population. The geometric MFI is plotted for three or two independent experiments. *, P < 0.05; **, P < 0.01; ***, P < 0.001, paired Student's *t* test.

Notably, the expression pattern of Tfh markers paralleled the one of our positive controls, represented by sorted tonsillar GC Tfh (CD4⁺CD45RO⁺CXCR5^{hi}PD1^{hi}) and Tfh (CD4⁺CD45RO⁺CXCR5^{lo}PD1^{lo}), and differed from non-Tfh CD4 (CD4⁺CD45RO⁺CXCR5⁻PD1⁻; Fig. 4). TSLP-induced CXCR5^{hi}/PD1^{hi} cells down-regulated the lymph node homing receptors CXCR4 and CCR7 at the mRNA level, suggesting peripheral effector functions. As a control naive CD4 T cells expressed CCR7 and CXCR4 mRNA.

Additionally, we measured the expression of BCL6, BLIMP1, TBET, GATA3, RORGT, and FOXP3, transcription factors orchestrating Th subset differentiation. The mRNA expression of BCL6, a transcriptional repressor important for Tfh polarization, was lower in CXCR5^{hi}PD1^{hi} than

in CXCR5^{lo}PD1^{lo} cells polarized by TSLP-DC (Fig. 4). CXCR5^{hi}PD1^{hi} cells induced by TSLP-DC expressed higher levels of TBET, GATA3, and RORGT when compared with CXCR5^{lo}PD1^{lo} cells, similarly to tonsillar GC Tfh cells. Additionally, the CXCR5^{hi}PD1^{hi} cells induced by TSLP-DC did not express FOXP3, indicating that they were distinct from regulatory Tfh.

We measured by FACS analysis the expression of BTLA, CD200, SAP, and C-MAF proteins in naive CD4 T cells, as well as in CXCR5^{hi}PD1^{hi} and CXCR5^{lo}PD1^{lo} cells, after 4 d of co-culture in the presence of TSLP-DC and LPS-DC as a comparison (Fig. 5, A–D). CXCR5^{hi}PD1^{hi} cells induced by TSLP-DC expressed BTLA, CD200, SAP, and C-MAF at the protein level, thus validating our mRNA analysis. At the

protein level, we did not measure any significant difference in CCR7 protein levels between TSLP-induced CXCR5^{hi}PD1^{hi} and CXCR5^{lo}PD1^{lo}. However, CCR7 protein expression was significantly higher in LPS-DC-induced CXCR5^{hi}PD1^{hi} cells as compared with TSLP-DC-induced (Fig. 5 E). As a negative control, naive CD4 T cells did not express BTLA, CD200, SAP, or C-MAF protein. As expected, naive CD4 T cells expressed surface CCR7 at similar levels that TSLP-induced CXCR5^{hi}PD1^{hi} and CXCR5^{lo}PD1^{lo} cells.

Overall, CXCR5^{hi}PD1^{hi} cells polarized by TSLP-DC express markers characteristic of human tonsillar Tfh, suggesting that TSLP-DC are able to induce Tfh polarization from naive CD4 T cells.

CXCR5^{hi}PD1^{hi} cells polarized by TSLP-DC coexpressed BCL6 and GATA3

Our data showing the expression of BCL6, TBET, GATA3, and RORGT by TSLP-DC activated CD4 T cells are relevant to the coexistence of Th and Tfh polarization programs in a single cell. Therefore, we investigated their coexpression at the single-cell level.

We measured by intracellular FACS staining the expression of BCL6, TBET, GATA3, and RORGT in CD4 T cells co-cultured for 4 d with TSLP-DC. We included, as a negative control, a CXCR5⁻PD1⁻ population corresponding to cells that were co-cultured with TSLP-DC but did not display an activated profile (Fig. 6 A, bottom). We compared the expression of the same transcription factors in human tonsillar CD4 populations, identified by different expression levels of CXCR5 and PD1 (Fig. 6 B). TSLP-induced CXCR5^{hi}PD1^{hi} cells expressed significantly higher levels of BCL6, TBET, GATA3, and RORGT protein when compared with CXCR5^{lo}PD1^{lo} cells and naive CD4 T cells (Fig. 6, A and C). CXCR5^{hi}PD1^{hi} tonsillar cells expressed higher levels of BCL6, but lower levels of TBET, GATA3, and RORGT, as compared with TSLP-induced CXCR5^{hi}PD1^{hi} cells. These data validated that TSLP-DC-activated T cells expressed higher levels of lineage defining transcription factors, as suggested by our mRNA analysis of Fig. 4. CXCR5^{hi}PD1^{hi} cells, induced by TSLP-DC, expressed higher levels of BCL6 protein (Fig. 6 A) but lower levels of BCL6 mRNA (Fig. 4) as compared with CXCR5^{lo}/PD1^{lo} cells. One interpretation of this discrepancy is that there are some differences at the posttranscriptional level between CXCR5^{hi}/PD1^{hi} and CXCR5^{lo}/PD1^{lo} cells. Discrepancies between BCL6 mRNA and protein levels have been already reported (Kroenke et al., 2012).

Next, we investigated whether the IL-4⁺IL-21⁺ cells we characterized (Fig. 1) coexpressed BCL6 and GATA3. We FACS sorted CXCR5^{hi}PD1^{hi} cells and analyzed the expression of IL-4, IL-21, BCL6, and GATA3 by intracellular FACS staining. The majority (80%) of IL-4⁺IL-21⁺ cells coexpressed BCL6 and GATA3 proteins, as shown by a representative donor and quantification in Fig. 6 D. BCL6/GATA3 double-positive population was significantly enriched in IL-4⁺IL-21⁺ cells compared with single cytokine producers

or double-negative cells. This showed that TSLP-DC-activated CXCR5^{hi}PD1^{hi}IL-21⁺IL-4⁺ cells preferentially coexpressed BCL6 and GATA3.

Overall, these data showed that TSLP-DC-induced the expression of BCL6 in combination with Th lineage defining transcription factors, in particular GATA3, at the protein level.

IL-21 and CXCL13 secretion from memory CD4 T cells are increased by TSLP-DC

TSLP-DC are potent inducers of memory Th2 responses (Wang et al., 2006). To establish whether TSLP-DC stimulated IL-21 and CXCL13 secretion by memory CD4 T cells, we cultured TSLP-DC with allogeneic memory CD4 purified by sorting (99% purity) from healthy donor peripheral blood (CD4⁺CD25⁻CD45RA⁻CD45RO⁺). Memory CD4 T cells secreted increased amounts of IL-21 after 6 d of co-culture in the presence of TSLP-DC, when compared with CD4 memory co-cultured with untreated DCs or LPS-activated DCs (Fig. 7 A).

To gain insight into the dynamic of cytokine secretion by memory T cells activated by TSLP-DC, we washed and restimulated cells after 2, 4 or 6 d of co-culture. IL-21 secretion by memory CD4 T cells was detected after 2 d of co-culture with TSLP-DC, and was higher after 4 and 6 d (Fig. 7 B). CXCL13 was induced at day 6 of co-culture, but barely detectable before (Fig. 7 C). We compared the expression of IL-21 and CXCL13 with the expression of Th2 cytokines (IL-3, IL-4, and IL-5) in the same experiment. IL-3 was induced at day 2, whereas the secretion profiles of IL-4 and IL-5 over time were comparable to the one of CXCL13 (Fig. 7 D, left column). In the same settings, we were unable to detect any statistically significant difference in TNF secretion (Fig. 7 D, right column). The secretion profiles of IL-21 and CXCL13 were different from the ones of IL-17A and IFN- γ (Fig. 7 D, right column), characteristics of Th17 and Th1 cells, respectively. This indicated that TSLP-DC-activated memory CD4 T cells to express Tfh cytokines IL-21 and CXCL13 with a kinetic of secretion similar to Th2 cytokines.

Detection of CXCL13 and IL-21 in the co-culture of memory CD4 T cells with TSLP-DC suggested that memory Tfh, which have been described as CXCR5⁺CD4⁺CD45RA⁻CD45RO⁺ cells in human peripheral blood (Morita et al., 2011), might be activated by TSLP-DC. To test this hypothesis, we sorted blood memory CD4 based on CXCR5 expression, and co-cultured the CXCR5⁻ and CXCR5⁺ memory CD4 populations separately with either nonactivated DCs or TSLP-DC (Fig. 7 E, top). TSLP-DC significantly induced IL-21 and CXCL13 secretion by CXCR5⁺ memory Tfh in comparison to nonactivated DCs after 6 d of co-culture, followed by 1 d of restimulation with anti-CD3/CD28 beads (Fig. 7 E). At day 6, we measured by FACS the expression of ICOS, PD1, CXCR5, and BCL6 in the same experimental conditions as in Fig. 7 E. TSLP-DC significantly induced ICOS, CXCR5, and BCL6 compared with unstimulated DCs (Fig. 7 F) in memory CXCR5⁻ cells.

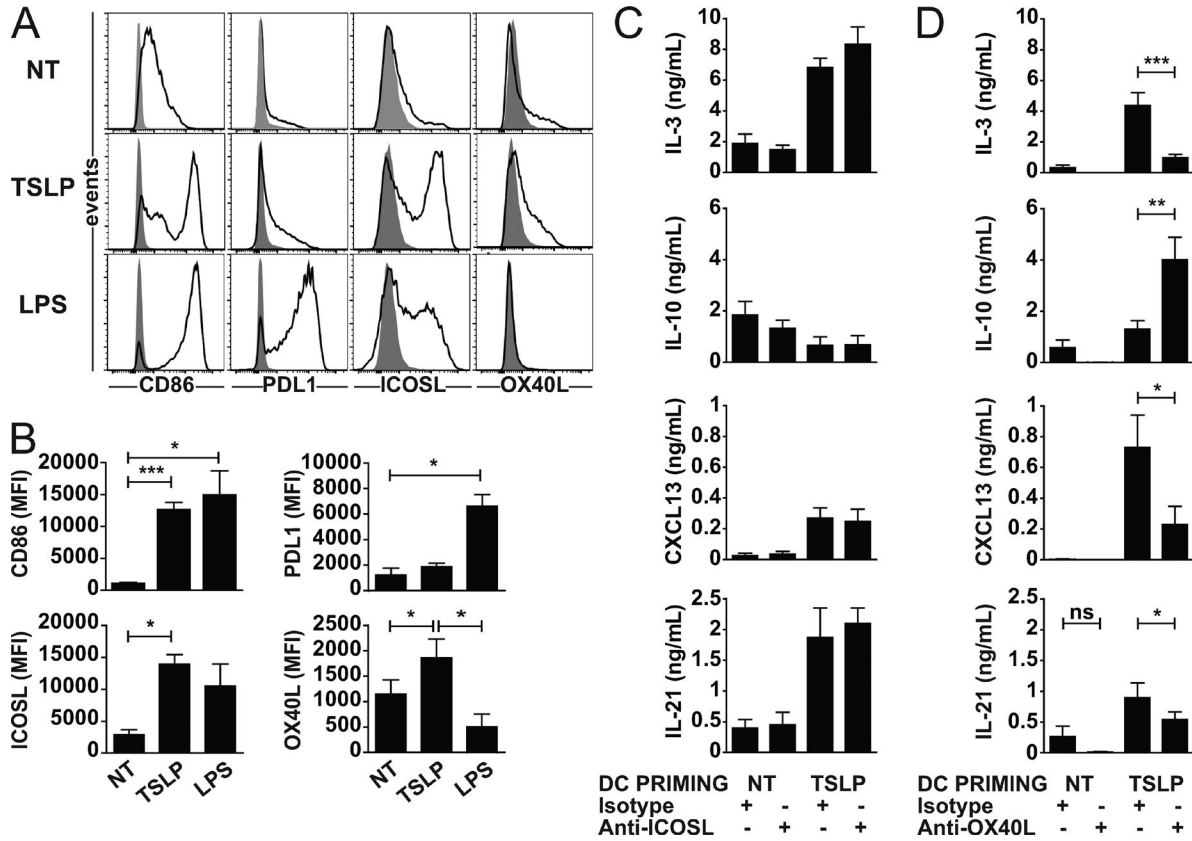


Figure 8. TSLP-DC induce IL-21 and CXCL13 production through OX40L. (A) FACS analysis of surface expression of CD86, PDL1, ICOSL, and OX40L by DCs cultured without any stimulation (NT), TSLP, or LPS for 48 h. Filled gray histogram shows matched isotype control. Black histogram shows antibody staining. One representative donor is shown. (B) Quantification of MFI as in A. Mean \pm SEM for seven experiments. (C) Quantification of cytokine by CBA (IL-3 and IL-10) or ELISA (CXCL13 and IL-21) by CD4 T cells differentiated during 6 d with DCs or TSLP-DC. Anti-ICOSL blocking antibody or isotype control antibody (25 μ g/ml) were kept all along the culture. Mean \pm SEM for four experiments, is plotted. (D) Cells were cultured as in C, and instead of ICOSL blocking antibody, an anti-OX40L antibody or isotype control (50 μ g/ml) were used. Mean \pm SEM for seven experiments. *, $P < 0.05$; **, $P < 0.01$; ***, $P < 0.001$, paired Student's *t* test.

Overall, we concluded that TSLP-DC preferentially stimulated CXCR5⁺ CD4 T cells to secrete IL-21 and CXCL13. Additionally, TSLP-DC induced expression of ICOS, CXCR5, and BCL6 on CXCR5⁻ memory CD4 T cells.

TSLP-DC induce IL-21 and CXCL13 production through OX40L

To gain mechanistic insight into TSLP-DC induction of IL-21 and CXCL13 expression, we focused on the Th-polarizing molecules induced by TSLP in DCs. Because TSLP-DC produce low levels of inflammatory cytokines, and no IL-12 (Soumelis et al., 2002), we explored the contribution of surface co-stimulatory molecules associated with Tfh differentiation. We measured by flow cytometry the expression of CD86, PDL1, ICOSL, and OX40L on DCs cultured for 48 h with TSLP, LPS, or untreated.

We observed that TSLP-DC expressed high levels of ICOSL (Fig. 8, A and B), a molecule important in Tfh polarization (Choi et al., 2011). To assess the role of ICOSL, we

cultured TSLP-DC with CD4 T cells in the presence of an anti-ICOSL blocking antibody and measured cytokines after 6 d. ICOSL blocking did not affect IL-3 or IL-10 levels, and more importantly, did not inhibit polarization by TSLP-DC into Th cells secreting IL-21 and CXCL13 (Fig. 8 C). As a control of the functional blocking of the ICOSL antibody, we detected a decrease in IL-10 production by naive CD4 T cells cultured with plasmacytoid DCs activated with CpGB (pDCs; Fig. 9 A), as previously reported (Ito et al., 2007).

We confirmed OX40L as being induced by TSLP in comparison to DCs or LPS-DC (Fig. 8 A and quantification in Fig. 8 B; Ito et al., 2005). Given the controversial role of OX40L in mouse Tfh development (Deenick et al., 2011), and a recent study on the role of OX40L in human Tfh polarization (Jacquemin et al., 2015), we investigated its role in TSLP-DC-induced Tfh polarization. We used an anti-OX40L blocking antibody during the TSLP-DC CD4 T cell co-culture. OX40L blocking inhibited IL-3 secretion, whereas enhancing IL-10 expression (Fig. 8 D), as previously

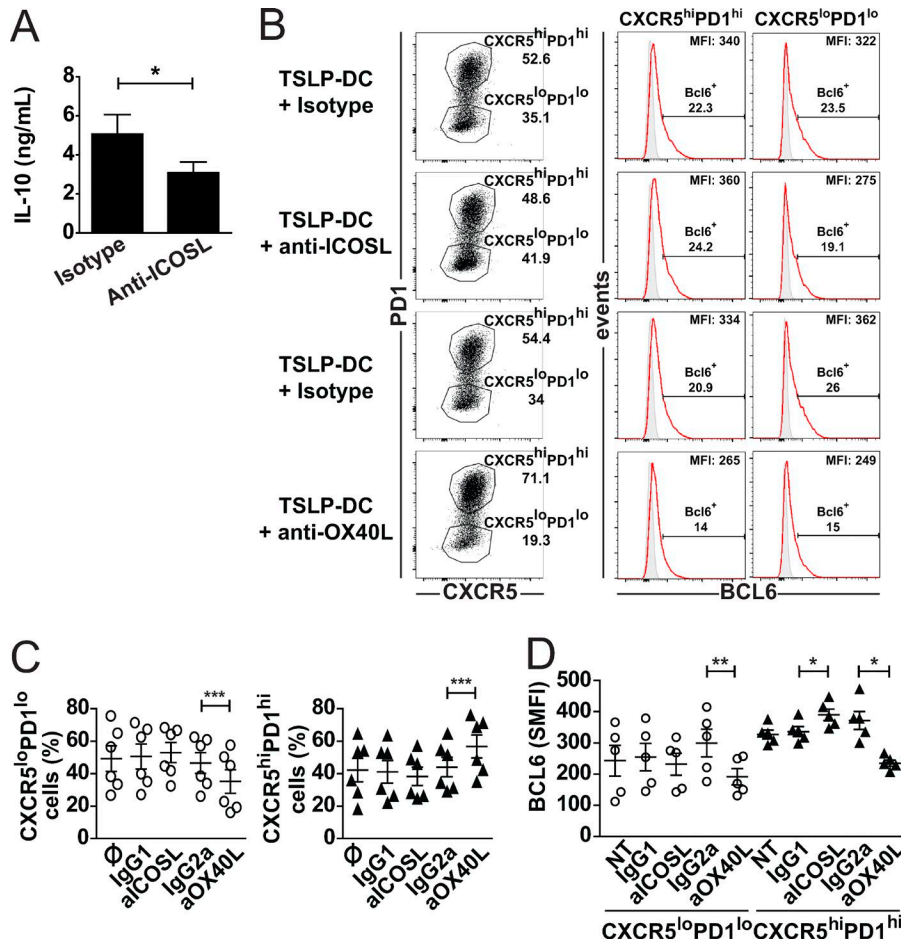


Figure 9. OX40L blocking reduces BCL6 induction by TSLP-DC. (A) Quantification of IL-10 production using CBA by CD4 T cells differentiated during 6 d with pDC activated with CpGB (15 μ g/ml during 24 h). Anti-ICOSL blocking antibody or isotype control antibody (25 μ g/ml) were added at the beginning of the culture. Mean \pm SEM for six experiments is plotted. *, $P < 0.05$ Wilcoxon matched pair test. (B) Quantification by FACS analysis of the percentage of CXCR5^{hi}PD1^{hi}, CXCR5^{lo}PD1^{lo} cells in TSLP-DC co-culture at day 4, treated with functional blocking antibodies or isotype controls as indicated. The percentage of each gate is shown. For BCL6 expression, gray histograms represent the FMO signal, and red histograms represent specific BCL6 staining. MFI of specific staining and percentage of BCL6⁺ cells are plotted for one representative experiment. (C and D) Quantification as in B, from six independent experiments. SMFI for BCL6 was calculated by subtracting the FMO from BCL6-specific staining in CXCR5^{hi}PD1^{hi} and CXCR5^{lo}PD1^{lo} cells. *, $P < 0.05$; **, $P < 0.01$; ***, $P < 0.001$, paired Student's t test.

reported (Ito et al., 2005). We found that OX40L inhibition significantly decreased both CXCL13 and IL-21 secretion by CD4 T cells polarized by TSLP-DC (Fig. 8 D). We investigated the effect of ICOSL and OX40L functional blocking on the expression of CXCR5, PD1, and BCL6. We measured the percentage of CXCR5^{hi}PD1^{hi} and CXCR5^{lo}PD1^{lo} cells, and their respective expression of BCL6 in the presence of blocking antibodies and isotype controls, after 4 d of co-culture with TSLP-DC. ICOSL functional blocking increased BCL6 expression by CXCR5^{hi}PD1^{hi} cells compared with the isotype control (Fig. 9 B, and quantification in D). OX40L functional blocking decreased the percentage of CXCR5^{lo}PD1^{lo} cells, paralleled by an increase in the percentage of CXCR5^{hi}PD1^{hi} cells (Fig. 9 C). In line with no significant changes in IL-21 and CXCL13 expression (Fig. 8 D), we could not observe any decrease of BCL6 expression in response to ICOSL functional blocking (Fig. 9 D). However, we observed that OX40L functional blocking induced a significant decrease of BCL6 expression in both CXCR5^{lo}PD1^{lo} and CXCR5^{hi}PD1^{hi} cells polarized by TSLP-DC (Fig. 9 D).

In summary, our data demonstrated that TSLP induced Tfh polarization through OX40L, and that OX40L controlled BCL6 expression.

In vivo evaluation of Tfh markers in atopic dermatitis (AD) and Netherton syndrome (NS) patients

We sought to assess the relevance of the TSLP-DC-polarized Tfh cells in human pathology. AD is a skin allergic pathology characterized by Th2 environments (Brandt and Sivaprasad, 2011), and the role of TSLP in the pathogenesis of AD is well established (Ziegler and Artis, 2010).

We first asked whether Tfh were infiltrating the lesional skin of AD patients. By immunofluorescence, we could not detect CXCL13⁺ cells in frozen AD skin sections (Fig. S3 A). By FACS, we identified very low percentages (<0.5%) of CXCR5⁺ CD4⁺ cells in T cell emigrated from lesional skin biopsies of 2 AD donors (Fig. S3 B). Lack of significant Tfh cell infiltration of AD skin prompted us to look for circulating Tfh within AD PBMCs. Circulating human Tfh cells comprise a population of IL-4⁻ and IL-21⁻ producing cells that induce IgE switch in B cells (Morita et al., 2011).

We quantified by FACS the percentage of this Tfh subset cells, gated as CD4⁺CD45RO⁺CXCR5⁺CXCR3⁻CCR6⁻, in PBMCs obtained from age- and gender-matched AD and healthy donors. The percentage of Tfh2 was higher in AD donors as compared with healthy donors (64 vs. 30% of CXCR5⁺CD45RA⁺CD4⁺ cells). In parallel, we observed a dramatic decrease of CXCR3⁺CCR6⁻ cells (Fig. 10 A).

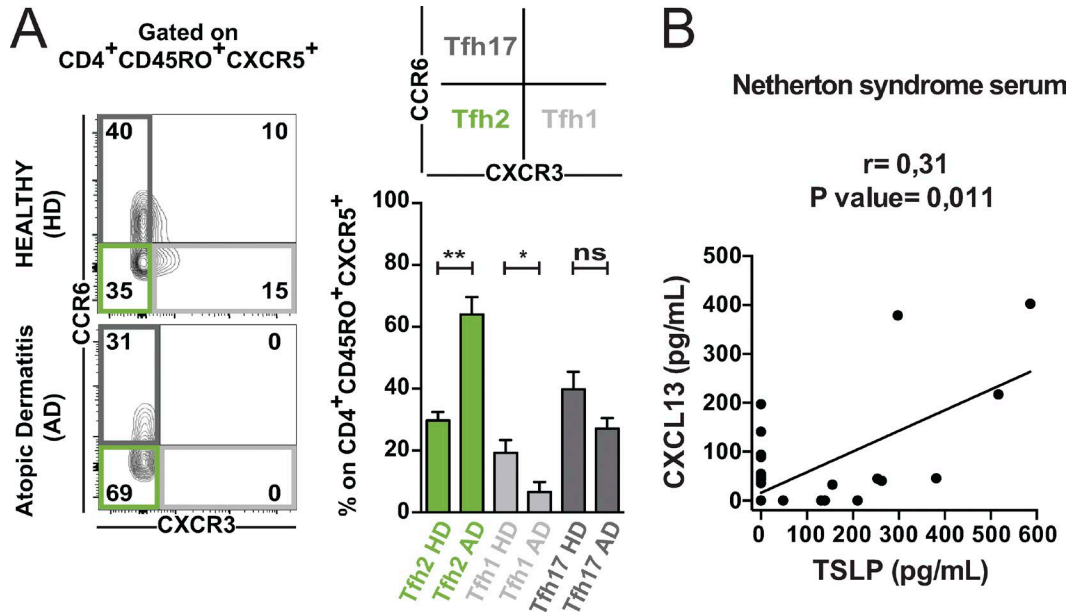


Figure 10. In NS patients, serum TSLP levels positively correlate with CXCL13. (A) FACS analysis showing the frequency of CCR6⁻CXCR3⁻ (green), CCR6⁻CXCR3⁺, and CCR6⁺CXCR3⁻ populations in the CD4⁺CD45RO⁺CXCR5⁺ gate. Representative plots are shown for a healthy donor and AD donor, respectively. Frequency distribution in six AD donors, and four healthy donors are plotted. *, P < 0.05; **, P < 0.01; ***, P < 0.001, paired Student's *t* test. (B) Linear correlation between serum TSLP and CXCL13, measured by ELISA, is shown. Spearman *r* and P-values are plotted. 64 samples from 13 NS patients are plotted.

In addition to AD, which includes predominantly local inflammatory manifestations, we looked for a systemic disease in which TSLP is expressed. This is the case of NS, a rare genetic skin disease characterized by a severe skin barrier defect, atopic manifestations, and elevated IgE levels (Hovnanian, 2013). It has recently been shown that TSLP is highly expressed in a mouse model for NS and in the skin of NS patients (Briot et al., 2009). We analyzed the levels of TSLP in 64 serum samples obtained from 13 NS patients by ELISA. In parallel, we measured CXCL13 as a Tfh marker in the same samples. We found a significant positive correlation between TSLP and CXCL13 in the sera of NS patients (Fig. 10 B).

Collectively, AD and NS patient samples suggest that TSLP and Tfh might be linked in humans in vivo.

DISCUSSION

In this study, we provide definitive evidence for a key role of TSLP-activated DCs in the differentiation of naive CD4 T cells into cells possessing Tfh characteristics through the co-stimulatory molecule OX40L.

IL-12, the main driver of Th1 polarization, promotes Tfh differentiation in humans (Schmitt et al., 2009, 2013; Ma et al., 2012). It has been recently shown that the Th17-inducing cytokines IL-23 and TGF-β could trigger Tfh differentiation too (Schmitt et al., 2014). However, Tfh cells are also present in Th2-dominated environments (Glatman Zaretsky et al., 2009; Yusuf et al., 2010; Liang et al., 2011; Kemeny, 2012), and may have an important physiopathological role in mouse models of airway hyperresponsiveness (Coquet et al., 2015;

Ballesteros-Tato et al., 2016). However, how Tfh differentiation can occur in such Th2 environments is not known. The cytokine TSLP was until now associated with human Th2 polarization (Liu et al., 2007; Ziegler and Artis, 2010). Here, we show a novel function of TSLP as the driver of the differentiation of Tfh cells expressing CXCR5, IL-21, CXCL13, BCL6, and helping memory B cells to produce IgG and IgE. How to reconcile the induction of Tfh cell differentiation in a Th2 context, and the reported negative role of IL-4 on human Tfh development (Schmitt et al., 2014), must still be answered. In our data, we observed a co-occurrence of IL-21- and IL-4-producing T cells in TSLP-DC-polarized cultures. However, TSLP-DC do not produce IL-4 (Soumelis et al., 2002), and TSLP-DC-activated T cells start secreting IL-4 around day 4 (Leyva-Castillo et al., 2013), when we could already identify the CXCR5^{hi}PD1^{hi} population of cells expressing Tfh markers. Therefore, there is an IL-4-free window for Tfh differentiation during the first 48 h of culture, a time when the decision making about Tfh differentiation likely occurs (Choi et al., 2011). Importantly, IL-4 inhibits IL-21 secretion in DC-free settings (Schmitt et al., 2014), different from our DC/T cell co-cultures. We cannot exclude the possibility that, in the context of TSLP-DC-driven Tfh polarization, IL-4 might not inhibit IL-21 production.

The relationship and plasticity between Tfh and Th subsets are still debated. Here, we show that TSLP-DC-induced CXCR5^{hi}PD1^{hi}IL-21⁺IL-4⁺ cells coexpressed the Th2 transcription factor GATA3 and the Tfh transcription factor BCL6. Our data suggest that, in TSLP-DC-activated cells,

GATA3 drives IL-4 expression in the presence of BCL6. In contrast, previous observations showed that BCL6 represses GATA3 in GC Tfh (Kusam et al., 2003; Hatzi et al., 2015). From our data, we could not elucidate the mechanisms underlying GATA3 and BCL6 coexpression. However, our cellular system, based on human primary cells, represents a unique tool to understand the relationship and plasticity between Th2 and Tfh in humans.

Co-stimulatory molecules, in particular ICOS–ICOSL interactions, were shown to be important in Tfh cell development (Choi et al., 2011; Crotty, 2014). The role of other co-stimulatory molecules, and in particular OX40L, is controversial and seems to depend on the experimental mouse model used (Deenick et al., 2011). A recent work shows that OX40L promotes human Tfh responses, particularly in Lupus (Jacquemin et al., 2015). In our work, by using functional blocking of co-stimulatory molecules, we established that OX40L, and not ICOSL, is the main driver of IL-21, CXCL13, and BCL6 expression in T cells by TSLP-DC. Nonetheless, as OX40L functional blocking did not completely abolish IL-21 and CXCL13 production, we cannot exclude that other factors may contribute to the induction of Tfh differentiation by TSLP-DC.

We show that TSLP-DC not only stimulated naive CD4 T cells to acquire Tfh markers, but strongly induced IL-21 and CXCL13 secretion by memory circulating Tfh cells. Additionally, TSLP-DC induced the expression of Tfh markers ICOS, PD1, CXCR5 and BCL6 in memory non Tfh (CXCR5⁻) cells. This result is particularly relevant to Tfh biology because, to our knowledge, this is the first report of reprogramming of human memory non-Tfh CD4 T cells into Tfh-like cells. The frequency of memory circulating Tfh and their activation states have been linked to antibody responses in human subjects (He et al., 2013; Locci et al., 2013). Therefore, it has been proposed that boosting memory Tfh responses could improve vaccine efficacy (Ma and Deenick, 2014). Our study, in combination with published data on the effect of TSLP on mouse antibody responses (Van Roey et al., 2012), provides the rationale to further explore TSLP as a vaccine adjuvant in humans. Additionally, our findings suggest that TSLP, which is produced by epithelial cells, could activate memory Tfh cells in inflamed peripheral tissues through DCs.

How CXCR5^{hi}PD1^{hi} CD4 cells induced by TSLP-DC relate to reported Tfh subsets is of major importance. We directly compared CXCR5^{hi}PD1^{hi} cells polarized by TSLP-DC to human tonsillar Tfh (Kim et al., 2004; Bryant et al., 2007; Weinstein et al., 2014). Our data show that the expression profile of key Tfh markers (PD1, CXCR5, ICOS, BTLA, SAP, CD200, CXCL13, IL-21, C-MAF, BCL6, and BLIMP1) by TSLP-DC-induced CXCR5^{hi}PD1^{hi} cells was similar to tonsillar Tfh and GC Tfh cells.

A characteristic of the IL-21⁺ cells we identified, distinguishing them from previously reported Tfh subsets, is the co-production of TNF. 20% of CD4 activated by TSLP-DC coexpressed IL-21 and TNF. We propose that IL-21⁺TNF⁺ cells may correspond to a distinct inflammatory Tfh cell

subset. In addition, we also detected cells producing IL-21, but not IL-4, TNF, or IFN- γ (16% of IL-21 producers), IL-21⁺IL-4⁺ (3% of IL-21 producers), and IL-21⁺IL-4⁺TNF⁺ (11% of IL-21 producers). This reveals that TSLP induced a large diversity of Th cells, with potential diverse functions depending on the physiopathological contexts. We observed the co-induction of IFN- γ ⁺ cells, a hallmark of Th1 cells, together with Th2 effector cells. This co-induction reproduces the coexistence of Th1 and Th2 cells in AD (Grewe et al., 1998), where TSLP plays a role in T cell polarization (Ziegler and Artis, 2010).

By co-culturing CXCR5^{hi}PD1^{hi} and CXCR5^{lo}PD1^{lo} cells polarized by TSLP-DC with memory B cells, we showed that CXCR5^{hi}PD1^{hi} cells selectively induced IgE secretion. Therefore, in addition to Tfh markers, cells polarized by TSLP-DC presented Tfh2 functional features (Ueno et al., 2015). We found that IgE secretion was accompanied by IgG4 production. Both IgE and IgG4 have been linked to allergic disorders in humans (Gould et al., 2003). Mechanistically, using anti-IL-4R β functional blocking antibody, we showed that IgE induction depended on IL-4 and/or IL-13. Therefore, we described a pathway linking TSLP to IgE production, and involving interactions between epithelial cells, DCs, T cells and B cells.

TSLP is expressed in a broad spectrum of diseases. This is the case of AD (Soumelis et al., 2002), psoriasis (Volpe et al., 2014), NS (Hovnanian, 2013; Furio and Hovnanian, 2014), keloid (Shin et al., 2016), and helminthic infections (Ramalingam et al., 2009; Ziegler and Artis, 2010; Giacomini et al., 2012). In some of these diseases, Tfh cells have been reported (Glatman Zaretsky et al., 2009; Niu et al., 2015). Our analysis on AD clinical samples show that there is an enrichment of Tfh2 and a decrease of Tfh1 in the circulation. A decrease in Th1 cells in PMBC of chronic AD patients has been previously shown (Nakazawa et al., 1997; Lonati et al., 1999). In NS serum samples, we found a positive correlation between TSLP and the GC activity marker CXCL13.

Collectively, our study provides the rationale to exploit TSLP as a pharmacological target to manipulate Tfh polarization in allergic and inflammatory disorders. Acting on an upstream inducer mechanism of Tfh and Tfh2 differentiation may result in additional clinical benefit in the complex pathogenicity of allergy.

MATERIALS AND METHODS

Cell purification

Buffy coats were obtained from healthy adult blood donors (Etablissement Français du Sang, Paris, France) in conformity with Institut Curie ethical guidelines. Human blood primary DCs were purified according to an established protocol (Alculumbre and Pattarini, 2016). In brief, after FICOLL (GE Healthcare) gradient centrifugation, total PBMCs were enriched in DCs using the EasySep Human Pan-DC Pre-Enrichment kit (StemCell Technologies). Enriched DCs were sorted to obtain 98% purity on a FACSVantage (Miltenyi

Biotec), as Lineage (CD3, CD14, CD16, and CD19)⁻ CD4⁺ (Beckman Coulter), CD11c⁺ (BioLegend), whereas pDCs were sorted as Lineage⁻ CD4⁺ CD11c⁻. When detailed, DCs were further separated into subsets by FACS sorting using anti CD1c (eBioscience) and CD141 (Miltenyi Biotec) staining. After enrichment from total PBMCs using the CD4⁺ T cell isolation kit (Miltenyi Biotec), naive and memory CD4 T cells were sorted on a FACSARIA (BD) as CD4⁺, CD25⁻, and CD45RA⁺ and CD45RO⁺, respectively (BD). Blood Tfh were sorted as CD4⁺CD25⁻CD45RO⁺CXCR5⁺ (R&D Systems). Human tonsils were obtained from the Necker Hospital (Paris, France) in conformity with Institut Curie ethical guidelines. Tonsillar CD4 T cells were purified from human tonsils by mechanical disruption (C tube and gentleMACS, Miltenyi), followed by a FICOLL gradient centrifugation. For FACS analysis, total cells were analyzed. For PCR analysis, tonsillar Tfh were enriched using a CD4⁺ T cell isolation kit (Miltenyi) and then sorted as CD4⁺, CD19⁻, CD45RO⁺, CXCR5^{hi/lo/-}, and PD1^{hi/lo/-} (BioLegend) on a FACSARIA (BD).

DC and pDC activation

DC and pDC were cultured in RPMI 1640 Medium GlutaMAX (Life Technologies) containing 10% Fetal Calf Serum (Hyclone), 100 U/ml Penicillin/Streptomycin (Gibco), MEM Non-Essential Amino Acids (Gibco), and 1 mM NA pyruvate (GIBCO). DCs were cultured at 10⁶/ml in flat bottom plates for 24 h in the presence of 50 ng/ml rhTSLP where not differently specified (R&D Systems) or 100 ng/ml ultrapure LPS (InvivoGen).

pDCs were cultured at 10⁶/ml in flat-bottom plates for 24 h in the presence of 15 µg/ml CpGBODN2006 (InvivoGen).

DC/T co-culture

For co-culture, DCs were washed twice in PBS and put in culture with allogeneic either naive or memory CD4 (10⁴ DCs and 5 × 10⁴ T cells) in X-VIVO 15 medium (LONZA) for the indicated time. For co-culture, pDC were washed twice and put in culture with allogeneic naive CD4 cells (10⁴ pDC and 5 × 10⁴ T cells) in Yssel's medium for 6 d. For co-culture, CD4 T cells were freshly purified from PBMC the day after DC purification. Each co-culture experiment was performed by coupling exclusively a single DC donor with a single CD4 T cell donor.

For blocking experiments, DCs or pDCs were incubated at 37°C with 50 µg/ml anti-human OX40L antibody (clone ik-5; provided by T. Hori, Ritsumeikan University, Japan), 25 µg/ml anti-human ICOSL (clone MIH-12; eBioscience), or matched isotype controls (R&D Systems and eBioscience). After 60 min, CD4 naive T cells were added to the culture. Antibodies were maintained for the duration of the co-culture.

At indicated time points, cells were either FACS sorted or used for surface or intracellular staining, or washed and reseeded at 10⁶/ml and treated with anti-CD3/CD28 beads (LifeTech) for 24 h, after which supernatants and cells were collected for analysis.

For primary and secondary co-cultures, CD4 naive T cells were co-cultured with DCs as described at the beginning of this section. At day 5, cells were counted and divided. One part was analyzed for intracellular cytokine production; the other part was put in a secondary culture in the absence of any DCs, in the presence of TSLP-DC or LPS-DC (24 h activation), at the ratio 1:5 in X-VIVO 15 medium. DCs used in the secondary co-culture were purified from donors independent from the DC donors of the primary co-culture and the CD4 T cell donors. Cells were kept in culture for 6 d, and half of the medium was replaced at day 5 with fresh medium.

DC-free Th cell polarization

Sorted naive CD4 T cells were cultured with anti CD3/CD28 beads to obtain Th0 or beads plus IL-1β, IL-23, TGF-β, and IL-6 (PeproTech) to obtain Th17 as already published (Volpe et al., 2008) for 5 d. When indicated, 50 ng/ml TSLP was added at the beginning of the culture, and cells were cultured for 6 d. At the end of the culture, cells were washed, reseeded at 10⁶/ml, and treated with anti-CD3/CD28 beads; supernatants and cells were collected for analysis after 24 h.

T/B co-culture

After 4 d of co-culture with TSLP-DC, activated CD4 T cells were FACS sorted as CXCR5^{hi}/PD1^{hi} or CXCR5^{lo}/PD1^{lo}. The same day, autologous PBMC were thawed and, after a round of human memory B cell Enrichment (Miltenyi Biotec), memory B cells were FACS sorted as CD3⁻CD19⁺CD27⁺IgD⁻ cells. T and B cells were co-cultured in X-VIVO medium in round-bottom plates (2.5 × 10⁵ T and 2.5 × 10⁵ memory B). Memory B cells alone were cultured with 1 µg/ml rhCD40L (Alexis) and 2.5 µg/ml CpG B or left untreated. At day 14 of culture, cells were harvested for flow cytometry analysis and supernatants stored at -80°C to quantify Igs.

For IL4R-α functional blocking, sorted CXCR5^{hi}/PD1^{hi} or CXCR5^{lo}/PD1^{lo} cells were incubated at 37°C with 20 µg/ml of anti-IL4R-α or IgG2a isotype control (R&D Systems). After 1 h, autologous-sorted memory B cells were added (2.5 × 10⁵ T cells and 2.5 × 10⁵ memory B cells). Supernatants were recovered after 14 d of co-culture, stored at -80°C for IgG and IgE measurement by cytometric bead array (CBA).

Flow cytometry analysis

Antibodies and matched isotypes were titrated on the relevant human PBMC population. For surface FACS analysis, the antibodies recognizing these proteins were used: PDL1 (BD), CD86 (BD), OX40L (Ansell), ICOSL (R&D Systems), ICOS (eBioscience), PD1 (BD), CXCR5 (R&D Systems or BD), BTLA (BioLegend), CD200 (eBioscience), CCR7 (BD), TSLPR (BioLegend), IL7Ra (eBioscience), CD27 (BD), and CD38 (Miltenyi Biotec). Dead cells were excluded using DAPI (Miltenyi Biotec).

For intracellular cytokine staining, CD4 T cells were stimulated with 100 ng/ml PMA plus 500 ng/ml Ionomycin.

cin. When cells were sorted before intracellular staining, they were cultured overnight in X-VIVO medium at 10^6 cells/ml before PMA and Ionomycin stimulation. After 90 min, 3 $\mu\text{g/ml}$ Brefeldin A (eBioscience) was added and kept for 4 h. To exclude dead cells, CD4 T cells were stained using the LIVE/DEAD Fixable yellow dead cell stain kit, following manufacturer's instructions (LifeTech). Cells were fixed and permeabilized using the IC Fix and Permeabilization buffers (eBioscience). Intracellular cytokines were revealed with fluorescently conjugated antibodies against IL-21 (BD), TNF (BioLegend), IL-4, and IFN- γ , or matched isotype controls (eBioscience) and acquired on a LSR Fortessa instrument (BD).

For transcription factor intracellular staining, dead cells were first stained with a Zombie-NIR dye (BioLegend), followed by PD1 and CXCR5 (BD) staining. After fixation and permeabilization using the FOXP3 IC buffer kit (eBioscience), cells were stained with an anti-BCL6 antibody (BD), TBET, GATA3, RORC, C-MAF, or SAP (eBioscience) and acquired on a LSR Fortessa instrument. As a control for intracellular staining of transcription factors, cells were stained using PD1, CXCR5, and CD4 (to define the populations) and matched isotype controls at the same concentration as the transcription factor antibodies. The fluorescence obtained in each channel and in each population in the presence of isotype control antibody (Fluorescence minus one [FMO]) was subtracted from the fluorescence obtained by the specific staining of transcription factors in each population. Sorted naive CD4 T cells were analyzed in parallel as a control.

Flow cytometry data processing

FACS data were analyzed using the FlowJo software (Tree Star).

Cytokine quantification

Cytokines were quantified in the supernatants using ELISA for IL-21 (BioLegend) and CXCL13 (R&D Systems) or CBA flex set for IL-3, IL-4, IL-5, IL-10, IL-13, IL-17A, TNF, and IFN- γ (BD), following the manufacturer's protocol. Total human IgG, IgE, IgG4, and IgM were quantified using the Human IgGs Flex Sets (BD).

PCR

Cells were sorted and lysed in RLT buffer. RNA extraction was performed using the RNeasy micro kit (QIAGEN) according to manufacturer's instructions. Total RNA was retrotranscribed using the superscript II polymerase (Invitrogen) in combination with random hexamers, oligo dT, and dNTPs (Promega).

Transcripts were quantified by real time PCR on a 480 LightCycler instrument (Roche). Reactions were performed in 10 μl , using a master mix (Eurogentec), with the following TaqMan Assays (all from Life Technologies): BCL6 (Hs00153368_m1), PRMD1 (Hs00153357_m1), BTLA (Hs00699198_m1), CXCR4 (Hs00607978_s1), CXCR5 (Hs00540548_s1), CXCL13 (Hs00757930_m1), ICOS (Hs00359999_m1), IL-21 (Hs00222327_m1), PDCD1 (Hs01550088_m1), SH2D1A (Hs00158978_m1), CCR7 (HS 00171054_m1), CD200 (Hs01033303_m1), IL-4 (Hs00174122_m1), TNF (Hs00174128_m1), MAF (Hs00193519_m1), GATA-3 (Hs00231122_m1), TBX-21 (Hs00203436_m1), RORC (Hs01076112_m1), FOXP3 (Hs00203958_m1), IL-5 (Hs00174200_m1), IL-13 (Hs99999038_m1), IFNG (Hs00174143_m1), and IL-17A (Hs00174383_m1). Crossing points (Cp) from each analyte were obtained using the second derivative maximum method, and the transcripts were quantified as fold changes in comparison to the mean of the two housekeeping genes (B2M [Hs99999907_m1] and RPL34 [Hs00241560_m1]).

Analysis of AD and HD PBMCs

After obtaining informed consent from patients, whole blood was taken from AD patients ($n = 6$, Table 1). PBMCs were purified using CPT tubes (BD) and immediately frozen. Local ethics committees of the Heinrich-Heine University (Düsseldorf, Germany) approved the study. Healthy age- and gender-matched controls were also included in the study, and were processed as AD samples at the Heinrich-Heine University.

Total PBMCs from healthy donors and from AD patients (5×10^6 each), were thawed and immediately stained for sorting. Cells were stained using CD4 (BD), CD45RO (BD), CXCR5 (R&D Systems), CXCR3 (BD), and CCR6 (BioLegend) for 30 min at 37°C .

Table 1. **Clinical data**

Patient no.	Gender	Year of birth	Diseases	SCORAD
1	M	1975	AD	41
2	W	1957	AD	41
3	M	1962	AD	39
4	W	1997	AD	35.4
5	W	1998	AD	38.2
6	W	1989	AD	44.4
7	M	1980	HD	
8	W	1970	HD	
9	W	1987	HD	
10	W	1969	HD	

M, man; W, woman. SCORAD (Scoring of AD) was assessed following the Consensus report of the European task force on AD.

Immunofluorescence

Frozen tissue slides (human tonsils and skin) were stained with rat anti-human TSLP (clone 12F3; gift from L. Bover, MD Anderson Cancer Center, Houston, Texas), goat anti-human CXCL13 (R&D Systems), followed by incubation with fluorescence-conjugated secondary antibodies. Slides were stained with DAPI, mounted with Vectashield (Vector) and acquired using an Eclipse microscope (Nikon).

Cell purification from human skin

Fresh AD lesional skin biopsies were washed in PBS, minced with a scalpel, and placed in culture at 37°C with 5% CO₂ in RPMI 1640 complemented with 2 mmol/liter glutamine, 1 mmol/liter sodium pyruvate, 1% nonessential amino acids, 0.05 mmol/liter 2-mercaptoethanol, 100 U/ml penicillin, and 100 µg/ml streptomycin (Lonza) with 5% autologous plasma and 60 U/ml recombinant human IL-2 (Novartis) to obtain enriched skin T cells. Medium was replaced every third day, and after 8 to 10 d, T cells that emigrated from tissue samples were collected and placed in starvation with low IL-2 before phenotypic characterization.

Statistical analysis

Statistical analysis was performed using the Prism software v7 (GraphPad). Paired Wilcoxon or *t* test were applied as detailed to compare two groups. Mann-Whitney test was used for nonpaired analysis. Significance was retained for *P* < 0.05.

qPCR data were normalized and center reduced using Box-Cox transformation, and plotted using heat map package in the R software.

Online supplemental material

Fig. S1 shows that human naive CD4 T cells do not express TSLPR, and do not respond to TSLP stimulation by expressing IL-21. Fig. S2 details the expression of Tfh and Th markers shown in Fig. 4. Fig. S3 displays the expression of CXCL13 and CXCR5 in AD and healthy donor skin samples, by IHC and FACS staining, respectively.

ACKNOWLEDGMENTS

We thank the Cytometry Core facility of IC for cell sorting. We thank Hideki Ueno, Elodie Segura, and Luigia Pace for discussions and reading of the manuscript. We thank Giovanni Marchiori for R programming advice.

This work was supported by funding from Institut National de la Santé et de la Recherche Médicale (BIO2014-08), FRM, ANR-13-BSV1-0024-02, ANR-10-IDEX-0001-02 PSL* and ANR-11-LABX-0043, ERC (IT-DC 281987 and HEALTH 2011-261366) and CIC IGR-Curie 1428. L.P. had a post-doctoral fellowship from CIDF, M.G. a PhD fellowship from ANRS.

The authors have no conflicting financial interests.

Author contributions: L.P. designed, performed and analyzed experiments and wrote the manuscript, C.T. performed experiments, analyzed data and prepared Figures, S.B. performed experiments, M.G. performed intracellular staining, M.D. purified tonsillar Tfh and performed PCR, T.H. provided the anti-OX40L ab. V.S. supervised the study.

Submitted: 5 March 2015

Revised: 30 December 2016

Accepted: 2 March 2017

REFERENCES

- Alcolumbre, S., and L. Pattarini. 2016. Purification of human dendritic cell subsets from peripheral blood. *Methods Mol. Biol.* 1423:153–167. http://dx.doi.org/10.1007/978-1-4939-3606-9_11
- Ballesteros-Tato, A., T.D. Randall, F.E. Lund, R. Spolski, W.J. Leonard, and B. León. 2016. T follicular helper cell plasticity shapes pathogenic T helper 2 Cell-mediated immunity to inhaled house dust mite. *Immunity* 44:259–273. <http://dx.doi.org/10.1016/j.immuni.2015.11.017>
- Bernasconi, N.L., E. Traggiai, and A. Lanzavecchia. 2002. Maintenance of serological memory by polyclonal activation of human memory B cells. *Science* 298:2199–2202. <http://dx.doi.org/10.1126/science.1076071>
- Brandt, E.B., and U. Sivaprasad. 2011. Th2 Cytokines and atopic dermatitis. *J. Clin. Cell. Immunol.* 2:3–5. <http://dx.doi.org/10.4172/2155-9899.1000110>
- Briot, A., C. Deraison, M. Lacroix, C. Bonnart, A. Robin, C. Besson, P. Dubus, and A. Hovnanian. 2009. Kallikrein 5 induces atopic dermatitis-like lesions through PAR2-mediated thymic stromal lymphopoietin expression in Netherton syndrome. *J. Exp. Med.* 206:1135–1147. <http://dx.doi.org/10.1084/jem.20082242>
- Bryant, V.L., C.S. Ma, D.T. Avery, Y. Li, K.L. Good, L.M. Corcoran, R. de Waal Malefyt, and S.G. Tangye. 2007. Cytokine-mediated regulation of human B cell differentiation into Ig-secreting cells: predominant role of IL-21 produced by CXCR5+ T follicular helper cells. *J. Immunol.* 179:8180–8190. <http://dx.doi.org/10.4049/jimmunol.179.12.8180>
- Choi, Y.S., R. Kageyama, D. Eto, T.C. Escobar, R.J. Johnston, L. Monticelli, C. Lao, and S. Crotty. 2011. ICOS receptor instructs T follicular helper cell versus effector cell differentiation via induction of the transcriptional repressor Bcl6. *Immunity* 34:932–946. <http://dx.doi.org/10.1016/j.immuni.2011.03.023>
- Coquet, J.M., M.J. Schuijs, M.J. Smyth, K. Deswarte, R. Beyaert, H. Braun, L. Boon, G.B. Karlsson Hedestam, S.L. Nutt, H. Hammad, and B.N. Lambrecht. 2015. Interleukin-21-producing CD4⁺ T cells promote type 2 immunity to house dust mites. *Immunity* 43:318–330. <http://dx.doi.org/10.1016/j.immuni.2015.07.015>
- Crotty, S. 2014. T follicular helper cell differentiation, function, and roles in disease. *Immunity* 41:529–542. <http://dx.doi.org/10.1016/j.immuni.2014.10.004>
- Deenick, E.K., C.S. Ma, R. Brink, and S.G. Tangye. 2011. Regulation of T follicular helper cell formation and function by antigen presenting cells. *Curr. Opin. Immunol.* 23:111–118. <http://dx.doi.org/10.1016/j.coi.2010.10.007>
- Furio, L., and A. Hovnanian. 2014. Netherton syndrome: defective kallikrein inhibition in the skin leads to skin inflammation and allergy. *Biol. Chem.* 395:945–958. <http://dx.doi.org/10.1515/hsz-2014-0137>
- Giacomin, P.R., M.C. Siracusa, K.P. Walsh, R.K. Grencis, M. Kubo, M.R. Comeau, and D. Artis. 2012. Thymic stromal lymphopoietin-dependent basophils promote Th2 cytokine responses following intestinal helminth infection. *J. Immunol.* 189:4371–4378. <http://dx.doi.org/10.4049/jimmunol.1200691>
- Glatman Zaretsky, A., J.J. Taylor, I.L. King, F.A. Marshall, M. Mohrs, and E.J. Pearce. 2009. T follicular helper cells differentiate from Th2 cells in response to helminth antigens. *J. Exp. Med.* 206:991–999. <http://dx.doi.org/10.1084/jem.20090303>
- Gould, H.J., B.J. Sutton, A.J. Beavil, R.L. Beavil, N. McCloskey, H.A. Coker, D. Fear, and L. Smurthwaite. 2003. The biology of IGE and the basis of

- allergic disease. *Annu. Rev. Immunol.* 21:579–628. <http://dx.doi.org/10.1146/annurev.immunol.21.120601.141103>
- Grewe, M., C.A. Bruijnzeel-Koomen, E. Schöpf, T. Thepen, A.G. Langeveld-Wildschut, T. Ruzicka, and J. Krutmann. 1998. A role for Th1 and Th2 cells in the immunopathogenesis of atopic dermatitis. *Immunol. Today.* 19:359–361. [http://dx.doi.org/10.1016/S0167-5699\(98\)01285-7](http://dx.doi.org/10.1016/S0167-5699(98)01285-7)
- Gringhuis, S.I., T.M. Kaptein, B.A. Wevers, M. van der Vlist, E.J. Klaver, I. van Die, L.E. Vriend, M.A. de Jong, and T.B. Geijtenbeek. 2014. Fucose-based PAMPs prime dendritic cells for follicular T helper cell polarization via DC-SIGN-dependent IL-27 production. *Nat. Commun.* 5:5074. <http://dx.doi.org/10.1038/ncomms6074>
- Hatzi, K., J.P. Nance, M.A. Kroenke, M. Bothwell, E.K. Haddad, A. Melnick, and S. Crotty. 2015. BCL6 orchestrates Tfh cell differentiation via multiple distinct mechanisms. *J. Exp. Med.* 212:539–553. <http://dx.doi.org/10.1084/jem.20141380>
- He, J., L.M. Tsai, Y.A. Leong, X. Hu, C.S. Ma, N. Chevalier, X. Sun, K. Vandenberg, S. Rockman, Y. Ding, et al. 2013. Circulating precursor CCR7(lo)PD-1(hi) CXCR5⁺ CD4⁺ T cells indicate Tfh cell activity and promote antibody responses upon antigen reexposure. *Immunity.* 39:770–781. <http://dx.doi.org/10.1016/j.immuni.2013.09.007>
- Hovnanian, A. 2013. Netherton syndrome: skin inflammation and allergy by loss of protease inhibition. *Cell Tissue Res.* 351:289–300. <http://dx.doi.org/10.1007/s00441-013-1558-1>
- Ito, T., Y.H. Wang, O. Duramad, T. Hori, G.J. Delespesse, N. Watanabe, F.X. Qin, Z. Yao, W. Cao, and Y.J. Liu. 2005. TSLP-activated dendritic cells induce an inflammatory T helper type 2 cell response through OX40 ligand. *J. Exp. Med.* 202:1213–1223. <http://dx.doi.org/10.1084/jem.20051135>
- Ito, T., M. Yang, Y.H. Wang, R. Lande, J. Gregorio, O.A. Perng, X.F. Qin, Y.J. Liu, and M. Gilliet. 2007. Plasmacytoid dendritic cells prime IL-10-producing T regulatory cells by inducible costimulator ligand. *J. Exp. Med.* 204:105–115. <http://dx.doi.org/10.1084/jem.20061660>
- Jacquemin, C., N. Schmitt, C. Contin-Bordes, Y. Liu, P. Narayanan, J. Seneschal, T. Maurouard, D. Dougall, E.S. Davizon, H. Dumortier, et al. 2015. OX40 ligand contributes to human lupus pathogenesis by promoting T follicular helper response. *Immunity.* 42:1159–1170. <http://dx.doi.org/10.1016/j.immuni.2015.05.012>
- Kemeny, D.M. 2012. The role of the T follicular helper cells in allergic disease. *Cell. Mol. Immunol.* 9:386–389. <http://dx.doi.org/10.1038/cmi.2012.31>
- Kim, C.H., H.W. Lim, J.R. Kim, L. Rott, P. Hillsamer, and E.C. Butcher. 2004. Unique gene expression program of human germinal center T helper cells. *Blood.* 104:1952–1960. <http://dx.doi.org/10.1182/blood-2004-03-1206>
- Kroenke, M.A., D. Eto, M. Locci, M. Cho, T. Davidson, E.K. Haddad, and S. Crotty. 2012. Bcl6 and Maf cooperate to instruct human follicular helper CD4 T cell differentiation. *J. Immunol.* 188:3734–3744. <http://dx.doi.org/10.4049/jimmunol.1103246>
- Kusam, S., L.M. Toney, H. Sato, and A.L. Dent. 2003. Inhibition of Th2 differentiation and GATA-3 expression by BCL-6. *J. Immunol.* 170:2435–2441. <http://dx.doi.org/10.4049/jimmunol.170.5.2435>
- Leyva-Castillo, J.M., P. Hener, P. Michea, H. Karasuyama, S. Chan, V. Soumelis, and M. Li. 2013. Skin thymic stromal lymphopoietin initiates Th2 responses through an orchestrated immune cascade. *Nat. Commun.* 4:2847. <http://dx.doi.org/10.1038/ncomms3847>
- Liang, H.E., R.L. Reinhardt, J.K. Bando, B.M. Sullivan, I.C. Ho, and R.M. Locksley. 2011. Divergent expression patterns of IL-4 and IL-13 define unique functions in allergic immunity. *Nat. Immunol.* 13:58–66. <http://dx.doi.org/10.1038/ni.2182>
- Liu, Y.J., V. Soumelis, N. Watanabe, T. Ito, Y.H. Wang, R. W. Malefyt, M. Omori, B. Zhou, and S.F. Ziegler. 2007. TSLP: an epithelial cell cytokine that regulates T cell differentiation by conditioning dendritic cell maturation. *Annu. Rev. Immunol.* 25:193–219. <http://dx.doi.org/10.1146/annurev.immunol.25.022106.141718>
- Locci, M., C. Havenar-Daughton, E. Landais, J. Wu, M.A. Kroenke, C.L. Arlehamm, L.F. Su, R. Cubas, M.M. Davis, A. Sette, et al. International AIDS Vaccine Initiative Protocol C Principal Investigators. 2013. Human circulating PD-1⁺CXCR3⁺CXCR5⁺ memory Tfh cells are highly functional and correlate with broadly neutralizing HIV antibody responses. *Immunity.* 39:758–769. <http://dx.doi.org/10.1016/j.immuni.2013.08.031>
- Lonati, A., S. Licenziati, A.D. Canaris, S. Fiorentini, G. Pasolini, M. Marcelli, S. Seidenari, A. Caruso, and G. De Panfilis. 1999. Reduced production of both Th1 and Tc1 lymphocyte subsets in atopic dermatitis (AD). *Clin. Exp. Immunol.* 115:1–5. <http://dx.doi.org/10.1046/j.1365-2249.1999.00773.x>
- Ma, C.S., and E.K. Deenick. 2014. Human T follicular helper (Tfh) cells and disease. *Immunol. Cell Biol.* 92:64–71. <http://dx.doi.org/10.1038/icb.2013.55>
- Ma, C.S., D.T. Avery, A. Chan, M. Batten, J. Bustamante, S. Boisson-Dupuis, P.D. Arkwright, A.Y. Kreins, D. Averbuch, D. Engelhard, et al. 2012. Functional STAT3 deficiency compromises the generation of human T follicular helper cells. *Blood.* 119:3997–4008. <http://dx.doi.org/10.1182/blood-2011-11-392985>
- Morita, R., N. Schmitt, S.E. Bentebibel, R. Ranganathan, L. Bourdery, G. Zurawski, E. Foucat, M. Dullaers, S. Oh, N. Sabzghabaei, et al. 2011. Human blood CXCR5(+)CD4(+) T cells are counterparts of T follicular cells and contain specific subsets that differentially support antibody secretion. *Immunity.* 34:108–121. <http://dx.doi.org/10.1016/j.immuni.2010.12.012>
- Nakazawa, M., N. Sugi, H. Kawaguchi, N. Ishii, H. Nakajima, and M. Minami. 1997. Predominance of type 2 cytokine-producing CD4⁺ and CD8⁺ cells in patients with atopic dermatitis. *J. Allergy Clin. Immunol.* 99:673–682. [http://dx.doi.org/10.1016/S0091-6749\(97\)70030-7](http://dx.doi.org/10.1016/S0091-6749(97)70030-7)
- Nies, J.H., C. Bär, G. Schlenvoigt, B. Fahlbusch, G. Zwacka, and U.R. Markert. 2002. IL-4 supplemented B-cell cultures of allergic children show reduced IgA and IgG production in response to additional stimulation with IL-10. *J. Invest. Allergol. Clin. Immunol.* 12:99–106.
- Niu, J., Z. Song, X. Yang, Z. Zhai, H. Zhong, and F. Hao. 2015. Increased circulating follicular helper T cells and activated B cells correlate with disease severity in patients with psoriasis. *J. Eur. Acad. Dermatol. Venereol.* 29:1791–1796. <http://dx.doi.org/10.1111/jdv.13027>
- O’Shea, J.J., and W.E. Paul. 2010. Mechanisms underlying lineage commitment and plasticity of helper CD4⁺ T cells. *Science.* 327:1098–1102. <http://dx.doi.org/10.1126/science.1178334>
- Pène, J., F. Rousset, F. Brière, I. Chrétien, X. Paliard, J. Banchereau, H. Spits, and J.E. De Vries. 1988. IgE production by normal human B cells induced by alloreactive T cell clones is mediated by IL-4 and suppressed by IFN- γ . *J. Immunol.* 141:1218–1224.
- Ramalingam, T.R., J.T. Pesce, M.M. Mentink-Kane, S. Madala, A.W. Cheever, M.R. Comeau, S.F. Ziegler, and T.A. Wynn. 2009. Regulation of helminth-induced Th2 responses by thymic stromal lymphopoietin. *J. Immunol.* 182:6452–6459. <http://dx.doi.org/10.4049/jimmunol.0900181>
- Schmitt, N., R. Morita, L. Bourdery, S.E. Bentebibel, S.M. Zurawski, J. Banchereau, and H. Ueno. 2009. Human dendritic cells induce the differentiation of interleukin-21-producing T follicular helper-like cells through interleukin-12. *Immunity.* 31:158–169. <http://dx.doi.org/10.1016/j.immuni.2009.04.016>
- Schmitt, N., J. Bustamante, L. Bourdery, S.E. Bentebibel, S. Boisson-Dupuis, F. Hamlin, M.V. Tran, D. Blankenship, V. Pascual, D.A. Savino, et al. 2013. IL-12 receptor β 1 deficiency alters in vivo T follicular helper cell response in humans. *Blood.* 121:3375–3385. <http://dx.doi.org/10.1182/blood-2012-08-448902>

- Schmitt, N., Y. Liu, S.E. Bentebibel, I. Munagala, L. Bourdery, K. Venuprasad, J. Banchereau, and H. Ueno. 2014. The cytokine TGF- β co-opts signaling via STAT3-STAT4 to promote the differentiation of human TFH cells. *Nat. Immunol.* 15:856–865. <http://dx.doi.org/10.1038/ni.2947>
- Shin, J.U., S.H. Kim, H. Kim, J.Y. Noh, S. Jin, C.O. Park, W.J. Lee, D.W. Lee, J.H. Lee, and K.H. Lee. 2016. TSLP is a potential initiator of collagen synthesis and an activator of CXCR4/SDF-1 axis in keloid pathogenesis. *J. Invest. Dermatol.* 136:507–515. <http://dx.doi.org/10.1016/j.jid.2015.11.008>
- Soumelis, V., P.A. Reche, H. Kanzler, W. Yuan, G. Edward, B. Homey, M. Gilliet, S. Ho, S. Antonenko, A. Lauerma, et al. 2002. Human epithelial cells trigger dendritic cell mediated allergic inflammation by producing TSLP. *Nat. Immunol.* 3:673–680.
- Tangye, S.G., C.S. Ma, R. Brink, and E.K. Deenick. 2013. The good, the bad and the ugly - TFH cells in human health and disease. *Nat. Rev. Immunol.* 13:412–426. <http://dx.doi.org/10.1038/nri3447>
- Trinchieri, G. 2003. Interleukin-12 and the regulation of innate resistance and adaptive immunity. *Nat. Rev. Immunol.* 3:133–146. <http://dx.doi.org/10.1038/nri1001>
- Ueno, H., J. Banchereau, and C.G. Vinuesa. 2015. Pathophysiology of T follicular helper cells in humans and mice. *Nat. Immunol.* 16:142–152. <http://dx.doi.org/10.1038/ni.3054>
- Van Roey, G.A., M.A. Arias, J.S. Tregoning, G. Rowe, and R.J. Shattock. 2012. Thymic stromal lymphopoietin (TSLP) acts as a potent mucosal adjuvant for HIV-1 gp140 vaccination in mice. *Eur. J. Immunol.* 42:353–363. <http://dx.doi.org/10.1002/eji.201141787>
- Volpe, E., N. Servant, R. Zollinger, S.I. Bogiatzi, P. Hupé, E. Barillot, and V. Soumelis. 2008. A critical function for transforming growth factor-beta, interleukin 23 and proinflammatory cytokines in driving and modulating human T(H)-17 responses. *Nat. Immunol.* 9:650–657. <http://dx.doi.org/10.1038/ni.1613>
- Volpe, E., L. Pattarini, C. Martinez-Cingolani, S. Meller, M.H. Donnadieu, S.I. Bogiatzi, M.I. Fernandez, M. Touzot, J.C. Bichet, F. Reyat, et al. 2014. Thymic stromal lymphopoietin links keratinocytes and dendritic cell-derived IL-23 in patients with psoriasis. *J. Allergy Clin. Immunol.* 134:373–381. <http://dx.doi.org/10.1016/j.jaci.2014.04.022>
- Wang, Y.H., T. Ito, Y.H. Wang, B. Homey, N. Watanabe, R. Martin, C.J. Barnes, B.W. McIntyre, M. Gilliet, R. Kumar, et al. 2006. Maintenance and polarization of human TH2 central memory T cells by thymic stromal lymphopoietin-activated dendritic cells. *Immunity*. 24:827–838. <http://dx.doi.org/10.1016/j.immuni.2006.03.019>
- Weinstein, J.S., K. Lezon-Geyda, Y. Maksimova, S. Craft, Y. Zhang, M. Su, V.P. Schulz, J. Craft, and P.G. Gallagher. 2014. Global transcriptome analysis and enhancer landscape of human primary T follicular helper and T effector lymphocytes. *Blood*. 124:3719–3729. <http://dx.doi.org/10.1182/blood-2014-06-582700>
- Ying, S., B. O'Connor, J. Ratoff, Q. Meng, K. Mallett, D. Cousins, D. Robinson, G. Zhang, J. Zhao, T.H. Lee, and C. Corrigan. 2005. Thymic stromal lymphopoietin expression is increased in asthmatic airways and correlates with expression of Th2-attracting chemokines and disease severity. *J. Immunol.* 174:8183–8190. <http://dx.doi.org/10.4049/jimmunol.174.12.8183>
- Yusuf, I., R. Kageyama, L. Monticelli, R.J. Johnston, D. Ditoro, K. Hansen, B. Barnett, and S. Croty. 2010. Germinal center T follicular helper cell IL-4 production is dependent on signaling lymphocytic activation molecule receptor (CD150). *J. Immunol.* 185:190–202. <http://dx.doi.org/10.4049/jimmunol.0903505>
- Ziegler, S.F., and D. Artis. 2010. Sensing the outside world: TSLP regulates barrier immunity. *Nat. Immunol.* 11:289–293. <http://dx.doi.org/10.1038/ni.1852>

SUPPLEMENTAL MATERIAL

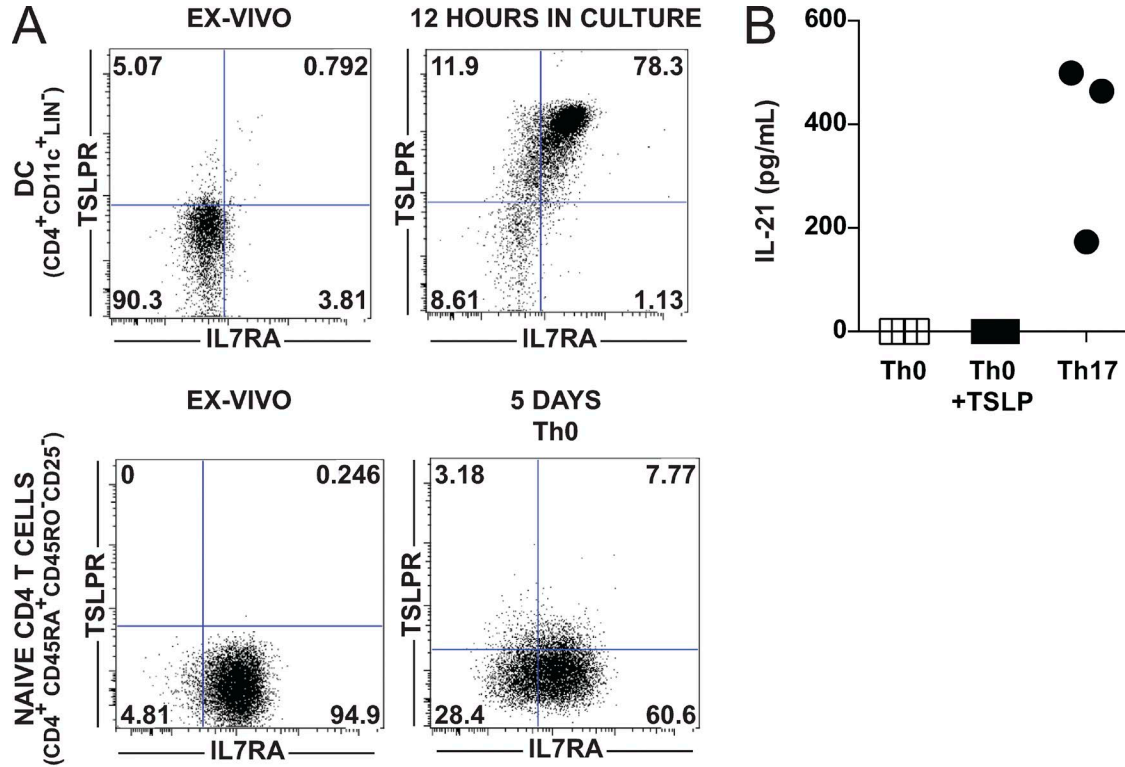
Pattarini et al., <https://doi.org/10.1084/jem.20150402>

Figure S1. TSLP does not induce IL-21 production by naive CD4 T cells in the absence of DCs. (A) FACS analysis of the surface expression of TSLPR and IL7R α in sorted DCs (ex vivo and after 12 h of culture) and sorted naive CD4 T cells (ex vivo and after 5 d in culture with anti-CD3/CD28 beads; Th0) in one representative donor. Quadrant gates were established using matched isotype controls. (B) IL-21 secretion measured by ELISA after 6 d of culture of sorted naive CD4 T cells in Th0 condition (squares), in the presence of 50 ng/ml of TSLP (filled squares) or in Th17 polarizing conditions (circles), and 24 h of restimulation using anti-CD3/CD28 beads. Three independent experiments are plotted.

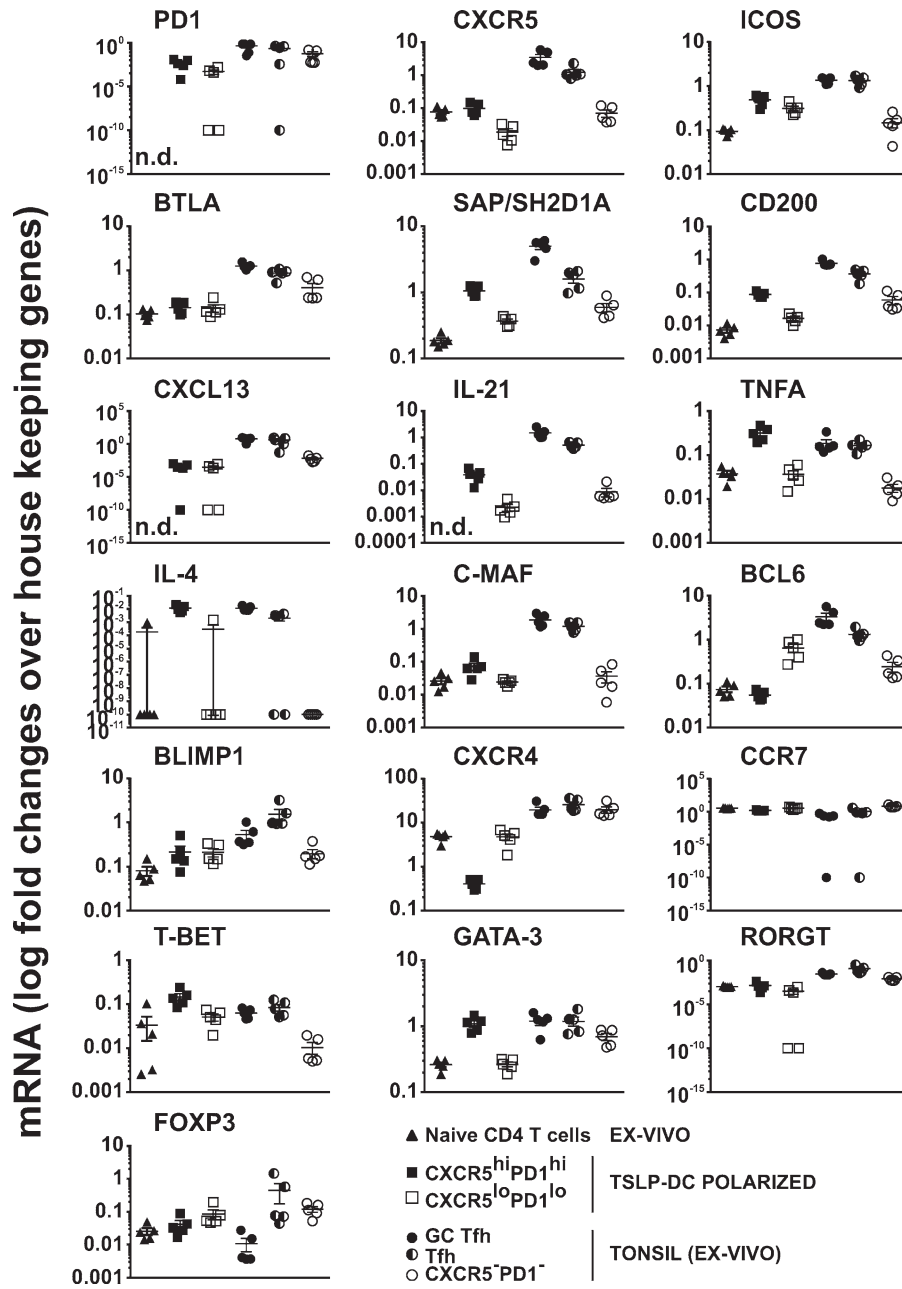


Figure S2. CXCR5^{hi}/PD1^{hi} cells induced by TSLP-DC expressed mRNA of Tfh markers. mRNA levels quantified by qPCR are shown for individual Tfh and Th markers in naive CD4 T cells, TSLP-DC activated cells and ex-vivo tonsillar CD4 subsets as indicated. mRNA levels are shown as fold changes over the mean of housekeeping genes (RPL34, B2M). Five independent donors for each population are shown from two independent experiments.

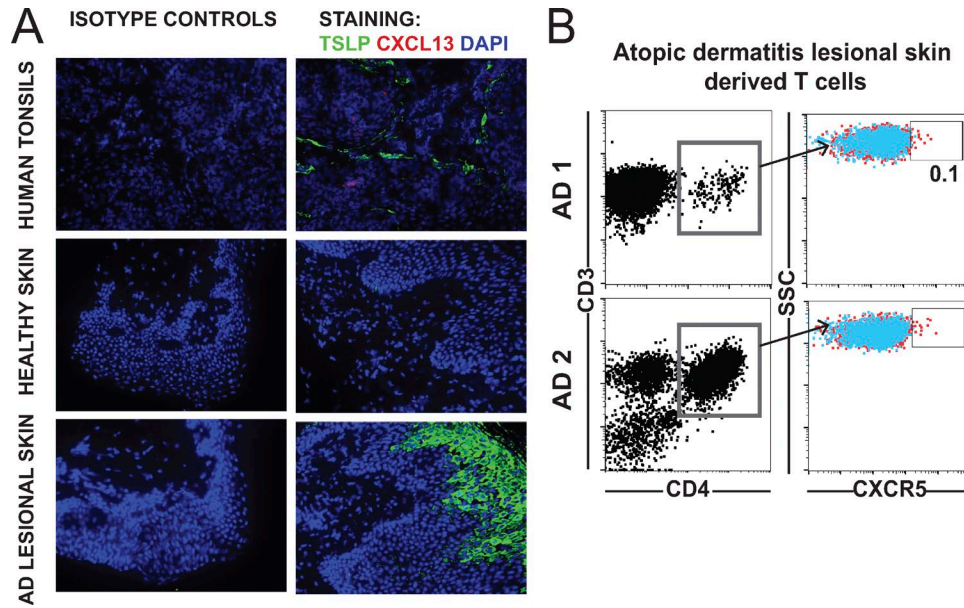


Figure S3. **Tfh cells do not infiltrate in the skin of AD patients.** (A) Immunofluorescence staining for TSLP (green), CXCL13 (red), and DAPI (blue) in sections of human tonsil, healthy skin, and AD lesional skin. One representative donor is shown for each tissue (three tonsils, 10 AD, and 5 HD donors analyzed), 20X magnification. (B) FACS analysis of CXCR5 expression in CD4⁺CD3⁺ T cells, derived from lesional AD skin biopsies. Gates for CXCR5⁺ cells were set using isotype staining. Two donors shown.

2. Publication n°2

A quantitative multivariate model of human dendritic cell-T helper cell communication

Cell. 2019 Oct 3;179(2):432-447.e21.

The combinatorial diversity of DC communication molecules that can be expressed at the surface of a DC and modulate the T helper polarization is virtually unlimited. So far, most studies have focused on studying the role of one DC communication molecule or a small set of them, which limits the understanding of their interactions. Here there was a need of a systematic study, taking into account a larger number of molecules and studying their combined impact on T helper cell polarization. Harnessing this complexity of signals could be achieved only using mathematical modeling.

For this project, I was involved in the experimental part. I helped for the experiments from which the dataset was generated, and I mainly performed the experimental validations.

Using the same DC/T coculture system than previously, Maximilien Grandclaude, measured in parallel 36 parameters on the DC (7 cytokines and 29 surface molecules) before coculture and 18 parameters (17 cytokines and expansion fold) on the T cells at the end of the coculture, generating a total of 428 coupled measures on DC and T cells. From those data, Marie Perrot-Dockès, biostatistician, generated an innovative statistical model able to predict the behavior of the 18 T helper parameters in response to the 36 DC-derived signals.

First this model has been extensively validated computationally. It has also been confronted to the literature knowledge. By screening 178 articles, 56 predictions were validated by literature, showing a validation score of 70%, while 290 predictions were novel. Finally, it has been systematically experimentally validated. Using a CD28 blocking antibody during MoDC/T coculture, we were able to demonstrate that the model predicted properly for 11/15 predictions. Then, using a DC-free Th polarization system we were able to validate 7/10 predictions for IL-1, 10/16 for ICOSL and 13/15 for IL-12p70. At the end, the model was able to predict successfully a mean of 73.2% of the input-output relationships examined through experimental validation.

In addition to these systematic validations, we were also able to validate predictions of completely new mechanisms, not known from the literature. First, we demonstrated, using a CD2 agonist antibody in a

Th17 context of DC-free Th polarization, that CD2 induced both IL-17F and IL-17A production. Going further into the characterization of IL-12p70, which has been associated to Th1 polarization until now, we established that combining IL-12p70 with IL-1 β (or IL-1 α) induced high levels of IL-17F without co-production of IL-17A. On the opposite, adding IL-12p70 to an IL-23+IL-1 β context induced IL-17A production, with similar levels of IL-17F than IL-12p70+IL-1 β alone. All these new mechanisms were never described before, but predicted by an advanced version of the model taking into account context-dependent variables.

This DC-T communication model as a potential to be a great resource for the scientific community to provide hypotheses not only on single molecules impact on Th parameters but also of context-dependent associations. Beyond the DC/T system, this strategy can have broad applications to any input-output communication systems.

Title: A quantitative multivariate model of human dendritic cell-T helper cell communication

Authors: Maximilien Grandclaudon^{1,2,8}, Marie Perrot-Dockès^{3,8}, Coline Trichot^{1,2,8}, Léa Karpf^{1,2}, Omar Abouzid^{1,2}, Camille Chauvin^{1,2}, Philémon Sirven^{1,2}, Wassim Abou-Jaoudé⁴, Frédérique Berger^{1,5,6}, Philippe Hupé^{1,6,7}, Denis Thieffry⁴, Laure Sansonnet³, Julien Chiquet³, Céline Levy-Leduc³, Vassili Soumelis^{1,2*}

Authors affiliations

¹ Institut Curie, Centre de Recherche, PSL Research University, F-75005 Paris, France

² INSERM U932, Immunity and Cancer, F-75005 Paris, France

³ UMR MIA-Paris, AgroParisTech, INRA - Université Paris-Saclay, F-75005 Paris, France

⁴ Computational Systems Biology Team, Institut de Biologie de l'École Normale Supérieure, Centre National de la Recherche Scientifique UMR8197, INSERM U1024, École Normale Supérieure, PSL Université, F-75005, Paris, France

⁵ Institut Curie, PSL Research University, Unit of Biostatistics, F-75005, Paris, France

⁶ Institut Curie, PSL Research University, INSERM U900, F-75005, Paris, France

⁷ Mines Paris Tech, F-77305, Cedex Fontainebleau, France

⁸ These authors contributed equally to this work

* Lead contact: vassili.soumelis@curie.fr

Summary

Cell-cell communication involves a large number of molecular signals that function as words of a complex language, the grammar of which remaining mostly unknown. Here, we describe an integrative approach involving: i) protein-level measurement of multiple communication signals coupled to output responses in receiving cells; ii) mathematical modeling to uncover input-output relationships and interactions between signals. Using human dendritic cell (DC)-T helper (Th) cell communication as a model, we measured 36 DC-derived signals, and 17 Th cytokines broadly covering Th diversity, in 428 observations. We developed a data-driven computationally validated model capturing 56 already described, and 290 potentially novel mechanisms of Th cell

specification. By predicting context-dependent behaviors, we demonstrated a new function for IL-12p70 as inducer of Th17 in an IL-1 signaling context. This work provides a unique resource to decipher the complex combinatorial rules governing DC-Th cell communication, and guide their manipulation for vaccine design and immunotherapies.

Key Words: Cell-cell communication, systems immunology, mathematical modeling, signal Integration, immunology, T helper cell differentiation, dendritic cells.

Introduction

Cell-cell communication involves the exchange of molecular signals produced by a given cell and transmitting an effect through specific receptors expressed on target cells. This process requires the integration of multiple communication signals of different nature during homeostatic or stress-related responses. For example, the differentiation of pluripotent hematopoietic stem cells into mature myeloid or lymphoid blood cells requires the collective action of multiple cytokines, growth factors and Notch ligands (Balan et al., 2018). In the context of a stress, multiple signals need to be integrated by innate and adaptive immune cells, including cytokines, growth factors, inflammatory mediators, and immune checkpoints (Chen and Flies, 2013; Macagno et al., 2007). In most studies, these communication molecules have been studied as individual stimuli to a target cell, by gain- and loss-of-function experiments. This provided important knowledge on the downstream effects of the signals, but prevented from widely addressing their function in various contexts of other co-expressed communication signals.

Context-dependency is an important aspect of verbal language communication, which can directly affect the meaning of individual words, but also modify the logic of syntactic rules (Cariani and Rips, 2017; Kintsch and Mangalath, 2011). Similarly, context-dependencies may dramatically affect the function of biologically active communication signals. For example, we have shown that 90% of the transcriptional response to type I interferon in human CD4 T cells depended on the cytokine context (Th1, Th2 or Th17) (Touzot et al., 2014). Other studies have identified major context-dependent functions of immune checkpoints, such as OX40-ligand (Ito et al., 2005), and regulatory cytokines, such as TGF-beta (Ivanov et al., 2006; Manel et al., 2008; Volpe et al., 2008). These studies suggest that communication molecules function as words of a

complex language, with a grammar defining combinatorial rules of co-expression, and mutual influence of one signal over the function/meaning of another signal.

Three levels of biological complexity need to be integrated in order to decipher those combinatorial rules: 1) the multiplicity of input communication signals, in order to include as many possible contextual effects; 2) communication signals at their naturally occurring concentrations; 3) a large number of output responses in target cells, reflecting the impact of cell-cell communication, quantitatively and qualitatively. Those three levels create a bottleneck in deciphering cell-cell communication.

Here, we have developed an integrative approach combining 1) the coupled protein-level measurement of multiple communication signals and output response molecules in target cells, 2) a multivariate mathematical modeling strategy enabling to infer the input-output relationships for individual signals, taking into account the context/configuration of all other signals, and 3) experimental validation of model-derived hypotheses. We have applied this framework to decipher human dendritic cell (DC)-Th cell communication, which potentially involves over 70 individual molecular stimuli (Chen and Flies, 2013), including cytokines, TNF family members, integrins, nectins, notch-ligands, and galectins (Tindemans et al., 2017; Zhu et al., 2010; Zygmunt and Veldhoen, 2011). These molecules can all be expressed by DC, and function as communication signals to T cells (hereafter Th stimuli). They can be measured at the protein level by highly specific assays in order to optimize biological relevance.

By using this unbiased data-driven approach, we could capture the simultaneous effects of large numbers of DC-T communication signals, in naturally occurring patterns and expression levels. Our systems level model revealed novel emergent and context-dependent mechanisms controlling Th cell differentiation. A similar framework can be applied to systematically decipher the communication of other cell types.

Results

Generation of a unique multivariate dataset of human DC-Th cell communication

In order to induce a broad range of DC molecular states, expressing various patterns of communication signals, human monocyte-derived-DC (MoDC) and primary blood CD11c⁺ DC (bDC), were activated for 24 hours with a diversity of DC-modulating signals (hereafter “DC perturbators”). These included 14 distinct stimuli that were

grouped in three categories reflecting various physiopathological contexts: 1) Endogenous factors: IFN- β , GM-CSF, TSLP, PGE₂; 2) Toll-like receptor ligands: LPS (TLR4 agonist), PAM3CSK4 (TLR1/2 agonist), Curdlan (Dectin1 agonist), Zymosan (TLR2 /Dectin1 agonist), R848 (TLR 7/8 agonist), Poly(I:C) (TLR3 agonist), Aluminum potassium sulfate (Alum, NLRP3 inflammasome inducer); 3) Whole pathogens: Heat-Killed *Candida Albicans* (HKCA), Heat-Killed *Listeria monocytogenes* (HKLM), Heat-Killed *Staphylococcus aureus* (HKSA), Heat Killed *Streptococcus pneumoniae* (HKSP), influenza virus (Flu). These 14 DC perturbators were used in distinct doses and combinations to further increase the diversity of DC communication molecules, and downstream functional effects (Table S1). In each independent experiment, we included a Medium condition as negative control, and LPS (100 ng/mL) and/or Zymosan (10 μ g/mL) as positive controls. A total of 66 perturbators were used on MoDC, and 16 on bDC, totaling 82 distinct “DC conditions” (C1-C82, see Table S1). In each DC condition, we measured 36 DC-expressed molecules, which influence Th cell differentiation in at least one published study (Star methods), and can be measured with a highly specific antibody-based assay. Twenty-nine were measured by FACS at the DC surface (Figure S1A), and 7 were measured in the 24 hours DC culture supernatant (Star methods).

Following 24h culture in each of the 82 DC perturbation conditions, the same DC batch was used to stimulate naive CD4 T cells in a heterologous co-culture system. At day 6 of the co-culture, we measured Th cell expansion fold (Exp Fold), and a total of 17 distinct Th cytokines broadly representing the spectrum of Th cell output responses (Star methods). In total, we produced a unique dataset of coupled measurements of DC-derived Th stimuli, and Th response cytokines in 428 independent observations, from 44 independent donors (Figure 1A, Table S2).

Variability and specificity of DC communication signals

We asked whether our systematic DC stimulation strategy could generate important variations in the expression of individual DC-derived Th stimuli. All Th stimuli were expressed over at least three logs (Figure 1B), with high coefficients of variation (>0.44) (Figure 1C). Interleukins had the higher variability, (10^4 to 10^5), and high coefficient of variation, from 2.72 for IL-12p70 (IL-12) to 1.43 for IL-6. CD11a had a wide expression range (10^4) but the smallest coefficient of variation (0.44), with values

distributed around the mean (Figure 1C). Hence, we were able to generate highly variable expression patterns for all Th stimuli.

We sought to identify conserved, and specific patterns of Th stimuli in response to standard DC perturbators. We compared the expression levels of DC-derived Th stimuli in three conditions belonging to distinct classes of microbes, LPS (100 ng/mL) (Bacteria), Zymosan (10 µg/mL) (Fungi), and Flu (1X) (Virus), which were used across at least 17 MoDC biological replicates (Figure 1D). Medium-MoDC (negative control) expressed lower levels of activation-associated communication molecules (Figure 1D and S1B). We confirmed previous findings validating our experimental system: 1) Zymosan induced specifically IL-10 and IL-23, 2) Flu induced large amount of IL-28 α , and 3) LPS and Zymosan induced large amount of IL-12 (Figure 1D and S1B). In addition, we identified novel specific inductions of DC-derived Th stimuli: Zymosan-treated MoDC expressed the highest levels of CD54 and PVR, Flu-treated MoDC specifically induced ICOSL, and LPS-treated MoDC induced the highest level of CD30L and CD83 (Figure 1D). Specificity of expression of a given signal for a given DC stimulation was determined using Wilcoxon statistical test (Figure S1B). Hence, standard DC perturbators induced specific patterns of Th stimuli.

Defining the spectrum of DC communication states

Next, we aimed at assessing the spectrum of DC communication states, as defined by their expression pattern of communication signals, across the 82 DC conditions. We computed the mean expression of biological replicates for each DC-derived Th stimuli and performed unsupervised hierarchical clustering, in order to identify classes of the most similar conditions (C1 to C82, y axis) and DC-derived Th stimuli (x axis) (Figure 2A). This revealed five groups of DC conditions (Figure 2B). Each of the four standard DC conditions (Figure 1D), belonged to different groups (Figure 2A).

Group 1 was defined by the high expression of adhesion molecules such as CD18, ICAM-2, ICAM-3, and CD29, low levels of co-stimulatory molecules and cytokines, with the exception of high IL-28a. Group 2 showed low expression for most DC-derived Th stimuli, but high levels of integrins, VISTA and B7H3, suggesting a capacity to interact with T cells and transmit co-inhibitory signals. Group 3 showed a complimentary pattern, lack of Group 1- and Group 2-specific molecules, and intermediate or high levels of co-stimulatory molecules, such as CD83, CD86, HLA-DR, 4-1BBL and OX40L. This suggested potent T cell stimulating functions. Group 4 exhibited high

levels of molecules from the B7 and TNF super-families, such as CD80, CD86, PDL1, PDL2, CD40 but intermediate or low cytokine levels. In contrast, Group 5 showed the highest level of cytokines, and molecules of the B7 and TNF super-families (Figure 2B).

Next, we sought to analyze intra-cluster heterogeneity. We selected three pairs of perturbators being the most closely related as defined by Euclidian distance (C32 (MoDC HKLM MOI1) and C33 (MoDC HKCA MOI1), C47 (bDC LPS 100 ng/mL) and C48 (bDC HLKM MOI1), C61 (MoDC R848 1 µg/mL) and C62 (MoDC PAM3 10 µg/mL)), and compared them for the expression of the 36 DC-derived Th stimuli (Figure 2C). C32 and C33 did not exhibit significant differences in CD80 and CD86 expression reflecting equal level of DC activation. They were statistically different only for IL-6, with levels ranging from complete absence in C33 to over 1 ng/mL in C32 (Figure 2C). In contrast, the pairs C47/C48 and C61/C62 showed significant differences for multiple Th stimuli. C47 expressed significantly more CD86, PDL1 and IL-1 than C48. On the contrary, C48 expressed higher levels of 4-1BBL. C61 and C62 showed marked differences in CD70 and IL-12 (higher in C61), and OX40L (higher in C62) levels. Hence, each DC condition expressed unique combinations of DC-derived Th stimuli, suggesting different communication potential with CD4 T cells.

An unsupervised Gaussian mixture model showed that the highest BIC value corresponded to 82 groups, confirming that each DC condition induced a unique profile of the 36 communication molecules (Figure 2D).

Using principal component analysis (PCA), we showed that neither the date of the experiment, nor the donor batch had major impact on the clustering (Figure S1C, and Star methods).

The heterogeneity of DC-induced Th cytokine responses

We characterized the diversity of CD4 T cell output responses, as assessed by Th cytokine profiles following co-culture of naive CD4 T cells with activated DC across the 82 conditions previously described. Th cytokines exhibited important variations across the 428 observations (Figure 3A). Some cytokines such as IL-2, TNF- α , GM-CSF, TNF- β , IL-3 were always detected (Figure S2A).

To identify Th subset signatures, we compared cytokine expression in our four standard conditions, Medium (negative control), LPS, Zymosan and Flu. The Th17 cytokines, IL-17A and IL-17F were induced predominantly in Zymosan-MoDC. LPS-

MoDC induced mixed Th1, Th2 and Th9 responses characterized by high IFN- γ , IL-13, IL-3, and IL-9, as compared to medium. Flu-MoDC, induced the Th2 cytokines IL-4, IL-5, IL-31 (Figure 3B and S2B). These results indicated that in LPS, Zymosan and Flu conditions, each DC state induced a distinct set of Th cytokine responses, corresponding to prototypical Th signatures or mixed Th profiles.

Th cytokine responses mirror the variability in DC communication states

We asked whether Th cytokine responses would reveal distinct patterns, or a continuum of responses mirroring each of the DC communication states (Figure 2A). We performed a hierarchical Pearson clustering on our 18 distinct Th-derived variables, across the entire 82 DC-activating conditions (Figure 3C). This revealed 6 distinct groups, although intra-group heterogeneity was evident in almost all groups. Interestingly, DC perturbation conditions (C1-C82) did not appear in the same order as compared to the DC communication signal clustering (Figure 2A), indicating that closely related patterns of DC-derived Th stimuli did not necessarily induce the closest patterns in Th cytokine responses.

Group 1 was dominated by production of IL-10, IL-22, IL-5, GM-CSF, IL-3, IL-31, IL-13, IL-4 (Figure S2C). Group 2 was the most heterogeneous, and included the inflammatory cytokines TNF- α and IL-6, co-expressed with variable levels of Th1 (IFN- γ) and Th2 (IL-4, IL-13) cytokines (Figure S2C). Group 3 expressed IL-21, IFN- γ and IL-17F, but no or low IL-17A, suggesting the possibility of differential regulatory mechanisms (Figure S2C). Group 4 was dominated by the Th17 cytokines IL-17A and F, group 5 by IL-22, and group 6 by IL-2. Distinct sets of DC perturbation condition, hence patterns of DC-derived communication molecules, were associated with each of these groups (Figure 3C). This was the first suggestion of specific rules underlying input-output relationships in DC-Th communication.

Because of intra-group heterogeneity, we asked whether most correlated conditions within the same cluster would differ from each other (Figure 3D). C12 and C33 were associated to different levels in IL-17F, while C42 and C47 were different in IL-2, and C46 and C49 were different in IL-6 and GM-CSF levels (Figure 3D). As for the DC dataset, we found that 82 was the best number of groups in our Th-derived dataset based on a Gaussian mixture model (Figure 3E). This suggested that a single DC profile of communication molecules would induce a unique set of Th cytokines.

A data-driven Lasso penalized regression- model predicts Th cytokine responses from combinations of DC-derived Th stimuli

Having generated distinct patterns of DC-derived communication signals, associated with a diversity of induced CD4 T cell cytokine responses, the question of their relationship appeared critical in order to decipher DC-Th communication. Given the complexity of the dataset, and the lack of clear hypotheses concerning the majority of DC-derived Th stimuli, we applied an unsupervised mathematical modeling strategy (Figure 4A).

The MultivarSel strategy with stability selection performed similar to the internal positive control, and better than other methodologies tested (Figure S3A and Star methods). Therefore, we applied MultivarSel to the modeling of our experimental data (Figure 4A). This methodology takes into account the dependencies that may exist among Th cell cytokines, and combines Lasso criterion and stability selection to select associations between DC-derived signals (INPUTS) and Th cytokines (OUTPUTS) (Star methods).

Our multivariate model identified a large number of significant positive (red) and negative (blue) associations of the 36 DC-derived Th stimuli with the 17 Th-derived cytokines (Figure 4B). White squares represent the absence of significant association (Figure 4B). The frequency of selection obtained for each input-output association is provided in Figure S3B.

Our mathematical model revealed 1) the impact of each DC communication signal on Th output responses, and 2) the critical regulators for each Th cytokine. For example, negative regulators of IL-10 were OX40L, 4-1BBL, IL-12, TNF- α , CD58, VISTA, Galectin-3, CD80, CD29, IL-1, ICAM-3, SLAMF3, IL-28 α , CD83, and positive regulators were Jagged-2, PDL1, IL-10, CD11a, HLA-DR, ICOSL, CD100, CD30L, CD18, ICAM-2, CD86 (Figure 4B). Hence, the model can predict the IL-10 production by responding Th cells for any DC, given the expression level of these molecules. It allows simulating loss or gain-of-function of an input. Similar insight can be obtained for each of the 17 Th cytokine responses, which may be explained by a combination of DC-derived communication signals.

We used computational cross-validation to evaluate the error of prediction of our model (Figure 4C). For all Th cytokines, the multivariate outperformed the best univariate model (Figure S3C). We ranked Th cytokines based on their prediction errors: Th

variables best explained by our model were IL-6, IL-17F, Exp Fold, and IL-3 (Figure 4C).

In order to address DC type specificity in model performance, we calculated the cross-validation error for each Th output of the MoDC and bDC dataset, respectively. Our model predicted equally well the majority of the outputs for the two DC types (Figure S3D). For a few outputs, mostly IL-22 and TNF- β , the model was more error prone in bDC than MoDC (Figure S3D). Interestingly, a higher prediction error was found for TNF- β only in 5 out of 118 observations (Figure S3E), where TNF- β levels were very high (range 6.7-22.2). This suggested that a TNF- β -promoting input signal might be involved in those 5 cases but not included in our model. For IL-22, more observations had a higher prediction error in bDC as compared to MoDC, but the prediction error range and distributions were similar, suggesting that the input-output relationship was conserved (Figure S3E).

We performed hierarchical clustering for both DC and T cell-derived variables to identify co-regulations between Th outputs. We retrieved relevant clusters of Th cytokines belonging classically to the same Th subset (Figure 4B). Th2-related cytokines IL-13, IL-31, IL-5, IL-4, IL-10 and GM-CSF were found in the same cluster, suggesting that their induction would be controlled by similar mechanisms. IL-17A and IL-17F were also in the same cluster, implying that the model associated them with closely related DC communication signals (Figure 4B). Surprisingly, our model closely related IL-9 expression to IL-17A and IL-17F, suggesting common regulators. It also clustered IL-22 closer to the Th2 than to the Th17 cytokines. IL-21 was associated with the Th1 cytokines IL-2 and IFN- γ (Figure 4B).

Multivariate DC-Th model reveals novel regulators of Th cytokine responses

We systematically confronted our model results to the literature, as a knowledge-based validation, but also novelty assessment. We screened 178 relevant articles (Star methods) and extracted information on specific molecular control of a given Th cytokine by DC-derived signals measured in our model (Table S3). We computed a validation score based on the number of articles identifying the same associations than our model (Star methods). IL-12 ranked as the top DC communication signal for which our model predictions globally recapitulate existing knowledge (8 out of 13 predicted

associations). Among other known associations, IL-23 was positively associated with IL-17A and F, IL-10 was positively associated with IL-10 and negatively with IFN- γ , and CD40 was positively associated with IFN- γ .

However, the model also predicted 290 associations that were not previously described. Putative novel regulators were identified for all Th outputs (Table S4). The robustness of each prediction could be estimated by the value of the coefficient and by the frequency of detection of the association (Table S4). Examples of high scores were for B7H3 and CD83 association with IL-4, 4-1BBL association with IL-9, ICOSL association with IL-13, and OX40L negative association with IL-22 (Table S4). Overall, literature knowledge was retrieved for 80 distinct input-output relationships presented in our model (Figure 4B), 56 were in agreement with our model, representing a global literature validation score of 70%.

Systematic and independent experimental validation of model's predictions

We performed a systematic experimental validation by selecting a subset of target inputs and measuring systematically the Th outputs selected by our model. We assessed the novelty of each validated prediction (Table S3).

First, we addressed systematic validations of model predictions by blocking experiments (Figure 5A). We performed a double in silico knock out for CD80 and CD86 in the three conditions, LPS (100 ng/mL), Flu (1X) and Zymosan (10 μ g/mL) MoDC, in which CD80 and CD86 were highly expressed, and predicted an impact on 15 distinct Th outputs (Figure 5B), 11 of which being successfully experimentally validated (Star Methods). The positive role of CD80 and CD86 on IL-3 and IL-31 were to our knowledge not described elsewhere. The predictions that we failed to validate were for IL-4, IL-5, IL-10 and TNF- α (Figure S4A), all predicted to be decreased by CD80/CD86.

Then, we validated the effects of three additional inputs: IL-1, ICOSL and IL-12 used as exogenous factors (Figure 5C). First, we gave the selected input together with anti CD3/CD28 signals (Th0), and measured systematically all Th outputs predicted by the model to be influenced by that input. In the absence of any effect, we gave the selected input in a Th2 (IL-4) or Th17 (IL-6, IL-1 β , IL-23 and TGF- β) condition, in order to detect additional synergistic or inhibitory effects required to validate the predicted effect. For

example, it is not possible to validate the inhibition of a Th2 cytokine without a significant production of this cytokine at baseline.

We focused on the ten predictions made by our model for IL-1 (Figure 5D). By adding IL-1 β to the Th0 condition, we were able to detect significant up-regulation of IL-6 and IL-17F, and significant down-regulation of IL-10 and IL-13. IL-10 down-regulation and IL-6 up-regulation were also significant in the Th2 context (Figure S4B). In a Th2 condition, we validated the significant up-regulation of TNF- α and down regulation of IL-9 by IL-1 β (Figure S4B), not seen in Th0 (Figure S4B). In a Th17 condition we observed the positive effect of IL-1 β on IL-17A. We could not validate the predictions regarding IL-21, IL-31 and IL-22 (Figure S4B). In total, 7 out of 10 predicted effects of IL-1 were validated. Interestingly, the positive role of IL-1 β on the induction of IL-6 by Th cells was not known (Table S3), and may suggest new biology and amplification loops in an inflammatory context.

We used a similar strategy to validate predictions regarding ICOSL, using an anti-ICOS agonistic antibody. Overall, we validated 10 out of 16 predictions (Figure 5E, S4C, and Star Methods). Interestingly, five out of the 10 validated predictions were novel (Table S3): IL-5, IL-13, IL-3, GM-CSF and IL-22, suggesting common pathways to induce IL-22 and Th2 responses.

Finally, we experimentally tested the predictions regarding IL-12 (Figure 5F). Adding IL-12 to the Th0 validated an induction of IFN- γ , IL-21, Exp Fold and TNF- β . We also validated the inhibitory role of IL-12 on Th2 cytokines (IL-4, IL-5, IL-13), IL-6, and IL-22 production. Using the Th2 condition we further validated the inhibitory role of IL-12 on IL-10 and IL-31. The effects of IL-12 on TNF- β , IL-31 and IL-6 have not been previously described (Table S3).

Since using our anti-CD3/CD28 system did not allow validating IL-12 effects on IL-2, IL-17F, IL-3 and IL-9 (Figure S4D), we wondered if DC-dependent factors could impact the role of IL-12 on these cytokines. We selected DC conditions with very low production of IL-12 (C51 and C55) (Figure 2A), and performed a co-culture with naive T cells adding or not IL-12. As a positive control, IL-12 was able to induce IFN- γ in both Zymosan and HKSA conditions (Figure S4E). We did not validate the role of IL-12 on

IL-2 or IL-17F regulation (data not shown). However, we validated that IL-3 was induced by IL-12 in both Zymosan-DC (C51) and HKSA-DC (C54) (Figure 5G), while IL-9 was significantly up-regulated only in HKSA-DC. Overall, we were able to experimentally validate 13 out of 15 predictions regarding IL-12.

Our systematic strategy established a validated prediction of the input-output relationship in 41 out of 56 cases (73.2%), 13 representing new mechanisms identified by the model. This number is similar or higher to the computational cross-validation (Figure 4C). Predictions with higher stability selection frequencies were more validated than those with low stability selection (Figure S4F). However, the value of the model's coefficients was not statistically different between the two groups (Figure S4F), indicating that the model efficiently captured associations with low coefficient values.

Although IL-12 was the input best explained by our model, we could not validate the predicted association between IL-12 and IL-17F (Figure S4D), neither in the literature nor in our systematic experimental validation. Previous studies have shown either no impact (Volpe et al., 2008) or a negative impact (Acosta-Rodriguez et al., 2007) of IL-12 on Th17 differentiation. We hypothesized that context-dependent effects may lead to new functions of IL-12, not accomplished by IL-12 as a single agent.

Context-dependent model reveals a role for IL-12 in Th17 differentiation

We designed a strategy to capture context-dependent effects of one input on any given output by integrating new composite variables into the model (Figure 6A). These new input variables were based on the co-occurrence of a given input with other DC-derived communication signals (i.e. contexts). They adopted the value of the given input (for instance IL-12) in each observation where the co-expressed DC signal was present, and they took a zero value when the co-signal was absent. We could derive 455 context-dependent variables.

The model including all context-dependent variables performed less well (higher error of prediction) than our classical MultiVarSel strategy (Figure S5A), most likely due to over fitting issues dependent on the dataset size, with a number of input variables exceeding the number of data points used to fit the model. Therefore, we derived 36 models, each one integrating the context-dependencies of one input (Table S5). For each of these models, we reported the coefficient and the stability selection

frequencies of each input (Table S5). In order to globally estimate the influence of context-dependencies within our data we quantified the number of times an input variable was selected, either “alone” or “with” another one. We derived percentages of context-dependencies and represented the results either per input (Figure S5B) or per output (Figure S5C). The inputs most likely to present “context-dependent” functions were PDL1 and SLAMF3, while CD11a and CD70 were mostly context-independent (Figure S5B). When analyzing the outputs, the models revealed that all cytokines could be regulated by context-dependent mechanisms, with relatively similar percentages (range: 0.13-0.22) (Figure S5C).

We used this strategy to explain the role of IL-12 in the control of Th17 differentiation through the identification of context-dependent effects. We found that adding context-dependent variables for IL-12 improved the model predictions for IL-17F and performed equally well for IL-17A (Figure 6B). We then focused on DC-derived signals that were kept significant by the model, and observed distinct associations of the new IL-12 context-dependent variables with IL-17A and IL-17F (Figure 6C), including some differentially associated with IL-17A and IL-17F, respectively. Among various contexts, we found that IL-12 in the context of IL-1, ICAM-2 or Jagged-2 was associated with IL-17F, while IL-12 in the context of CD70, IL-23 or LIGHT was associated with IL-17A.

As a first level of *in silico* validation, we selected a DC condition in which IL-12 was co-expressed with many of these contexts, and DC-derived signals induced IL-17A and F by responder Th cells. Zymosan (10 µg/mL) on MoDC fulfilled these criteria (Figure 1D and 3C). To study the specific effects of IL-12 in the context of all other DC communication signals induced by Zymosan, we performed *in silico* IL-12 knock-out in the IL-12 context-dependent model. We compared predicted values for IL-17A and IL-17F when IL-12 was kept or not in the model (Figure 6D). *In silico* knock-out of IL-12 diminished the production of both IL-17A and IL-17F in the Zymosan (10 µg/mL) condition. As experimental validation, we performed independent DC/T coculture experiments using MoDC treated with 10 µg/mL Zymosan, in the presence and absence of IL-12 neutralizing antibody (Figure 6E). Blocking IL-12 significantly decreased the production of IL-17A and IL-17F, as predicted (Figure 6E), and inhibited IFN-γ production (Figure S5D). The same model predicted no effect of blocking IL-12 in Curdlan-MoDC (Figure S5E), which we experimentally validated (Figure S5F).

Synergistic interaction between IL-12 and IL-1 explains induction of IL-17F without IL-17A

Our model predicted distinct roles of IL-12 on IL-17A and IL-17F production depending on the context in which IL-12 is expressed. Interestingly, IL-12, IL-1 and CD80 were the top variables almost systematically selected by the model to explain the differences between IL-17A and IL-17F (Figure 7A). This corroborated the results in Figure 6C where we found that IL-12 in the context of IL-1 was associated to IL-17F but not IL-17A. The model estimate for a stability selection of <0.8 indicated that IL-12, IL-1 and CD80 were positive contributors to the differences between IL-17A and IL-17F (Figure S6A). Consequently, we hypothesized that the combination of IL-12 with IL-1 would induce IL-17F independently of IL-17A.

To experimentally validate our hypothesis, we used a DC-free Th polarization assay, allowing us to specifically study the interaction between IL-12 and IL-1 regardless of any other molecular context. Naive CD4 T cells were polyclonally activated with anti-CD3/CD28 beads, and put in distinct cytokine treatments: Th0 (no cytokine) and Th2 (IL-4), as negative controls, Th17 (IL-1 β +IL-23+IL-6+TGF- β) as a positive control, IL-12, IL-1 β , and IL-12+IL-1 β . IL-12 alone induced IFN- γ and IL-21, and inhibited Th2-related cytokines, as expected (Figure S6B). IL-12 alone induced neither IL-17F nor IL-17A, but combining IL-12 to IL-1 β dramatically induced IL-17F at levels comparable to the positive control, without detectable amount of IL-17A, which fully validated the model predictions (Figure 7B).

This effect was specific to the IL-12+IL-1 β combination, since neither IL-6, nor IL-23, nor TGF- β alone or combined to IL-12, could induce IL-17F expression (Figure S6C). The exact same pattern of Th cytokine expression was obtained by combining IL-1 α or IL-1 β to IL-12, which fitted model predictions since those two variables were highly correlated (Figure S6D). The capacity of IL-12+IL-1 β to induce IL-17F was resistant to the presence of other Th differentiation factors, such as IL-4 (Figure S6E). Using cell trace violet (CTV) (Figure S6F) we could show that the production of IL-17F could not be attributed to distinct proliferation capacity of Th cells in the IL-12+IL-1 β condition.

Next, we questioned whether Th cells generated in the IL-12+IL-1 β condition would express transcription factors classically associated to Th17 differentiation. We

measured 63 RNA transcripts by qPCR in Th0, Th2, IL-1 β , IL-12, IL-12+IL-1 β , and Th17 conditions (Table S6). The 63 genes included master regulators of the Th1 and Th2 subsets, such as T-bet and GATA3, respectively, and Th17 regulators, such as RORc, STAT3, BATF, and SATB1 (Ciofani et al., 2012). IL-17A and IL-17F regulation at the mRNA level mirrored the protein level (Figure S6H). IL-12+IL-1 β induced significantly more RORc, BATF, and Bcl6, than IL-12 or IL-1 β alone (Figure S6H), which could explain the induction of IL-17F and IL-21. Still, the levels of RORc and Bcl6 were lower in IL-12+IL-1 β than in Th17 condition (Figure S6H). T-bet was highly induced in IL-12+IL-1 β in comparison to IL-12 or Th17 conditions, indicating that Th1 differentiation was maintained, and that T-bet did not inhibit IL-17F production. IL-12Rb2, a Th1 marker, was downregulated by IL-1 β when added to IL-12, while IL-12, IL-12+IL-1 β and Th17 conditions all induced the IL-23 receptor (Figure S6H). SATB1 was specifically up-regulated in IL-12+IL-1 β in comparison to Th17 or IL-1 β alone (Figure S6H), suggesting that it could play a role in the specific up-regulation of IL-17F. In order to globally assess the expression of the various Th lineage-specific factors, across IL-12- and IL-1-containing conditions, we performed a PCA including all 63 mRNA variables (Figure S7A). Cells from the IL-12+IL-1 β condition had an intermediate expression pattern, between the IL-12 (Th1) and Th17 conditions. By decomposing the PCA space into vectors for each variable, we found that IL-17F, IL-23R, ICOS, and T-bet, projected predominantly along the IL-12+IL-1 β condition (Figure S7B), again pointing at mixed Th1/Th17 features.

We then addressed the link between IL-12 and IL-17A, in various contexts. IL-12 with IL-23 were predicted to induce IL-17A but not IL-17F (Figure 6C). In a DC-free Th polarization assay, we used IL-12, IL-23, or IL-12+IL-23, and found that none of these conditions induced IL-17A (Figure 7C). We hypothesized that a third input could explain the positive link between “IL-12_with_IL-23” and IL-17A. Using an unsupervised analysis, we found IL-1 as a top variable with the highest correlation (Figure S7C). In addition, IL-12 and IL-17A positive correlation was significant specifically in the group of data points where IL-23 and IL-1 were expressed (Figure S7D and S7E), and was lost when only IL-1 or IL-23 were expressed with IL-12 (Figure S7D). Therefore, we tested if IL-12+IL-23 would induce IL-17A in the presence of IL-1 β . We validated a significant induction of IL-17A, with no effect on IL-17F, when IL-12 and IL-23 were given in the presence of IL-1 β , as compared to IL-12 or IL-23 (Figure

7C). We measured IL-17A and IL-17F by qPCR and retrieved the same induction pattern (Figure S7F). Last, we could show that RORc was higher in IL-12+IL-23+IL-1 β than in IL-12+IL-1 β (Figure S7F).

Finally, we observed that our modeling strategy always identified CD58 as a main Th17 inducer since it impacted positively both IL-17A and IL-17F (Figure 4B and 6C), an association that we had not seen through our systematic literature review (Figure 4D and Table S3). To test this hypothesis, we used an agonist anti-CD2 antibody that mimics the presence of CD58 (Star Methods). As predicted, IL-17A or IL-17F were not induced by anti-CD2 alone in Th0 condition. However, anti-CD2 significantly induced the production of IL-17A and IL-17F in Th17 conditions (Figure 7D), which was confirmed by intracellular FACS staining (Figure S7H and S7I), with IL-17F upregulation restricted to IL-17A positive cells (Figure S7I).

In order to establish the cytokine co-expression profiles of IL-12+IL-1 β -treated Th cells at single cell level, we performed intracellular cytokine staining (Figure 7E). We confirmed that IL-12+IL-1 β induced significantly more IL-17F-positive Th cells without co-production of IL-17A (Figure 7F). In naive CD4 T cells polarized with the Th17 cytokine cocktail (IL-1 β , IL-6, TGF- β , IL-23) we mainly found two subsets of Th17 cells, producing either IL-17A or IL-17F, with very few cells co-producing both cytokines. To check for in vivo existence of those IL-17A and IL-17F single producers, we analyzed the human CD4 T cell memory compartment by intracellular FACS in healthy donor PBMC. We could identify a small fraction of Th cells expressing only IL-17F in the absence of IL-17A, suggesting that this phenotype constitutes a differentiation endpoint (Figure 7G).

To gain more insight into the functional properties of these “Th17F” cells, we studied their co-production with IL-21, IFN- γ , and IL-22, all being relevant to the Th17 and/or IL-12 pathways, in vitro (Figure S7J) and ex vivo (Figure S7K). Among IL-17F⁺IL-17A⁻ cells generated with IL-12 and IL-1 β , the majority co-produced IFN- γ (41.8%), IL-21 (10.5%) or both (24.1%) (Figure 7H) reflecting a dominant role for IL-12. IL-17F⁺IL-17A⁻ memory CD4 preferentially co-expressed IL-21 (30.3%), and IL-21 together with IFN- γ (17.5%) (Figure 7I), which matched the in vitro differentiated CD4 T cells. In addition, the percentage of IL-17F⁺IL-17A⁻IL-22⁻IL-21⁻IFN- γ ⁻ cells between in vitro IL-12+IL-1 β stimulation, and the ex vivo restimulated memory compartment was similar

(22.2%), which indirectly supported that IL-12+IL-1 β induced the emergence of IL-17F single producers.

Taken together, our results demonstrated a synergy between IL-12 and IL-1 in inducing IL-17F single producing Th cells, with possible physiopathological relevance.

Discussion

Cell-cell communication may involve several tens of communication signals functioning concomitantly and possibly interacting with each other. These signals in turn modify many molecular and functional parameters in target cells. Such complexity cannot be captured and formalized without an integrated mathematical modeling approach. Theoretical models of Th cell differentiation have already been established (Abou-Jaoude et al., 2014; Naldi et al., 2010), and include a large number of possible inputs to T cells. However, they suffer from three limitations: 1) they include input signals that may be expressed by diverse cell types, in different anatomical locations, 2) they do not recapitulate combinations of input signals in their naturally occurring patterns and concentrations, 3) they use prior knowledge to infer input-output relationships, which does not integrate possible context-dependencies and interactions. In parallel, data-driven models have been developed in response to predefined stimuli, such as Th17 (Yosef et al., 2013) or Th1/Th2 (Antebi et al., 2013), which do not recapitulate the integration of multiple communication signals. In our study, we applied an unbiased data-driven approach specifically designed to model DC-Th communication. Combinations and concentrations of input communication signals were measured as naturally determined by their intrinsic biological regulation. Subsequently, the input-output relationships were learned from the experimental data, and integrated any underlying context-dependency and interaction, even when not previously described. This maximizes the relevance of the model and the potential for novel discoveries.

Cells can change state in response to environmental cues, a concept defined as plasticity (da Silva-Diz et al., 2018; Liu et al., 2001). Each cell state may be associated to different communication potential, i.e. different expression patterns of communication signals (Soumelis et al., 2002; Wang et al., 2014). In order to broadly cover the possible DC states, we used various DC stimulatory conditions (cytokines, virus, bacteria, fungi), at various doses, and combinations, and across a large number of observations (>400). This prevented from biasing our observations towards certain quantitatively or qualitatively extreme behaviors. After the model has learned the rules

from such an extended range of observations, we anticipate that it should be able to predict behaviors in situations not necessarily covered in our original dataset, as confirmed in our computational and experimental validations. This opens possibilities of applications in many areas of immunology, inflammation, and immunotherapy.

RNAseq has offered a means of capturing the expression of many communication signals and their receptors, in order to infer cell-cell communication between various cell types (Vento-Tormo et al., 2018). However, the RNA-to-protein correlation can be rather low (Liu et al., 2016), and varies a lot depending on the gene (Edfors et al., 2016). Consequently, RNA copies of a gene cannot be associated to a given functional output, preventing quantitative mathematical modeling. Functional response in target cells can only be estimated indirectly, through surrogate activation markers, which is most often not performed. In our approach, all measurements of communication signals and output variables were done at the protein level, hence directly measuring the bioactive communication molecules, with a direct link to a specific response in target cells. This ensures robustness of the modeling strategy, as evidenced by our model's ability to recapitulate most of the known relationships in DC-Th cell communication.

Modeling complex biological behaviors in a quantitative manner is challenging. In data-driven models, it relies in large parts on the choice of explanatory (input) variables, which drive the induction/regulation of output variables. Here, we have selected DC-derived communication molecules through an exhaustive literature mining. The model was able to integrate 36 input and 18 output variables in a quantitative manner, which makes it a reference in the field. We have been able to describe patterns of DC communication molecules in a way that goes beyond the classical view of immature versus mature DC (Banchereau and Steinman, 1998; Guermonprez et al., 2002). In fact, we showed that almost each DC stimulatory condition leads to a distinct DC state. This is a first step into defining general combinatorial rules of DC-derived communication molecules: co-expressed molecules form the basis of putative context-dependent effects. Through the large number of variables handled by the model, we have identified 290 novel associations explaining major immunoregulatory cytokines, which may lead to the discovery of novel functions of known DC molecules, and suggest novel therapeutic targets.

Going further into the complexity of communication, we explored context-dependencies of communication signals. In verbal communication, the context may

dramatically alter the meaning of an individual word. Currently, there is no systematic way to search for context-dependencies in biological communication. In our modeling strategy, we have devised a method that introduces context-dependent variables for a given molecule. This allows for unbiased identification of context-dependent functions, which would have been missed by classical regression models. For example, we identified a new function for IL-12 in promoting IL-17F production by Th cells, which was completely unexpected based on prior knowledge (Korn et al., 2009). Identifying such context-dependencies before therapeutic targeting of a DC-Th communication molecule, may improve the prediction of its effect.

Given that DC-Th communication is central to a large number of physiopathological conditions (Keller, 2001), we can foresee multiple applications of the model. Based on expression pattern of DC molecules, the model can predict the induced Th cytokine profile. Quantitative measurements of DC communication molecules in a given disease or in an individual patient *ex vivo* can be used to simulate the corresponding Th response. Depending on the outcome, strategies may be devised to re-orient the response towards a protective or less pathogenic profile, again through model-based predictions. Alternatively, starting from a Th profile (cytokine or groups of cytokines), the appropriate molecular targets can be manipulated through gain- or loss-of-function experiments in order to amplify or inhibit a given Th cytokine. Last, the model can help predict the most appropriate vaccine adjuvant to obtain a protective immunity to some microbes, or to re-orient a pathogenic Th response. For example, all DC molecules positively associated in the model to Th2 responses are potential targets to decrease pathogenic Th2 allergic inflammation (Ito et al., 2005; Nakayama et al., 2017; Soumelis et al., 2002).

Using DC-Th communication as a model, we have established a framework that can now be applied to other types of cell-cell communication following 5 major steps: 1) systematic perturbation of the “sender” cell in order to generate a diversity of communication states, 2) broad, quantitative and protein level measurement of communication molecules relevant to the “sender” cell, 3) systematic quantitative assessment of the response in “receiver/target” cells, 4) MultivarSel modeling of the input-output relationship, which defines communication rules, 5) *in silico* and experimental validation. Currently, we believe that cell type-specificities in the expression of communication molecules and in their function would prevent from generalizing our DC-Th model to other cell types. Comparing different quantitative

models of cell-cell communication will ultimately tell us whether cells speak the same language, i.e. whether they express similar patterns of communication molecules, and whether the same communication molecule has the same meaning/function when expressed by two different cell types.

Author Contributions

M.G., C.T., L.K., C.C., and P.S. performed experiments; M.G. and V.S., designed the experiments, M.P.D. performed statistical analysis. O.A., W.A-J. and M.G. performed literature mining. P.H., D.T., F.B., L.S., J.C., C.L-L., V.S., participated and supervised the statistical analysis. M.G. and V.S. wrote the manuscript. V.S. supervised the study.

Acknowledgments

We thank the Institut Curie Cytometry platform for cell sorting, P. Gestraud and F. Coffin for advice in statistical analyses, O. Lantz and N. Manel for important discussions. We wish to thank L. Pattarini, B. Fould, W. Cohen, O. Geneste, B. Lockhart, V. Blanc and their teams, from the Institut de Recherche Servier for having produced and generously shared the anti-ICOS antibody. This work was supported by funding from ANR-16-CE15-0024-01, ANR-10-IDEX-0001-02 PSL*, ANR-11-LABX-0043 and CIC IGR-Curie 1428. M.G. was funded by ANRS and ARC.

Declaration of Interests

The authors declare no competing interests.

Figure Legends

Figure 1: Variability and specificity of DC communication signals. A) Experimental strategy B) Raw expression values of the 36 DC communication signals (n=428 data points) C) Statistical descriptors of the 36 DC communication signals: expression range (log magnitude), percentage of positive observations among the 428 datapoints, coefficient of variation. D) Average expression values and Standard Deviation (SD) shown for the four indicated DC signals for MoDC.

Figure 2: The diversity of DC states is defined by unique combinations of communication molecules. A) Heatmap showing expression values of each 36 DC derived signals performed with hierarchical clustering on Pearson metrics for the DC signals and Euclidian distances for the 82 DC conditions B) Expression profiles of the

36 communication molecules within the five groups of DC conditions defined by hierarchical clustering. Expression data were logged and scaled so as μ represents the mean and σ the SD of the expression of a given DC signal across the whole dataset. C) Average expression values and SD for selected DC signals for pairs of stimulatory conditions defined as being the most correlated within our dataset by Pearson correlation. D) Best number of groups by gaussian mixture model determined using the 428 points of the 36 DC parameters.

Figure 3: Th cytokine responses mirror the variability in DC communication states. A) Raw expression values of each of the 18 Th derived parameters (n=418 data points). B) Average expression values and SD for all Th derived signals in MoDC conditions, Medium, LPS, Zymosan and Flu. C) Heatmap of expression values of each 18 Th parameters performed with hierarchical clustering on Pearson metrics for the DC signals and Euclidian distances for the T cell conditions. D) Mean expression values and SD of Th signals for pairs of conditions selected as being the most correlated within our dataset by Pearson correlation. t-test. E) Best number of groups by gaussian mixture model determined only using the 428 points of the 18 Th parameters.

Figure 4: A data-driven Lasso penalized regression model predicts Th differentiation outcomes from DC-derived communication signals. A) Mathematical modeling strategy. B) Heatmap of the model's coefficient values of the MultivarSel derived model explaining the 18 Th parameters based on the 36 DC derived signals. Pearson correlation-based hierarchical clustering. C) Prediction error values obtained by 10-fold cross-validation for Th parameters using the multivariate model (yellow) and the best univariate model (grey) within the 36 DC signals. D) Literature-based validation score. For each DC signal, all predicted associations with Th cytokines were categorized as “new”, “validated” or “contradictory”.

Figure 5: Independent and systematic experimental validation of model's prediction. A) CD28 blocking experimental design in DC-T coculture B) Comparison of the predicted versus observed Fold change following CD28 blocking. n=6 donors. C) Experimental scheme of the “adding” validation procedure used in D-F. D) DC-free validation experiment studying the effect of adding IL-1 β in Th0, Th2 and Th17. Naive T cells were stimulated by anti-CD3/CD28 beads. n=6 donors. E) DC-free validation experiment studying the effect of adding ICOS in Th0, and Th17. Naive T cells were stimulated by coated anti-CD3 and ICOS antibodies and soluble anti-CD28. n=6

donors. F) IL-12 validation experiments in DC-free system. Naive T cells were stimulated by anti-CD3/CD28 beads in Th0 and Th2 conditions. n=8 donors. G) Validation of IL-12 predictions regarding IL-3 and IL-9. bDC were cultured with naive CD4 T cells. IL-12 at 10 ng/mL was added for 6 days. n= 6 donors. For B, D-G, each panel shows the mean and SD of cytokine concentration measured on restimulated Th supernatants. Wilcoxon test.

Figure 6: Context-dependent model reveals a role for IL-12 in Th17 differentiation. A) Context-dependent modeling and application to IL-12. I: input. O: output. B) Error of prediction values obtained by 10-fold cross-validation for IL-17A and IL-17F, comparing the best univariate model (grey), MultivarSel (yellow), and MultivarSel with context-dependencies (blue). C) Heatmap of model's coefficient value of the context-dependent multivariate model explaining IL-17A and IL-17F. D) Model predictions on IL-12 in silico KO in the condition Zymosan-MoDC for IL-17A and IL-17F values (blue), compared to experimental values in the presence of IL-12 (yellow). E) Concentrations of IL-17A and IL-17F produced by Th cells after differentiation with zymosan-MoDC, in the presence of anti-IL-12 neutralizing antibody or matched isotype. n=6 donors. Paired t-test.

Figure 7: Synergistic interaction of IL-12 and IL-1 promotes IL-17F without IL-17A. A) Stability selection frequencies of selection of the different DC signals by a multivariate model explaining the difference between IL-17F and IL-17A. B) Concentration of cytokines measured on restimulated Th supernatants. Naive CD4 T cells were differentiated 5 days with anti-CD3/CD28 beads in the indicated conditions. n=6 donors, paired t-test. C) Same experimental design as in B) with conditions as annotated, n=6 donors, Wilcoxon test. D) Coated anti-CD2 and anti-CD3 together with soluble anti-CD28 were given 5 days to naive CD4 T cells in Th0 or Th17 conditions. Cytokine concentrations were measured after 24h restimulation at day 5. Mean and SD shown. n=8. Wilcoxon test. E) Day 5 Intracellular FACS analysis of Th cells differentiated as in B. Dot plots show a representative donor. F) Quantification of live total CD4 T cells producing either IL-17A or IL-17F. n=6 donors. Paired t-test. G) Representative donor of CD4 memory T cells with intracellular FACS staining for IL-17A versus IL-17F. H) Venn Diagrams of IL-17F⁺/IL17A⁻ Th cells co-producing IL-22, IFN- γ , IL-21 of naive CD4 T cells in the condition IL-12+IL-1 β . Mean percentage and confidence interval, n=6 donors. I) Venn Diagrams of IL-17F⁺/IL17A⁻ Th cells co-

producing IL-22, IFN- γ , IL-21 of memory CD4 T cells stimulated 5 hours with PMA/ionomycin. Mean percentage of 6 donors with confidence interval.

Supplementary Figure Legends

Figure S1 Related to Figure 1 and Figure 2: Descriptive analysis of 36 DC-derived communication molecules. A) Example of raw FACS staining of MoDC communication molecules after 24 hours stimulation with Medium, LPS, Zymosan or Flu. 29 surface markers measured of one representative donor are shown. B) Statistical analysis comparing a given DC stimulation to the other 3 for each signal annotated. P-values are annotated in the table, red should be considered as significant. Paired Wilcoxon test was used (n=14). C) PCA performed either on the whole dataset (left and middle panel) or on the 6 most frequent perturbators (right panel) used across MoDC and bDC stimulations. From left to right colors respectively indicates, the dates of experiments, the DC subset, the 6 most frequent DC stimulations.

Figure S2 Related to Figure 3: Mathematical description and statistical analysis of Th cytokine profiles. A) Table showing three key mathematical parameters of the Exp Fold and the 17 Th derived cytokines. First column: the range of expression (the number of log on which the data are expressed). Second column: the percentage of positive observations among the 428 datapoints. Third column: the coefficient of variation. Communication molecules were ranked based on their range of expression and their coefficient of variation. B) Statistical analysis comparing selected Th cytokines within the following groups: Medium-MoDC, LPS-MoDC, Zymosan-MoDC and Flu-MoDC. The statistical test used is paired Wilcoxon test on n=14 donors. C) Expression profiles of the Exp Fold and the 17 Th derived cytokines within the six groups of DC conditions defined by hierarchical clustering. Expression data were logged transformed and scaled so as μ represents the mean and σ the SD of the expression of a given communication molecule across the whole dataset (n=428).

Figure S3 Related to Figure 4: Multivariate modeling strategies applied to our DC-T datasets. A) Comparative analysis of distinct modeling strategies on simulated data. Using ROC curves, we applied the annotated strategies in terms of true and false discovery. The simulated dataset mimics the features of our DC and T cell experimental data but for which we artificially attributed a link between DC signals and Th cytokines. This allowed us to compare four different types of modeling strategies

(Raw, OR, MultivarSel and sPLS) and different variable selection methods (Lasso, Stability Selection and CV) by analyzing their false and true positive rates. B) Frequency of selection of input variables established through model stability selection. Stability selection was applied after our MultivarSel strategy to the full DC-T dataset (n=428). C) Table showing for each output (Th signals) the input that minimizes its mean squared error of prediction in an univariate model, with its spearman correlation coefficient and its adjusted p-value. D) Error of prediction (obtained by 10-fold cross-validation) of the model respectively on blood DC dataset (n=118) and MoDC dataset (n =310) E) Example of distribution of the squared error of prediction per DC-type for IL-22, TNF- β and Exp Fold. Allows to see the number of data points with the highest error of prediction.

Figure S4 Related to Figure 5: Complementary Th secretion profiles of the tested conditions for systematic model validation. A) Fold change of the cytokine concentration estimated versus experimentally measured for the four indicated cytokines. n=6 independent donors B) Mean cytokine concentration and SD indicated for each condition. n=6 C) Mean cytokine concentration and SD indicated for each condition. n=6 D) and E) Mean cytokine concentration and SD indicated for each condition. n=6 F) Boxplot of the coefficient and stability selection frequencies in the two conditions: True (validated predictions) and False (not validated), Wilcoxon test. Performed only for IL-12, IL-1 and ICOSL validations.

Figure S5 Related to Figure 6: Quantification of context-dependent input-output associations. A) Prediction of error comparison between MultiVarSel and “all_with model” performed for each Th output. B) Quantification per input of the number of times it is selected as associated to an output in the 36 context-dependent models (Table S5). The total number of associations (resp. the number associations of the input alone, resp. the input with another) is represented in the column ‘Number’ (resp. Number alone, resp. Number with) the ratio (Number with / Number) is represented in the column ‘Percentage’ C) Same as panel B but per output instead of input. D) On 8 distinct donors of coculture MoDC/naive CD4 T cells experiments IL-12 was blocked using neutralizing antibody. After the coculture at day 6, Th cells were restimulated 24 hours at 1 million cells/mL and the amount of IFN- γ was determined using CBA. Paired student’s t-test was applied to compare two conditions. E) Model predictions on IL-12 in silico KO in the condition MoDC-curdan (10 μ g/mL) for IL-17A and IL-17F values. Real values in the presence of IL-12 are compared to predicted values obtained in the

absence of IL-12. F) Concentrations of IL-17A, IL-17F and IFN- γ produced by Th cells after coculture with MoDC treated with 10 $\mu\text{g}/\text{mL}$ curdlan, in the presence of neutralizing antibody specific for IL-12 or matching isotype. n=4 donors. Paired t-test was performed to compare the means.

Figure S6 Related to Figure 7: In depth characterization of Th cells polarized in the IL-1+IL-12 condition. A) Multivariate model explaining the differences between IL-17F and IL-17A for a stability selection threshold of 0.8. B) Cytokine profiles of Th cells differentiated in distinct cytokine condition: Th0 (medium), Th2 (IL-4), IL-12, IL-1 (IL-1 β), IL-12+IL-1 and Th17 (IL-6+IL-1 β +TGF- β +IL-23), measured by CBA on 6 donors. Paired student's t-test was used for statistical analysis. C) IL-17A and IL-17F were measured by CBA in the supernatants of Th cells differentiated in distinct cytokine condition: Med, IL-12, IL-1 β , IL-6, IL-23, TGF- β , IL-12+IL-1 β , IL-6+IL-12, IL-23+IL-12, TGF- β +IL-12, IL-6+IL-23+IL-1 β +TGF- β . This experiment was performed on 3 donors. D) Comparison in the same naive CD4 DC-free culture system of the effect of IL-1 α and IL-1 β on the production of six distinct cytokines: IFN- γ , IL-17A, IL-17F, TNF- α , IL-13, IL-10. This experiment was performed on 3 donors. E) DC-free differentiation assay performed using anti CD3/CD28 beads in the indicated cytokine conditions. n=6, Wilcoxon test was used for statistics. F) Example of FACS CTV staining for Th proliferation assessment at day 5. G) Quantification of the % of alive cells in each peak of the CTV staining for each condition. n=3, paired t-test was performed H) qPCR expression profiles for selected genes in the following conditions Th0, Th2, IL-12, IL-1 β , IL-12+IL-1 β , Th17 (IL-6+IL-23+IL-1 β +TGF- β). n=6. Wilcoxon test was used.

Figure S7 Related to Figure 7: Detailed description of distinct experimentally validated predictions. A) PCA using 63 genes measured by qPCR in the 6 indicated Th conditions B) Detailed descriptions of the contribution of each 63 genes to the two first dimensions of the PCA represented in A). C) Systematic univariate analysis evaluating the Pearson correlation between IL-17A and IL-12 in the presence of IL-23 and another input (listed in the column 'Inputs') the number of samples having both of these inputs is in column 'Number'. D) Pearson correlation between IL-17A and IL-12 in the presence or absence of IL-1 and IL-23. E) Dot plot representing the correlation between IL-12 and IL-17A on IL-23 positive data points. F) qPCR measuring RORc, IL-17A and IL-17F in the indicated conditions. n=6 independent donors. Wilcoxon test was used for statistical analysis G) Positive control showing the validation of the anti-CD2 agonist antibody through the measure of Exp Fold in the Th0 condition n=8 H)

Representative intracellular cytokine staining for IL-17A and IL-17F performed in the Th17 and Th17+anti-CD2 conditions. I) Quantification of the intracellular FACS staining performed in H) for 8 distinct donors. Wilcoxon analysis. J) Representative raw data staining of intracellular FACS for IFN- γ , IL-21, IL-22, IL-17A and IL-17F in 6 distinct conditions, Th0 (medium), Th2 (IL-4), IL-12, IL-1 (IL-1 β), IL-12+IL-1 and Th17 (IL-6+IL-1 β +TGF- β +IL-23) for naive CD4 culture. K) Representative raw data staining of intracellular FACS for IFN- γ , IL-21, IL-22, IL-17A and IL-17F for memory CD4 purified cells, previously isolated by magnetic sorting, and restimulated 5 hours with PMA/ionomycin.

STAR★Methods

LEAD CONTACT AND MATERIALS AVAILABILITY

Further information and requests for resources and reagents should be directed to and will be fulfilled by the Lead Contact, Vassili Soumelis (vassili.soumelis@curie.fr).

This study did not generate new unique reagents.

EXPERIMENTAL MODEL AND SUBJECT DETAILS

Human subjects

Apheresis blood from healthy human blood donors were obtained from Etablissement Français du Sang (French Blood Establishment) after written informed consent and in conformity with Institut Curie ethical guidelines. Gender identity and age from anonymous donors were not available, but all donors were between 18 and 70 years old (age limits for blood donation in France).

METHOD DETAILS

PBMCs purification

PBMCs were isolated by centrifugation on a density gradient (Lymphoprep, Proteogenix).

MoDC generation and activation

CD14⁺ cells were selected from PBMCs using magnetically labeled anti-CD14 Microbeads and MACS LS columns following manufacturer's instructions (MiltenyiBiotec). CD14⁺ cells were then cultured with IL-4 (50 ng/mL) and GM-CSF (10

ng/mL) (MiltenyiBiotec) for 5 days in RPMI 1640 Medium, GlutaMAX (Life Technologies) with 10% Fetal Calf Serum. Monocyte-derived Dendritic Cells (MoDC) were activated for 24 hours using one or a combination of perturbators as described in Table S1.

Blood dendritic cells purification

A step of DC pre-enrichment was performed from PBMCs using the EasySep Human Pan-DC Pre-Enrichment kit (StemCell Technologies). Total DC were sorted on a MoFloAstrios (Beckman Coulter) as Lineage (CD3, CD14, CD16, and CD19)⁻, CD4⁺ (Beckman Coulter), CD11c⁺ (BD), as described in (Alculumbre and Pattarini, 2016).

CD4⁺ T lymphocytes purification

Naive CD4⁺ T lymphocytes were purified from PBMCs using the EasySep™ Human Naive CD4⁺ T Cell Isolation Kit (StemCell Technologies). Memory CD4⁺ T cells were purified from PBMCs using the Memory CD4⁺ T cell isolation Kit (MiltenyiBiotec).

Paired protein measurement in DC/T coculture

After 24 hours DC or MoDC activation with DC stimuli listed in Table S1, culture supernatants were kept for cytokine analysis for IL-23, IL-28 α , IL-1, IL-10, IL-12p70, IL-6, TNF- α , while cells were washed in PBS. Some cells were used for surface staining of the following markers: B7H3, CD30L, 4-1BBL, PDL2, VISTA, CD40, CD54, CD58, ICAM-2, ICAM-3, CD18, CD29, SLAMF5, SLAMF3, PVR, CD11a, CD100, LIGHT, Nectin-2, Jagged-2, Galectin-3, CD70, CD80, CD83, OX40L, PDL1, CD86, ICOSL and HLA-DR. And the remaining cells were put in coculture with allogeneic naive CD4 T cells, at a ratio of 1 DC for 5 T cells, in X-VIVO 15 medium (Lonza). For FACS staining, a single batch of commercially available antibodies was used across the study. After 6 days of coculture, T cells were washed and live cells were counted at the microscope using trypan blue to calculate Exp Fold. T cells were reseeded at 1×10^6 /mL and restimulated with anti-CD3/CD28 Dynabeads (LifeTechnologies). 24 hours later supernatants were collected to measure the following T cell cytokines: IL-2, IL-3, IL-4, IL-5, IL-6, IL-9, IL-10, IL-13, IL-17A, IL-17F, IL-21, IL-22, IL-31, GM-CSF, IFN- γ , TNF- α , TNF- β . In each coculture experiment, one single DC donor was coupled to a different single CD4 T cell donor. For each DC/T cell pair, the measurement of DC

derived signals and Th cytokines were performed in parallel, leading to the acquisition of paired data for the 36 DC derived signals and the 18 T cell parameters measured.

IL-12 blocking experiment

For IL-12 blocking experiment, after 24 hours activation with Zymosan (10 μ g/mL) or curdlan (10 μ g/mL), MoDC were incubated during one hour at 37°C in the presence of 20 μ g/mL of anti-IL-12p70 blocking antibody or its matched isotype control. Then, naive CD4 T cells were added to the culture. Antibodies were maintained for the duration of the co-culture. After 6 days of coculture cells were washed and reseeded at 1x10⁶/mL and restimulated with anti-CD3/CD28 Dynabeads (LifeTechnologies). 24 hours later supernatants were collected to measure T cell cytokines.

CD28 blocking experiment

For CD28 blocking experiment, MoDC were first activated for 24 hours with Flu (1X), LPS (100ng/mL) or Zymosan (10 μ g/mL). Then, activated DC were cocultured with allogeneic naïve CD4 T cells in the presence of 5 μ g/mL anti-CD28 blocking antibody or its matched isotype control (Figure 5A). Antibodies were maintained for the duration of the co-culture. After 6 days of coculture cells were washed and reseeded at 1x10⁶/mL and restimulated with anti-CD3/CD28 Dynabeads (LifeTechnologies). 24 hours later supernatants were collected to measure T cell cytokines. We systematically measured all Th outputs predicted to be associated either to CD80 or CD86 (Figure 5B). Finally, we compared the estimated (in silico prediction) and the real (experimental) fold change (FC) (Figure 5B). A FC higher or lower than one for a given Th output indicated an inhibitory versus inducer role of CD80/CD86, respectively.

Addition of rhIL-12p70 during DC/T coculture

Sorted myeloid-DC were activated for 24 hours with zymosan (10 μ g/mL) or HKSA (MOI 1). Then, 10,000 activated DC were cocultured with 50,000 allogeneic naive CD4 T cells in the presence or absence of 10 ng/mL rhIL-12p70. After 6 days of coculture, 100,000 T cells were restimulated for 24 hours with anti-CD3/CD28 Dynabeads. Supernatants were then collected for cytokine measurements.

DC-free Th cell polarization

Naive CD4 T cells were cultured for 5 days with only anti-CD3/CD28 Dynabeads (Life Technologies) to obtain Th0 or in combination with either 10 ng/mL IL-12 (Th1), 25ng/mL IL-4 (Th2), 10 ng/mL IL-1 β or IL-1 α , 100 ng/mL IL-23, IL-12 plus IL-1 β or a mix of IL-1 β , IL-23, 1 ng/mL TGF- β and 20 ng/mL IL-6 to obtain Th17 (Peprotech) as already published (Touzot et al., 2014). At the end of the culture cells were used for intracellular staining or washed, reseeded at 1x10⁶/mL and restimulated with anti-CD3/CD28 Dynabeads (Life Technologies) for 24 hours before collecting supernatants for cytokine measure and lysing cells in RLT buffer (Qiagen) for qPCR analysis.

ICOS agonism

For experiments with anti-ICOS antibody, prior to culture 5 μ g/mL anti-CD3 (OKT3 clone, Biolegend) with 5 μ g/mL anti-ICOS or matching isotype control were coated on a flat-bottom 96 well plate (TPP) and incubated overnight at 4°C. The plate was then washed 3 times with PBS before seeding 32,000 naive CD4 T cells with 1 μ g/mL anti-CD28 (CD28.2 clone, Biolegend) and cytokines as described above in X-vivo medium (Lonza). After 5 days culture, T cells were counted and 100,000 cells were restimulated with anti-CD3/CD28 Dynabeads for 24 hours before collecting supernatants for cytokine measure.

We were able to induce the following Th outputs in the Th0 condition: Exp Fold, IL-3, IL-5, IL-6, IL-10, IL-13, IL-22, TNF- α and GM-CSF (Figure 5E). In a Th17 condition, we were able to demonstrate a positive effect of the ICOS pathway on the production of IL-17A (Figure 5E). All these observations were statistically significant, and validated the model predictions. However, six predictions on TNF- β , IL-2, IL-21, IL-17F, IL-4 and IL-31 could not be validated using these experimental settings (Figure S4C). For IL-17F, IL-4 and IL-31 we could not detect a significant effect of ICOS (Figure S4C), suggesting possible lack of a co-factor. However, for TNF- β , IL-2, IL-21 we found significant but opposite effects to the one predicted by the model, including the positive role of ICOSL in the induction of IL-21 (Table S3).

CD2 agonism

For experiments with anti-CD2 agonist antibody, prior to culture 5 μ g/mL anti-CD3 (OKT3 clone, Biolegend) with 5 μ g/mL anti-CD2 or matching isotype control were coated on a flat-bottom 96 well plate (TPP) and incubated overnight at 4°C. The plate was then washed 3 times with PBS before seeding 32,000 naive CD4 T cells with 1

µg/mL anti-CD28 (CD28.2 clone, Biolegend) and cytokines as described above in X-vivo medium (Lonza). After 5 days culture, T cells were counted and 100,000 cells were restimulated with anti-CD3/CD28 Dynabeads for 24 hours before collecting supernatants for cytokine measure.

We showed that our anti-CD2 antibody worked by studying the Exp Fold of naive T cells, cultured with anti-CD3 and CD28 with or without anti-CD2. We found that anti-CD2 significantly induced T cell Exp Fold (Figure S7G).

Flow cytometry analysis

Antibodies and matched isotypes were titrated on the relevant human PBMC population. For surface FACS analysis on activated MoDC and blood DC the complete list of antibodies and important information such as brand, final dilutions, reference, clone and colors are given in Key Resources Table. Dead cells were excluded using DAPI (Miltenyi Biotec).

For intracellular cytokine staining, naive or memory CD4 T cells were stimulated with 100 ng/mL PMA, 500 ng/mL ionomycin and 3 µg/mL Brefeldin A (ThermoFisher) for 5 hours. To exclude dead cells, CD4 T cells were stained using the LIVE/DEAD Fixable yellow dead cell stain kit, following manufacturer's instructions (LifeTechnologies). Cells were fixed and permeabilized using the IC Fix and Permeabilization buffers (ThermoFisher). Intracellular cytokines were revealed with fluorescently conjugated antibodies against IL-17A (BioLegend), IL-17F (ThermoFisher), IL-21 (BioLegend), IL-22 (ThermoFisher), and IFN-γ (BD), or matched isotype controls and acquired on a Fortessa instrument (BD).

Cytokine quantification

Cytokines were quantified in dendritic cell supernatants using CBA flex set for IL-1α, IL-1β, IL-6, IL-10, TNF-α and IL-12p70 (also named IL-12) and using Luminex for IL-23 and IL-28α. Cytokines from T cell supernatants were quantified using CBA flex set for, IL-2, IL-3, IL-4, IL-5, IL-6, IL-9, IL-10, IL-13, IL-17A, IL-17F, TNF-α, IFN-γ and GM-CSF (BD) and Luminex for IL-21, IL-22, IL-31 and TNF-β following the manufacturer's protocol.

Gene expression quantification

At the end of the 5 days Th polarization and 24 hours restimulation, total RNA was extracted from 100,000 cells using RNA easy micro kit (Qiagen). Total RNA was retrotranscribed using Superscript II Reverse Transcriptase (ThermoFisher Scientific) in combination with random primers, Oligo(dT) and dNTP (Promega). Transcripts were then quantified by real time PCR on a 480 LightCycler Instrument (Roche). Reactions were performed using a qPCR Master Mix Plus (Eurogentec) and TaqMan assays listed in the Key Resources Table. Raw expression data (ct values) were normalized on the mean of two housekeeping genes (B2M and RPL34).

QUANTIFICATION AND STATISTICAL ANALYSIS

Dataset quality control – batch effect

As quality control of our procedure we asked whether experimental batch effect could play a role in the differences we observed across our dataset. Selecting the 6 most frequent perturbators within our MoDC dataset we performed principal component analysis to look for batch effects related to the date of the experiments or the donor variability (Figure S1C).

Dataset quality control – T cell expansion

As a control, we could see that the Exp Fold profiles of CD4 T cells matched the activation profiles of DC observed in Figure 1C. Indeed, T cells co-cultured with either LPS-MoDC, Zymosan-MoDC or Flu-DC induced significantly more expansion than the negative Medium-DC control reflecting good quality controls of the experiments (Figure 3B).

Statistical tests

In the figure legends, n is indicated and corresponds to the number of donors used for each experiment. Paired Wilcoxon or t test were applied as detailed in figure legends to compare two groups. Significance was retained for *, $P < 0.05$.

Statistical analysis

Each variable of the dataset was transformed using first the Box-Cox transformation and then a scaling step on both the mean and the variance (using TBoCo package). For all analyses performed, cytokine values inferior to 20 pg/mL were considered as

0, as 20 pg/mL corresponds to the general detection limit of the assay. In order to cluster the inputs, outputs and the samples a hierarchical clustering approach was applied by using different criterions: Ward's criterion and Pearson correlation metric were used to cluster the inputs and the outputs, while Ward's criterion and the Euclidean metric were used to cluster the samples or DC conditions. The heatmaps were generated by using the heatmap.2 package. The correlations between the continuous variables were computed by using the Pearson correlation. All statistical tests are called "significant" if their p-value is smaller than 0.05. The p-values were corrected using Benjamini-Hochberg correction.

Boxplots represented are Tukey Boxplot, meaning that the box goes from the first to the third quartile, it is cut by the median and the whisker goes from the upper (resp. the lower) whisker extends from the third (resp. the first) quartile to the largest (resp. the smallest) value no further than $1.5 * IQR$ from the third (resp. The first) quartile (where IQR is the inter-quartile range, or distance between the first and third quartiles). Data beyond the end of the whiskers points and are plotted individually.

The fold change represented in Figure 5B and Figure S4A represent the value (real or estimated) of an output in the absence of CD80 and CD86 divided by the value of the output in the same sample when CD80 and CD86 are present.

Model comparison and ROC Curves

In order to test different multivariate statistical modeling strategies, and to compare them in terms of false and true positive rates, we generated a simulated dataset that mimics the features of our DC and T cell experimental data, but for which we arbitrarily attributed a link between DC communication signals and Th cytokines, the whole strategy is detailed below.

The Figure S3A aims at assessing the performance of our modelling strategy in terms of variable selection and comparing it with other variable selection methodologies. In order to do this, we performed numerical experiment: we used the real input dataset called hereafter X , simulated a random error matrix (E) with a block covariance matrix to mimic the Th subset and a matrix of coefficients (B) to mimic the effect of the inputs on the outputs. Using these three matrices we created a new output matrix $Y=XB+E$. On this new matrix Y we applied different modeling strategies. 1) The sPLS, 2) the classical Lasso, applied to each column of Y (namely each output) independently

(Lasso without covariance) 3) Our methodology, called MultivarSel, (described in the Modeling strategy section), which consists in estimating the covariance matrix of E and use it to remove the dependence between the outputs before applying the Lasso methodology (Lasso empirical covariance) 4) Lasso with real covariance matrix, the same methodology than ours, but with the real covariance matrix of E, corresponding to the internal positive control of this analysis. We also assessed stability selection by adding this analysis step to the three last methods (Lasso with stability selection and without covariance, Lasso with stability selection and empirical covariance, Lasso with stability selection and real covariance matrix). For each part of this methodology, we varied the threshold to vary the number of variables that were kept and calculated for each threshold the True Positive Rate (TPR) and the False Positive Rate (FPR). The TPR is the number of variables that have been properly identified as being relevant for explaining the response divided by the total number of explanatory variables. We also wanted to assess the sparsity: the percentage of non-zeros in the matrix B. Namely the percentage of pairs of input-output that actually interact together. To do this, we made different scenarios with high and low sparsity (0.01 and 0.3). For all of these scenarios we simulated 1000 different Y, so we performed all this methodology 1000 times each and we calculated at each time, for each methodology and for each threshold the TPR and the FPR. We then took the mean of this TPR and FPR for each methodology and for each threshold. We also assessed the importance of the stability selection.

We can see that our MultivarSel Strategy (Lasso empirical covariance) provides better results than sPLS and Lasso without covariance. Moreover, we observed that its performance is similar to Lasso with the real covariance matrix (the positive control), which means that we greatly estimated the dependence among the outputs. We also noted that the larger the sparsity level, the smaller the differences of performance between MultivarSel (Lasso empirical covariance) and Lasso without covariance, while the differences between Lasso empirical covariance and sPLS are bigger. We can see that adding the stability selection step improves a lot the results.

Modeling strategy

In order to select the most relevant inputs for modeling the outputs, we used the linear model methodology recently developed in (Perrot-Dockès et al., 2018) which has already been successfully applied to metabolomics data in (M. Perrot-Dockès, 2018).

The great advantage of such an approach is to propose a Lasso-based criterion (Tibshirani, 1996) taking into account the dependence that may exist between the outputs. The parameters involved in the criterion are chosen thanks to 10-fold cross-validation and stability selection with 1000 resampling (Nicolai Meinshausen and Bühlmann, 2010). The numerical experiments were performed using the real inputs data set. Then, in order to mimic the Th groups, a random error matrix having a blockwise constant covariance matrix was generated.

The ROC curves display the True positive rate (TPR) as a function of the False positive rate (FPR) where the TPR is the number of variables that have been properly identified as being relevant for explaining the response divided by the total number of explanatory variables. The FPR is the number of variables that have been wrongly identified as being relevant for explaining the response divided by the total number of variables that do not explain the response. To look for a context dependent role of IL-12p70 in the presence of another input we performed the same methodology but instead of modeling the outputs by using only the inputs, some new variables were added: they correspond to a combination of IL-12p70 with the other inputs. More precisely, for instance, the variable “IL-12p70 with IL-1” is equal to the value of IL-12p70 for the samples having a positive concentration in IL-1 and to zero for the samples for which the concentration in IL-1 is equal to zero.

We propose the following modeling for the outputs:

$$(1) \quad Y = XB + E,$$

where Y denotes the $n \times q$ output matrix, X denotes the $n \times p$ design matrix containing the inputs, B is an unknown $p \times q$ coefficient matrix and E is the $n \times q$ random error matrix. Here, n corresponds to the number of samples, q is the number of outputs and p denotes the number of inputs. In order to take into account the potential dependence that may exist between the outputs, we shall assume that each row i of E satisfies:

$$(2) \quad (E_{i,1}, \dots, E_{i,q}) \sim N(\mathbf{0}, \Sigma_q),$$

where Σ_q denotes the covariance matrix of the i th row of the random error matrix.

In order to select the most relevant inputs for explaining the outputs, the methodology that we propose can be summarized in the following three steps:

First step: Fitting a multiple regression model to each output to have an estimation of the error matrix: \hat{E} and computing its empirical covariance matrix.

Second step: Using this empirical covariance matrix to remove the dependence in E , namely between the outputs.

Third step: Selecting among the inputs the most relevant for explaining the outputs by applying a Lasso approach to the transformed data as explained in the second step.

First step: Residuals and covariance matrix

We obtained an ordinary least square (OLS) estimator of B by fitting a multiple regression model which is not a variable selection method. More precisely, the corresponding estimator \hat{B}^{OLS} is defined by

$$\hat{B}^{OLS} = \text{Argmin}_B \{ \|Y - XB\|_2^2 \},$$

Using \hat{B}^{OLS} we got an estimation of E : $\hat{E} = Y - X\hat{B}^{OLS}$. Then, we computed the empirical covariance matrix $\hat{\Sigma}_q$ of \hat{E} .

Second step: Transformation

Let us recall that the standard Lasso criterion, proposed by (Tibshirani, 1996) estimates B in the following univariate linear model:

$$(3) \quad Y = XB + E,$$

by

$$(4) \quad \hat{B}(\lambda) = \text{Argmin}_B \{ \|Y - XB\|_2^2 + \lambda \|B\|_1 \},$$

where Y , B and E are vectors. Usually, the components of E are assumed to be independent.

Thus, we proposed to transform Model (1) to be able to use the Lasso criterion as follows. First, we removed the dependence among the outputs:

$$(5) \quad Y\hat{\Sigma}_q^{-1/2} = X B \hat{\Sigma}_q^{-1/2} + E \hat{\Sigma}_q^{-1/2},$$

where $\hat{\Sigma}_q^{-1/2}$ denotes the inverse of the square root of Σ_q .

Then, we applied the *vec* operator which consists in stacking the columns of a matrix into a single column vector.

$$\begin{aligned} Y &= \text{vec}(Y\hat{\Sigma}_q^{-1/2}) = \text{vec}(XB\hat{\Sigma}_q^{-1/2}) + \text{vec}(E\hat{\Sigma}_q^{-1/2}) \\ &= \text{vec}\left(\left(\hat{\Sigma}_q^{-1/2}\right)' \otimes X\right) \text{vec}(B) + \text{vec}(E\hat{\Sigma}_q^{-1/2}) \\ &= Xb + \varepsilon. \end{aligned}$$

Third step: Variable selection

Thanks to the previous transformation, the Lasso criterion can be applied to $y = \text{vec}(Y\hat{\Sigma}_q^{-1/2})$. Since $B = \text{vec}(B)$, estimating the coefficient of B boils down to estimating the coefficients of B . The parameter λ in (4) is chosen by 10-fold cross-

validation followed by a stability selection step with 1000 resamplings, as proposed by (Nicolai Meinshausen and Bühlmann, 2010).

The squared error of prediction of the different models were assessed using 10-fold cross-validation (Figures 4A, 6B, S3D, S3E and S5A).

Systematic literature review

To assess the literature and evaluate the generated multivariate model of Figure 4B, we conducted a systematic literature review to identify articles indexed on the PubMed database by March 1st 2017, examining the effects of inputs on naive CD4+ cells.

One of three different search strategies was used to export references from the PubMed database into the reference management software EndNote™.

We started by performing the first search strategy which consisted of using free text to search English language articles for the input (or any of its aliases) and the output (or any of its aliases). If the search yielded 20 or less results, the references were exported into EndNote™.

If not, then we performed the second search strategy, which consisted of searching English language articles for the input (or any of its aliases) and the output (or any of its aliases), both in the title or abstract, and at least one of the following medical subject heading terms: “cell differentiation” or “CD4-positive T-lymphocytes” or “lymphocyte activation». If the search returned 50 or less results, the references were exported into EndNote™. If not, then we carried out the third search strategy which returned English language articles that had both the input (or any of its aliases) and the output (or any of its aliases) in the title or abstract, as well as indexes to both of the following medical subject heading terms: “cell differentiation” and “CD4-positive T-lymphocytes”. Results were exported into EndNote™.

The electronic searches generated a total of 14,748 references that were managed through EndNote™. A manual search of references from review articles and other records identified 21 additional publications that were not included in the search results. Of these 14,769 articles, 9,780 duplicates were removed, leaving 4,989 records to be screened.

Titles and abstracts were screened by 2 independent reviewers. Publications were selected for further in-depth consideration if they met all of the following inclusion criteria: 1) Journal Article, 2) Examining the effect of one input at a time, 3) Testing on naive CD4+ T cells, which were defined as CD4+ and CD45RA+ and/or CD45RO- and/or

CD25⁻ cells. Studies were excluded from the analysis if: 1) Full-text article, Title and/or abstract were not available, 2) Methods and/or experiments and/or results were unclear or inconclusive or of low quality. Reasons for removing articles included not performing proper experimental controls, insufficient information, lack of replicates and/or statistical analysis.

The reviewers excluded 4,589 articles because they did not meet the inclusion and exclusion criteria, leaving 400 articles of which, at least, the figures and materials and methods sections were examined. Finally, 178 publications met all the inclusion criteria and underwent data extraction.

Extracted information included the PubMed identifier, the input, the output, the input's effect on naive CD4⁺ T cells in regards to the output, the experimental context and setup (e.g., details about T cell stimulation context, input's concentration, duration...) and the organism. Data were cross-checked by the 2 reviewers, and any ambiguities were discussed and resolved through a consensus.

The Exp Fold was not included in the literature review so it was not included in the following literature validation score.

Calculation of the literature validation score: an association predicted by our model (Figure 4B) between an input and an output was considered as “new” if none of the 178 publications found that the input induces or inhibits the output. Absence of effect depicted in some articles was not considered relevant to assess novelty of the prediction. It was “validated” if at least one of the 178 publications found similar results than our model and “contradictory” if none of the study found the same results than our model but at least one found an opposite result. Opposite result would be an induction if the model predicted a negative coefficient or an inhibition if our model predicted a positive coefficient.

DATA AND CODE AVAILABILITY

The dataset generated during this study is available in Table S2.

All references from literature mining are listed in Table S3.

Software used for flow cytometry data analysis was FlowJo software (TreeStar).

Software used for CBA analysis was FCAP Array v3.

Software used for statistical analysis was Prism software v5 (GraphPad).

Software used for statistical analysis and modeling was R version 3.5.2.

The R packages used to perform this study are: package MultiVarSel 1.0.0 used for modelling and package TBoCo 0.0.1 for boxcox transformation available at <https://CRAN.R-project.org/package=MultiVarSel>.

This study did not generate code.

Supplementary Tables

Table S1 Related to Figure 1: Number of data point generated per stimulation per DC subset:

This table recapitulates the number of distinct data points corresponding to the biological replicates (column Frequency) generated for each DC stimulation on bDC or MoDC.

Table S2 Related to Figure 1, 2 and 3: Complete input-output numerical dataset:

This table recapitulates all the raw data used to perform the statistical models. For all surface markers, the mean fluorescence intensity (MFI) was computed using FlowJo analysis software. Each parameter was considered individually and the MFI was calculated on live events determined by DAPI staining. For both DC and Th cytokines values correspond to pg/mL.

Table S3 Related to Figure 4 and 5: Literature data extracted under the form of input-output and their relationship.

Literature table) This tab recapitulates all the data used for the Figure 4D to construct our literature validation. Each DC-derived communication molecule for which literature data were found are represented in the column “input” and is associated to a given Th cytokine as indicated in the column “output”. For each input/output association, the type of association (induction, inhibition, no effect, no induction) was extracted from the given figure and the reference can be retrieved through its PMID number. This tab also provides the molecular and experimental context, the species, the experiment type (in vitro versus in vivo). Prediction classification) In this tab we use our global literature assessment to recapitulate, for each prediction made by the model of Figure 4, if the prediction was considered as “new” (never studied in the literature), “validated” (found in at least one other study) or “contradictory” (not validated and contradictory to at least one of the studies in the literature).

Table S4 Related to Figure 4: New input-output associations predicted by our data-driven Lasso penalized regression model. This table provides the list of all input/output associations found by our modeling strategy as presented in Figure 4B and retrieved as novel when confronted to the literature validation analysis in Figure

4D. Depicted scores correspond to model coefficient and frequencies obtained in the stability selection analysis.

Table S5 Related to Figure 6: Context-dependent models. Table showing the 36 distinct “context dependent” models. The context dependencies of each input one by one is addressed in a specific model following the strategy detailed in Figure 6. The threshold of the stability selection has been put to 0.6 for all the models.

Table S6 Related to Figure 7: Normalized expression values of the 63 genes Th related genes measured by qPCR. Each column shows the normalized value, in arbitrary units, of expression of the indicated genes. Six donors were included and stimulated with anti CD3/28 beads in the indicated conditions: Th0, Th2, IL- β , IL-12, IL-12+IL-1 β and Th17. Normalization of the expression values was performed for each data point on the value of the mean of two housekeeping genes (RPL34 and B2M).

References

- Abou-Jaoude, W., Monteiro, P.T., Naldi, A., Grandclaoudon, M., Soumelis, V., Chaouiya, C., and Thieffry, D. (2014). Model checking to assess T-helper cell plasticity. *Frontiers in bioengineering and biotechnology* 2, 86.
- Acosta-Rodriguez, E.V., Napolitani, G., Lanzavecchia, A., and Sallusto, F. (2007). Interleukins 1beta and 6 but not transforming growth factor-beta are essential for the differentiation of interleukin 17-producing human T helper cells. *Nature immunology* 8, 942-949.
- Alcumbre, S., and Pattarini, L. (2016). Purification of Human Dendritic Cell Subsets from Peripheral Blood. *Methods in molecular biology* 1423, 153-167.
- Antebi, Y.E., Reich-Zeliger, S., Hart, Y., Mayo, A., Eizenberg, I., Rimer, J., Putheti, P., Pe'er, D., and Friedman, N. (2013). Mapping differentiation under mixed culture conditions reveals a tunable continuum of T cell fates. *PLoS biology* 11, e1001616.
- Balan, S., Arnold-Schrauf, C., Abbas, A., Couespel, N., Savoret, J., Imperatore, F., Villani, A.C., Vu Manh, T.P., Bhardwaj, N., and Dalod, M. (2018). Large-Scale Human Dendritic Cell Differentiation Revealing Notch-Dependent Lineage Bifurcation and Heterogeneity. *Cell reports* 24, 1902-1915 e1906.
- Banchereau, J., and Steinman, R.M. (1998). Dendritic cells and the control of immunity. *Nature* 392, 245-252.
- Cariani, F., and Rips, L.J. (2017). Conditionals, Context, and the Suppression Effect. *Cognitive science* 41, 540-589.
- Chen, L., and Flies, D.B. (2013). Molecular mechanisms of T cell co-stimulation and co-inhibition. *Nature reviews Immunology* 13, 227-242.

- Ciofani, M., Madar, A., Galan, C., Sellars, M., Mace, K., Pauli, F., Agarwal, A., Huang, W., Parkhurst, C.N., Muratet, M., *et al.* (2012). A validated regulatory network for Th17 cell specification. *Cell* 151, 289-303.
- da Silva-Diz, V., Lorenzo-Sanz, L., Bernat-Peguera, A., Lopez-Cerda, M., and Munoz, P. (2018). Cancer cell plasticity: Impact on tumor progression and therapy response. *Seminars in cancer biology* 53, 48-58.
- Edfors, F., Danielsson, F., Hallstrom, B.M., Kall, L., Lundberg, E., Ponten, F., Forsstrom, B., and Uhlen, M. (2016). Gene-specific correlation of RNA and protein levels in human cells and tissues. *Molecular systems biology* 12, 883.
- Guermonprez, P., Valladeau, J., Zitvogel, L., Thery, C., and Amigorena, S. (2002). Antigen presentation and T cell stimulation by dendritic cells. *Annual review of immunology* 20, 621-667.
- Ito, T., Wang, Y.H., Duramad, O., Hori, T., Delespesse, G.J., Watanabe, N., Qin, F.X., Yao, Z., Cao, W., and Liu, Y.J. (2005). TSLP-activated dendritic cells induce an inflammatory T helper type 2 cell response through OX40 ligand. *The Journal of experimental medicine* 202, 1213-1223.
- Ivanov, I.I., McKenzie, B.S., Zhou, L., Tadokoro, C.E., Lepelley, A., Lafaille, J.J., Cua, D.J., and Littman, D.R. (2006). The orphan nuclear receptor ROR γ t directs the differentiation program of proinflammatory IL-17+ T helper cells. *Cell* 126, 1121-1133.
- Keller, R. (2001). Dendritic cells: their significance in health and disease. *Immunology letters* 78, 113-122.
- Kintsch, W., and Mangalath, P. (2011). The construction of meaning. *Topics in cognitive science* 3, 346-370.
- Korn, T., Bettelli, E., Oukka, M., and Kuchroo, V.K. (2009). IL-17 and Th17 Cells. *Annual review of immunology* 27, 485-517.
- Liu, Y., Beyer, A., and Aebersold, R. (2016). On the Dependency of Cellular Protein Levels on mRNA Abundance. *Cell* 165, 535-550.
- Liu, Y.J., Kanzler, H., Soumelis, V., and Gilliet, M. (2001). Dendritic cell lineage, plasticity and cross-regulation. *Nature immunology* 2, 585-589.
- M. Perrot-Dockès, C.L.-L., J. Chiquet, L. Sansonnet, M. Brégère, M.-P. Étienne, S. Robin, G. Genta-Jouve (2018). A variable selection approach in the multivariate linear model: an application to LC-MS metabolomics data. *Statistical Applications in Genetics and Molecular Biology* 17(5).
- Macagno, A., Napolitani, G., Lanzavecchia, A., and Sallusto, F. (2007). Duration, combination and timing: the signal integration model of dendritic cell activation. *Trends in immunology* 28, 227-233.
- Manel, N., Unutmaz, D., and Littman, D.R. (2008). The differentiation of human T(H)-17 cells requires transforming growth factor-beta and induction of the nuclear receptor ROR γ t. *Nature immunology* 9, 641-649.
- Nakayama, T., Hirahara, K., Onodera, A., Endo, Y., Hosokawa, H., Shinoda, K., Tumes, D.J., and Okamoto, Y. (2017). Th2 Cells in Health and Disease. *Annual review of immunology* 35, 53-84.

- Naldi, A., Carneiro, J., Chaouiya, C., and Thieffry, D. (2010). Diversity and plasticity of Th cell types predicted from regulatory network modelling. *PLoS computational biology* 6, e1000912.
- Nicolai Meinshausen, and Bühlmann, P. (2010). Stability selection. *Series B Statistical Methodology*.
- Perrot-Dockès, M., Lévy-Leduc, C., Sansonnet, L., and Chiquet, J. (2018). Variable selection in multivariate linear models with high-dimensional covariance matrix estimation. *Journal of Multivariate Analysis* 166, 78-97.
- Soumelis, V., Reche, P.A., Kanzler, H., Yuan, W., Edward, G., Homey, B., Gilliet, M., Ho, S., Antonenko, S., Lauerma, A., *et al.* (2002). Human epithelial cells trigger dendritic cell mediated allergic inflammation by producing TSLP. *Nature immunology* 3, 673-680.
- Tibshirani, R. (1996). Regression Shrinkage and Selection via the Lasso. *Journal of the Royal Statistical Society* 58.
- Tindemans, I., Peeters, M.J.W., and Hendriks, R.W. (2017). Notch Signaling in T Helper Cell Subsets: Instructor or Unbiased Amplifier? *Frontiers in immunology* 8, 419.
- Touzot, M., Grandclaudon, M., Cappuccio, A., Satoh, T., Martinez-Cingolani, C., Servant, N., Manel, N., and Soumelis, V. (2014). Combinatorial flexibility of cytokine function during human T helper cell differentiation. *Nature communications* 5, 3987.
- Vento-Tormo, R., Efremova, M., Botting, R.A., Turco, M.Y., Vento-Tormo, M., Meyer, K.B., Park, J.E., Stephenson, E., Polanski, K., Goncalves, A., *et al.* (2018). Single-cell reconstruction of the early maternal-fetal interface in humans. *Nature* 563, 347-353.
- Volpe, E., Servant, N., Zollinger, R., Bogiatzi, S.I., Hupe, P., Barillot, E., and Soumelis, V. (2008). A critical function for transforming growth factor-beta, interleukin 23 and proinflammatory cytokines in driving and modulating human T(H)-17 responses. *Nature immunology* 9, 650-657.
- Wang, Y., Chen, X., Cao, W., and Shi, Y. (2014). Plasticity of mesenchymal stem cells in immunomodulation: pathological and therapeutic implications. *Nature immunology* 15, 1009-1016.
- Yosef, N., Shalek, A.K., Gaublomme, J.T., Jin, H., Lee, Y., Awasthi, A., Wu, C., Karwacz, K., Xiao, S., Jorgolli, M., *et al.* (2013). Dynamic regulatory network controlling TH17 cell differentiation. *Nature* 496, 461-468.
- Zhu, J., Yamane, H., and Paul, W.E. (2010). Differentiation of effector CD4 T cell populations (*). *Annual review of immunology* 28, 445-489.
- Zygmunt, B., and Veldhoen, M. (2011). T helper cell differentiation more than just cytokines. *Advances in immunology* 109, 159-196.

KEY RESOURCES TABLE

REAGENT or RESOURCE	SOURCE	IDENTIFIER
Antibodies		
FITC Mouse anti-human CD3 (Clone HIT3a)	BD	Cat# 555339
FITC Mouse anti-human CD14 (Clone TÜK4)	Miltenyi Biotec	Cat# 130-080-701
FITC Mouse anti-human CD16 (Clone NKP15)	BD	Cat# 335035
FITC Mouse anti-human CD19 (Clone LT19)	Miltenyi Biotec	Cat# 130-091-328
APC-Cy7 Mouse anti-human CD11c (Clone Bu15)	BioLegend	Cat# 337218
PE-Cy5 Mouse anti-human CD4 (Clone 13B8.2)	Beckman Coulter	Cat# A07752
R-PE Mouse anti-human OX40L (Clone ANC10G1)	Ancell	Cat# 400-050
R-PE Mouse IgG1, κ Isotype Control (Clone MOPC31C)	Ancell	Cat# 278-050
BV711 Mouse anti-human CD54 (Clone HA58)	BD	Cat# 564078
BV711 Mouse IgG1, κ Isotype Control (Clone X40)	BD	Cat# 563044
BV786 Mouse anti-human CD273 (Clone MIH18)	BD	Cat# 563843
BV786 Mouse anti-human CD80 (Clone L307.4)	BD	Cat# 564159
BV786 Mouse IgG1, κ Isotype Control (Clone X40)	BD	Cat# 563330
FITC Mouse anti-human CD70 (Clone Ki-24)	BD	Cat# 555834
FITC Mouse IgG3, κ Isotype Control (Clone J606)	BD	Cat# 555578
Alexa Fluor® 700 Mouse anti-human CD29 (Clone TS2/16)	BioLegend	Cat# 303020
Alexa Fluor® 700 Mouse IgG1, κ Isotype Control (Clone MOPC-21)	BioLegend	Cat# 400144
APC Mouse anti-human ICAM-3 (Clone CBR-IC3/1)	BioLegend	Cat# 330011
APC Mouse anti-human Jagged-2 (Clone MHJ2-523)	BioLegend	Cat# 346906 (Discontinued)
APC Mouse IgG1, κ Isotype Control (Clone MOPC-21)	BioLegend	Cat# 400121
BV650 Mouse anti-human CD86 (Clone IT2.2)	BioLegend	Cat# 305428
BV650 Mouse IgG2b, κ Isotype Control (Clone MPC-11)	BioLegend	Cat# 400352
BV711 Mouse anti-human HLA-DR (Clone L243)	BioLegend	Cat# 307644
BV711 Mouse IgG2a, κ Isotype Control (Clone MOPC-173)	BioLegend	Cat# 400272
FITC Mouse anti-human CD100 (Clone A8)	BioLegend	Cat# 328406
FITC Mouse IgG1, κ Isotype Control (Clone MOPC-21)	BioLegend	Cat# 400108
FITC Mouse anti-human ICAM-2 (Clone CBR-IC2/2)	BioLegend	Cat# 328507
FITC Mouse IgG2a, κ Isotype Control (Clone MOPC-173)	BioLegend	Cat# 400209
PE Mouse anti-human CD18 (Clone TS1/18)	BioLegend	Cat# 302107
PE Mouse anti-human Nectin-2 (Clone TX31)	BioLegend	Cat# 337410
PE Mouse anti-human PVR (Clone SKII.4)	BioLegend	Cat# 337610
PE Mouse IgG1, κ Isotype Control (Clone MOPC-21)	BioLegend	Cat# 400112
PE/Cy7 Mouse anti-human CD40 (Clone 5C3)	BioLegend	Cat# 334321
PE/Cy7 Mouse IgG1, κ Isotype Control (Clone MOPC-21)	BioLegend	Cat# 400126
PE/Cy5 Mouse anti-human CD58 (Clone TS2/9)	BioLegend	Cat# 330909
PE/Cy5 Mouse IgG1, κ Isotype Control (Clone MOPC-21)	BioLegend	Cat# 400117
PerCP/Cy5.5 Mouse anti-human CD83 (Clone HB15e)	BioLegend	Cat# 305320
PerCP/Cy5.5 Mouse IgG1, κ Isotype Control (Clone MOPC-21)	BioLegend	Cat# 400150
Alexa Fluor® 488 Goat anti-human Galectin-3	R&D Systems	Cat# IC1154G
Alexa Fluor® 488 Normal Goat IgG	R&D Systems	Cat# IC108G
Alexa Fluor® 700 Mouse anti-human VISTA (Clone 730804)	R&D Systems	Cat# FAB71261N
Alexa Fluor® 700 Mouse IgG _{2B} Isotype Control (Clone 133303)	R&D Systems	Cat# IC0041N
APC Mouse anti-human SLAMF3 (Clone 249936)	R&D Systems	Cat# FAB1898A
APC Mouse IgG _{2A} Isotype Control (Clone 20102)	R&D Systems	Cat# IC003A
APC Mouse anti-human 4-1BBL (Clone 282220)	R&D Systems	Cat# FAB2295A
APC Mouse anti-human ICOSL (Clone 136726)	R&D Systems	Cat# FAB165A
APC Mouse IgG _{2B} Isotype Control (Clone 133303)	R&D Systems	Cat# IC0041A
FITC Mouse anti-human B7H3 (Clone 185504)	R&D Systems	Cat# FAB1027F
FITC Mouse IgG ₁ Isotype Control (Clone 11711)	R&D Systems	Cat# IC002F

FITC Goat anti-human SLAMF5	R&D Systems	Cat# FAB1855F (Discontinued)
FITC Normal Goat IgG	R&D Systems	Cat# IC108F
PE Mouse anti-human LIGHT (Clone 115520)	R&D Systems	Cat# FAB664P
PE Mouse IgG ₁ Isotype Control (Clone 133303)	R&D Systems	Cat# IC002P
PE Mouse anti-human CD30L (Clone 116614)	R&D Systems	Cat# FAB1028P
PE Mouse IgG2B Isotype Control (Clone 133303)	R&D Systems	Cat# IC0041P
PerCP Mouse anti-human CD11a (Clone CR38)	R&D Systems	Cat# FAB35951C (Discontinued)
PerCP Mouse IgG _{2A} Isotype Control (Clone 20102)	R&D Systems	Cat# IC003C
PerCP-eFluor710 Mouse anti-human PDL1 (Clone MIH1)	ThermoFisher Scientific	Cat# 46-5983-42
PerCP-eFluor710 Mouse IgG1, κ Isotype Control (Clone P3.6.2.8.1)	ThermoFisher Scientific	Cat# 46-4714-82
Alexa Fluor® 488 Mouse anti-human IL-17A (Clone BL168)	BioLegend	Cat# 512308
Alexa Fluor® 488 Mouse IgG1, κ Isotype Control (Clone MOPC-21)	BioLegend	Cat# 400134
PE-Cy7 Rat anti-human IL-17F (Clone SHLR17)	ThermoFisher Scientific	Cat# 25-7169-42
PE-Cy7 Rat IgG1, κ Isotype Control (Clone eBRG1)	ThermoFisher Scientific	Cat# 25-4301-82
PE Mouse anti-human IL-21 (Clone 3A3-N2)	BioLegend	Cat# 513004
PE Mouse IgG1, κ Isotype Control (Clone MOPC-21)	BioLegend	Cat# 400112
eFluor 660 Mouse anti-human IL-22 (Clone 22URTI)	ThermoFisher Scientific	Cat# 50-7229-42
eFluor 660 Mouse IgG1, κ Isotype Control (Clone P3.6.2.8.1)	ThermoFisher Scientific	Cat# 50-4714-82
BV605 Mouse anti-human IFN-γ (Clone B27)	BD	Cat# 562974
BV605 Mouse IgG1, κ Isotype Control (Clone X40)	BD	Cat# 562652
Ultra-LEAF™ Purified anti-human CD3 Antibody (Clone OKT3)	Biolegend	Cat# 317347
Ultra-LEAF™ Purified anti-human CD28 Antibody (Clone CD28.2)	Biolegend	Cat# 302943
Mouse IgG1 kappa Isotype Control (Clone P3.6.2.8.1)	ThermoFisher Scientific	Cat# 14-4714-85
Human IL12 monoclonal blocking antibody (Clone B-T21)	ThermoFisher Scientific	Cat# BMS152
Mouse IgG1 isotype control	R&D Systems	Cat# MAB002
Human CD2 monoclonal blocking antibody (Clone 299808)	R&D Systems	Cat# MAB18562
Mouse IgG2A isotype control	R&D Systems	Cat# MAB003
Anti-human CD28 monoclonal blocking antibody (Clone 9.3)	BioXcell	Cat# BE0248
Anti-Unknown Specificity (Isotype control) Human IgG1,k	Absolute Antibody	Cat# Ab00178-10.0
Anti-human ICOS monoclonal blocking antibody	N/A	The agonist ICOS antibody was produced for research purposes from the sequence made publicly available by JOUNCE THERAPEUTICS in the patent US 2016/0304610, INC. The produced antibody corresponded to the following sequences of the clone 37A10S713 with a human IgG1 isotype. Heavy chain: EVQLVESGGGLVQPGGSL RLSCAASGFTFSDYWMD WVRQAPGKGLVWVSNIDE DGSITEYSPFVKGRFTISR DNAKNTLYLQMNSLRAED

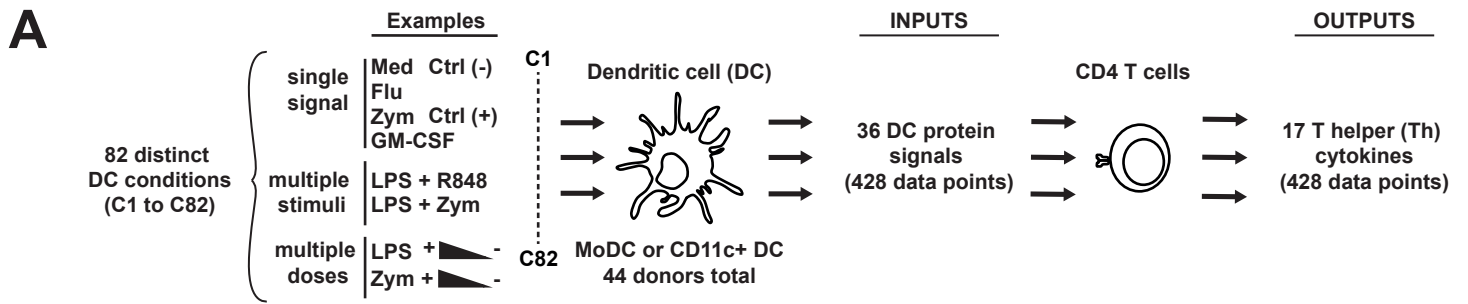
		<p>TAVYYCTRWGRFGFDSW GGQTLTVSSASTKGPSV FPLAPSSKSTSGGTAALG CLVKDYFPEPVTVSWNSG ALTSGVHTFPAVLQSSGLY SLSSVTVPSSSLGTQTYI CNVNHKPSNTKVDKKVEP KSCDKTHTCPPAPELL GGPSVFLFPPKPKDTLMIS RTPEVTCVVVDVSHEDPE VKFNWYVDGVEVHNAKTK PREEQYNSTYRVVSVLTVL HQDWLNGKEYKCKVSNKA LPAPIEKTISKAKGQPREP QVYTLPPSREEMTKNQVS LTCLVKGFYPSDIAVEWES NGQPENNYKTTTPVLDSD GSFFLYSKLTVDKSRWQQ GNVFSCSVMHEALHNHYT QKSLSLSPGK</p> <p>Light chain: IVMTQSPDSLAVSLGERAT INCKSSQSLLSGSFNLYLTW YQQKPGQPPKLLIFYASTR HTGVPDRFSGSGSGTDFT LTISSLQAEDVAVYYCHHH YNAPPTFGPGTKVDIKRTV AAPSVFIFPPSDEQLKSGT ASVVCLLNNFYPREAKVQ WKVDNALQSGNSQESVTE QDSKDSTYLSSTLTLSKA DYEKHKVYACEVTHQGLS SPVTKSFNRGEC</p> <p>Classical quality controls were performed to check that the produced anti-ICOS antibody had a correct, Purity (SDS-PAGE reducing), Homogeneity (SEC-MALS) Mass (LC-MS) and binding to target (FACS).</p>
Biological Samples		
Human Healthy blood donors for primary MoDC, bDC, naive and memory CD4 T cells	Etablissement Français du Sang (French Blood Bank)	N/A
Human serum	Sigma-Aldrich	Cat# H4522
Chemicals, Peptides and Recombinant Proteins		
Lymphoprep	StemCell Technologies	Cat# 07861
RPMI 1640 Medium, GlutaMAX™ Supplement	ThermoFisher Scientific	Cat# 61870010
Penicillin-Streptomycin	ThermoFisher Scientific	Cat# 15140122
Foetal Bovine Serum Research Grade	Hyclone/Perbio	Cat# CH30160.03
MEM Non-essential Amino Acids Solution (100X)	ThermoFisher Scientific	Cat# 11140050
Sodium pyruvate (100 mM)	ThermoFisher Scientific	Cat#11360070
X-VIVO 15 Chemically Defined, Serum-Free Hematopoietic Cell Medium	Ozyme	Cat# BE02-060F
Hepes Buffer	ThermoFisher Scientific	Cat# 15630056
UltraPure EDTA	ThermoFisher Scientific	Cat# 15575020

Phorbol 12-myristate 13-acetate	Sigma-Aldrich	Cat# P8139
Ionomycin calcium salt from Streptomyces conglobatus	Sigma-Aldrich	Cat# I0634
Brefeldin A Solution 1000X	ThermoFisher Scientific	Cat# 00-4506-51
Intracellular Fixation & Permeabilization Buffer Set	ThermoFisher Scientific	Cat# 88-8824-00
DAPI (4',6-Diamidino-2-Phenylindole, Dihydrochloride)	ThermoFisher Scientific	Cat# D1306
Zombie NIR Fixable Viability Kit	BioLegend	Cat# 423105
LIVE/DEAD™ Fixable Yellow Dead Cell Stain Kit	ThermoFisher Scientific	Cat# L34959
CellTrace™ Violet Cell Proliferation Kit, for flow cytometry	ThermoFisher Scientific	Cat# C34557
Recombinant human IL-1 α	R&D Systems	Cat# 200-LA
Recombinant human IL-1 β	Peptotech	Cat# 200-01B
Recombinant human IL-4	R&D Systems	Cat# 204-IL-010
Recombinant human IL-6	Peptotech	Cat# 200-06
Recombinant human IL-12p70	R&D Systems	Cat# 219-IL
Recombinant human IL-23	R&D Systems	Cat# 1290-IL
Recombinant human TGF- β 1	Peptotech	Cat# 100-21
Recombinant human IL-4	Miltenyi Biotec	Cat# 130-093-922
Recombinant human GM-CSF	Miltenyi Biotec	Cat# 130-093-865
PAM3CSK4	Invivogen	Cat# tlr1-pms
Aluminium potassium sulfate	Invivogen	Cat# tlr1-alk
Heat-killed Staphylococcus aureus	Invivogen	Cat# tlr1-hksa
Heat-killed Candida albicans	Invivogen	Cat# tlr1-hkca
Heat-killed Listeria monocytogenes	Invivogen	Cat# tlr1-hklm
Heat-killed Streptococcus pneumoniae	Invivogen	Cat# tlr1-hksp
Poly(I:C) High molecular weight	Invivogen	Tlr1-pic
Curdlan	Invivogen	Cat# tlr1-curd
Zymosan	Sigma-Aldrich	Cat# Z4250
LPS-EB Ultrapure	Invivogen	Cat# tlr1-3pelps
Prostaglandin E2	Sigma-Aldrich	Cat# P0409
R848	Invivogen	Cat# tlr1-r848
Recombinant Human IFN- β	Preprotech	Cat# 300-02BC
Influenza A/PR/8/34 (H1N1) Allantoic Fluid	Charles River	Cat# 10100781
Recombinant human TSLP	R&D Systems	Cat# 1398-TS
Critical Commercial Assays		
EasySep™ Human Pan-DC Pre-Enrichment Kit	StemCell Technologies	Cat# 19251
EasySep™ Human Naïve CD4+ T Cell Isolation Kit	StemCell Technologies	Cat# 19555
CD14 MicroBead human	Miltenyi Biotec	Cat# 130-050-201
LS columns	Miltenyi Biotec	Cat# 130-042-401
Memory CD4+ T Cell Isolation Kit, human	Miltenyi Biotec	Cat# 130-091-893
Dynabeads® Human T-Activator CD3/CD28 for T Cell Expansion and Activation	ThermoFisher Scientific	Cat# 11131D
Easy 50 EasySep™ Magnet	StemCell Technologies	Cat# 18002
Big Easy EasySep™ Magnet	StemCell Technologies	Cat# 18001
QuadroMACS Starting Kit (LS)	Miltenyi Biotec	Cat# 130-091-051
BD™ Cytometric Bead Array (CBA) Human Soluble Protein Master Buffer Kit	BD	Cat# 558265
BD™ Cytometric Bead Array (CBA) Human IL-1 α Flex Set	BD	Cat# 560153
BD™ Cytometric Bead Array (CBA) Human IL-1 β Flex Set	BD	Cat# 558279
BD™ Cytometric Bead Array (CBA) Human IL-2 Flex Set	BD	Cat# 558270
BD™ Cytometric Bead Array (CBA) Human IL-3 Flex Set	BD	Cat# 558355

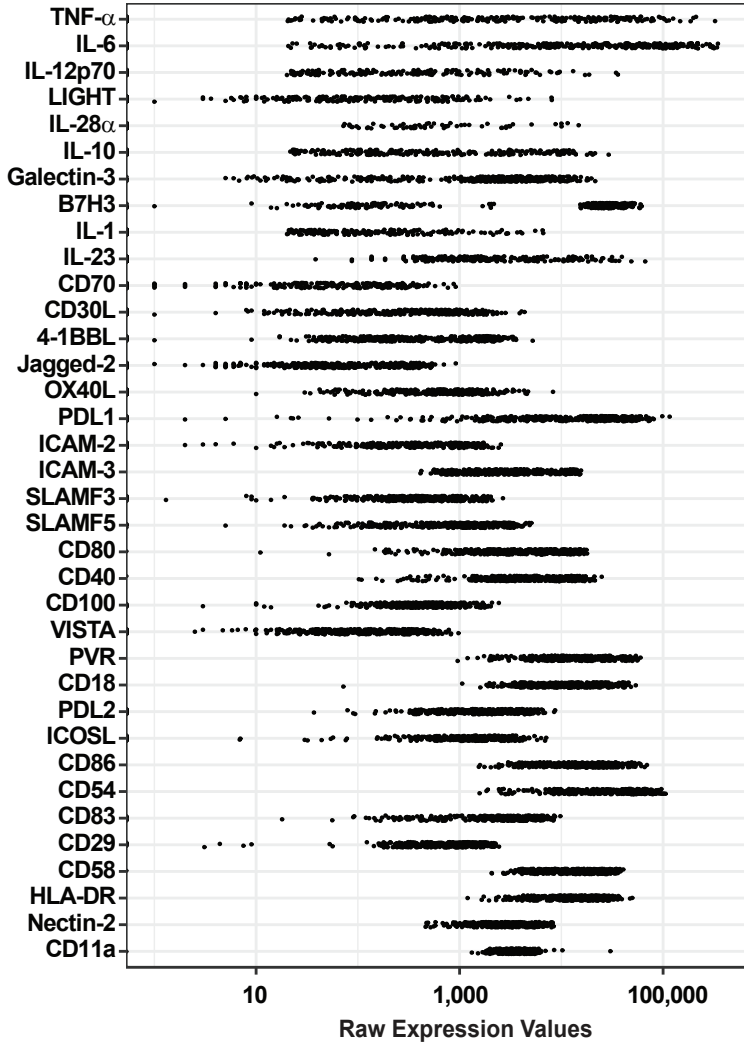
BD™ Cytometric Bead Array (CBA) Human IL-4 Flex Set	BD	Cat# 558272
BD™ Cytometric Bead Array (CBA) Human IL-5 Flex Set	BD	Cat# 558278
BD™ Cytometric Bead Array (CBA) Human IL-6 Flex Set	BD	Cat# 558276
BD™ Cytometric Bead Array (CBA) Human IL-9 Flex Set	BD	Cat# 558333
BD™ Cytometric Bead Array (CBA) Human IL-10 Flex Set	BD	Cat# 558274
BD™ Cytometric Bead Array (CBA) Human IL-12p70 Flex Set	BD	Cat# 558283
BD™ Cytometric Bead Array (CBA) Human IL-13 Flex Set	BD	Cat# 558450
BD™ Cytometric Bead Array (CBA) Human IL-17A Flex Set	BD	Cat# 560383
BD™ Cytometric Bead Array (CBA) Human IL-17F Flex Set	BD	Cat# 562151
BD™ Cytometric Bead Array (CBA) Human GM-CSF Flex Set	BD	Cat# 558335
BD™ Cytometric Bead Array (CBA) Human IFN-γ Flex Set	BD	Cat# 558269
BD™ Cytometric Bead Array (CBA) Human TNF-α Flex Set	BD	Cat# 558273
MILLIPLEX MAP Human TH17 Magnetic Bead Panel - Immunology Multiplex Assay IL-21, IL-22, IL-31, TNF-β	Merck Millipore	Cat# HTH17MAG-14K
MILLIPLEX MAP Human TH17 Magnetic Bead Panel - Immunology Multiplex Assay IL-23, IL-28α	Merck Millipore	Cat# HTH17MAG-14K
RNeasy Micro Kit (50)	Qiagen	Cat# 74004
SuperScript™ II Reverse Transcriptase	ThermoFisher Scientific	Cat# 18064-071
Random primers	Promega	Cat# C1181
Oligo(dT)15 Primer	Promega	Cat# C1101
RNasin® Ribonuclease Inhibitors	Promega	Cat# N2515
dNTP	Promega	Cat# U1240
qPCR MasterMix Plus dTTP	Eurogentec	Cat# 05-QP2X-03+WOUN
Oligonucleotides		
RORC [Hs01076112_m1]	ThermoFisher Scientific	Cat# 4331182
TBX21 [Hs00203436_m1]	ThermoFisher Scientific	Cat# 4331182
GATA3 [Hs00231122_m1]	ThermoFisher Scientific	Cat# 4331182
RORA [Hs00536545_m1]	ThermoFisher Scientific	Cat# 4331182
FOXP3 [Hs00203958_m1]	ThermoFisher Scientific	Cat# 4331182
FOXP1 [Hs00212860_m1]	ThermoFisher Scientific	Cat# 4331182
SH2D1A [Hs00158978_m1]	ThermoFisher Scientific	Cat# 4331182
PRDM1 [Hs00153357_m1]	ThermoFisher Scientific	Cat# 4331182
PDCD1 [Hs01550088_m1]	ThermoFisher Scientific	Cat# 4331182
BTLA [Hs00699198_m1]	ThermoFisher Scientific	Cat# 4331182
HLX [Hs00172035_m1]	ThermoFisher Scientific	Cat# 4331182
IRF1 [Hs00971965_m1]	ThermoFisher Scientific	Cat# 4331182
CMIP [Hs00286832_m1]	ThermoFisher Scientific	Cat# 4331182

MAF [Hs00193519_m1]	ThermoFisher Scientific	Cat# 4331182
RUNX1 [Hs00231079_m1]	ThermoFisher Scientific	Cat# 4331182
PU1 / SPI1 [Hs02786711_m1]	ThermoFisher Scientific	Cat# 4331182
CD200 [Hs01033303_m1]	ThermoFisher Scientific	Cat# 4331182
CXCL13 [Hs00757930_m1]	ThermoFisher Scientific	Cat# 4331182
IL-12RB2 [Hs00155486_m1]	ThermoFisher Scientific	Cat# 4331182
BCL6 [Hs00153368_m1]	ThermoFisher Scientific	Cat# 4331182
IRF4 [Hs00180031_m1]	ThermoFisher Scientific	Cat# 4331182
FOSL2 [Hs01050117_m1]	ThermoFisher Scientific	Cat# 4331182
BATF [Hs00232390_m1]	ThermoFisher Scientific	Cat# 4331182
KDM6B [Hs00996325_g1]	ThermoFisher Scientific	Cat# 4331182
NFKBIZ [Hs00230071_m1]	ThermoFisher Scientific	Cat# 4331182
SATB1 [Hs00962580_m1]	ThermoFisher Scientific	Cat# 4331182
BCL11B [Hs01102259_m1]	ThermoFisher Scientific	Cat# 4331182
EOMES [Hs00172872_m1]	ThermoFisher Scientific	Cat# 4331182
SKI [Hs01057032_m1]	ThermoFisher Scientific	Cat# 4331182
ATF6 [Hs00232586_m1]	ThermoFisher Scientific	Cat# 4331182
AES [Hs01081012_m1]	ThermoFisher Scientific	Cat# 4331182
CREM [Hs01582003_g1]	ThermoFisher Scientific	Cat# 4331182
DDIT3 [Hs00358796_g1]	ThermoFisher Scientific	Cat# 4331182
LEF1 [Hs01547250_m1]	ThermoFisher Scientific	Cat# 4331182
NFATC2 [Hs00905451_m1]	ThermoFisher Scientific	Cat# 4331182
ETV6 [Hs00231101_m1]	ThermoFisher Scientific	Cat# 4331182
SIRT2 [Hs01560289_m1]	ThermoFisher Scientific	Cat# 4331182
USP18 [Hs00276441_m1]	ThermoFisher Scientific	Cat# 4331182
NFATC1 [Hs00542675_m1]	ThermoFisher Scientific	Cat# 4331182
NFATC3 [Hs00190046_m1]	ThermoFisher Scientific	Cat# 4331182
SMAD3 [Hs00969210_m1]	ThermoFisher Scientific	Cat# 4331182
SMAD2 [Hs00998187_m1]	ThermoFisher Scientific	Cat# 4331182
SMAD7 [Hs00998193_m1]	ThermoFisher Scientific	Cat# 4331182
MINA [Hs01031255_m1]	ThermoFisher Scientific	Cat# 4331182
POUA2F1 [Hs01573369_m1]	ThermoFisher Scientific	Cat# 4331182

TNFRSF4/OX40 [Hs00937195_g1]	ThermoFisher Scientific	Cat# 4331182
TNFRSF8/CD30 [Hs00174277_m1]	ThermoFisher Scientific	Cat# 4331182
TIGIT [Hs00545087_m1]	ThermoFisher Scientific	Cat# 4331182
CD226/DNAM-1 [Hs00170832_m1]	ThermoFisher Scientific	Cat# 4331182
CD96 [Hs00976975_m1]	ThermoFisher Scientific	Cat# 4331182
IL17A [Hs00174383_m1]	ThermoFisher Scientific	Cat# 4331182
IL17F [Hs00369400_m1]	ThermoFisher Scientific	Cat# 4331182
STAT3 [Hs00374280_m1]	ThermoFisher Scientific	Cat# 4331182
ICOS [Hs00359999_m1]	ThermoFisher Scientific	Cat# 4331182
IL23R [Hs00332759_m1]	ThermoFisher Scientific	Cat# 4331182
AHR [Hs00169233_m1]	ThermoFisher Scientific	Cat# 4331182
IL1R2 [Hs01030384_m1]	ThermoFisher Scientific	Cat# 4331182
CCL20 [Hs01011368_m1]	ThermoFisher Scientific	Cat# 4331182
IL2RA [Hs00907779_m1]	ThermoFisher Scientific	Cat# 4331182
IL2RB [Hs01081697_m1]	ThermoFisher Scientific	Cat# 4331182
IL2RG [Hs00953624_m1]	ThermoFisher Scientific	Cat# 4331182
IL17RA [Hs01064648_m1]	ThermoFisher Scientific	Cat# 4331182
CCR6 [Hs00171121_m1]	ThermoFisher Scientific	Cat# 4331182
B2M [Hs99999907_m1]	ThermoFisher Scientific	Cat# 4331182
RPL34 [Hs00241560_m1]	ThermoFisher Scientific	Cat# 4331182
Software and Algorithms		
GraphPad Prism 6 – Version 6.01	GraphPad	https://www.graphpad.com/
FlowJo V10 – Version 10.0.8	FlowJo	https://www.flowjo.com
Bioplex Manager Software	BioRad	http://www.bio-rad.com/en-cn/product/bio-plex-manager-software-standard-edition?ID=5846e84e-03a7-4599-a8ae-7ba5dd2c7684
FCAP Array – Version 3.0	BD	http://www.bdbiosciences.com/us/applications/research/bead-based-immunoassays/analysis-software/fcap-array-software-v30/p/652099
R version 3.5.2	The R Foundation	https://www.r-project.org/



B DC surface and secreted communication signals (n=428 data points)



C

Input	Range (log)	% of positive observations	Coefficient of variation
TNF- α	5.00	63.32	2.04
IL-6	5.00	78.74	1.43
IL-12p70	4.00	41.12	2.72
LIGHT	4.00	50.00	2.30
IL-28 α	4.00	14.25	1.82
IL-10	4.00	56.54	1.70
Galectin-3	4.00	98.36	1.09
B7H3	4.00	97.66	0.67
IL-1	3.00	41.12	2.10
IL-23	3.00	54.67	1.64
CD70	3.00	47.20	1.19
CD30L	3.00	79.21	1.08
4-1BBL	3.00	96.26	1.06
Jagged-2	3.00	79.67	1.05
OX40L	3.00	74.53	0.97
PDL1	3.00	96.50	0.94
ICAM-2	3.00	73.13	0.90
ICAM-3	3.00	100.00	0.89
SLAMF3	3.00	96.73	0.83
SLAMF5	3.00	98.60	0.82
CD80	3.00	99.77	0.78
CD40	3.00	99.77	0.76
CD100	3.00	98.13	0.72
VISTA	2.00	92.76	0.97
PVR	2.00	100.00	0.75
CD18	2.00	100.00	0.72
PDL2	2.00	93.22	0.71
ICOSL	2.00	90.65	0.65
CD86	2.00	100.00	0.65
CD54	2.00	100.00	0.64
CD83	2.00	97.90	0.60
CD29	2.00	98.13	0.59
CD58	2.00	99.77	0.57
HLA-DR	2.00	100.00	0.56
Nectin-2	2.00	100.00	0.53
CD11a	1.00	99.77	0.44

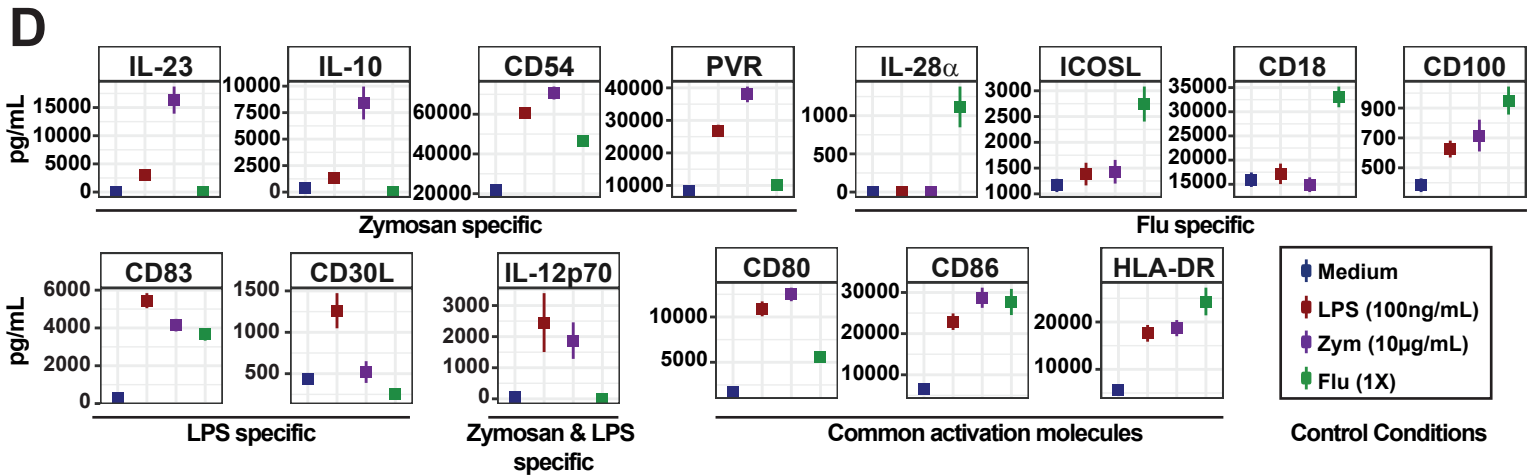


FIGURE 1: Variability and specificity of DC communication signals

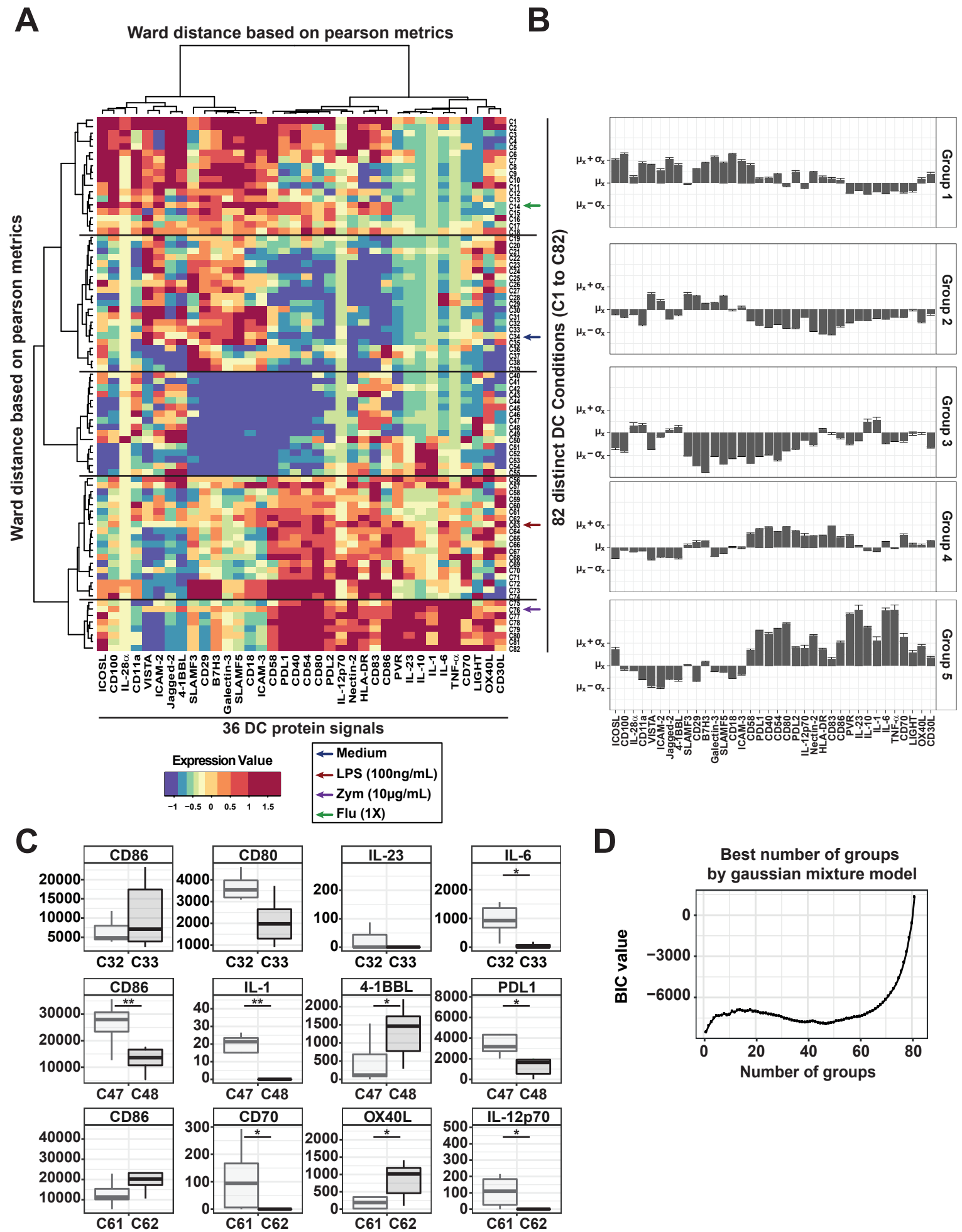
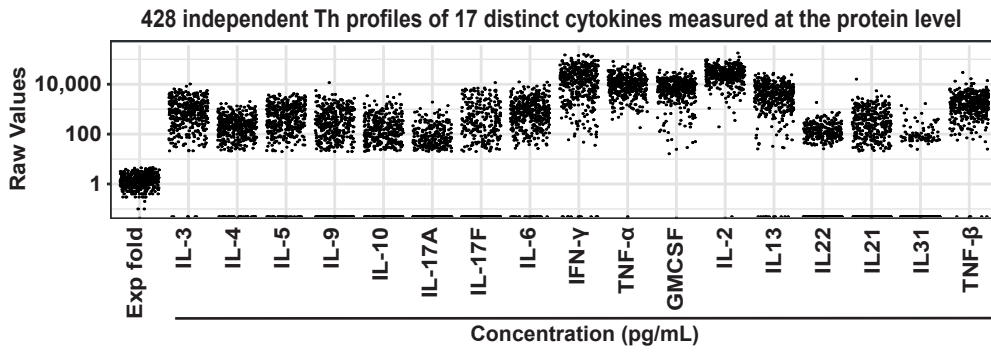
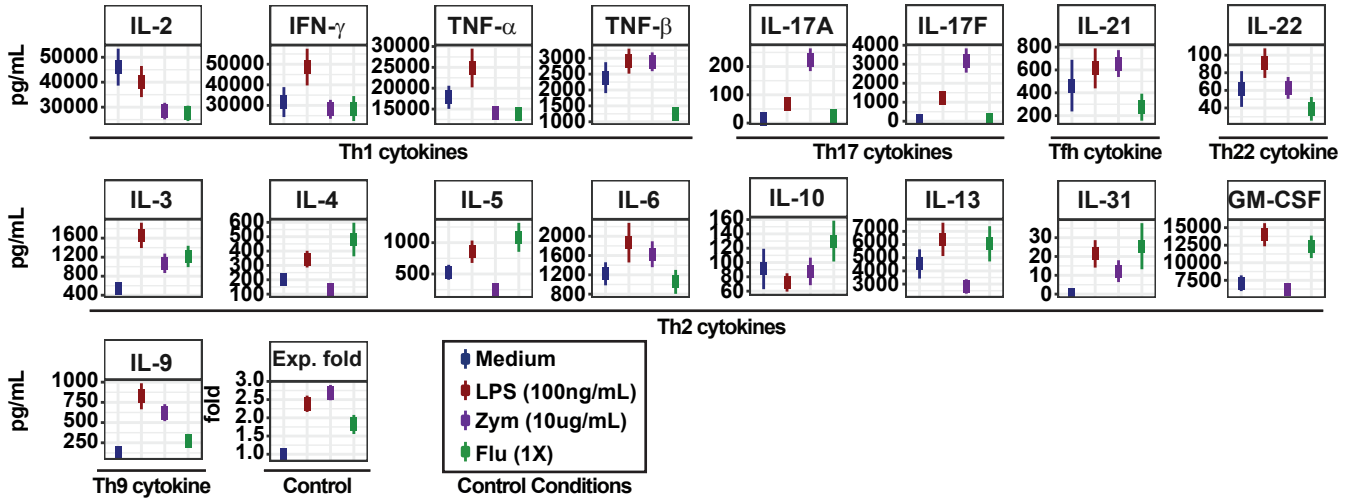


FIGURE 2: The diversity of DC states is defined by unique combinations of communication molecules

A**B****C**

Ward distance based on pearson metrics

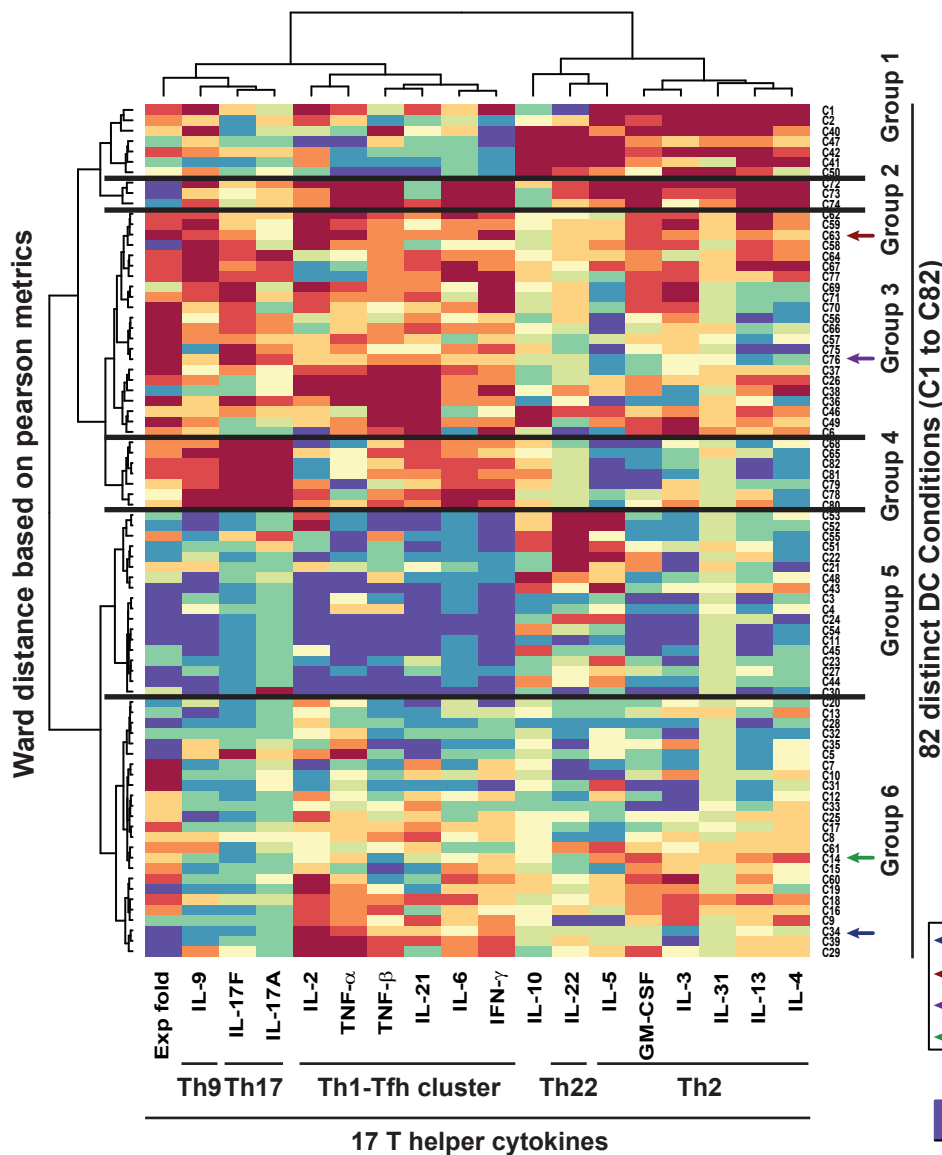
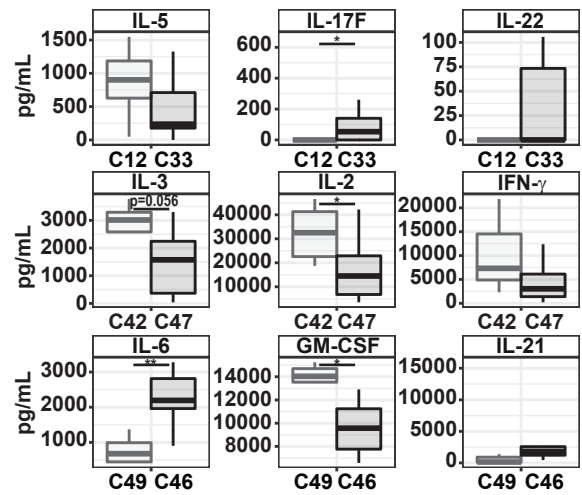
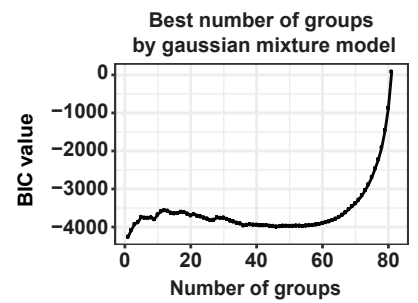
**D****E**

FIGURE 3: Th cytokine responses mirror the variability in DC communication states

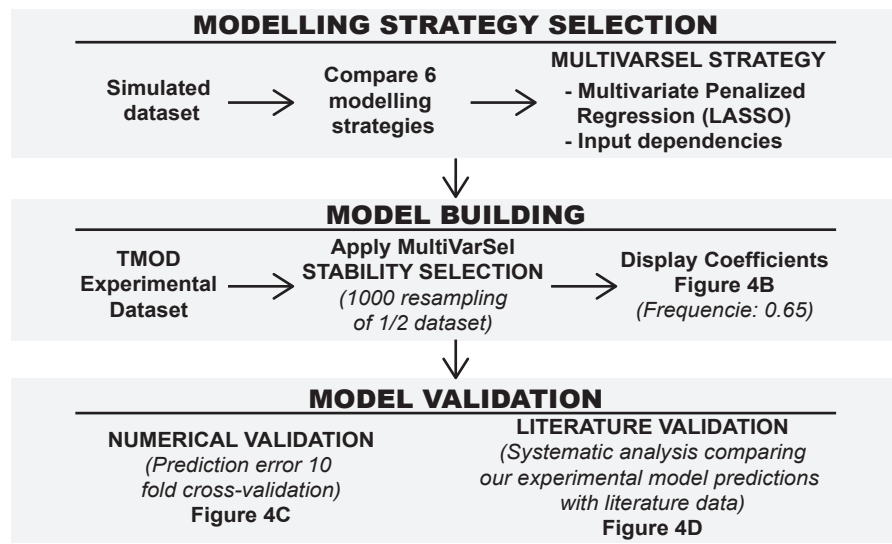
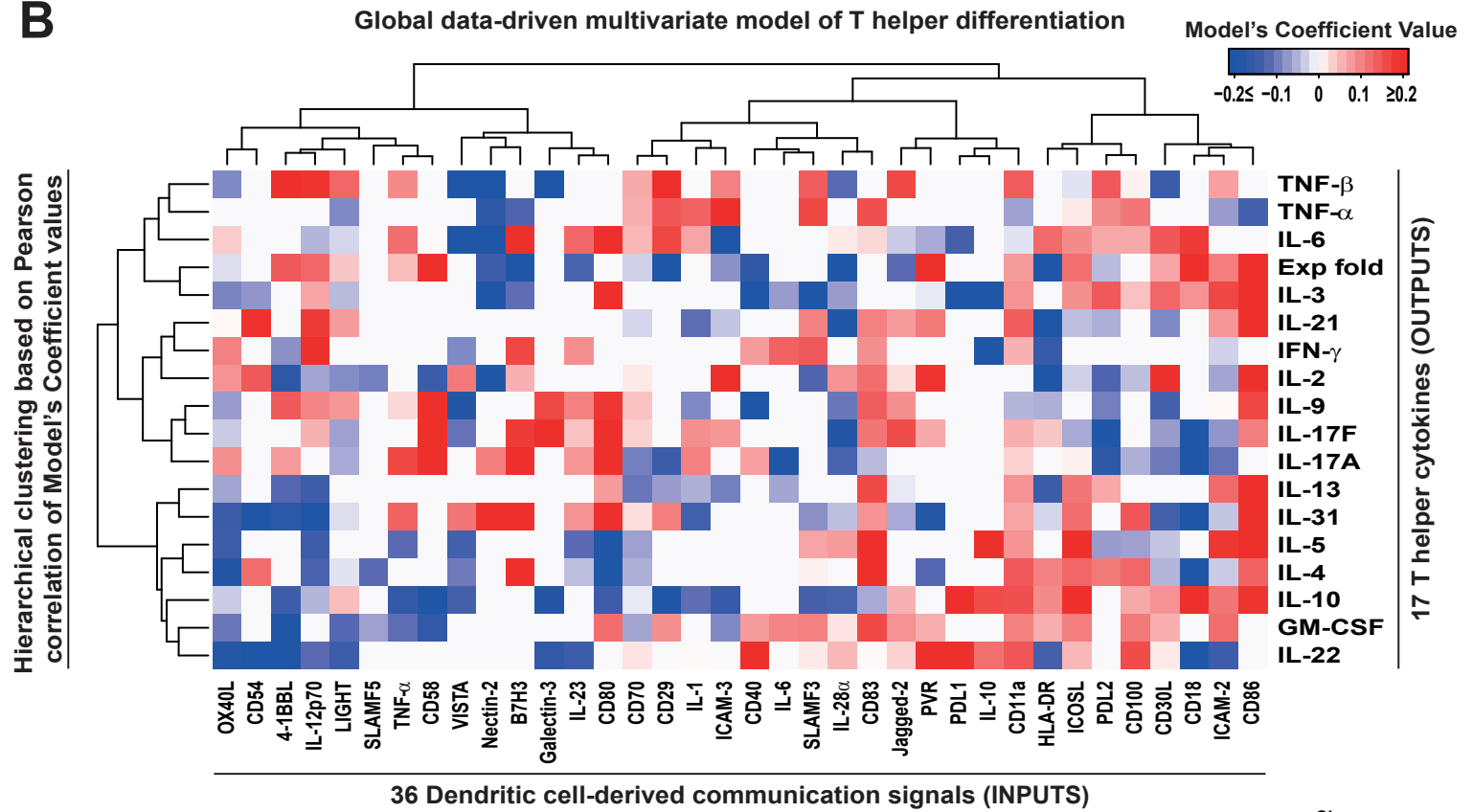
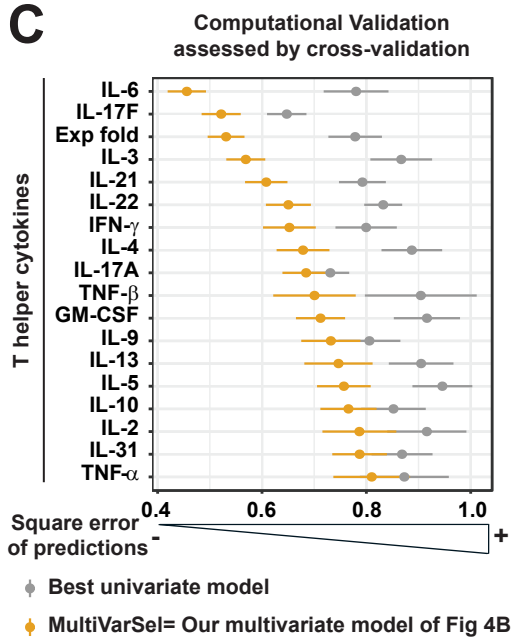
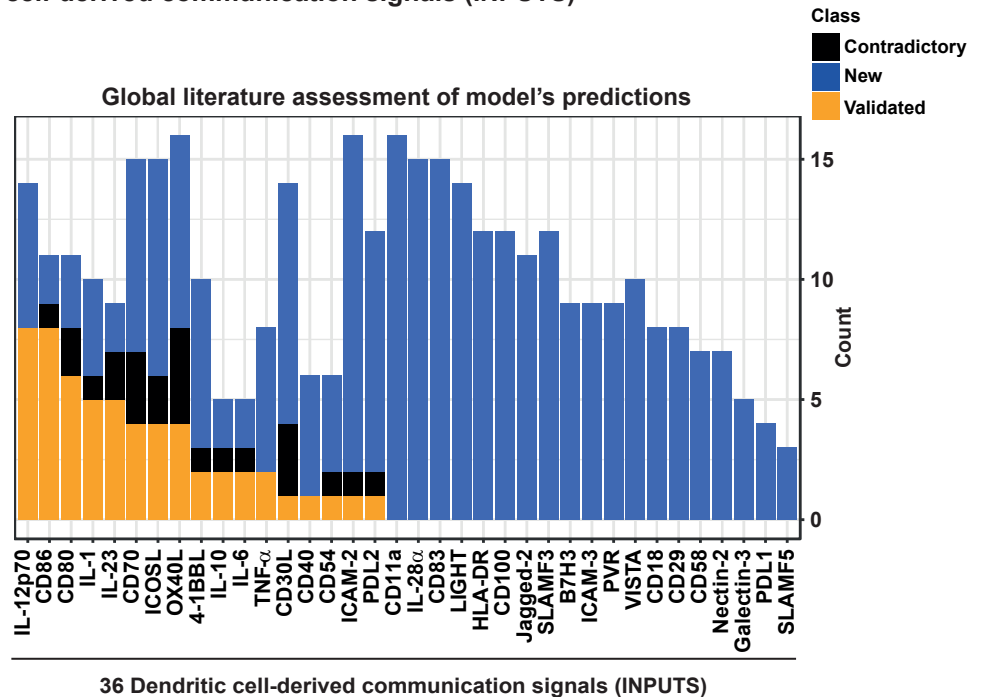
A**B****C****D**

FIGURE 4: A data-driven Lasso penalized regression model predicts multiple Th differentiation outcomes from DC-derived communication signals expression

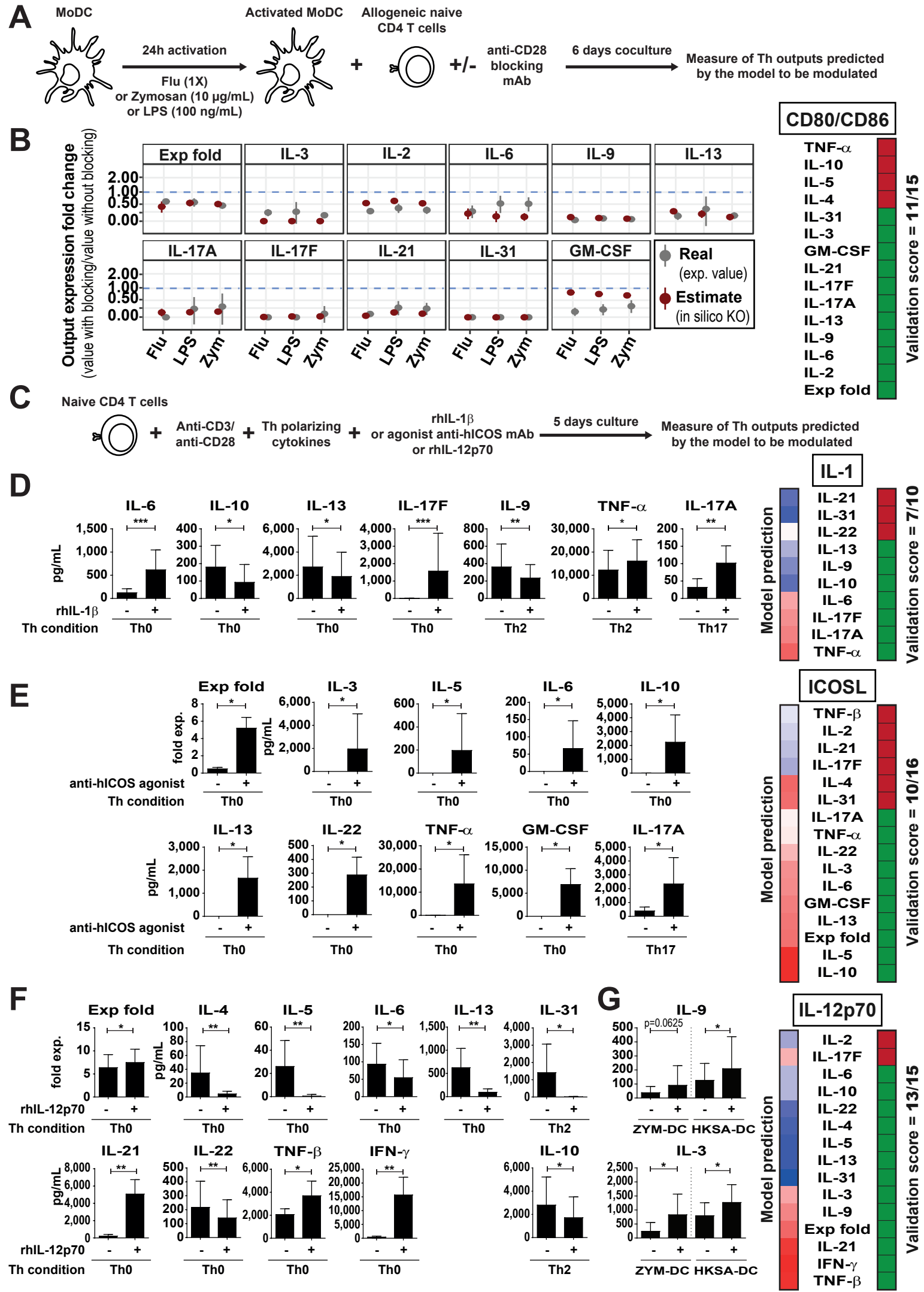
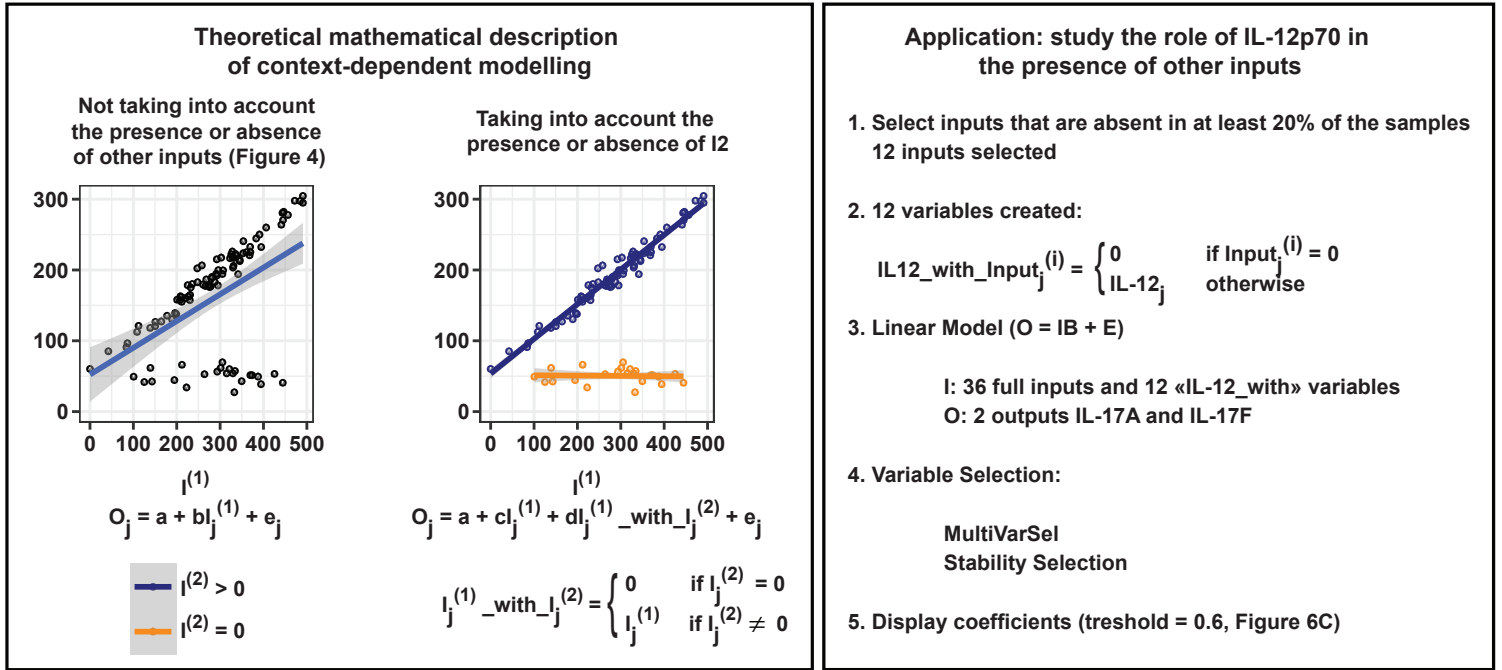
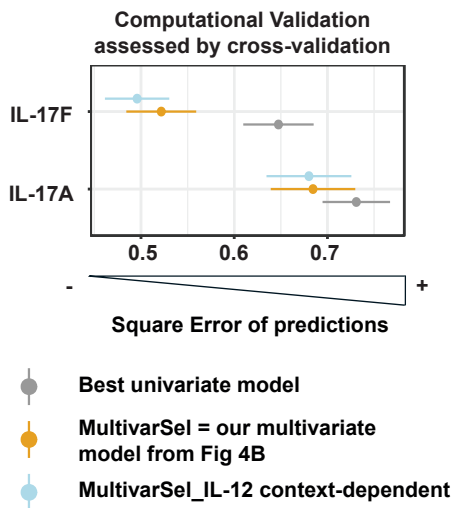


FIGURE 5: Independent and systematic experimental validation of model's prediction

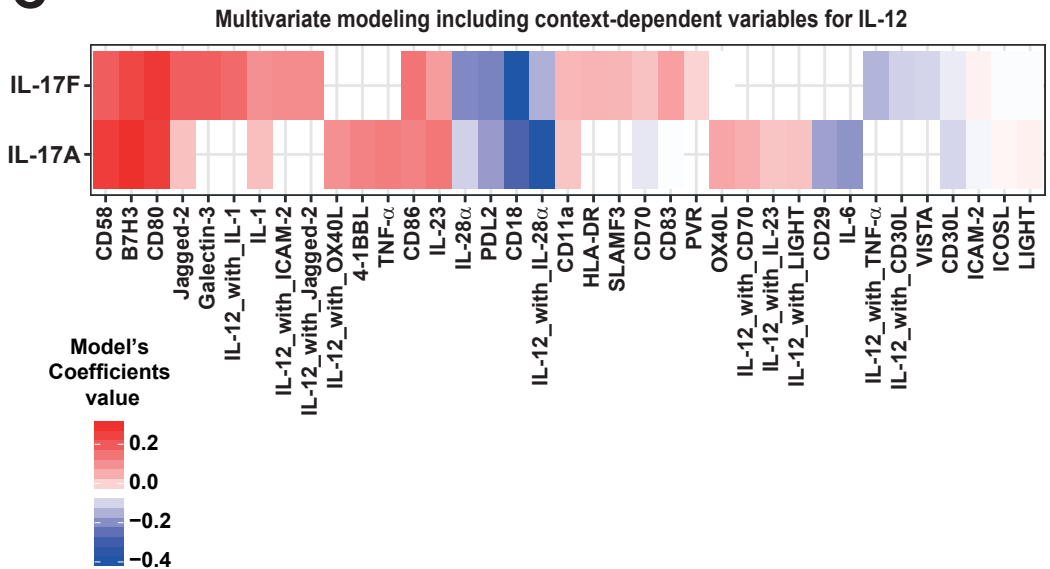
A



B

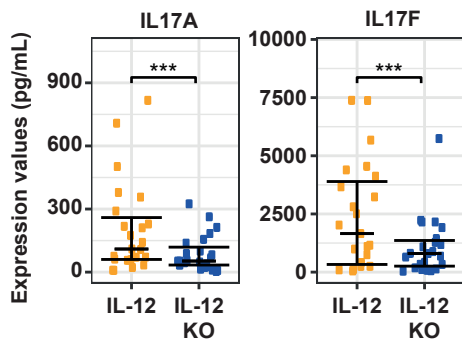


C



D

Model predictions on IL-12 in silico KO in 10 µg/mL zymosan treated MoDC



E

Experimental validation of IL-12 in silico knock-out on zymosan treated MoDC

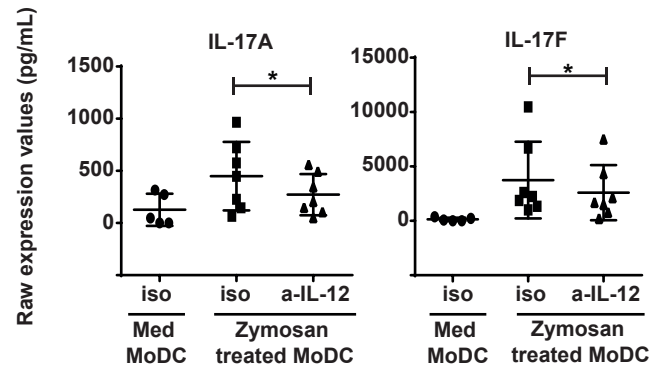


FIGURE 6: Context-dependent model reveals a role for IL-12p70 in Th17 differentiation

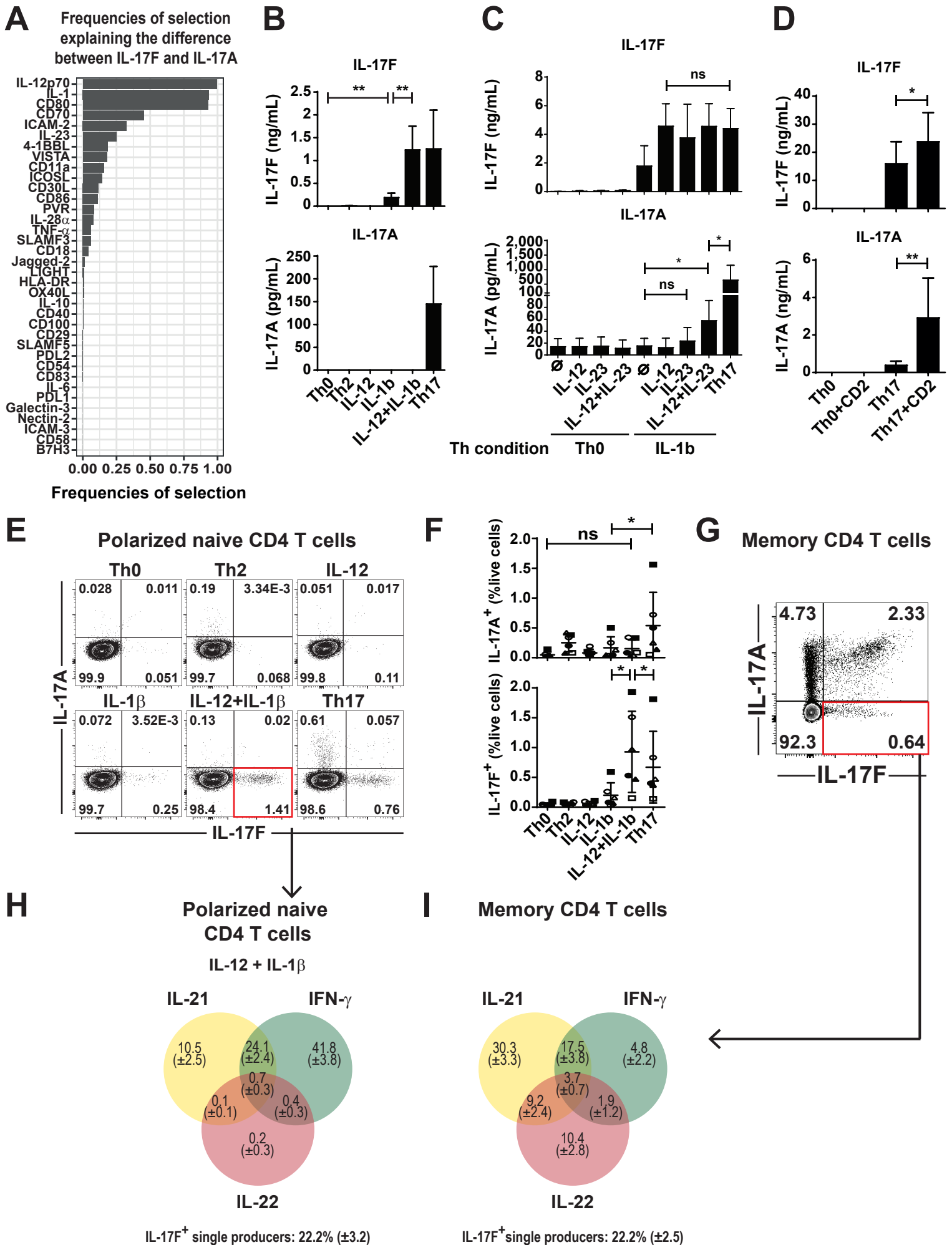
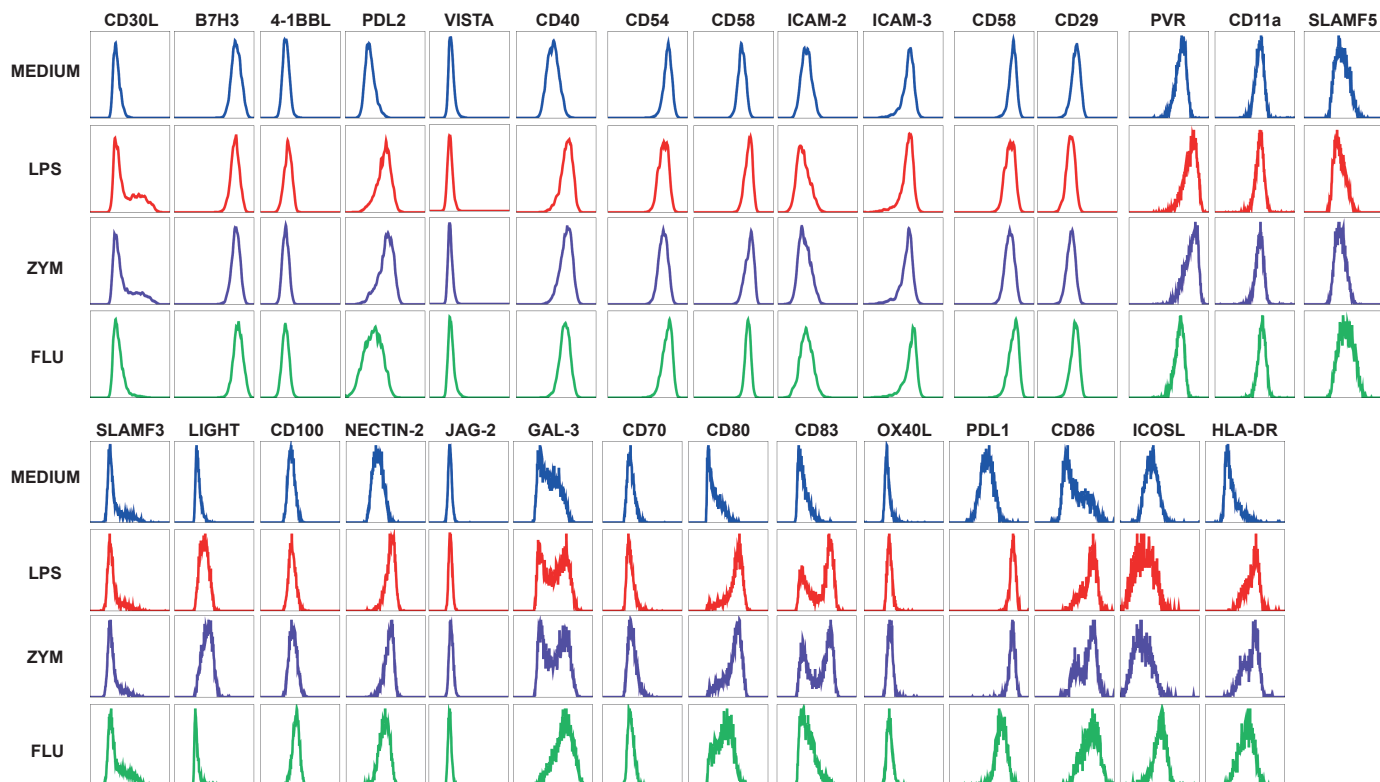


FIGURE 7: Synergistic interaction of IL-12p70 and IL-1 cytokines in the specific induction of IL-17F without production of IL-17A

A

Example of MoDC activation profile after 24 hours stimulation with Medium, LPS, Zymosan or Flu. 29 surface markers measured by flow cytometry shown on one representative donor.

**B**

Comparison with Zymosan (10 μ g/mL)

	IL-23	IL-10	CD54	PVR
Medium	0.000	0.000	0.000	0.000
LPS (100ng/mL)	0.000	0.000	0.044	0.003
Flu (1X)	0.000	0.000	0.000	0.000

Comparison with LPS (100ng/mL)

	IL-12p70	CD83	CD30L
Medium	<0.001	<0.001	0.005
Zymosan (10 μ g/mL)	0.432	0.002	0.008
Flu (1X)	<0.001	0.002	0.002

Comparison with Flu (1X)

	IL-28 α	ICOSL	CD18	CD100
Medium	<0.001	<0.001	<0.001	<0.001
LPS (100ng/mL)	<0.001	0.005	<0.001	0.017
Zymosan (10 μ g/mL)	<0.001	0.003	<0.001	0.017

Comparison with Medium

	CD86	CD80	HLA-DR
Zymosan (10 μ g/mL)	<0.001	<0.001	<0.001
LPS (100ng/mL)	<0.001	<0.001	<0.001
Flu (1X)	<0.001	<0.001	<0.001

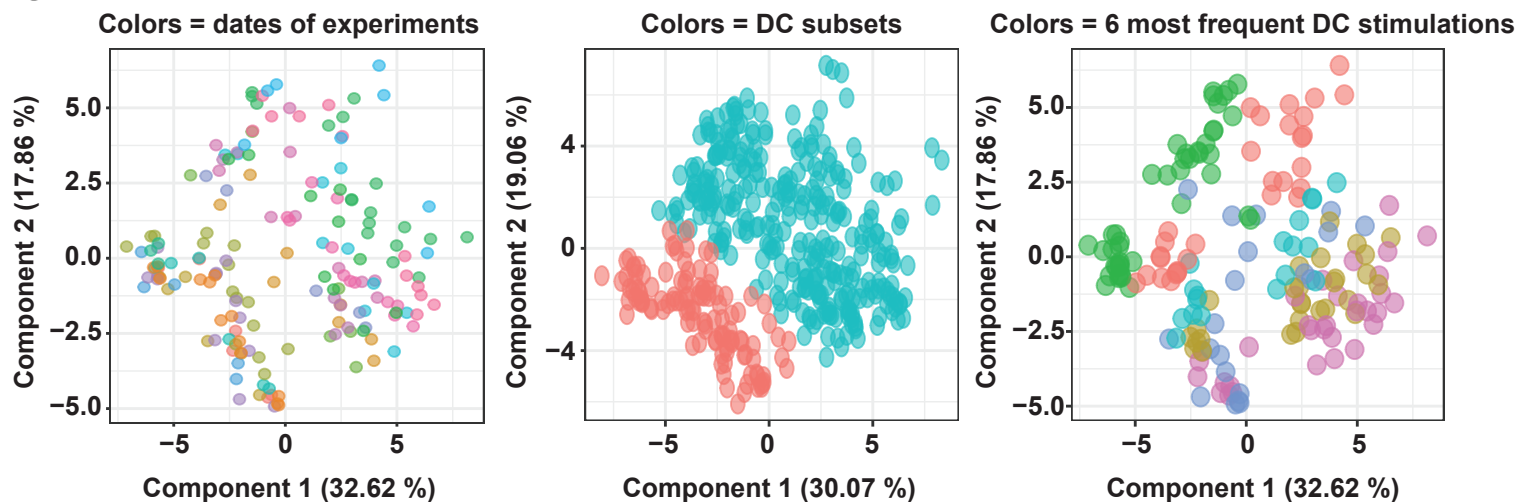
C

FIGURE S1: Descriptive analysis of 36 DC-derived communication molecules

A

Input	Range (log)	% of positive observations	Coefficient of variation
IL-21	4.00	86.45	1.89
IL-10	4.00	97.43	1.78
IL-17F	4.00	75.23	1.75
IL-9	4.00	94.39	1.67
IL-5	4.00	99.53	1.07
IL-4	4.00	98.83	1.06
IL-13	4.00	97.66	0.92
IL-17A	3.00	83.18	1.77
IL-6	3.00	98.83	1.28
IFN- γ	3.00	97.20	1.08
IL-3	3.00	99.77	1.05
TNF- α	3.00	99.77	0.86
GM-CSF	3.00	100.00	0.72
IL-31	2.00	21.03	1.54
TNF- β	2.00	98.83	1.08
IL-22	2.00	57.94	0.98
IL-2	2.00	99.77	0.68
Expansion-fold	1.00	100.00	0.61

B

Comparison with Medium

	IL-2
Zymosan (10 μ g/mL)	0,7439
LPS (100ng/mL)	0,0535
Flu (1X)	0,0579

Comparison with Zymosan (10 μ g/mL)

	Expansion fold	IL-17A	IL-17F	IL-21
Medium	<0,001	<0,001	<0,001	0,0054
LPS (100ng/mL)	0,3007	0,0013	0,0127	0,1983
Flu (1X)	0,0093	<0,001	<0,001	1

Comparison with LPS (100ng/mL)

	IL-3	IL-9	IL-6	IFN- γ
Medium	0,0003	<0,001	0,2698	0,0858
Zymosan (10 μ g/mL)	0,082	0,5334	0,9814	0,1154
Flu (1X)	0,281	0,0072	0,1136	0,1279

Comparison with Flu (1X)

	IL-4	IL-5	IL-10	IL-31
Medium	0,0584	0,0403	0,1287	0,0056
LPS (100ng/mL)	0,9769	0,504	0,1755	0,9149
Zymosan (10 μ g/mL)	0,0053	0,0003	0,2841	0,3998

	TNF- α	IL-22	IL-13	GM-CSF	TNF- β
Medium	0,3724	0,0579	0,0417	0,0008	0,1565
Zymosan (10 μ g/mL)	0,1823	0,2772	0,0019	<0,001	0,8342
Flu (1X)	0,1606	0,0188	0,4856	0,8391	0,0015

C

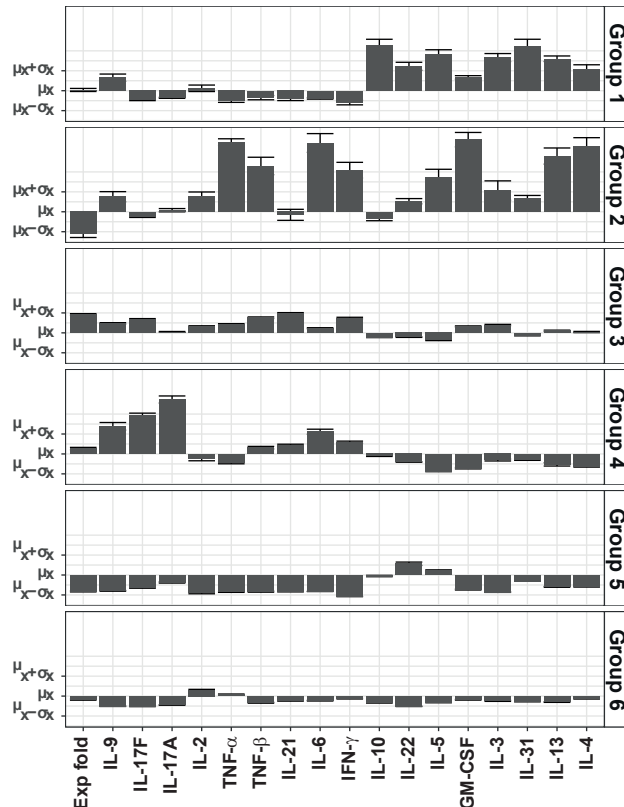
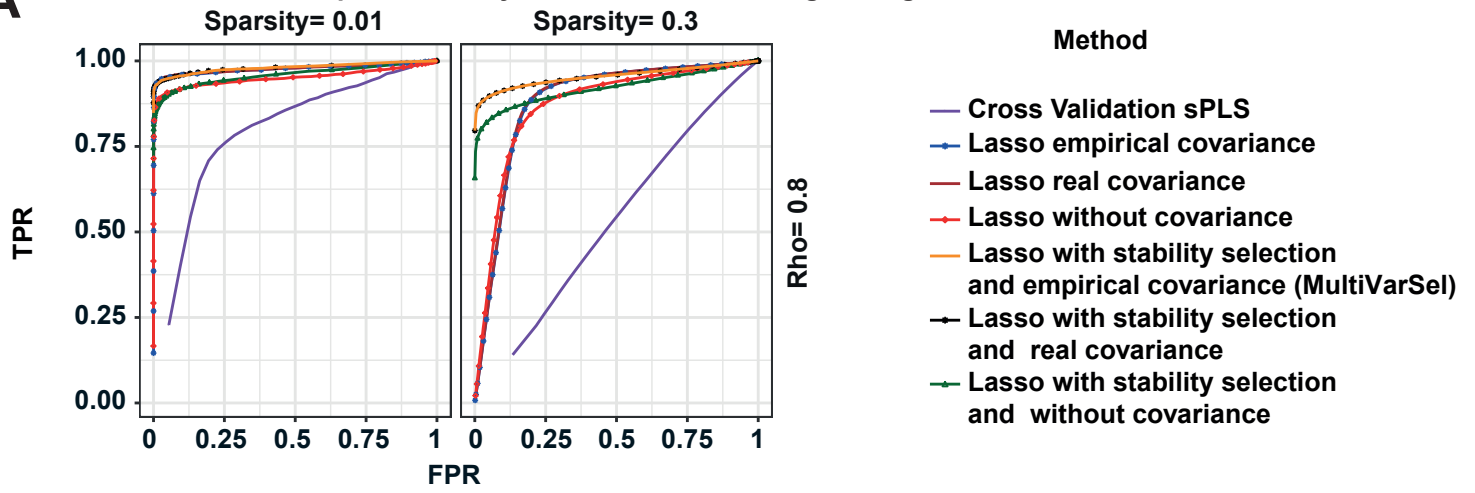


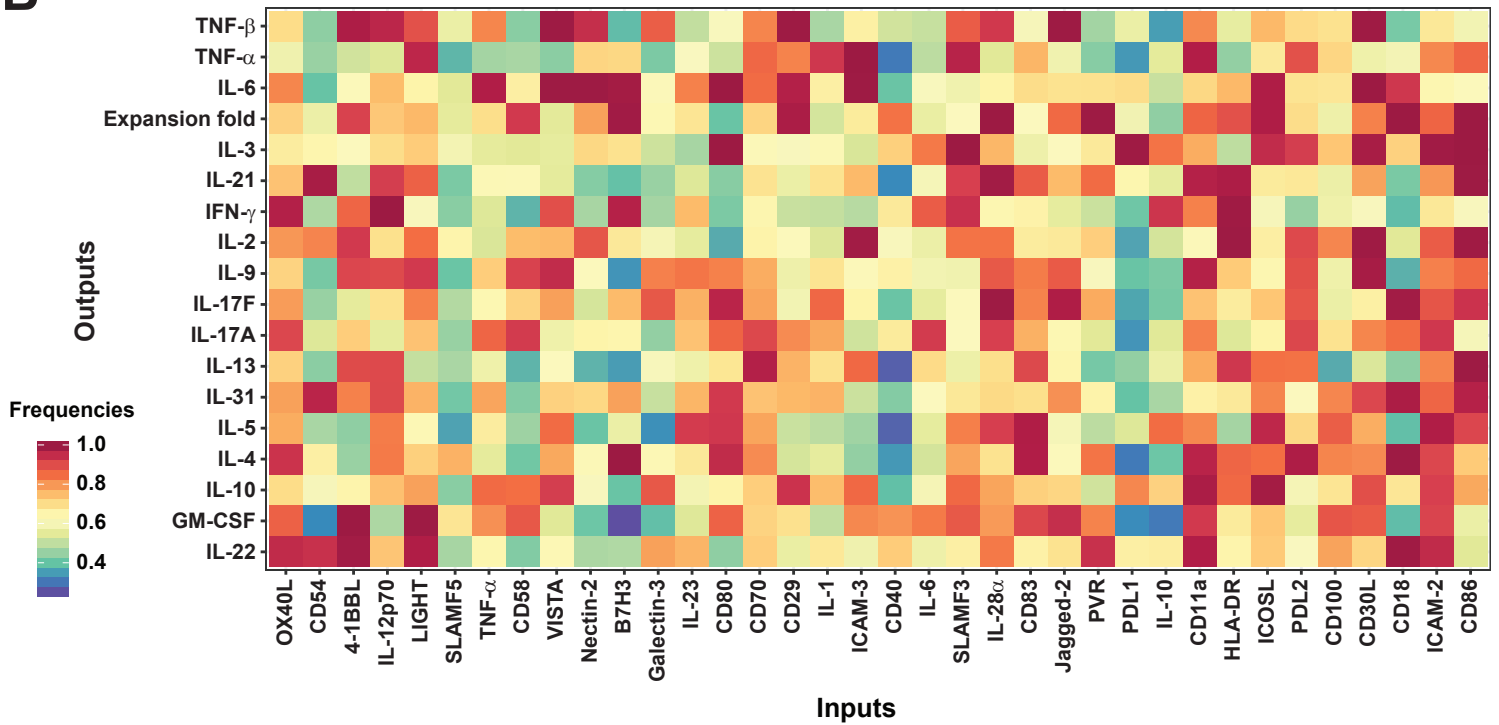
FIGURE S2: Mathematical description and statistical analysis of T helper cytokine profiles

A

Comparative analysis of distinct modelling strategies on simulated data

**B**

Frequency of selection of input variables established through model stability selection

**C**

Th signals	DC signals	Spearman correlation	Adjusted p-values
Exp fold	CD80	0.49	5.66e-27
GM-CSF	CD83	0.31	1.08e-10
IFN- γ	CD54	0.48	1.16e-25
IL-10	ICAM-3	-0.49	9.19e-27
IL-13	CD86	0.29	1.12e-09
IL-17A	CD80	0.52	1.38e-30
IL-17F	CD80	0.56	1.26e-35
IL-2	4-1BBL	-0.32	1.05e-11
IL-21	PVR	0.45	3.37e-22
IL-22	CD18	-0.45	1.17e-22
IL-3	CD80	0.39	5.00e-17
IL-31	CD86	0.38	5.17e-16
IL-4	CD86	0.30	1.83e-10
IL-5	IL-12p70	-0.18	1.58e-04
IL-6	CD80	0.46	4.38e-23
IL-9	CD80	0.50	3.35e-27
TNF- α	CD29	0.41	1.46e-18
TNF- β	SLAMF3	0.29	5.62e-10

D

Error of prediction of the model respectively on blood DC dataset and MoDC dataset

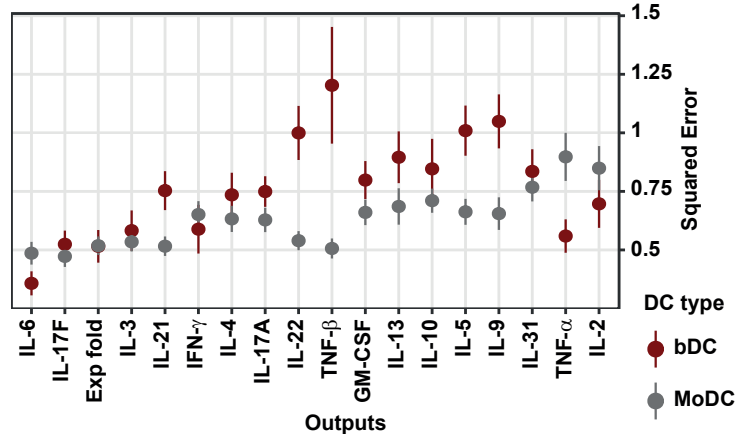
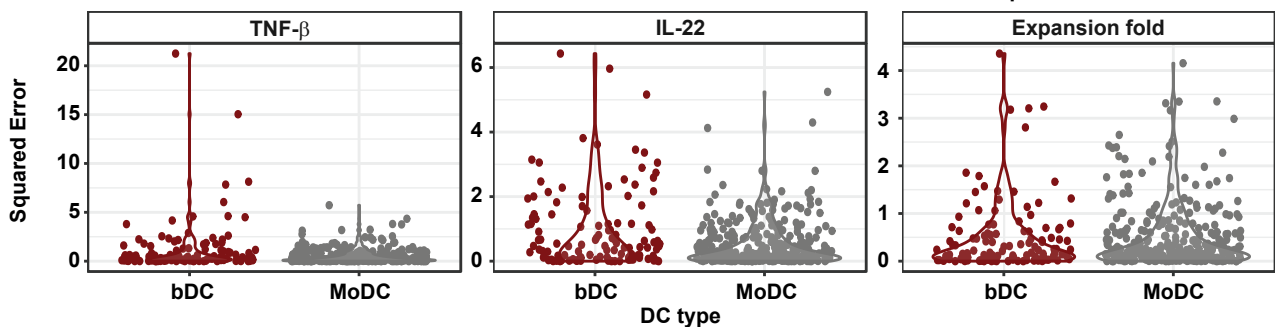
**E**

FIGURE S3: Multivariate modelling strategies applied to our DC-T datasets

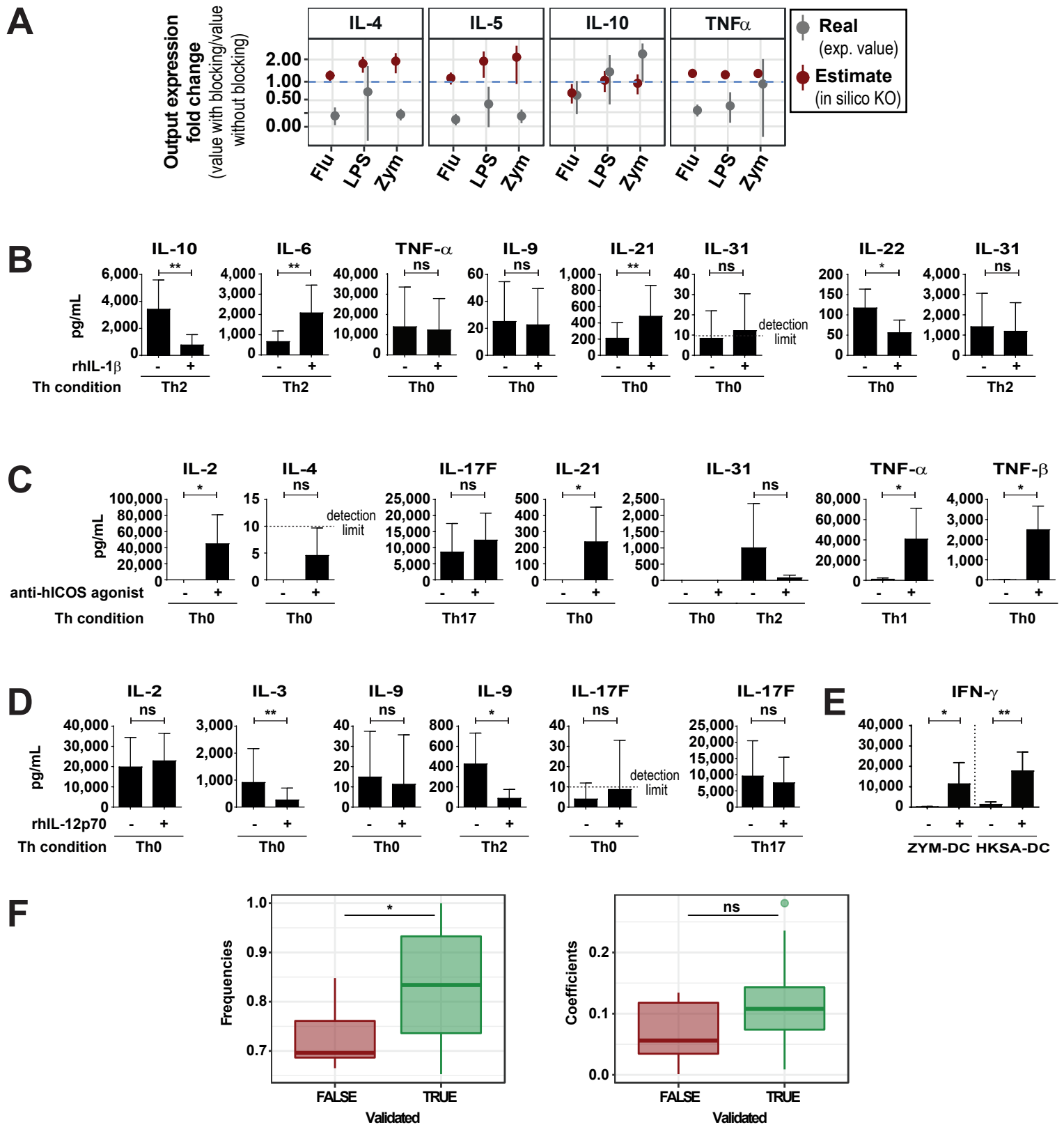
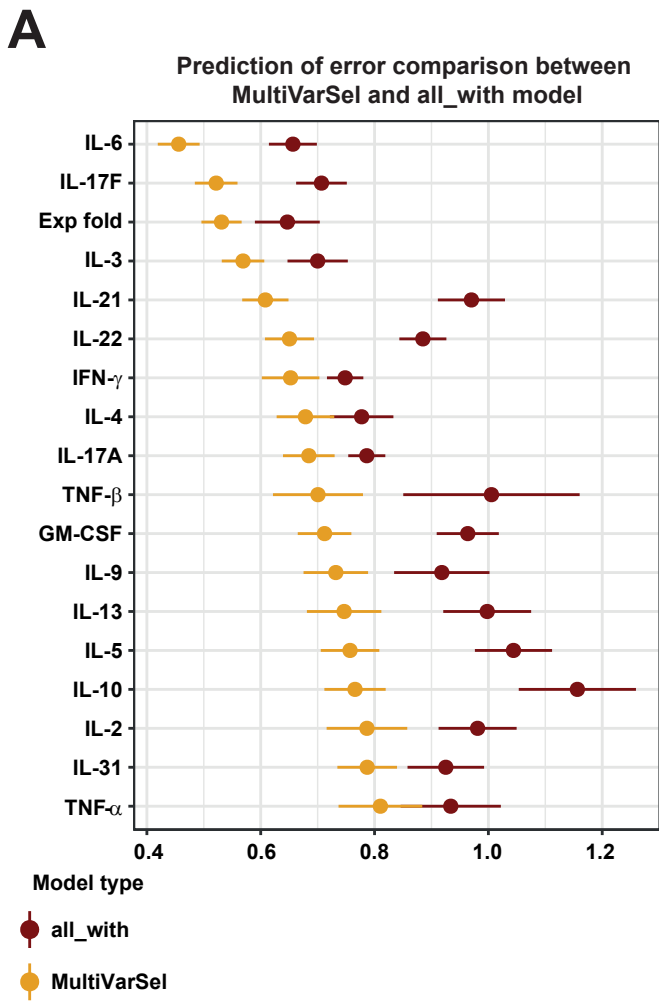


FIGURE S4: Complementary Th secretion profiles of the tested conditions for systematic model validation



B

Inputs	Number	Number alone	Number with	Percentage
CD70	638	580	58	0.09
CD11a	673	611	62	0.09
ICOSL	609	551	58	0.10
OX40L	622	562	60	0.10
IL-28 α	607	545	62	0.10
CD83	539	482	57	0.11
LIGHT	607	534	73	0.12
CD30L	606	533	73	0.12
ICAM-2	684	601	83	0.12
IL-23	389	339	50	0.13
Jagged-2	484	420	64	0.13
CD100	452	392	60	0.13
4-1BBL	482	418	64	0.13
VISTA	433	374	59	0.14
PDL2	493	420	73	0.15
IL-12p70	582	494	88	0.15
PVR	360	304	56	0.16
SLAMF3	515	433	82	0.16
TNF- α	416	346	70	0.17
CD86	569	471	98	0.17
CD80	440	362	78	0.18
HLA-DR	505	411	94	0.19
Nectin-2	316	254	62	0.20
IL-1	384	301	83	0.22
CD58	383	289	94	0.25
CD18	415	311	104	0.25
CD29	453	335	118	0.26
CD54	238	175	63	0.26
CD40	251	182	69	0.27
ICAM-3	454	325	129	0.28
IL-6	295	210	85	0.29
B7H3	432	307	125	0.29
Galectin-3	333	220	113	0.34
IL-10	241	159	82	0.34
PDL1	207	121	86	0.42
SLAFM5	217	72	145	0.67

C

Outputs	Number	Number alone	Number with	Percentage
IL-2	926	806	120	0.13
IL-4	932	802	130	0.14
IL-6	1013	865	148	0.15
IL-3	912	777	135	0.15
IL-13	741	631	110	0.15
GM-CSF	920	780	140	0.15
TNF- β	838	710	128	0.15
IL-10	1103	901	202	0.18
TNF- α	607	495	112	0.18
IL-17A	947	772	175	0.18
IL-17F	1030	839	191	0.19
IL-31	1088	884	204	0.19
IL-21	848	677	171	0.20
IL-9	955	762	193	0.20
Exp fold	1041	828	213	0.20
IL-5	773	613	160	0.21
IL-22	968	767	201	0.21
IFN- γ	682	535	147	0.22

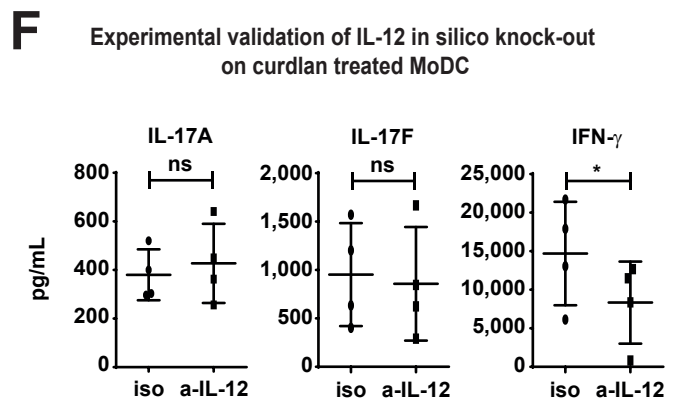
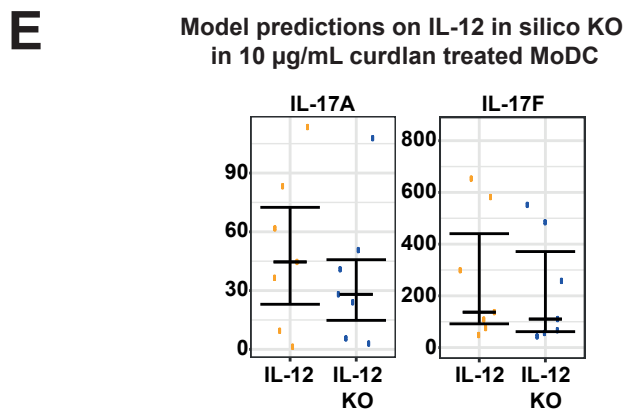
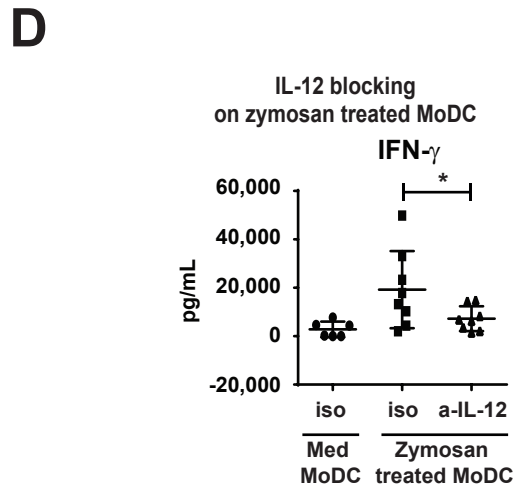


FIGURE S5: Quantification of context-dependent input-output associations

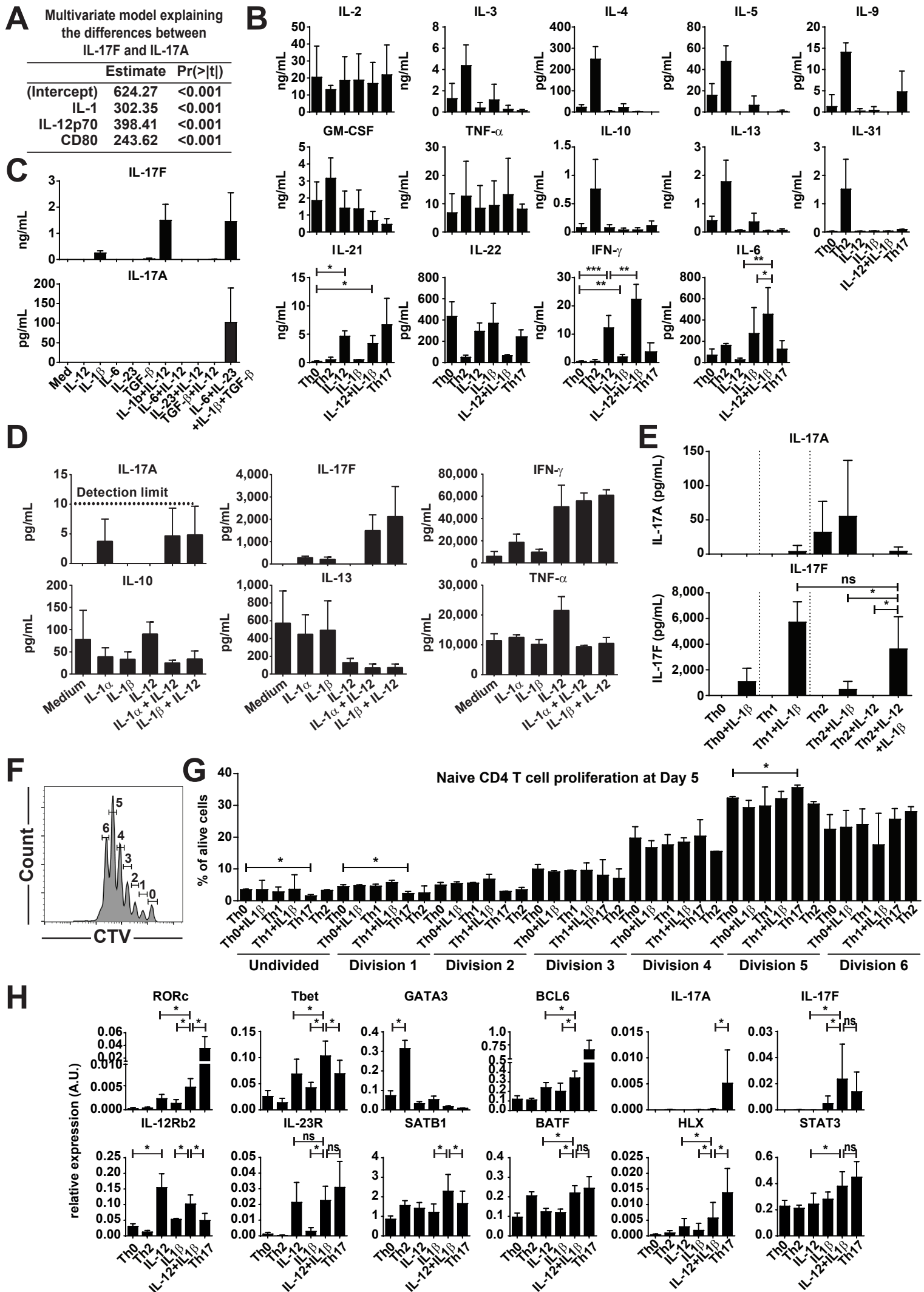


FIGURE S6: In depth characterization of Th cells polarized in the IL-1+IL-12 condition

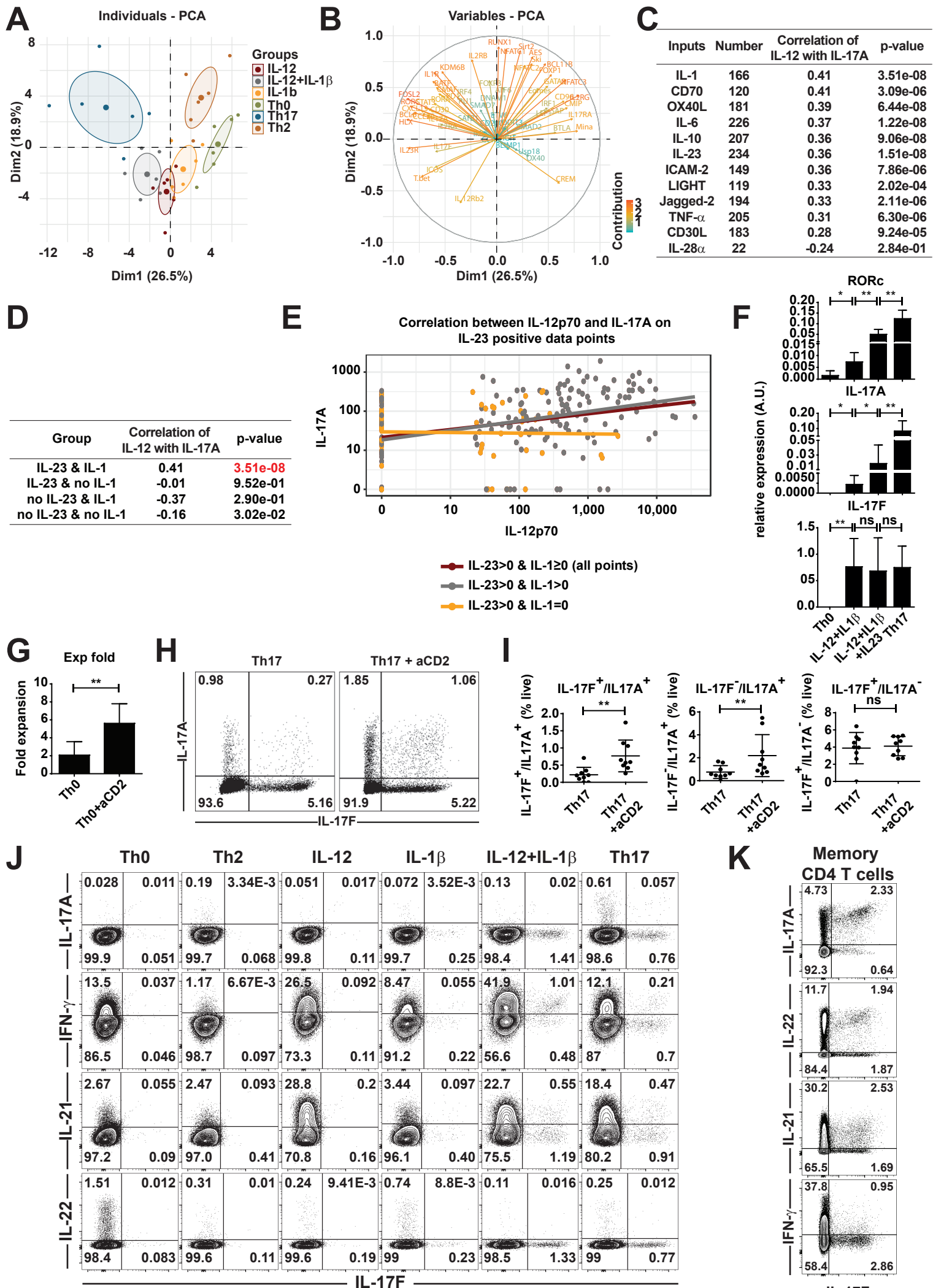


FIGURE S7: Detailed description of distinct experimentally validated predictions

DC Condition	Perturbators	Frequency
C1	Flu (1X) + PAM3 (1µg/mL)*MoDC	3
C2	Alum (200µg/mL) + Flu (1X)*MoDC	3
C3	Flu (1X) + HKSA (MOI 1)*MoDC	3
C4	Flu (1X) + HKCA (MOI1)*MoDC	3
C5	Flu (1X) + HKLM (MOI 1)*MoDC	3
C6	PolyIC (100µg/mL)*MoDC	2
C7	HKLM (MOI 10)*MoDC	2
C8	HKCA (MOI100)*MoDC	2
C9	GMCSF (100ng/mL)*MoDC	2
C10	Curdlan (20µg/mL)*MoDC	2
C11	Alum (200µg/mL)*MoDC	3
C12	PolyIC (50ng/mL)*MoDC	5
C13	Flu (0,1X)*MoDC	4
C14	Flu (1X)*MoDC	17
C15	Flu (0,5X)*MoDC	4
C16	PAM3 (0,1µg/mL)*MoDC	4
C17	HKSA (MOI 1)*MoDC	9
C18	PAM3 (1µg/mL)*MoDC	9
C19	Zymosan (0,1µg/mL)*MoDC	4
C20	LPS (1ng/mL)*MoDC	4
C21	Zymosan (1µg/mL) + PGE2 (1 µg/mL)*MoDC	2
C22	Zymosan (0,1µg/mL) + PGE2 (0,1µg/mL)*MoDC	2
C23	PGE2 (1 µg/mL)*MoDC	4
C24	PGE2 (0,1 µg/mL)*MoDC	2
C25	HKSA (MOI 0,1)*MoDC	4
C26	HKCA (MOI 10)*MoDC	4
C27	PGE2 (10 µg/mL)*MoDC	4
C28	R848 (10ng/mL)*MoDC	2
C29	R848 (100 ng/mL)*MoDC	2
C30	IFN β (50ng/mL)*MoDC	2
C31	GMCSF (50ng/mL)*MoDC	3
C32	HKLM (MOI 1)*MoDC	7
C33	HKCA (MOI1)*MoDC	9
C34	Med*MoDC	24
C35	HKSP (MOI1)*MoDC	3
C36	HKSA (MOI 20) + HKCA (MOI 10)*MoDC	2
C37	HKSA (MOI 1) + HKCA (MOI 1)*MoDC	2
C38	HKSA (MOI 0,1) + HKCA (MOI 0,1)*MoDC	2
C39	HKCA (MOI0,1)*MoDC	2
C40	TSLP (50ng/mL)*bDC	12
C41	PAM3 (1µg/mL)*bDC	2
C42	Curdlan (10µg/mL)*bDC	7
C43	Flu (1X)*bDC	13
C44	Med*bDC	20
C45	HKCA (MOI1)*bDC	4
C46	PAM3 (10µg/mL)*bDC	8
C47	LPS (100ng/mL)*bDC	8

C48	HKLM (MOI 1)*bDC	8
C49	GMCSF (50ng/mL)*bDC	6
C50	PolyIC (50µg/mL)*bDC	4
C51	Zymosan (10µg/mL)*bDC	8
C52	HKLM (MOI 100) *bDC	1
C53	HKSA (MOI 10)*bDC	1
C54	R848 (1µg/mL)*bDC	10
C55	HKSA (MOI 1)*bDC	6
C56	Zymosan (10µg/mL) + PGE2 (10µg/mL)*MoDC	4
C57	Curdlan (10µg/mL)*MoDC	7
C58	LPS (10ng/mL) + R848 (10ng/mL) *MoDC	2
C59	LPS (10ng/mL)*MoDC	4
C60	Zymosan (1µg/mL)*MoDC	4
C61	R848 (1µg/mL)*MoDC	10
C62	PAM3 (10µg/mL)*MoDC	10
C63	LPS (100ng/mL)*MoDC	21
C64	PAM3 (1µg/mL) + R848 (1µg/mL)*MoDC	3
C65	HKSA (MOI 20) + PAM3 (1µg/mL)*MoDC	3
C66	HKSA (MOI 20)*MoDC	7
C67	LPS (100ng/mL) + PAM3 (1µg/mL)*MoDC	3
C68	HKSA (MOI 20) + R848 (1µg/mL)*MoDC	3
C69	LPS (100ng/mL) + R848 (100 ng/mL)*MoDC	2
C70	LPS (1000ng/mL)*MoDC	4
C71	LPS (1000ng/mL) + R848 (1000ng/mL)*MoDC	2
C72	Flu (1X)+ PAM3 (10µg/mL)*MoDC	2
C73	Flu (0,5X) + PAM3 (1µg/mL)*MoDC	2
C74	Flu (0,1X) + PAM3 (0,1µg/mL)*MoDC	2
C75	Zymosan (20µg/mL)*MoDC	4
C76	Zymosan (10µg/mL)*MoDC	23
C77	LPS (100ng/mL) + R848 (1µg/mL)*MoDC	3
C78	Zymosan (10µg/mL) + PAM3 (1µg/mL)*MoDC	3
C79	Zymosan (10µg/mL) + HKSA (MOI 20)*MoDC	3
C80	LPS (100ng/mL) + Zymosan (10µg/mL) *MoDC	3
C81	LPS (100ng/mL) + HKSA (MOI 20)*MoDC	3
C82	Zymosan (10µg/mL) + R848 (1µg/mL)*MoDC	3

Table S1 Related to Figure 1: Number of data point generated per stimulation per DC subset: This table recapitulates the number of distinct data points corresponding to the biological replicates (column Frequency) generated for each DC stimulation on bDC or MoDC.

Publication n°3

Th17 cells decrease correlated with EASI improvement in atopic dermatitis patients during Dupilumab treatment

Manuscript in preparation for the Journal of Allergy and Clinical Immunology

In our previous work (Publication n°1) we observed a higher proportion of Tfh2 cells in AD patients compared to healthy donors [142]. We wanted to go deeper in understanding the involvement of the different T helper and T follicular helper cell subsets in AD.

Recently, a new immunotherapy for AD treatment, named Dupilumab, was developed by Regeneron/Sanofi. Dupilumab is a fully human monoclonal IgG4 antagonist antibody targeting IL-4 receptor alpha subunit, which can either interact with the common γ -chain to form the IL-4 receptor or with the IL-13R chain $\alpha 1$ to form the IL-13 receptor. Therefore, Dupilumab inhibits both IL-4 and IL-13 signal transduction and thus abnormal Th2 responses [182]. We were then interested in studying the evolution of the different Th/Tfh cell subsets in response to this treatment.

Thanks to the help of Professor Jean-David Bouaziz and his team, we received peripheral blood samples from 29 AD patients treated with Dupilumab at several timepoints along the course of treatment. These patients were also included in a real-life study whose results were published in the Journal of the American Academy of Dermatology in 2019 [195].

We were able to monitor by flow cytometry the evolution of eight Th and Tfh cell subsets (Th1, Th2, Th17, Th1/17, Tfh1, Tfh2, Tfh17 and Tfh1/17). These measures were associated to clinical scores (SCORAD, IGA, EASI, DLQI) controlled by clinicians at each sample collection.

We observed a significant decrease of Th2 cell percentage during Dupilumab treatment. This was the most important variation of Th cell percentages among all populations measured. Surprisingly, when we investigated potential associations between variations of Th cell percentages and improvement of EASI score, we observed a correlation between Th17 cell percentage decrease and improvement of EASI score.

This study demonstrates that evolution of Th cell populations can be followed in peripheral blood samples from patients during treatment. Additionally, it suggests that evolution of Th cell populations in patients could be linked to disease pathophysiology and might also serve as potential biomarker of treatment response.

1 **Title:** Th17 cells decrease correlated with EASI improvement in atopic dermatitis patients
2 during Dupilumab treatment

3
4 **Authors:**

5 Coline Trichot, MSc¹

6 Lilith Faucheux, MSc^{2,3,4}

7 Léa Karpf, MSc^{1,3}

8 Maximilien Grandclaudon, PhD¹

9 Lucia Pattarini, PhD¹

10 Thibault Mahévas, MD⁵

11 Marie Jachiet, MD⁵

12 Anne Saussine, MD⁵

13 Jean-David Bouaziz, MD, PhD⁵

14 Vassili Soumelis, MD, PhD^{1,3}

15

16 **Authors affiliations:**

17 ¹ Institut Curie, PSL Research University, INSERM U932, 26 rue d'Ulm, 75005, Paris, France

18 ² Statistic and epidemiologic research center Sorbonne Paris Cité, INSERM UMR-1153,
19 ECSTRRA Team, 75010 Paris, France

20 ³ Hôpital Saint-Louis, INSERM U976, Laboratoire d'Immunologie et Histocompatibilité, 1
21 avenue Claude Vellefaux, 75010 Paris

22 ⁴ Université de Paris, Paris, France

23 ⁵ Dermatology Department, and Université Paris Diderot Paris VII Sorbonne Paris Cité APHP,
24 Hôpital Saint-Louis, Paris, France

25

26 **Corresponding author:** Vassili Soumelis, U932 Immunity and Cancer, 26 rue d'Ulm, Paris,
27 75005, France, +33 1 44 32 42 27, vassili.soumelis@curie.fr

28

29 **Financial support:** ANR-10-IDEX-0001-02 PSL*, ANR-11-LABX-0043, ANR-15-CHIN-0002,
30 ANR-17-CE14-0025-02 and CIC IGR-Curie 1428.

31

32 **Disclosure of potential conflict of interest:** The authors declare no conflict of interests.

33

34 **Key words:** Atopic Dermatitis, Dupilumab, T helper cells, T follicular helper cells

35

36 **Abbreviations:**

37 AD: Atopic Dermatitis

38 Th: T helper

39 Tfh: T follicular helper

40

41 **Total word count:** 1139 words

42

43 *To the Editor:*

44 Using a panel of five colors, we were able to measure the evolution of eight T helper (Th) and
45 T follicular helper (Tfh) cell subpopulations in peripheral blood of atopic dermatitis (AD) patients
46 treated with Dupilumab.

47 Peripheral blood was obtained from 29 patients with moderate-to-severe AD at different
48 timepoints during their treatment with Dupilumab (at baseline (M0), and 1 (M1), 3 (M3), 6 (M6)
49 and superior or equal to 12 (\geq M12) months after beginning of treatment), and 25 age- and
50 gender-matched healthy subjects (Clinical data in Table 1).

51 Using a five-parameters surface flow cytometry staining, Morita et al. identified eight memory
52 Th and Tfh cell subpopulations in the peripheral blood of healthy donors (1). Using the same
53 surface staining (Gating strategy in Figure S1), we were able to measure the eight memory Th
54 and Tfh cell populations: Th1, Th2, Th17, Th1/17, Tfh1, Tfh2, Tfh17 and Tfh1/17, at different
55 timepoints during AD patient treatment with Dupilumab. First, we noticed that AD patients at
56 M0 had the same percentages of CXCR5⁻ (total Th cells) and CXCR5⁺ (total Tfh cells) cells
57 than healthy subjects (HD), and these two percentages did not vary significantly along patient
58 treatment with Dupilumab (Figure 1A).

59 When looking at the Tfh cell subpopulations, Tfh1, Tfh2 and Tfh1/17 percentages were not
60 significantly different between AD at M0 and HD, but percentage of Tfh17 cells was lower in
61 AD compared to HD. Additionally, we did not detect any significant variation of the Tfh2, Tfh17
62 and Tfh1/17 cell percentages during AD patient treatment with Dupilumab. Only a significant
63 decrease of Tfh1 cell percentage between M0 and M3 could be measured, but the percentage
64 was back to initial at M12 (Figure 1B).

65 The biggest variations were measured on the Th cell populations. First, when comparing AD
66 at M0 to HD, there was no significant difference of the Th1 cell percentage, but higher
67 percentages of Th2 and Th17 cells in AD compared to HD, and a lower percentage of Th1/17
68 in AD compared to HD. Then, we also detected a significant increase of Th1 cell percentage
69 between M0 and M12. Besides, we measured a significant increase of Th17 cell percentage
70 from M0 to M1 and M0 to M3, but this percentage decreased and was back to initial at M12.
71 Th1/17 cells variation started with a non-significant decrease from M0 to M1, followed by a
72 significant increase after M3. Finally, looking at the Th2 cell percentage, we could detect a
73 significant decrease from M0 to M3, M6 and M12 (Figure 1C).

74 In parallel of the blood withdrawal, clinicians performed an evaluation of the clinical scores:
75 EASI, SCORAD, DLQI and IGA at each timepoint. As reported by the different clinical trials
76 which evaluated Dupilumab efficacy (2), all scores significantly decreased from M0 to M12
77 during patient treatment with Dupilumab (Figure 2A).

78 Several teams measured Th cell populations in peripheral blood from AD patients compared
79 to HD (3-6). Although Th markers were already measured during Dupilumab treatment (7, 8),
80 this is the first study showing variations of memory Th cell populations in peripheral blood
81 samples from AD patients treated with Dupilumab. Indeed, the previous two studies measured
82 Th molecular signatures in lesional skin samples from AD patients treated with Dupilumab by
83 transcriptomic analysis (7, 8), while we were able to monitor memory Th cell populations
84 directly in peripheral blood.

85 Hamilton et al. were able to correlate reductions in CCL26 and CCL13 (Th2-associated
86 chemokines) expression with improvement in the EASI score (8). Therefore, we decided to
87 evaluate the association between variation of percentage of the Th and Tfh cell populations
88 and improvement of EASI score, which is the score the most used in clinical trials.

89 We calculated the percentage of variation of the EASI score and each Th and Tfh cell
90 percentage between M0 and M12 and determined the Pearson correlations of the variation
91 with treatment of each Th and Tfh cell percentage with evolution of EASI score. Surprisingly,
92 we observed that the highest improvement of EASI score significantly correlated with the
93 highest decrease in Th17 cell percentage. Even though the biggest variation of Th cell
94 percentage during Dupilumab treatment was the decrease of Th2 cell percentage, the
95 improvement of EASI score during Dupilumab treatment correlated only with decrease of Th17
96 cell percentage.

97 Our study suggests the potential of linking the evolution of Th cell populations in patient
98 peripheral blood with disease physiopathology and maybe serve as potential biomarker of
99 treatment response.

100

101 **Methods**

102

103 *Patient inclusion*

104 Consecutive patients over 18 years old evaluated during April 2017-July 2018 given AD
105 diagnoses according to the revised Hanifin and Rajka criteria were eligible for this study. The
106 patients received Dupilumab for moderate-to-severe AD due to inefficiency, loss of efficiency,
107 or contraindication of a previous systemic agent according to the French Early Access Program
108 set up during this period. Patients' non-opposition for the use of their deidentified records was
109 obtained for the noninterventional study, according to French legislation. Patients were given
110 300mg dupilumab every other week.

111
112
113
114
115
116
117
118
119
120
121
122
123
124
125
126
127
128
129
130
131
132
133
134
135
136
137
138
139
140
141
142
143
144
145
146
147

Sample processing

PBMCs were isolated by centrifugation on a density gradient (Lymphoprep) from whole blood samples collected from AD patients or healthy age- and gender-matched donors. Total PBMCs were then stained for 30 min at 37°C using the following antibodies: CD45RO FITC (Clone: UCHL1, BD), CD4 APC-Cy7 (Clone: RPA-T4, BD), CXCR5 APC (Clone: 51505, R&D Systems), CXCR3 PE (Clone: 1C6/CXCR3, BD), CCR6 PerCP-Cy5.5 (Clone: G034E3, Biologend) and analyzed on a BD Fortessa instrument. Cell percentages were extracted using FlowJo software (TreeStar).

Statistical analysis

Statistical analysis was performed using the Prism software v6 (GraphPad). Paired Wilcoxon test was applied to compare two groups. Significance was retained for *, $P < 0.05$; **, $P < 0.01$; ***, $P < 0.001$; ****, $P < 0.0001$.

Figure legends

Figure 1: Systematic analysis of Th and Tfh subpopulations in AD patients during Dupilumab treatment. A) Percentage of CXCR5⁺ and CXCR5⁻ cells among CD4⁺CD45RO⁺ cells in healthy donors (HD) and AD patients at each timepoint during Dupilumab treatment. Median ± interquartile range are plotted. B) Percentages of Tfh1, Tfh2, Tfh17 and Tfh1/17 cells among CD4⁺CD45RO⁺ cells in HD and AD patients at each timepoint during Dupilumab treatment. Median ± interquartile range are plotted. C) Percentages of Th1, Th2, Th17 and Th1/17 cells among CD4⁺CD45RO⁺ cells in HD and AD patients at each timepoint during Dupilumab treatment. Median ± interquartile range are plotted.

Figure 2: Improvement of EASI score correlates with decrease of Th17 cell percentage during Dupilumab treatment. A) Values of EASI, SCORAD, IGA and DLQI measured by clinicians at each timepoint during Dupilumab treatment. B) Correlation between variation of Th17 cell percentage between M0 and M12 and percentage of improvement of EASI score from M0 to M12 during Dupilumab treatment.

Supplementary Figure legends

Figure S1: Gating strategy. Gating strategy for identification of CXCR5⁺, CXCR5⁻, Th1, Th2, Th17, Th1/17, Tfh1, Tfh2, Tfh17 and Tfh1/17 cell populations from PBMCs by flow cytometry.

148

149 **References**

150

- 151 1. Morita R, Schmitt N, Bentebibel SE, Ranganathan R, Bourdery L, Zurawski G, et al.
152 Human blood CXCR5(+)CD4(+) T cells are counterparts of T follicular cells and contain specific
153 subsets that differentially support antibody secretion. *Immunity*. 2011;34(1):108-21.
- 154 2. Simpson EL, Bieber T, Guttman-Yassky E, Beck LA, Blauvelt A, Cork MJ, et al. Two
155 Phase 3 Trials of Dupilumab versus Placebo in Atopic Dermatitis. *The New England journal of*
156 *medicine*. 2016;375(24):2335-48.
- 157 3. Esaki H, Czarnowicki T, Gonzalez J, Oliva M, Talasila S, Haugh I, et al. Accelerated T-
158 cell activation and differentiation of polar subsets characterizes early atopic dermatitis
159 development. *The Journal of allergy and clinical immunology*. 2016;138(5):1473-7 e5.
- 160 4. Antunez C, Torres MJ, Mayorga C, Cornejo-Garcia JA, Santamaria-Babi LF, Blanca M.
161 Different cytokine production and activation marker profiles in circulating cutaneous-
162 lymphocyte-associated antigen T cells from patients with acute or chronic atopic dermatitis.
163 *Clinical and experimental allergy : journal of the British Society for Allergy and Clinical*
164 *Immunology*. 2004;34(4):559-66.
- 165 5. Teraki Y, Sakurai A, Izaki S. IL-13/IL-22-coproducing T cells, a novel subset, are
166 increased in atopic dermatitis. *The Journal of allergy and clinical immunology*.
167 2013;132(4):971-4.
- 168 6. Czarnowicki T, Esaki H, Gonzalez J, Malajian D, Shemer A, Noda S, et al. Early
169 pediatric atopic dermatitis shows only a cutaneous lymphocyte antigen (CLA)(+) TH2/TH1 cell
170 imbalance, whereas adults acquire CLA(+) TH22/TC22 cell subsets. *The Journal of allergy*
171 *and clinical immunology*. 2015;136(4):941-51 e3.
- 172 7. Beck LA, Thaci D, Hamilton JD, Graham NM, Bieber T, Rocklin R, et al. Dupilumab
173 treatment in adults with moderate-to-severe atopic dermatitis. *The New England journal of*
174 *medicine*. 2014;371(2):130-9.
- 175 8. Hamilton JD, Suarez-Farinas M, Dhingra N, Cardinale I, Li X, Kostic A, et al. Dupilumab
176 improves the molecular signature in skin of patients with moderate-to-severe atopic dermatitis.
177 *The Journal of allergy and clinical immunology*. 2014;134(6):1293-300.

178

	Healthy subjects (n=25)	Atopic Dermatitis patients				
		M0 (n=29)	M1 (n=27)	M3 (n=27)	M6 (n=23)	≥M12 (n=23)
Age (years) mean ± SD (Range)	39.9 ± 15 (19-67)	40 ± 14.3 (19-67)				
Male/Female (number)	16/9	18/11	17/10	16/11	14/9	14/9
SCORAD ± SD (Range)	NA	60.7 ± 16.1 (24.5-86)	40.9 ± 15.9 (12.6-81)	28.7 ± 16.9 (0-70.4)	28.2 ± 17.2 (0-80)	23.6 ± 14.2 (0-51)
EASI ± SD (Range)	NA	19.5 ± 12.9 (2-56.6)	12.1 ± 11.4 (0-54.3)	6.6 ± 7.6 (0-37)	7.1 ± 11.9 (0-59.7)	4.3 ± 3.3 (0-11.3)
DLQI ± SD (Range)	NA	12.6 ± 6.7 (2-29)	7.8 ± 7.2 (1-23)	6.2 ± 7.2 (0-25)	5.3 ± 6 (0-20)	4.1 ± 5.9 (0-24)
IGA ± SD (Range)	NA	3.2 ± 0.8 (1-4)	2.5 ± 0.9 (0-4)	1.7 ± 0.8 (0-3)	2 ± 1.2 (0-4)	1.5 ± 0.9 (0-4)
% CXCR5 ± SD (Range)	80.9 ± 4.6 (74.3-92.3)	79.8 ± 7.8 (60.6-95.7)	80.5 ± 8.6 (63.5-95.7)	81 ± 7.2 (64.8-96.8)	79.1 ± 10.8 (47.7-96.4)	79.1 ± 6.7 (63.2-93.6)
% CXCR5+ ± SD (Range)	18.1 ± 4.5 (6.71-24.2)	19.3 ± 7.6 (3.79-38.1)	18.7 ± 8.4 (3.87-34.9)	18 ± 6.9 (2.76-34.1)	19.4 ± 10.4 (2.93-48.7)	20.0 ± 6.7 (5.87-35.7)
% Th1 ± SD (Range)	20 ± 8.1 (9.05-40.9)	18.4 ± 7 (8.69-41.2)	16.8 ± 7 (4.36-33.8)	17.4 ± 5.8 (8.1-33.6)	18.3 ± 6.2 (10.3-32.1)	20.3 ± 6.3 (9.47-34)
% Th2 ± SD (Range)	13.7 ± 6.2 (2.91-33.4)	19.5 ± 7.7 (4.46-34.6)	19.1 ± 8.2 (3.58-34.1)	16.9 ± 8 (3.52-32.8)	16.5 ± 7.8 (2.49-36.4)	12.4 ± 5.9 (2.62-29.1)
% Th17 ± SD (Range)	18.8 ± 7.7 (6.61-38.1)	23.3 ± 7 (12.5-38.1)	28.8 ± 9.3 (11.5-45.4)	27 ± 8.4 (11.2-43.4)	26.5 ± 9.1 (11.7-46.2)	24.1 ± 7.1 (11.1-43.3)
% Th1/17 ± SD (Range)	28.3 ± 8.4 (10.8-53.3)	18.6 ± 8.2 (4.72-33.9)	15.8 ± 7.3 (6.48-36.9)	19.8 ± 8.9 (6.69-38.1)	17.9 ± 7.5 (5.58-36.1)	22.3 ± 8.1 (8.7-37.1)
% Tfh1 ± SD (Range)	4.8 ± 2.1 (1.04-9.13)	6 ± 2.4 (0.86-12.6)	5.2 ± 2.6 (1.05-9.75)	5.2 ± 2.1 (0.75-9.04)	5.6 ± 3.2 (1-15.4)	6.1 ± 2.4 (1.59-12.5)
% Tfh2 ± SD (Range)	3.7 ± 1.3 (2.26-7.02)	4.8 ± 2.7 (0.66-13.4)	4.7 ± 2.6 (0.71-10.5)	4.3 ± 2.4 (0.33-12.4)	4.5 ± 3 (0.44-12.8)	4.1 ± 1.7 (0.73-8.44)
% Tfh17 ± SD (Range)	6.6 ± 1.8 (2.86-10.3)	5.5 ± 2.9 (0.92-13.8)	5.8 ± 3.1 (1.02-13)	5.5 ± 2.8 (0.98-12.8)	5.9 ± 3.2 (0.76-12.7)	6.2 ± 2.8 (2.13-14.2)
% Tfh1/17 ± SD (Range)	3.1 ± 1.2 (0.55-5.82)	3 ± 1 (0.73-4.83)	3 ± 1.5 (0.55-5.61)	3 ± 1.3 (0.53-5.36)	3.3 ± 1.8 (0.67-8.32)	3.6 ± 1.4 (1.42-6.62)

Table 1: Subject characteristics

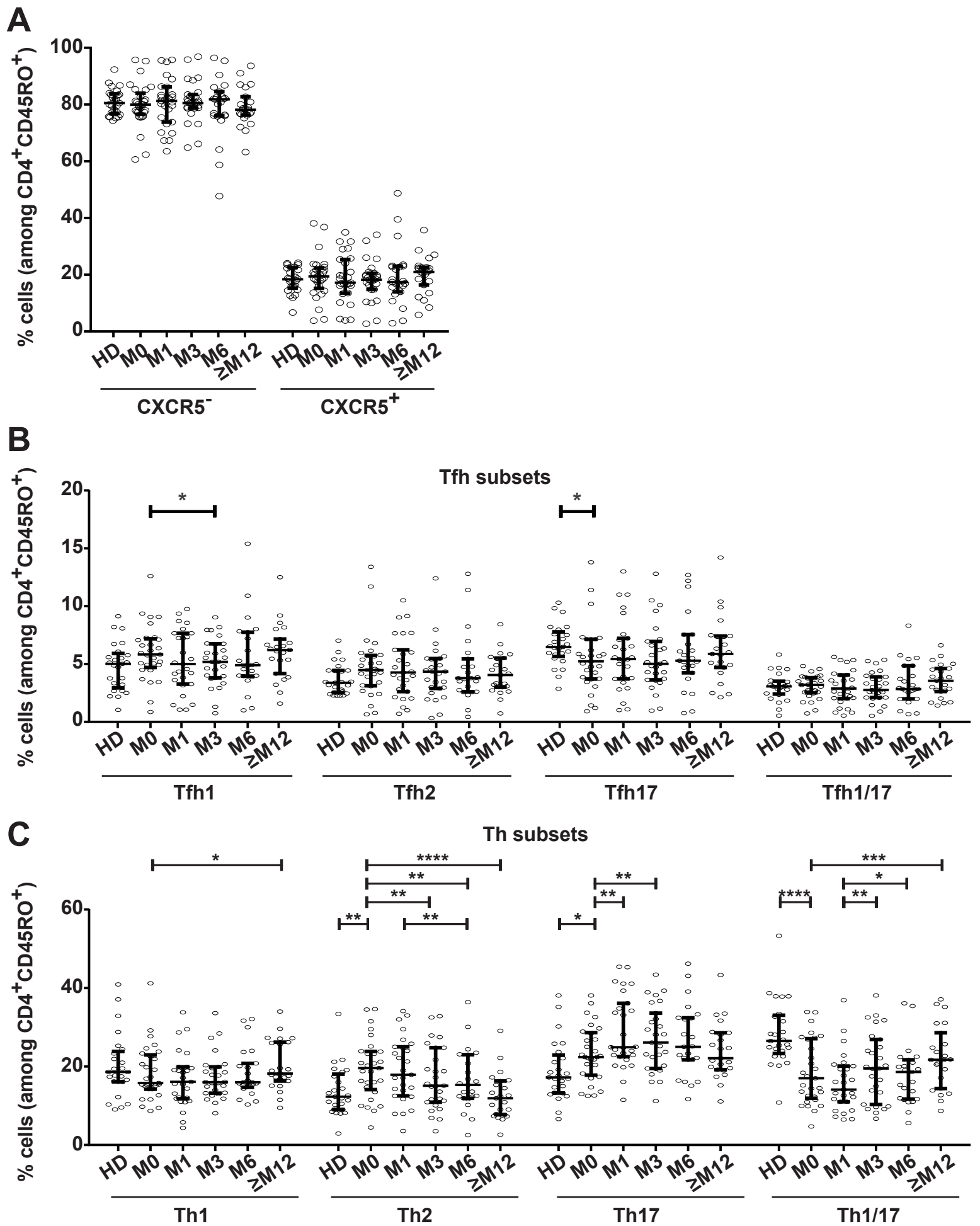


FIGURE 1: Systematic analysis of Th and Tfh subpopulations in AD patients during Dupilumab treatment

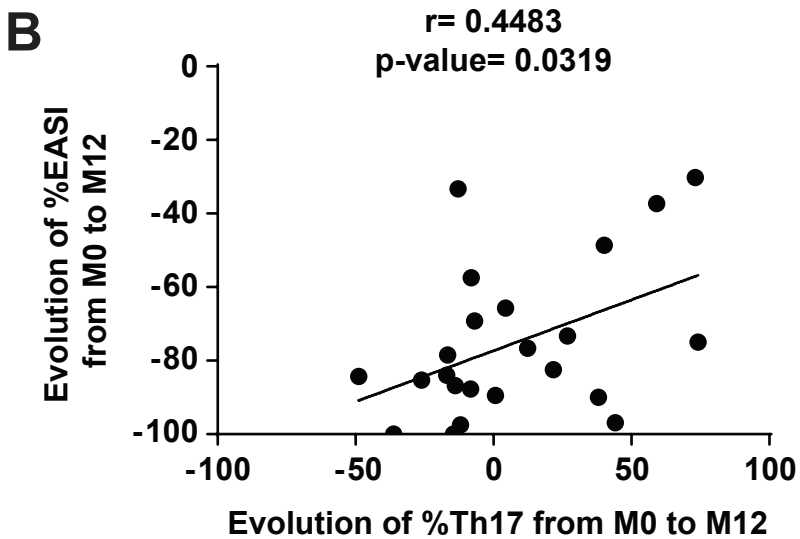
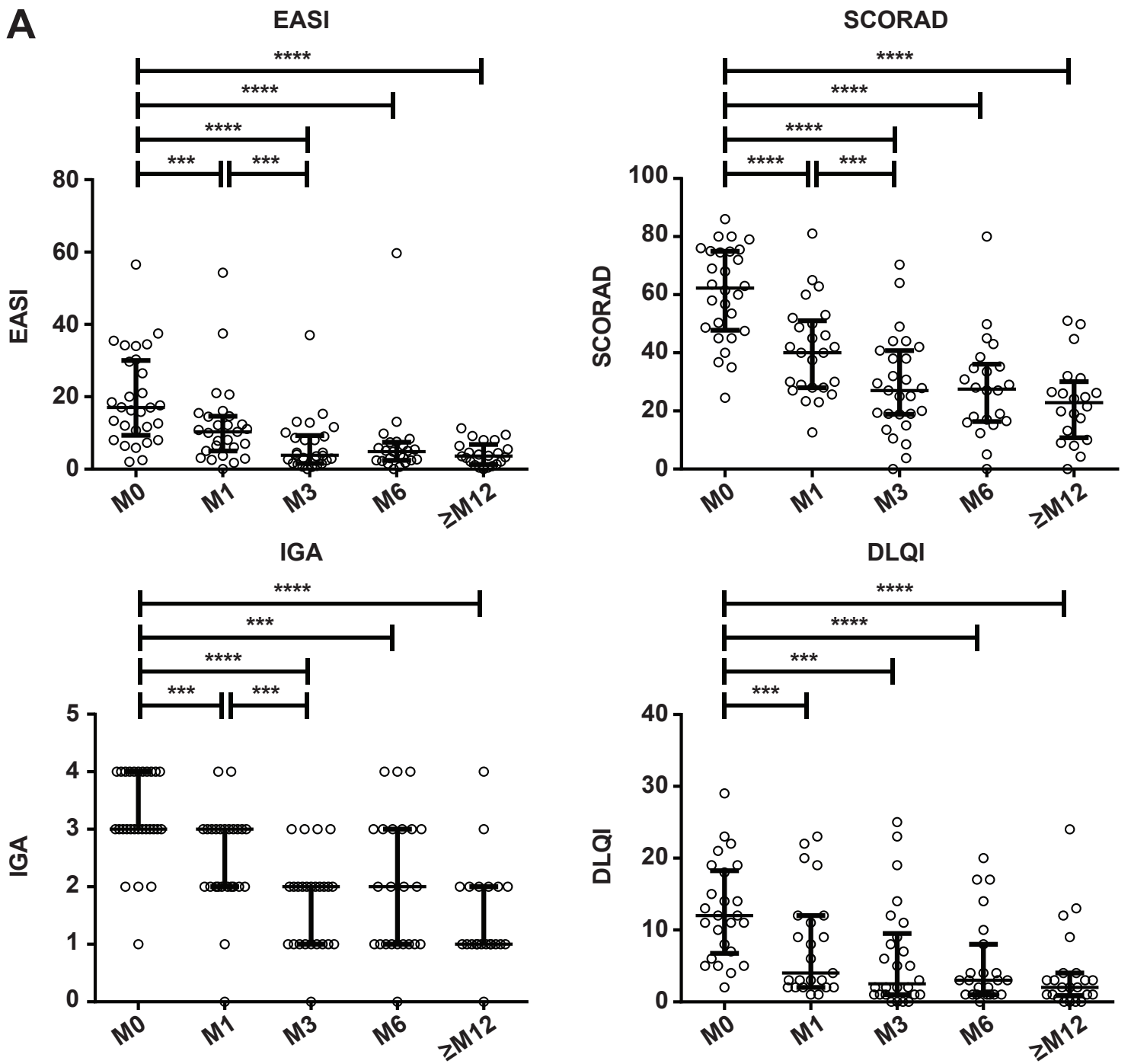


FIGURE 2: Improvement of EASI score correlates with decrease of Th17 cell percentage during Dupilumab treatment

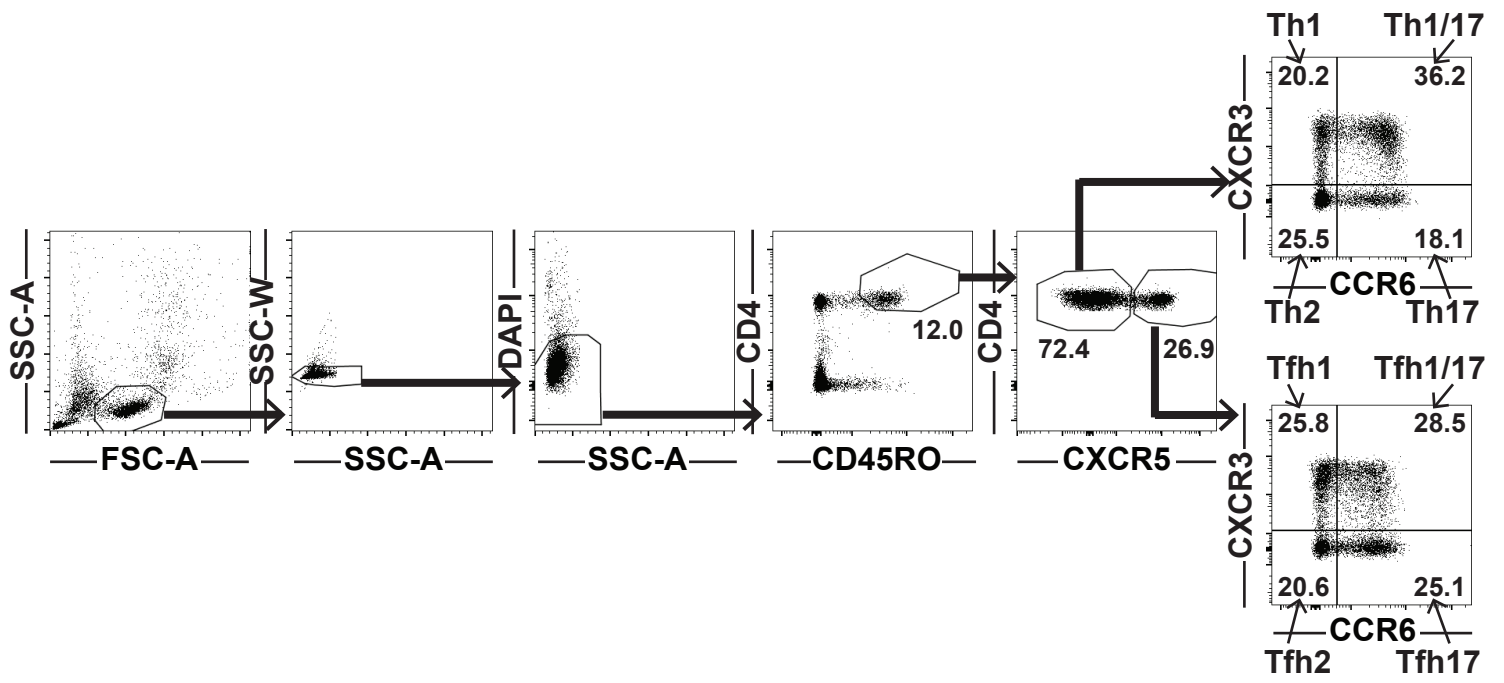


FIGURE S1: Gating strategy

GENERAL DISCUSSION AND PERSPECTIVES

Th cells are a very important component of the immune system. Through the combination of the cytokines they produce, Th cells are capable of shaping the appropriate immune response to the pathogen invading the host. The specific sets of cytokines they produce, depending on the subset, will allow them to attract and/or activate specifically other cell types on the inflammation site in order to clear the threat. However, if the process of Th polarization is not properly regulated, Th cells can become pathogenic. Indeed, Th cells have been described in a wide variety of diseases. Here I presented three projects studying different aspect of Th cell polarization: 1) Tfh cell polarization induced by TSLP-activated DC, 2) in depth study of Th cell polarization in response to DC communication molecule combinatorial and 3) monitoring of Th and Tfh cell populations in AD patients treated with Dupilumab and link with disease improvement. I will now review each of these projects and discuss their relevance, limitations and perspectives.

1. TSLP-activated DC induced Tfh cell polarization

In this work, we demonstrated that TSLP-activated DC are capable of polarizing naive CD4 T cells into Tfh-like cells presenting all features of Tfh cells: expression of the surface markers CXCR5, ICOS, PD1, of the transcription factor Bcl-6 and production of the cytokines IL-21 and CXCL13. Human Tfh cell polarization had mainly been shown to be driven by IL-12 [197]. Nevertheless, Tfh cell polarization in Th2 environments, such as allergy, had already been described [196]. However IL-4, a Th2 cytokine, had also been shown to inhibit Tfh cell polarization [145]. Since TSLP-activated DC have been demonstrated to induce high levels of IL-4 production from naive CD4 T cells [134], it was not expected to see Tfh cells emerge along with Th2 cells in response to TSLP-activated DC. We can wonder if other molecules described as Th2-inducing factors and involved in allergic diseases onset, such as IL-25 and IL-33 [198], could induce Tfh cell polarization.

Besides, we demonstrated that TSLP-activated DC induction of Tfh cells was going through OX40L. Using an OX40L blocking antibody, we targeted OX40L expressed by TSLP-DC during TSLP-DC/naive CD4 T cells coculture. We observed a significant decrease of IL-21 and CXCL13 production. Prior to our work, using a soluble OX40L recombinant protein in a DC-free T cell culture system, Jacquemin et al. demonstrated that OX40L was as efficient as IL-12 to induce naive CD4 T cell polarization into Tfh cells [141]. They also found increased levels of OX40L⁺ DC and Tfh cells in samples from patients with systemic lupus erythematosus, adding physiopathological relevance to OX40L role in Tfh cell induction.

Our work confirmed that OX40L role was conserved in a Th2-polarizing environment. Additionally, ICOS had been shown to be involved in Tfh cell polarization [199]. Since TSLP-activated DC highly expressed ICOSL, we used an ICOSL antagonist antibody in our TSLP-DC/T cell coculture system, however we did not detect any influence of ICOSL blocking on any cytokine we measured. This demonstrated that Tfh polarization by TSLP-DC does not go through ICOSL. However, since IL-21 and CXCL13 production were not entirely downregulated following OX40L blocking during coculture, probably other molecules might be involved. Since TSLP-DC have been described as not producing cytokine [134], Tfh polarization by TSLP-DC most probably go through other surface molecules in addition to OX40L.

Additionally, to prove that our TSLP-DC polarized Tfh cells were bona fide Tfh cells, we wanted to make sure they were capable of B cell help. We sorted TSLP-DC polarized CXCR5⁺PD1⁺ T cells and cocultured them with autologous memory B cells. We demonstrated that TSLP-DC polarized CXCR5⁺PD1⁺ T cells were capable of inducing plasma cell differentiation and IgE switch from memory B cells, while TSLP-DC polarized CXCR5⁻PD1⁻ T cells were not. These results demonstrated that TSLP-DC polarized CXCR5⁺PD1⁺ T cells were bona fide Tfh cells. This B cell help assay, even if complex, is a necessary step to definitely demonstrate T cells are Tfh cells. Several studies claim looking at Tfh cells without performing this experiment. For example, Durand and al. described that tonsillar cDC2 induced the polarization of IL-21⁺ Tfh cells, while tonsillar macrophages induced CXCL13⁺ Tfh cells. They even observed the two populations among tonsillar germinal center Tfh cells [89]. These results of differential Tfh polarization by tonsillar DC and macrophages are very interesting, however it would have been a real asset to demonstrate the B cell help capacities of each Tfh cell sub-population. Especially, it would have been interesting to show if the different Tfh cell populations induced different isotypic switches from B cells. Especially for the CXCL13⁺ Tfh cells, are they able to provide B cell help through their production of CXCL13? Besides, Schmitt et al. demonstrated that TGF- β combined with IL-12 or IL-23 induced Tfh-like cells, however they do not look at their B cell help capacities to prove they are bona fide Tfh cells [145], while they already have the assay set up since they used it in previous studies [45, 197].

Our study also demonstrated that IL-4 and/or IL-13 produced by TSLP-DC induced Tfh cells is responsible for the IgE switch on B cells, since blocking the IL-4R α led to the decrease of the IgE production. However, as shown by intracellular cytokine staining results, very

few TSLP-DC polarized T cells co-produce IL-21 together with IL-4, only a mean of 2% of the total polarized T cells. It has been demonstrated by Morita et al. that memory Th2 cells, which produce IL-4 but not IL-21, were capable of B cell help and IgE switch, though they were a lot less efficient than memory Tfh2 cells characterized by the production of IL-21 and IL-4 [45]. However again, Morita et al. never show cytokine coproduction at the single cell level. Are IL-21 and IL-4 co-produced by the same Tfh2 cells? Or is the memory Tfh2 cell population constituted of IL-21⁺ cells and IL-4⁺ cells? Thus, we can wonder if the minority of TSLP-DC polarized IL-21⁺IL-4⁺ T cells are responsible for all the plasma cell differentiation and IgE switch. Or if co-presence at the same location of IL-21 producing cells, with IL-4 producing cells allow B cell help and isotypic switch.

In our study we tried to identify Tfh cells in skin from AD patients, first by immunofluorescence staining on skin sections, and then in CD4 T cells emigrated from AD lesional skin. Our experimental settings did not allow us to identify Tfh cells within the skin of AD patients. For the immunofluorescence staining we wanted to see colocalization of TSLP with Tfh cells, thus we stained for TSLP and CXCL13. TSLP is strongly expressed on AD skin, as previously described [134], but we could not detect any CXCL13. And even in our tonsil section, used as a positive control, very few CXCL13 staining was detected, while it should be full of Tfh cells and B cells producing CXCL13. Maybe, CXCL13 is not the most sensitive marker to identify Tfh cells in tissue section. Additionally, for identification of Tfh cells among CD4 T cells after skin emigration, we used only CXCR5 as marker. However, it has been shown that chemokine receptors are not homogeneously expressed among tissues [65]. Already CXCR5 expression by memory Tfh cells is decreased in peripheral blood compared to germinal centers [38], we could imagine that Tfh cells completely shut down CXCR5 expression when migrating to the skin. What would be interesting, to look for Tfh cells in the skin, would be to take advantage of the new technologies allowing multiple tissue staining by sequential immunostaining and antibody quenching. This way we could use combination of markers, and in particular look for IL-21 rather than CXCL13, to stain the tissue section, and this would help to determine if Tfh cells are present in the skin and colocalize with TSLP.

To go further into the understanding of these TSLP-DC-induced Tfh cells, it would be particularly interesting to perform in parallel a single-cell RNA sequencing on in vitro polarized TSLP-DC induced Tfh cells and on memory Tfh cells from AD patient peripheral blood. We could compare their gene signature, identify differentially expressed genes

between the two populations. And this could help identify new therapeutic targets for treatment of AD and allergy in general.

2. Mathematical modeling of DC/T cell communication

We built the first data-driven unbiased statistical model able to predict the influence of 36 DC-derived molecules on 18 Th cell derived parameters. This model included two DC subsets: MoDC and myeloid DC (sorted from peripheral blood as LIN⁻CD4⁺CD11c⁺), activated with a total of 82 different DC conditions, and among others, TSLP. Since IL-21 is one of the outputs measured on T cells after coculture, we could make a parallel between this project and the TSLP-DC polarized Tfh cells. Surprisingly, the specific role of OX40L on IL-21 is not predicted by the model. This may appear as a main contradiction with our well-established results linking OX40L with IL-21, but several points may explain these discrepancies. First, OX40L expression by TSLP-DC specifically is not captured, since DC inputs are measured after 24 hours activation, while TSLP-DC upregulated OX40L only after 48 hours activation. Then, as shown on the first heatmap representing all DC inputs according to all DC activating conditions, OX40L can be expressed in many DC conditions. Finally, it has been shown that OX40L has a context-dependent influence on Th2 versus Th1 cytokine induction [135], so we cannot exclude that IL-21 induction by OX40L is also dependent on the context.

However, the model could be used to make new hypotheses on additional molecules involved in Tfh cell polarization. When looking at the model heatmap, we can see that 10 DC inputs are predicted to have a positive impact on IL-21, such as ICAM-2 and PVR for example, but also IL-12p70, which has been demonstrated by the literature to induce Tfh cell polarization [197]. On the opposite, eight DC inputs are predicted to have a negative impact on IL-21 production by T cells, including CD70, ICAM-3 and ICOSL, which is contradictory with what was previously published [199] but goes with our results [142]. Nevertheless, these predictions include cytokines, which might not be relevant in TSLP-DC precise case, since they do not produce any. Anyway, the model predictions can be interesting to consider as targets to better understand Tfh cell polarization by TSLP-DC.

Using our mathematical modeling strategy, we identified a context-dependent role of IL-12p70 in Th17 cell polarization. Indeed, the model predicted that IL-12p70 in combination with IL-1 was able to induce IL-17F production, but it also predicted a differential induction of IL-17F, without IL-17A. Besides, we were able to experimentally validate this

prediction by adding IL-12p70 and IL-1 on naive CD4 T cells in a DC-free culture. This was particularly surprising because up to now IL-12 had been linked to induction of IFN- γ [140]. Plus, IL-12 had even been shown to inhibit IL-17 production [200]. Thus, we described a novel context-dependent role for IL-12 in IL-17F induction.

Interestingly, differential regulation of IL-17A versus IL-17F had already been demonstrated. First, in mouse naive CD4 T cells differentiated under Th17 condition, Gomez-Rodriguez et al. showed that decreased TCR stimulation would lead to decreased IL-17A production with conserved level of IL-17F [201]. Then, Adamik et al. demonstrated that IL-17A and IL-17F could be differentially regulated in human memory Th17 cells. They showed that memory Th17 cells stimulated with PGE2 produced moderate amount of IL-17A but no IL-17F, when stimulated with IL-23+IL-1 β they produced high amount of IL-17F but low amount of IL-17A and finally when stimulated with combination of PGE2 and IL-23+IL-1 β , T cells produced high amounts of IL-17A but the level of IL-17F was similar to IL-23+IL-1 β alone. They also demonstrated that IL-17A and IL-17F present divergent epigenetic architectures in memory Th17 cells, which committed them to express IL-17A preferentially [202]. Our work further demonstrated that IL-12p70 in an IL-1 context can induce IL-17F without IL-17A. Unfortunately, the study by Wong et al. did not include IL-17F [65], because it would have been very interesting to find out if IL-17⁺IL-17A⁻ T cells could be identified in the different tissues they analyzed. Since Th17 cells have been broadly associated to diseases, it would be of interest to study if IL-17⁺IL-17A⁻ T cells specifically are involved in human diseases, such as psoriasis in which Th17 cells have been extensively described.

Our model was built using 428 observations on DC and the same amount on polarized Th cells, which represents an important amount of data. However, the dataset we used to build the model present some limitations. First, we measured only 36 inputs on the DC, and we know activated DC might express a lot more molecules than just 36. For example, just in terms of cytokines, we did not measure IL-18, IL-27 and IFN- α which are known to be produced by activated-DC and might have been produced in some of our DC activating conditions. The influence of the DC molecules not measured in our settings will not be captured by our model, or might be attributed to the DC molecules measured to which they are correlated. Overall, this might probably skew our model's predictions and explain the fact that 30% of the predictions are untrue.

Additionally, we only measured 17 Th cytokines in addition to T cell expansion, while we know Th cells can produce a lot more cytokines, like IL-26, IL-35 and TGF- β for instance.

As a consequence, the model does not represent the full spectrum of Th profiles that can arise in response to DC activation.

Also, the model has been constructed with an imbalance of observations towards MoDC conditions compared to myeloid DC conditions. Since technically it is easier to get high numbers of MoDC than myeloid DC, the model includes more MoDC datapoints than myeloid DC, which can again skew the model's predictions. Besides, the model has been built with an imbalanced number of observations among DC conditions. For example, 22 DC conditions contain only two donors, while some others include more than 15 donors. These underrepresented conditions are drowned by the others which are more represented, and do not influence the model the same way than if there were equal number of each DC condition.

As discussed in the introduction, this study aimed at fulfilling a real lack in the field of DC/T cell communication study. This original approach is not only useful to better understand DC/T cell communication but can also be applied more broadly to any cell/cell communication system.

3. Monitoring of Th cell populations in AD patients treated with Dupilumab

In this study, using a five-parameters flow cytometry surface staining, we were able to follow eight Th and Tfh cell populations in peripheral blood of AD patients treated with Dupilumab. Several studies had already been conducted to measure different Th subsets in AD patients compared to healthy donors. Esaki et al. performed a surface staining for CD3, CD4 and CLA associated to intracellular cytokine staining for IL-13, IL-22, IL-9 and IFN- γ on PBMC from 29 infants and 13 children with moderate-to-severe AD and age-matched controls [203]. In another work, they also performed quantitative real-time PCR to study 53 Th-associated markers on skin biopsies from AD children and adults, adults with psoriasis and matching controls [204]. Antunez et al. studied CD3, CD4, CD8, CLA and HLA-DR in combination to IL-2, IFN- γ , TNF- α , IL-10, IL-4 and IL-13 by flow cytometry on PBMC from 26 AD patients and 14 healthy controls [205]. Teraki et al. analyzed IL-13, IL-4, IFN- γ , IL-22 and IL-17 producing-cells among CD4 and CD8 T cells in PBMCs from AD patients [206]. Czarnowicki et al. performed a surface staining for CD3, CD4, CD69 and CLA with intracellular cytokine staining for IL-13, IL-22, IL-9, IFN- γ and IL-17 on 42 AD adults and 25 AD patients [207]. Additionally, in the specific context of Dupilumab treatment, one study involving 18 patients from four different trial studies had already

looked at Th associated markers. They looked at serum levels of Th2-associated markers TARC and IgE in addition to transcriptomic analysis of skin biopsies before and after four weeks of treatment. They observed a reduction of TARC levels correlated with reduction of pruritus and an improvement of lesional transcriptome associated with clinical enhancements [193, 194]. However, our study is the first to look for Th cell populations in the peripheral blood of patients during treatment with Dupilumab.

Our study shows variations of Th and Tfh cell populations in AD patient peripheral blood in response to Dupilumab treatment. In the study from Beck et al. [193, 194] they looked at the transcriptomic profile of lesional skin biopsies, which is the location where the treatment is applied and supposed to act. Hamilton et al. described a significant decrease of mRNA expression of Th2-associated chemokines (CCL17, CCL18, CCL22 and CCL26) but not of the Th2 cytokine genes (IL4, IL5, IL13 and IL31) in patients treated with Dupilumab compared to placebo group. In addition, they did not observe any variation neither in Th1-related genes nor in IL-17A and IL22 mRNA levels, but observed a significant decrease of IL-17 and IL-22-modulated genes in Dupilumab treated patients compared to placebo group [194]. The fact that variations of Th markers could be detected in the skin following treatment with Dupilumab could be expected since it is the location of the disease. On the opposite, being able to detect changes in Th cell populations in peripheral blood was not necessarily trivial. This is good news for two reasons: 1) blood withdrawal is a less invasive procedure than skin biopsy, 2) our work suggests the possibility of more complex studies to better understand what precise Th cell population, rather than just markers, are influenced during Dupilumab treatment.

In this work we used a simple surface flow cytometry staining of three chemokine receptors to identify eight Th and Tfh populations. This is a restrictive panel, especially knowing that nine additional populations could have been identified from Tfh1, Tfh2 and Tfh17 cells by adding staining for PD1, ICOS and CCR7 [49]. Another possibility would have been to look for intracellular cytokine production rather than chemokine receptors, since their expression is not reliable [65], all the more that Th2 and Tfh2 are identified by two negative markers. What would have been even more valuable, in order to improve the accuracy of the population identification, would have been to perform a similar analysis than Wong et al. using CyTOF and a panel including not only chemokine receptors but also intracellular cytokines [65]. This would have allowed us to be more certain of the

populations analyzed and might have led us to identify a biomarker of the response to treatment.

In our previous study (Publication n°1) [142] we measured a higher proportion of Tfh2 cells in six AD patients compared with four healthy donors. We did not confirm this observation with our new cohort of patients. Indeed, when comparing the 29 AD patients at M0 with the 25 age and gender matched healthy controls, there is a trend of higher Tfh2 cells in AD patients compared to healthy controls, but it is not statistically significant ($p=0.079$ by paired Wilcoxon test). In our previous work, we also showed a significantly higher percentage of Tfh1 cells in healthy donors compared to AD patients [142], while our new cohort present a non-significant higher percentage in AD patients compared to healthy donors. Finally, when looking at the Tfh17 cell percentage, we previously observed a non-significant higher proportion of Tfh17 cells in healthy donors compared to AD patients [142] and this is statistically significant in our new cohort. Additionally, we did not detect any significant variation of any Tfh cell subset in AD patients during Dupilumab treatment, suggesting Tfh cells are not influenced by Dupilumab treatment.

APPENDICES

1. Appendix 1

TSLP-DC-activated T cells express OX40 and OX40L and self-maintain their cytokine production

Coline Trichot, Léa Karpf, Vassili Soumelis

1.1. Results

The aim of this work was to understand better how OX40L molecule influences T helper polarization. For a long time OX40L has been associated to Th2 polarization. OX40L blocking in a TSLP-DC/T coculture has been shown to induce a decrease of the Th2 cytokines: IL-4, IL-5, IL-13 [135, 208]. And lately it has been demonstrated that OX40L is also implicated in Tfh polarization [141]. In our previous work [142], we additionally showed that blocking OX40L in a coculture between TSLP-DC and naive CD4 T cells lead to a decrease of the IL-21 and CXCL13 production. This confirmed that OX40L, in addition to its role on Th2 polarization, is involved in Tfh polarization as well. We wanted to go further into the characterization of OX40L role on Th and Tfh cell differentiation using different culture systems in order to study its impact in depth.

First, we used the same OX40L blocking antibody as in Ito et al. [135] and Inagaki-Katashiba et al. [208] (ik-5 clone provided by Pr Toshiyuki Hori in Japan), in the same TSLP-DC/naive CD4 T cell coculture system than in our previous work [142]. In this context, we reproduced the decrease of IL-13 production found by Ito et al. [135] and Inagaki-Katashiba et al. [208], as well as the decrease of TNF- α production, even though it was not significant. We measured a significant decrease of the fold expansion in the presence of OX40L blocking antibody. Contrary to the other two studies [135, 208], we did not detect any significant effect of blocking OX40L on IFN- γ production. And most surprisingly, we showed a significant increase of IL-4 production and a trend of increase of IL-5 production (Figure 14A) which is the opposite of what the other two studies using OX40L blocking in TSLP-DC/T coculture demonstrated [135, 208]. Even though Th2 cytokines: IL-4, IL-5 and IL-13 have been shown to be commonly regulated at the transcriptional level [209], our mathematical model predicted that they are not always associated and can arise separately.

Several factors could explain the discrepancies between results from the other two studies [135, 208] and ours. First, the dose of TSLP used for DC activation is different between our study and the other two, they used 15 ng/mL of TSLP, while we used 50 ng/mL. But most importantly, the medium used during the coculture is different, Ito et al. used Yssel's medium supplemented with 2% human serum,

Inagaki-Katashiba et al. used RPMI supplemented with 2% human serum while we used X-vivo medium without any serum complementation. The medium used for coculture, and even more the addition of serum, can greatly influence cytokine production, and thus the outcome of OX40L blocking.

In addition, we used a second OX40L blocking antibody: Oxelumab (Roche/Genentech) which has been initially developed for clinical applications and is also available for research. We blocked OX40L in the same TSLP-activated DC/naive CD4 T cell coculture as previously.

First, we observed a decrease in the fold expansion, just as with the ik-5 antibody (Figure 14D). Also, we were able to recapitulate the IL-21 decrease observed in our previous work [142]. When looking at IL-21 intracellular production by TSLP-activated DC polarized T cells in the presence of Oxelumab, we observed a decrease of IL-21⁺ cells compared to isotype (Figure 14B et C). Additionally, we confirmed the significant increase of IL-4 production observed with ik-5 antibody (Figure 14A). In the presence of Oxelumab we observed a significant increase of IL-4⁺ T cells by intracellular staining (Figure 14B and C) and a significant increase of IL-4 production by CBA (Figure 14D). We also observed a trend of increased IL-5 production by T cells with Oxelumab compared to isotype (Figure 14D), just as previously observed with ik-5 (Figure 14A). Besides, we discovered that OX40L blocking decreased IL-9 production by T cells, results were consistent between intracellular cytokine staining (Figure 14B, C) and by CBA (Figure 14D). With Oxelumab, as with ik-5, there was no significant effect of the blocking on TNF- α production (Figure 14 A & D). We did not retrieve a significant decrease of IL-3 [142] and IL-13 production (Figure 14A) when blocking OX40L with Oxelumab, compared with our blocking with ik-5. Indeed, OX40L blocking with Oxelumab did not affect significantly IL-3 and IL-13 production (Figure 14D). Finally, there was a discrepancy between intracellular cytokine staining (Figure 14B and C) and CBA (Figure 14D) for IFN- γ production. The blocking induced a significant increase of the IFN- γ ⁺ cells when looking by intracellular staining (Figure 14 B & C), while when IFN- γ was measured by CBA in the supernatant, there was a non-significant increase of IFN- γ level between isotype and blocking antibody (Figure 14D). In conclusion, the contradictory effect of OX40L blocking concerning IL-4 we found compared to the literature was reproducible with a different antibody. Minor differences between results obtained with ik-5 and Oxelumab blocking antibodies could come from the different DC used in each experiment. Blocking with ik-5 antibody was performed in a coculture between total myeloid DC and naive CD4 T cells, while blocking with Oxelumab was done in a coculture with cDC2 and naive CD4 T cells.

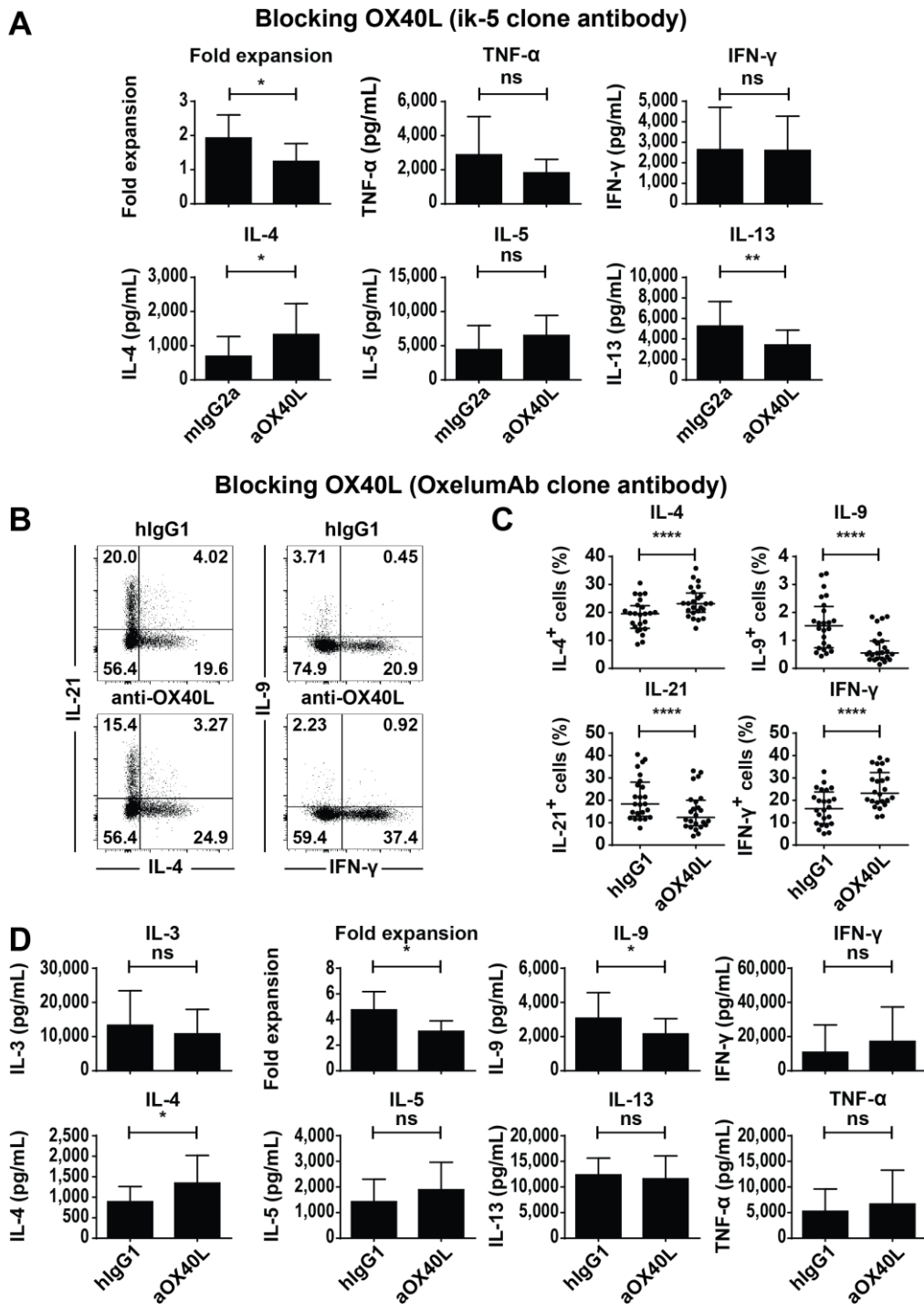


Figure 14: OX40L blocking decreases IL-21 and increases IL-4 production in TSLP-DC/T coculture
 A) Quantification of expansion fold and cytokines measured by CBA (IL-4, IL-5, IL-13, TNF-α, IFN-γ) produced by CD4 T cells differentiated for 6 days with TSLP-DC. 50 μg/mL anti-OX40L blocking antibody (ik-5 clone) or matching isotype control were kept during the entire coculture. Mean ± SEM for 7 independent donors is plotted. *, P < 0.05; **, P < 0.01, paired Student's t test. B) FACS plot of intracellular cytokine staining for IL-4, IL-21, IL-9 and IFN-γ of CD4 T cells differentiated for 6 days with TSLP-DC in the presence of 10 μg/mL of anti-OX40L blocking antibody (Oxelumab clone) or matching isotype. C) Quantification of intracellular cytokine staining as in B). Median ± interquartile range for 25 independent donors is plotted. ****, P < 0.0001, paired Wilcoxon test. D) Quantification of expansion fold and cytokines measured by CBA produced by CD4 T cells differentiated as in B). Mean ± SD for 6 independent donors is plotted. *, P < 0.05; paired Wilcoxon test.

In addition, we wanted to validate the robustness of our results using another experimental setting. We decided to confirm our results in a DC-free Th polarization system, using OX40L as a recombinant protein. We observed that the presence of rhOX40L induced a significant decrease of the IL-4 producing cells in the Th2 context (Figure 15A and B). There was no significant difference between presence or absence of rhOX40L in the culture in the Th0 context, while in the Th1 and Th17 contexts, the IL-4 production induced was not sufficient to see a decrease in the presence of rhOX40L. We also observed an increase of IL-21 in all Th0, Th1, Th2 and Th17 contexts when rhOX40L was added to the culture (Figure 15A and B). Finally, we were also able to detect a decrease of the IFN- γ in the presence of rhOX40L in the Th0, Th1 and Th17 contexts (Figure 15A and B). In the Th2 context, the induction of IFN- γ was not important enough to observe an effect of rhOX40L. These results demonstrate a mirror effect between the recombinant OX40L protein addition in DC-free T cell polarization system and the experiments of TSLP-DC/T coculture with OX40L blocking.

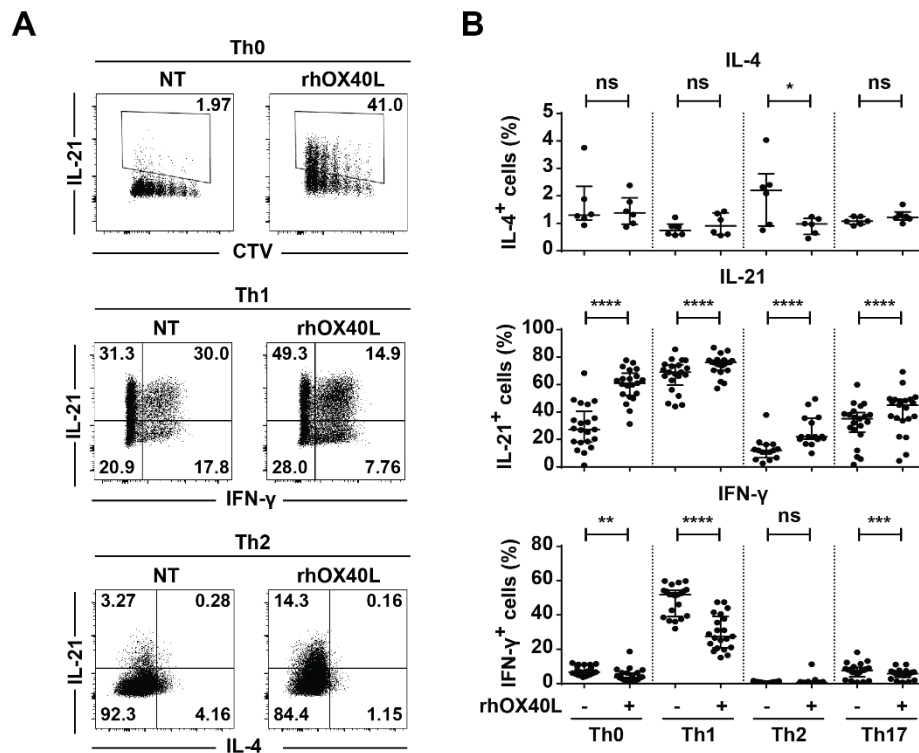


Figure 15: rhOX40L increases IL-21 and decreases IL-4 and IFN- γ in a DC-free Th polarization system

A) FACS plot of intracellular cytokine staining for IL-21 versus CTV in the Th0 condition, IL-21 versus IFN- γ in the Th1 condition and IL-21 versus IL-4 in the Th2 condition of CD4 T cells polarized for 5 days with anti-CD3/CD28 beads (Th0) and IL-12 (Th1) or IL-4 (Th2) and in the presence or not of 600 ng/mL of rhOX40L. B) Quantification of intracellular cytokine staining for IL-4, IL-21 and IFN- γ of CD4 T cells polarized for 5 days with anti-CD3/CD28 beads only (Th0), with IL-12 (Th1), IL-4 (Th2) or a cocktail of IL-1 β , IL-6, IL-23 and TGF- β (Th17) and in the presence or not of 600 ng/mL of rhOX40L. Median \pm interquartile range for 6 to 21 independent donors is plotted. *, P < 0.05; **, P < 0.01; ***, P < 0.001; ****, P < 0.0001, paired Wilcoxon test.

Finally, we wanted to validate our findings without manipulating the system. We have observed that OX40L expression by TSLP-DC at 48 hours activation is bimodal (Figure 16A), approximately 60% of the population expresses it, while the other part does not (Figure 16B).

We decided to sort both OX40L⁺ and OX40L⁻ DC after 48 hours activation with TSLP and cocultured them separately with naive CD4 T cells. We observed a significantly higher proliferation induced by OX40L⁺ DC compared to OX40L⁻ DC (Figure 16C). Which goes with our previous results, in which blocking OX40L decreased T cell expansion. We did not observe any difference between OX40L⁺ and OX40L⁻ DC for the production of IL-9 and IFN- γ (Figure 16C). We were able to detect a higher production of TNF- α in the presence of OX40L⁻ DC compared to OX40L⁺ DC. This did not confirm our previous results which showed an increase of IFN- γ , decrease of IL-9 and no effect on TNF- α in the presence of OX40L antibody compared to isotype control. We also observed a higher production of IL-4 from the T cells cocultured with OX40L⁻ DC and a higher production of IL-21 from T cells cocultured with OX40L⁺ DC (Figure 16C). These results confirmed the results from the OX40L blocking and Th polarization experiments for the IL-21 and IL-4 productions.

Then, we wondered whether OX40L expressed on OX40L⁺ DC was responsible for IL-4 and IL-21 regulation. In order to answer this question, we performed the same cocultures with OX40L⁺ and OX40L⁻ DC and naive CD4 T cells and added OX40L blocking antibody (Oxelumab) for the coculture duration. In the OX40L⁺ DC/T coculture we found that addition of OX40L blocking induced a significant increase of IL-4 associated to a significant decrease of the expansion fold and IL-21 production. There was no significant effect of the blocking on IL-9 and TNF- α production and a non-significant decrease of IFN- γ production (Figure 16D). The effect of OX40L blocking in the OX40L⁺ DC/T coculture observed on IL-4 and IL-21 production and expansion fold confirmed our previous results of OX40L blocking in total TSLP-DC/T coculture.

Surprisingly, we also observed an effect of OX40L blocking on the OX40L⁻ DC/T coculture. Indeed, we observed a significant decrease of the IL-21 production in the presence of OX40L blocking, associated to a non-significant increase of IL-4 production. TNF- α production was significantly decreased in the presence of OX40L blocking, while there was no significant effect of the blocking on IL-9 production and expansion fold. A contradictory effect of the blocking was observed concerning IFN- γ production. In the OX40L⁺ DC/T coculture there was a non-significant decrease, while in the OX40L⁻ DC/T coculture we observed a significant increase of IFN- γ production (Figure 16D). These results are particularly surprising that we could have expected an effect of OX40L blocking only in the coculture with the OX40L⁺ DC, which are the only one to actually express OX40L at their surface. Our first hypothesis was to think that OX40L expression could be induced on OX40L⁻ DC.

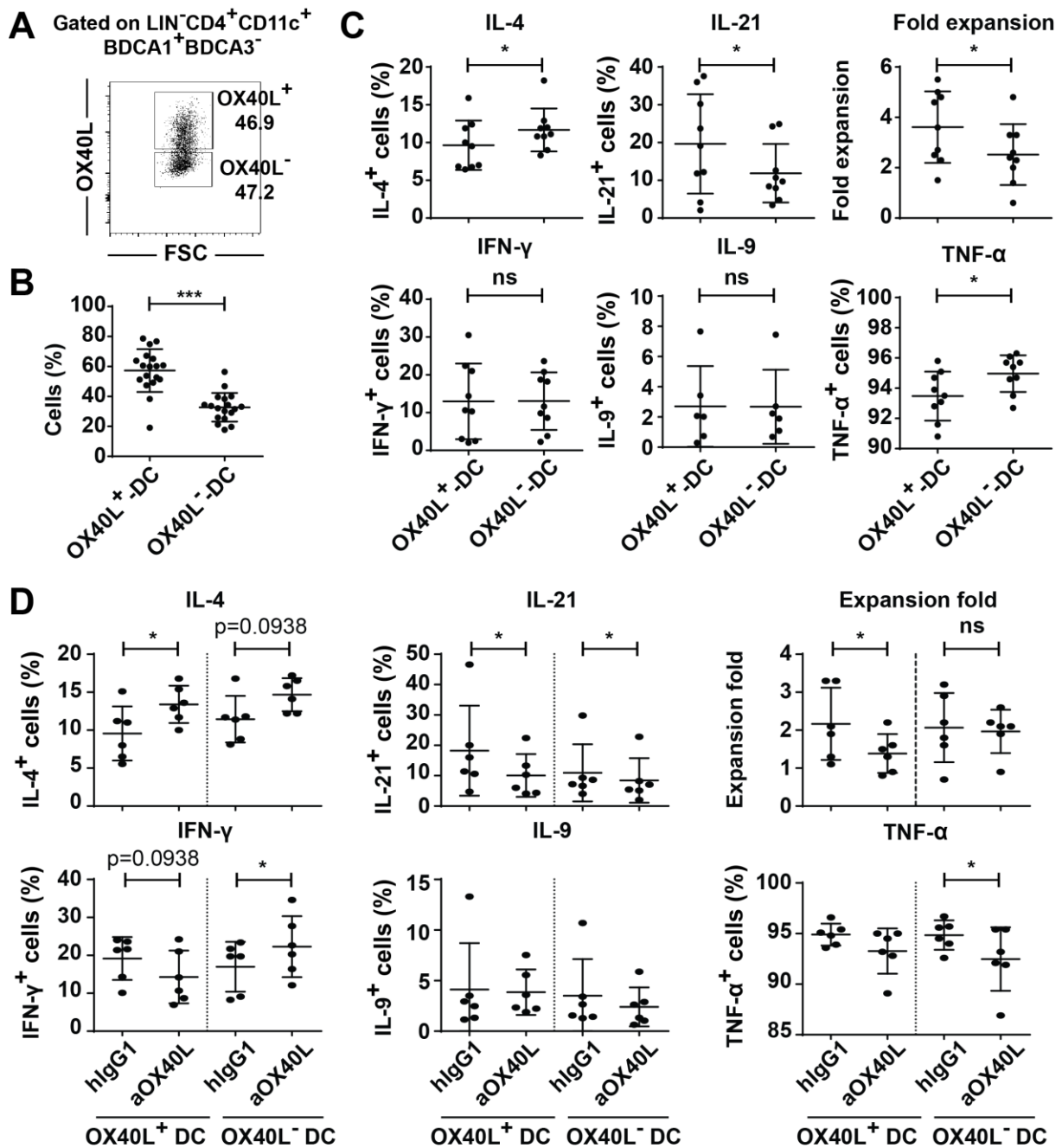


Figure 16: OX40L⁺ DC induce more IL-21 and less IL-4 producing cells than OX40L⁻ DC

A) FACS plot of OX40L surface staining of DC activated for 48 hours with 50 μg/mL of TSLP, gated on LIN⁻CD4⁺CD11c⁺BDCA1⁺BDCA3⁻. B) Quantification of the percentage of OX40L⁺ DC and OX40L⁻ DC. Mean ± SD of 18 independent donors is plotted. ***, P < 0.001, paired Wilcoxon test. C) Quantification of fold expansion and cytokines by intracellular cytokine staining for IL-4, IL-21, IL-9, IFN-γ and TNF-α of CD4 T cells polarized for 6 days in coculture with either OX40L⁺ DC or OX40L⁻ DC. Mean ± SD of 9 independent donors. D) Quantification of fold expansion and cytokines by intracellular cytokine staining for IL-4, IL-21, IL-9, IFN-γ and TNF-α of CD4 T cells polarized for 6 days in coculture with either OX40L⁺ DC or OX40L⁻ DC in the presence of 10 μg/mL OX40L blocking antibody (Oxelumab) or matching isotype control. Mean ± SD of 6 independent donors. *, P < 0.05, paired Wilcoxon test.

To verify if OX40L could be upregulated on OX40L⁻ DC, we re-cultured OX40L⁺ and OX40L⁻ DC after sorting in the presence or not of 50 µg/mL TSLP for 24 hours, before performing a surface staining for OX40L to measure its expression. We detected OX40L expression on OX40L⁺ DC both incubated with or without TSLP, while we did not detect any OX40L expression on OX40L⁻ DC neither cultured with TSLP nor without it (Figure 17A). This shows that OX40L⁻ DC are not able to express OX40L when activated a second time with TSLP. We cannot exclude that OX40L⁻ DC could upregulate OX40L during coculture, in which they receive different signals than just TSLP since they communicate with T cells in addition to DC, and this needs to be verified. But we decided to explore another possibility and study if we could detect an expression of OX40L by the T cells.

Indeed, we observed OX40L expression on T cells after 6 days coculture with TSLP-DC not only at the protein level (Figure 17B) but also at the mRNA level (data not shown). This OX40L expression was neither induced on naive CD4 T cells cultured with anti-CD3/CD28 beads in either cytokine polarizing condition (Th0, Th1, Th2, Th17), nor on memory T cells cultured in the same conditions (data not shown). Additionally, TSLP-DC polarized T cells almost exclusively expressed OX40L in combination with OX40 (Figure 17B).

In order to investigate if there could be a cross-talk between T cells through OX40-OX40L, we decided to re-culture TSLP-DC activated T cells. To avoid cell sorting, since we have observed an important cell death when sorting activated T cells, we preferred to re-culture T cells directly at the end of the coculture, for six additional days in the presence of anti-OX40L blocking antibody or its isotype control. At the end of the six days re-culture, T cell cytokine production was assessed by intracellular cytokine staining. We also decided not to sort activated T cells because we have already observed that at the end of the 6 days coculture, DC were all dead. But, in order to verify that, we performed a surface staining using several DC markers at the end of the six days coculture, just to make sure the OX40L expression we observed did not come from remaining DC. We did not observe any DC left and OX40L expression was found only on lymphoblastic T cells (data not shown).

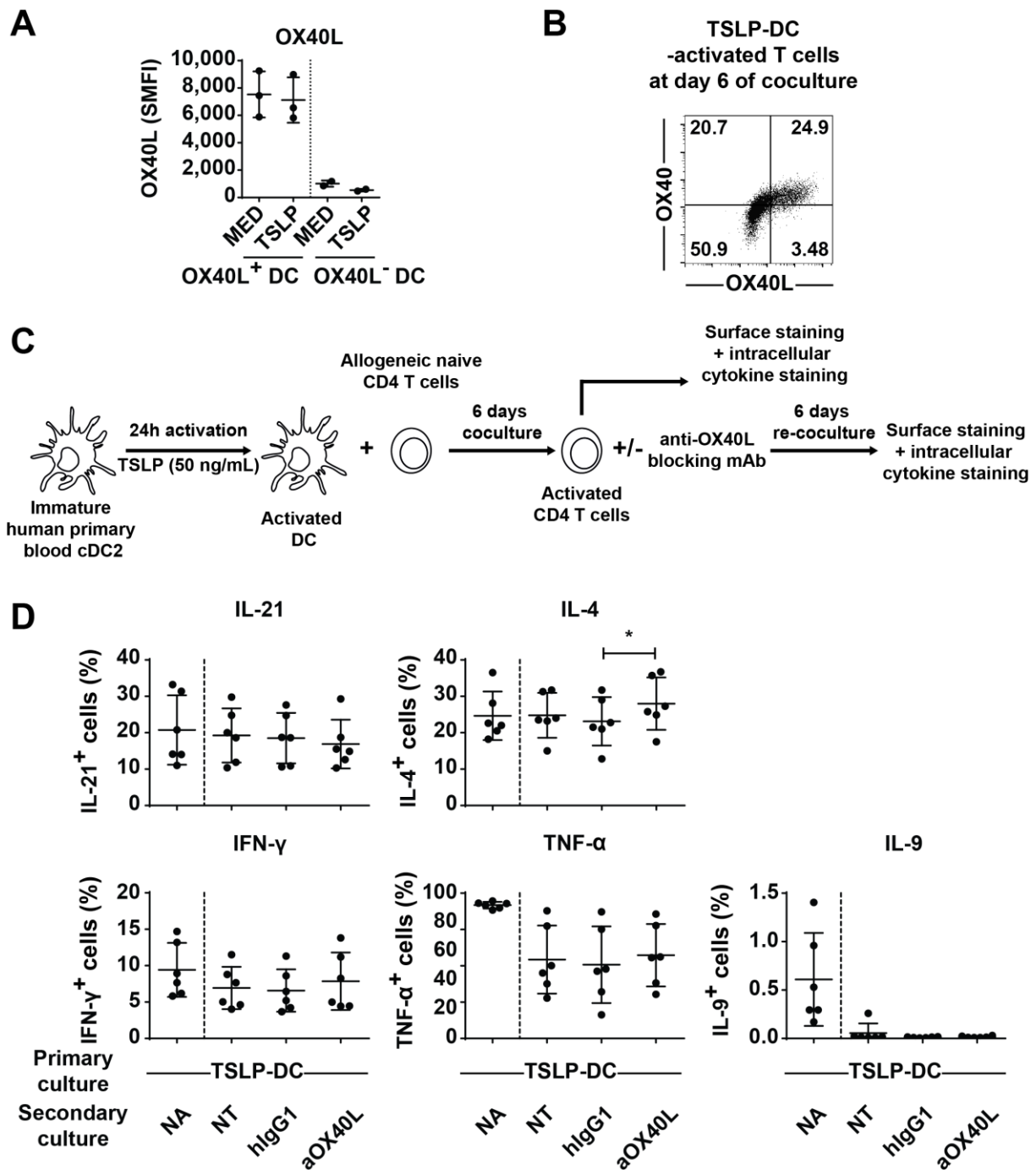


Figure 17: TSLP-DC-activated T cells express OX40L, and its blocking increases IL-4 production

A) Quantification of OX40L specific MFI (MFI staining - MFI isotype) of OX40L⁺ DC and OX40L⁻ DC re-cultured for 24 hours in the presence or not of 50 μg/mL TSLP. Mean ± SD of 3 independent donors. B) FACS plot of OX40L and OX40 surface staining on activated T cells after 6 days TSLP-DC coculture. One representative donor. C) Experimental scheme of TSLP-DC-activated T cell re-culture with anti-OX40L blocking. D) Quantification of cytokines by intracellular cytokine staining for IL-4, IL-21, IL-9, IFN-γ and TNF-α of TSLP-DC activated T cells re-cultured for 6 days with or without 10 μg/mL anti-OX40L blocking antibody or its isotype control. Mean ± SD of 6 independent donors. *, P < 0.05, paired Wilcoxon test.

First, we observed that after re-culture, IL-21 production was maintained at the same level than at the end of the initial coculture, and blocking OX40L did not affect it (Figure 17D). On the opposite, IL-9 production completely disappeared after re-culture compared to initial coculture and OX40L blocking did not influence it (Figure 17D). In addition, IFN- γ and TNF- α production were decreased after re-culture compared to initial coculture, and blocking OX40L did not significantly change their production (Figure 17D). Finally, IL-4 production was increased after re-culture compared to the end of the coculture, and blocking OX40L further increased the level of production (Figure 17D)

After seeing these results, we cannot exclude that OX40L blocking during total TSLP-DC/T cell coculture could act not only on OX40L expressed on the DC but also on OX40L expressed by T cells. Especially in the OX40L⁻ DC/T coculture system where the antibody, if not degraded or internalized when T cells start expressing OX40L, could target OX40L on the T cells. This needs more investigation, especially determining at which moment of the coculture T cells start expressing OX40L.

Besides, we could hypothesize a differential role for OX40L depending on the stage the T cells are in, either polarization or maintenance. For example, concerning IL-21, OX40L would be necessary during T cell polarization. This would explain the decrease in IL-21 production in initial coculture either with total TSLP-DC or OX40L⁺ DC or OX40L⁻ DC, while there is no effect of blocking OX40L during TSLP-DC polarized T cell re-culture. On the other hand, OX40L blocking either in total TSLP-DC/T coculture, in OX40L⁺ DC/T coculture, in OX40L⁻ DC/T coculture and even in TSLP-DC polarized T cell re-culture always induced an increase of IL-4 production. Thus, we can hypothesize that OX40L would be involved in IL-4 production regulation during both T cell polarization and maintenance.

1.2. Material and Methods

Cell purification

Apheresis blood was obtained from healthy adult blood donors (Etablissement Français du Sang, Paris, France) in conformity with Institut Curie ethical guidelines. PBMC were extracted from whole blood using a gradient centrifugation (Lymphoprep, Proteogenix). Myeloid-DC were purified using the EasySep Human Myeloid-DC Enrichment Kit (Stem Cell Technologies). Enriched DC were sorted on an MoFlo Astrios sorter (Beckman Coulter) to reach 98% purity as Lineage (CD3, CD14, CD16, CD19, CD20, CD56)⁻, CD4⁺ (BD), CD11c⁺ (Biolegend), BDCA1⁺ (ThermoFisher), BDCA3⁻ (Miltenyi Biotec) for cDC2. For the blocking experiments with ik-5 clone, DC were sorted as Lineage (CD3, CD14, CD16, CD19)⁻, CD4⁺ (BD), CD11c⁺ (Biolegend) for total myeloid DC.

Naive CD4 T cells were purified using EasySep Human Naive CD4 T Cell Isolation Kit (Stem Cell Technologies) to a 95% purity.

DC activation

Total myeloid DC or cDC2 were cultured in RPMI 1640 Medium GlutaMAX (Life Technologies) containing 10% Fetal Calf Serum (Hyclone) 100 U/mL Penicillin/Streptomycin (Gibco), MEM Non-Essential Amino Acids (Gibco) and 1 mM Sodium Pyruvate (Gibco). DC were seeded at 10^6 /mL in flat bottom plates for 24 hours in the presence of 50 ng/mL rhTSLP (R&D Systems)

DC/T coculture

After 24 hours activation, DC were washed in PBS and put in coculture with allogeneic naive CD4 T cells at a 1 to 5 ratio (10,000 DC + 50,000 T cells) in X-Vivo 15 medium (Lonza) for 6 days. For blocking experiments, DC were pre-incubated at 37°C with 50 µg/mL anti-human OX40L antibody (clone ik-5 provided by Pr. T. Hori, Ritsumeiken University, Japan), 10 µg/mL anti-human OX40L antibody (Oxelumab, Absolute Antibody) or matching isotype. After 60 minutes, naive CD4 T cells were added to the culture. Antibodies were maintained for the whole duration of the coculture. At the end of the coculture, T cells were either used for intracellular cytokine staining or washed and reseeded at 10^6 /mL and treated with anti-CD3/CD28 beads (Life Technologies) for 24 hours restimulation before harvesting supernatants.

OX40L^{+/-} DC coculture

After myeloid-DC selection from PBMC, bulk myeloid-DC were cultured at 10^6 /mL in RPMI 1640 Medium GlutaMAX (Life Technologies) with 50 ng/mL rhTSLP (R&D Systems). After 48 hours activation DC were sorted on an Aria IIIu sorter (BD) based on OX40L expression as Lineage (CD3, CD14, CD16, CD19, CD20, CD56), CD4⁺ (BD), CD11c⁺ (Biolegend), BDCA1⁺ (ThermoFisher), BDCA3⁻ (Miltenyi Biotec) and OX40L⁺ or OX40L⁻ (BD). Directly after sorting, OX40L⁺ and OX40L⁻ DC were cocultured with allogeneic naive CD4 T cells at a 1 to 5 ratio in X-Vivo 15 medium (Lonza). When indicated 10 µg/mL anti-human OX40L antibody (Oxelumab, Roche/Genentech) or matching isotype was added for the whole duration of the culture. After 6 days coculture, T cells were used for intracellular cytokine staining.

DC second culture

After 48 hours DC activation with 50 ng/mL rhTSLP and sorting as Lineage⁻, CD4⁺, CD11c⁺, BDCA1⁺, BDCA3⁻ and OX40L⁺ or OX40L⁻, DC were separately seeded at 10^6 /mL in RPMI 1640 Medium GlutaMAX (Life Technologies) with or without 50 ng/mL rhTSLP (R&D Systems). After 24 hours culture, DC were

stained with a fluorescently labeled antibody against OX40L (BD) and analyzed on a Fortessa analyzer (BD).

DC-free Th polarization

Naive CD4 T cells were cultured for 5 days with only anti-CD3/CD28 beads to obtain Th0, or in combination with either 10 ng/mL IL-12 (R&D Systems) to obtain Th1, 25 ng/mL IL-4 (R&D Systems) to obtain Th2 or a cocktail of 10 ng/mL IL-1 β (Peprotech), 100 ng/mL IL-23 (R&D Systems), 1 ng/mL TGF- β (Peprotech) and 20 ng/mL IL-6 (Peprotech) to obtain Th17 as already published [144]. When indicated 600 ng/mL rhOX40L (R&D Systems) was added to the culture. At the end of the culture, cells were washed, reseeded at 10⁶/mL and treated with anti-CD3/CD28 beads for 24 hours before harvesting supernatants for analysis.

TSLP-DC activated T cell re-culture

After 6 days of TSLP-DC/T cell coculture, activated T cells were either used for surface and intracellular cytokine staining or seeded at 0.5.10⁶ cells/mL and re-cultured for additional 6 days. When indicated 10 μ g/mL anti-human OX40L antibody (Oxelumab, absolute antibody) or matching isotype was added for the whole duration of the culture. After 6 days coculture, T cells were used for intracellular cytokine staining.

Surface staining

At the end of the coculture, T cells were washed and stained for 15 min at 4°C with antibodies recognizing human OX40 (Biolegend) and OX40L (BD). Dead cells were excluded using Live/Dead Fixable Yellow Dead Cell stain kit (LifeTechnologies).

Intracellular cytokine staining

At the end of the culture, CD4 T cells were restimulated with 100 ng/mL PMA, 500 ng/mL Ionomycin (Sigma) and 3 μ g/mL Brefeldin A (ThermoFisher) in X-Vivo medium. To exclude dead cells, T cells were stained using the Live/Dead Fixable Yellow Dead Cell stain kit (LifeTechnologies). Cells were fixed and permeabilized using the IC Fix and Permeabilization Buffers (ThermoFisher). Intracellular cytokines were revealed with fluorescently conjugated antibodies against IL-9 (ThermoFisher), IL-21 (Biolegend), IL-4 (ThermoFisher), TNF- α (Biolegend) and IFN- γ (BD).

Cytokine quantification

Cytokines were quantified in the culture supernatants using CBA flex set for IL-3, IL-4, IL-5, IL-9, IL-13, TNF- α , IFN- γ (BD) following manufacturer's instructions.

Statistical analysis

Paired Wilcoxon or student t test were applied as detailed to compare two groups. Significance was retained for $p < 0.05$.

Software availability

FACS data were analyzed using the FlowJo software (TreeStar).

Software used for CBA analysis was FCAP Array v3.

Statistical analysis was performed using the Prism software (GraphPad).

2. Appendix 2

A model for the integration of conflicting exogenous and endogenous signals by dendritic cells

Quentin Marcou, Irit Carmi-Levy, Coline Trichot, Vassili Soumelis, Thierry Mora and Aleksandra M Walczak

Phys Biol. 2018 May 16;15(5):056001



PAPER

A model for the integration of conflicting exogenous and endogenous signals by dendritic cells

To cite this article: Quentin Marcou *et al* 2018 *Phys. Biol.* **15** 056001

View the [article online](#) for updates and enhancements.

Related content

- [Dynamic interplay between tumour, stroma and immune system can drive or prevent tumour progression](#)
R J Seager, Cynthia Hajal, Fabian Spill *et al.*
- [Immunoadjuvant activity of nanoparticles surface modified with mannan](#)
Azita Haddadi, Samar Hamdy, Zahra Ghotbi *et al.*
- [Effects of titanium surface roughness on the mediation of osteogenesis via modulating the immune response of macrophages](#)
Xuezhong Li, Qianli Huang, Tarek A Elkhooly *et al.*



IOP | ebooks™

Bringing you innovative digital publishing with leading voices to create your essential collection of books in STEM research.

Start exploring the collection - download the first chapter of every title for free.

Physical Biology



PAPER

A model for the integration of conflicting exogenous and endogenous signals by dendritic cells

RECEIVED
18 August 2017

REVISED
13 January 2018

ACCEPTED FOR PUBLICATION
23 January 2018

PUBLISHED
16 May 2018

Quentin Marcou^{1,6}, Irit Carmi-Levy^{2,3,4,6}, Coline Trichot², Vassili Soumelis^{2,3,4}, Thierry Mora^{5,7} 
and Aleksandra M Walczak^{1,7} 

¹ Laboratoire de physique théorique, CNRS, UPMC and École normale supérieure, 75005 Paris, France

² INSERM U932, 26 rue d'Ulm, 75005 Paris, France

³ Institut Curie, Section Recherche, 26 rue d'Ulm, 75005 Paris, France

⁴ Laboratoire d'Immunologie Clinique, Institut Curie, 26 rue d'Ulm, 75005 Paris, France

⁵ Laboratoire de physique statistique, CNRS, UPMC and École normale supérieure, 75005 Paris, France

⁶ Equal contribution.

⁷ Corresponding authors with equal contribution.

E-mail: tmora@lps.ens.fr and awalczak@lpt.ens.fr

Keywords: signaling, immunology, modeling

Supplementary material for this article is available [online](#)

Abstract

Cells of the immune system are confronted with opposing pro- and anti-inflammatory signals. Dendritic cells (DC) integrate these cues to make informed decisions whether to initiate an immune response. Confronted with exogenous microbial stimuli, DC endogenously produce both anti- (IL-10) and pro-inflammatory ($\text{TNF}\alpha$) cues whose joint integration controls the cell's final decision. Backed by experimental measurements we present a theoretical model to quantitatively describe the integration mode of these opposing signals. We propose a two step integration model that modulates the effect of the two types of signals: an initial bottleneck integrates both signals (IL-10 and $\text{TNF}\alpha$), the output of which is later modulated by the anti-inflammatory signal. We show that the anti-inflammatory IL-10 signaling is long ranged, as opposed to the short-ranged pro-inflammatory $\text{TNF}\alpha$ signaling. The model suggests that the population averaging and modulation of the pro-inflammatory response by the anti-inflammatory signal is a safety guard against excessive immune responses.

1. Introduction

Cells constantly integrate signals to adapt to their environment. In the immune system, activating signals are critical to initiate and sustain an efficient immune response, and co-exist with inhibitory signals in order to avoid excessive and uncontrolled immune responses [1, 2]. Immune cells must often integrate such opposing signals, the outcome being key to decision making between immunity versus tolerance [3–5]. This signal integration process in immune cells involves many check points that can involve kinetic proofreading [6–8] or multiple feedback loops [9, 10]. In general, feedback allows the system to adjust its output in response to monitoring itself. Both positive and negative feedback loops have been found crucial to control the strength and duration of the system's activation in order to achieve optimal responses. Such loops represents a fundamental feature in cell development and differentiation [11],

hormonal homeostasis [12], intracellular signalling [13] and in the immune response [1]. Cells can receive feedback through paracrine signals coming from their neighbours or from their own autocrine signals [14, 15]. Since the adaptation to the environment occurs at the population level, autocrine and paracrine feedback may play a different role in a cell population responding to opposing signals, notably as a function of cell density.

Dendritic cells (DC) are an essential component of the innate immune system. Acting as the body's sentinels, they are equipped with a diversity of innate receptors, including pattern recognition receptors such as toll like receptors (TLRs). Engagement of TLRs by TLR ligands leads to DC maturation, a complex process which includes migration to draining lymph nodes, secretion of a diversity of chemokines and cytokines, as well as up-regulation of major histocompatibility class II (MHC-II) and co-stimulatory molecules, such as CD80 and CD86 [16]. The latter represent crucial

molecular checkpoints for orchestrating DC-T cell communication, playing a key role in the activation and expansion of CD4 T cells [17].

A critical question is how the diversity of signals sensed by DC controls the outcome of the DC maturation program. In this process, we can discriminate exogenous signals, i.e the nature and dose of microbial stimuli, and endogenous signals, such as autocrine factors induced by exogenous stimulation. When DC are activated by the bacterial component LPS (exogenous signal), they respond with an increased secretion of TNF- α (TNF α) and interleukin (IL)-10, generally considered as prototypical pro- and anti-inflammatory signals, respectively [18, 19]. As DC are equipped with the corresponding receptors, both TNF α and IL-10 act as endogenous auto-regulatory feedback signals that control the output response of the cell, and influence the final decision to initiate an immune response or not. Current and past studies have mostly studied each of these signals separately. LPS effect on DC has been extensively studied, including at various concentrations revealing dose-dependent effects [20, 21]. Few studies have addressed the role of the IL-10 negative feedback loop, showing that it dampens LPS-induced maturation [22]. TNF α is a DC-activating pro-inflammatory cytokine [19], but its role as a putative positive feedback factor on DC remains elusive. Studies of these DC-targeting regulatory signals suggest strong dependencies and cross-regulatory mechanisms between LPS, IL-10 and TNF α , but the underlying rules remain unexplored. Here we study MoDC (dendritic cells matured from monocytes) that do not express IL-12 receptors and are not strongly affected by TGF- β signaling [23]. In these cells IL-10 has a strong signaling impact, so we consider its role in DC maturation. We also note that the pro- and anti-inflammatory nature of the signals can depend on the cellular context. In the MoDC maturation system TNF α and IL-10 do behave as pro- and anti-inflammatory signals, respectively [18, 19]. Mechanistic understanding requires the integrated analysis of variations in the three signals level, and their consequences on the behaviour of the system.

In this study, motivated by measurements, we propose a minimal theoretical model that explains the experimentally observed effects of LPS, IL-10, and TNF α effects on human DC. Our original model describes the interplay between contradictory exogenous and endogenous signals in the control of DC maturation.

2. Results

2.1. LPS-induced TNF α and IL-10 differentially control DC maturation

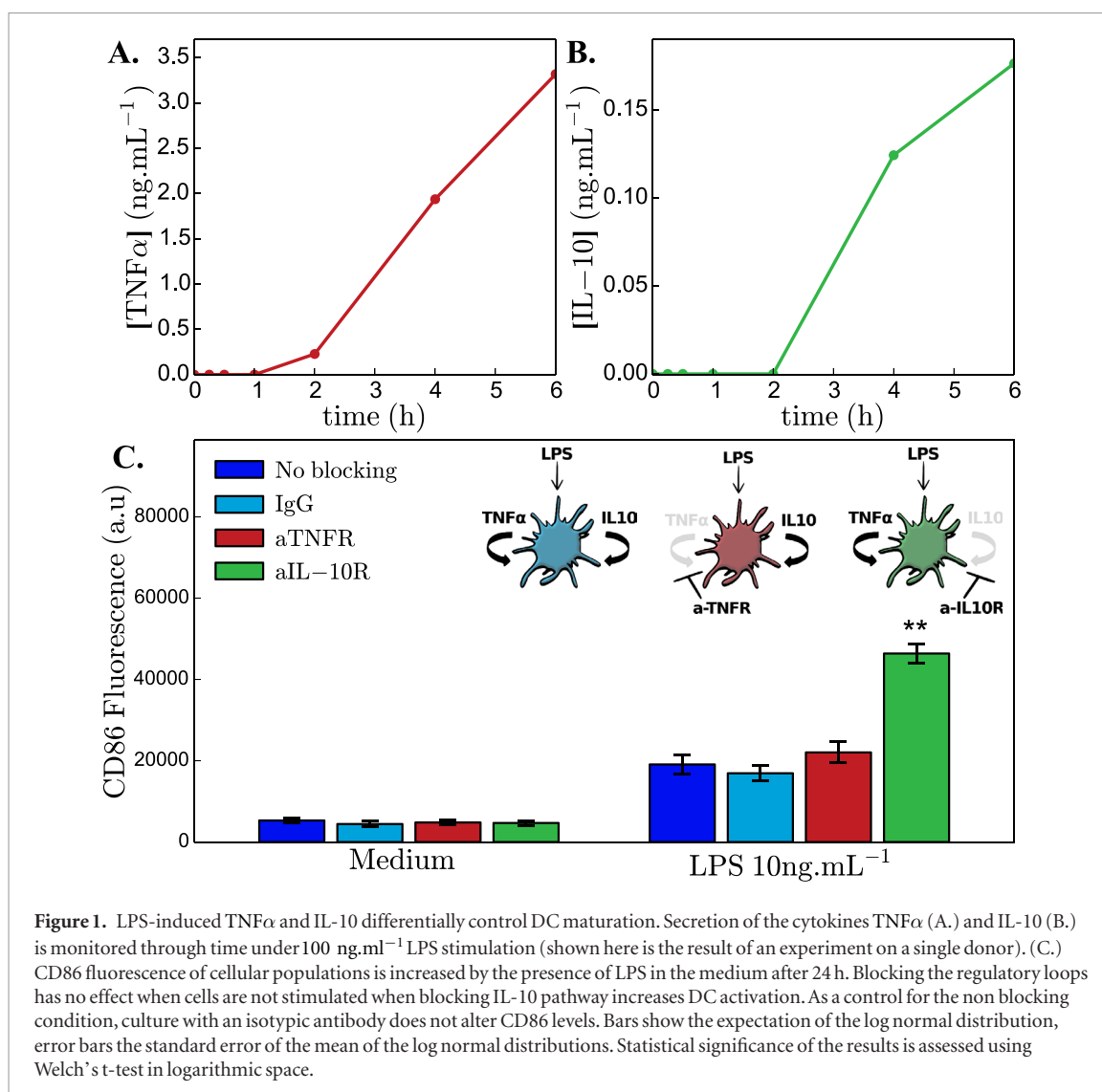
Upon activation by the TLR4 ligand LPS, DC undergo a maturation process leading to an upregulation of costimulatory molecules, such as CD86, but also production of pro- and anti-inflammatory cytokines.

CD86 is a classical marker for DC maturation [24], and we will use its expression as a surrogate for it. LPS is not toxic when incorporated into the bacterial outer membrane, but is toxic in solution [25]. We designed an *in vitro* setup to study how it regulates the expression of the downstream cytokines in solution. First, we measured the production of TNF α and IL-10 in response to a standard LPS concentration of 100 ng ml⁻¹ [26, 27]. The secretion of TNF α was more rapid and was significant already after 2 h, while IL-10 was detected only after 4 h following LPS stimulation (figure 1(A)), as previously reported [28]. After 4 h, both cytokines were detected concomitantly in the cellular supernatant (figure 1(A)). TNF α and IL-10 reached concentrations of 3.3 ng ml⁻¹ and 0.18 ng ml⁻¹, respectively after 6 h figure 1(A). In order to address the contribution of these two endogenous cytokines on DC maturation, we monitored CD86 using flow cytometry, in the presence and absence of blocking antibodies (Ab) to TNF α or IL-10 (figure 1(B)). LPS induced significant upregulation of CD86, consistent with an increase in DC maturation (figure 1(B)). Blocking the IL-10 loop induced a significant increase in CD86 expression. This suggested that IL-10 had a dominant negative effect in controlling LPS-induced DC maturation.

2.2. LPS dose determines the endogenous IL-10 and TNF α control of DC maturation

Microbial-derived signals occur at various concentrations in infected tissue, in relationship to the *in situ* microbial load. This process is also linked to microbial clearance, which induces a local decrease in microbial signals. First, we addressed the impact of various LPS doses on endogenous TNF α and IL-10 production (figure 2(A)). Both cytokines exhibited a similar LPS dose-dependent pattern, reaching maximum levels at a LPS concentration of 100 ng ml⁻¹ (figure 2(A)).

Given that TNF α and IL-10 co-exist at variable LPS concentrations, we asked whether LPS levels impact the way these endogenous signals are being integrated by DC. To address this question, we cultured DC in the presence or absence of blocking Abs to the TNF α and IL-10 receptors (TNFR and IL10R) while stimulating them with different concentrations of LPS achieved by serial dilutions (figure 2(B)). As for the standard LPS dose, DC maturation was quantified by CD86 expression 24 h following LPS activation. When none of the loops were altered (no blocking or IgG control), the level of activation increased with LPS concentration and reached a plateau for sufficiently high LPS doses (\sim 100 ng ml⁻¹) (blue curve in figure 2(B)). Blocking the pro-inflammatory TNF α loop led to a decreased expression of CD86 (red curve in figure 2(B)), while blocking the anti-inflammatory IL-10 loop led to an increased expression of CD86 (green curve in figure 2(B)). However, TNF α loop-blocking decreased CD86 levels mostly at LPS concentrations lower than



10 ng ml $^{-1}$ (red curve in figure 2(B)). By contrast, the impact of IL-10 loop-blocking on CD86 expression was constant along a wide spectrum of medium to high LPS doses, but absent at low LPS doses (green curve in figure 2(B)). The impact of the two opposite/contradictory loops differed not only in the directionality of the effect but also in mode of the effect: blocking the TNF α loop shifted the onset of the response towards higher LPS dose, while blocking the IL-10 loop affected mainly the amplitude of the response, which significantly increased in the presence of IL-10 blocking compared to its value in the absence of any blocking.

DC maturation with or without blocking the loops in the different LPS doses was quantified using the expression of a second maturation marker CD83. The expression of this marker also increased with increasing LPS dose (figure S1 (stacks.iop.org/Phys-Bio/15/056001/mmedia)). Blocking the TNF α loop led to a similar trend as with CD86, with a strong effect at low LPS doses, and weaker effect at high LPS doses (figure S1). Although both maturation markers were significantly upregulated by LPS, their distribution across the DC population was different. While

CD86 demonstrated a unimodal distribution, CD83 demonstrated a bi-modal one (figure S2). In addition to surface markers, blocking the loops also had a significant effect on cytokine secretion (figures 2(C) and (D)). Importantly, the TNF α and IL-10 loops reciprocally affected each other, as blocking the IL-10 loop increased TNF α secretion (green curve in figure 2(C) compared to the other curves), and blocking the TNF α loop strongly decreased IL-10 production (red curve in figure 2(D)). This suggests potential cross-regulation of TNF α and IL-10 through DC.

2.3. Modulated bottleneck model explains DC maturation control by opposing endogenous and exogenous signals

In order to qualitatively understand the mechanism behind microbial-induced signal integration in DC, we used the above experimental observations to build a minimal phenomenological steady state mathematical model of CD86 response to LPS stimulation. Our phenomenological model aims at reproducing all the experimental observations (summarized in this paragraph) and previously known facts about the interactions between the three signaling molecules in

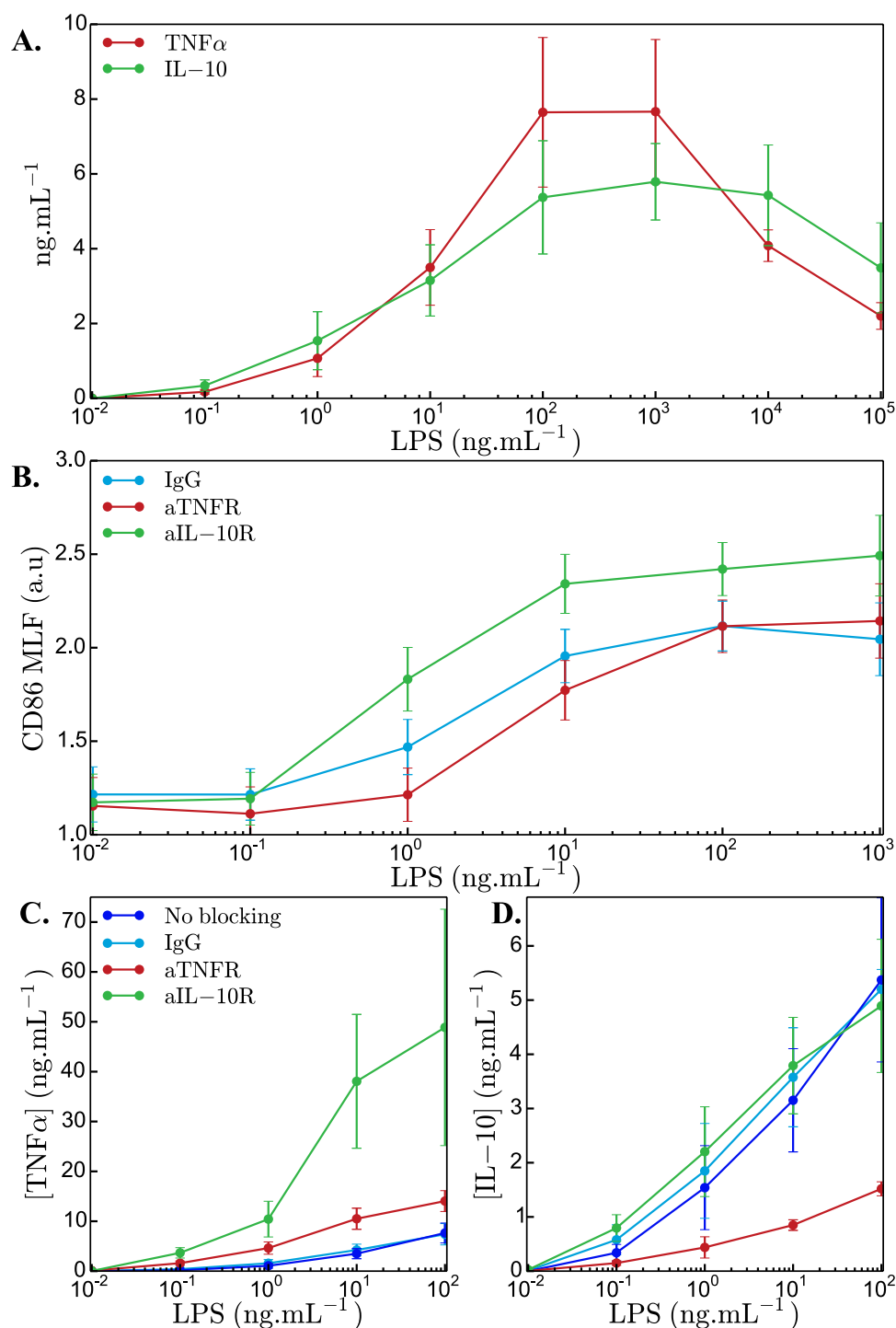
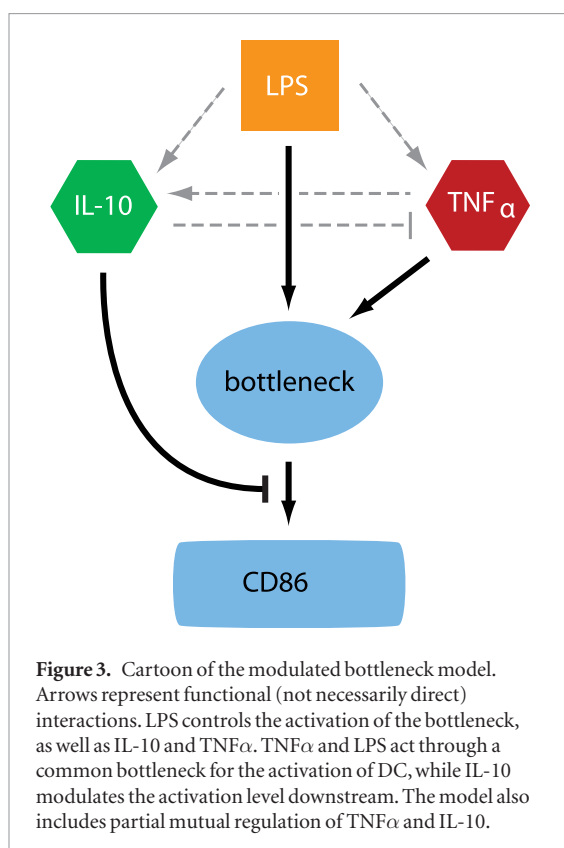


Figure 2. LPS dose determines the endogenous IL-10 and TNF α control of DC maturation. (A.) Titration of TNF α and IL-10 concentrations (ng.mL $^{-1}$) for a wide range of LPS doses after 24 h. Increasing LPS doses increase both TNF α (red) and IL-10 (green) secretion levels. (B.) Activation of DC is monitored by flow-cytometry labeling the co-stimulatory molecule CD86. CD86 mean log-fluorescence (MLF) is shown for a range of LPS concentration incubated for 24 h with isotypic control (blue), anti-TNFR (red) or anti-IL-10R (green) antibodies. CD86 has a sigmoidal dependence on LPS doses. Blocking IL-10 increases the maximal activation level while blocking TNF α decreases the sensitivity. Cytokine response of DC in different conditions, medium (dark blue), isotypic control (blue), anti-TNFR (red), anti-IL-10R antibodies, is measured for different doses of LPS. (C.) Blocking IL-10 increases TNF α secretion (D.) Blocking TNF α decreases IL-10 secretion.

the simplest way, without assuming additional modes of regulation. From figure 2(B) we see that the CD86 response follows a sigmoidal dependence on LPS concentration, which we denote as L and saturates at high LPS level. Additionally, both IL-10 (denoted as I) and TNF α (T) expressions are sigmoidal functions of LPS (figures 2(C) and (D) and see supplementary

material equations (1)–(4)). As we noted above, TNF α upregulates IL-10 expression [29], while IL-10 downregulates TNF α secretion [30, 31] (figures 2(C) and (D)). To avoid behavior that is not observed in the data, we assume there is a basal expression level of both TNF α and IL-10, even in the absence (presence) of the regulator. Results of blocking IL-10 show that



additionally to repressing TNF α , IL-10 also decreases the amplitude of the response (figure 2(B)). Lastly, it has previously been shown that TNF α alone, in the absence of LPS, activates and induces DC [19]. This observation suggested that TNF α does not just act downstream of LPS, but that TNF α and LPS act through a common intermediate in an additive way creating a bottleneck. This last assumption is the main idea behind our model: LPS and TNF α signals are integrated in the expression of one regulatory molecule. The expression of CD86 itself is not regulated directly by TNF α and LPS, but by the concentration and status of this central integrator (figure 3). Since there is no experimental evidence of direct interactions between TNF α and IL-10, and as we will see below we do not need to invoke these interactions to explain the data, we will not consider models with direct regulation.

A schematic representation of the effective regulatory pathway described above is shown in figure 3. A central signal integrator combines the two pro-inflammatory signals, TNF α and LPS, in a single common pathway making this integrator the key regulator of DC decision. The integrator acts as a molecular bottleneck for the pro-inflammatory signals (see figure 3): it responds to increases in the pro-inflammatory signal concentrations only until a certain total concentration. This concentration can be reached either purely by TNF α or purely by LPS, or by their combination (see figure 4(B)). Above this total concentration, set by the effective EC50 (dose at which the response is half of the maximum), the response is saturated and increasing pro-inflammatory signals has no effect on the output. Without the bottleneck effect of the central integra-

tor, the TNF α and LPS pathways would independently control the CD86 response. In this case blocking the TNF α loop would not change the EC50 of the response to LPS. Adding more LPS while the TNF α loop was blocked would lead to a lower saturation level at infinite LPS dose than without blocking. LPS and TNF α are known to control common downstream pathways [32], giving for example NF- κ B as a possible candidate for the bottleneck, which we discuss below. In turn IL-10 has been shown to inhibit NF- κ B activation in human monocytes [33, 34].

The concentration of the integrator molecule controls the amplitude of the response, which is further modulated downstream by the IL-10 anti-inflammatory signal (figures 3 and 4(B)). A plumbing analogy helps illustrate the role of the bottleneck and downstream anti-inflammatory regulation: there is a very high source of water distributed to each house, but the amount of available water is limited by the throughput capacity of the main pipeline (this is the bottleneck that regulates the amount of pro-inflammatory signals—see figure 4(B)). However when you take a shower, you can regulate the waterflow directly at the faucet (this is the inhibitory action of IL-10). In the absence of IL-10, the bottleneck still limits the scale of the inflammatory response. IL-10 can further downregulate it.

The bottleneck model reproduces all the experimentally observed features in figure 2(B). It further predicts the combined effect of blocking both the IL-10 and TNF α loops (figure 4(A)). We graphically represent the predictions of the model for the four blocking conditions at low and high LPS concentrations in figure 4(B). At high LPS dose the bottleneck limits the signaling of the master integrator, regardless of whether both TNF α or LPS are sensed or only LPS, and the IL-10 further reduces the strength of the response. At low LPS concentrations the effect of the bottleneck is reduced but IL-10 further modulates the output. We experimentally validated the bottleneck model by blocking both loops simultaneously in LPS stimulated DC. In agreement with the prediction, the condition in which both loops were blocked affected the CD86 EC50 expression similarly to blocking the TNF α loop (figure 4(C)) (the data from figure 2(B) is replotted in figure 4(C) adding the yellow curve that describes the simultaneous blocking of the two signaling channels). At higher LPS doses the CD86 amplitude increased similarly to blocking IL-10 alone, also in agreement with the model predictions. We also note that the secondary interactions of TNF α activating IL-10 and IL-10 repressing TNF α explain the experimentally observed results presented in figures 2(C) and (D). Since TNF α effectively represses itself (figure 3), blocking the TNF α receptor (red line in figure 2(C)) decreases the response of TNF α directly from LPS signaling, decreasing IL-10 concentrations, and effectively alleviating the IL-10s repression of TNF α , which results in the observed increase of TNF α concentrations in figure 2(C). Similarly, blocking the

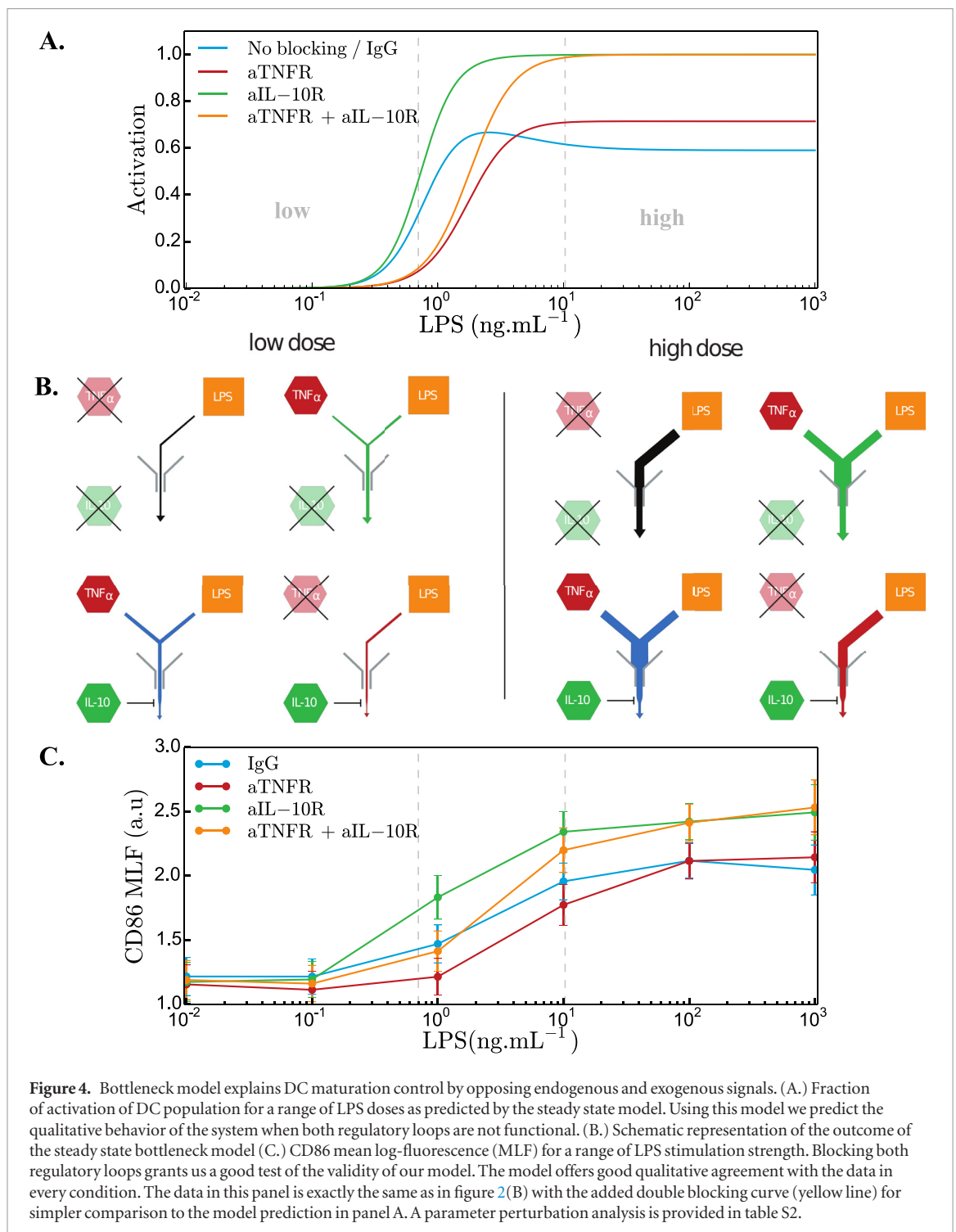


Figure 4. Bottleneck model explains DC maturation control by opposing endogenous and exogenous signals. (A.) Fraction of activation of DC population for a range of LPS doses as predicted by the steady state model. Using this model we predict the qualitative behavior of the system when both regulatory loops are not functional. (B.) Schematic representation of the outcome of the steady state bottleneck model (C.) CD86 mean log-fluorescence (MLF) for a range of LPS stimulation strength. Blocking both regulatory loops grants us a good test of the validity of our model. The model offers good qualitative agreement with the data in every condition. The data in this panel is exactly the same as in figure 2(B) with the added double blocking curve (yellow line) for simpler comparison to the model prediction in panel A. A parameter perturbation analysis is provided in table S2.

IL-10 receptor effectively increases IL-10 concentrations, although the effect is much smaller in magnitude (figure 2(D)).

The model proposes a possible mechanism for signal integration. To test whether the features of the model are constrained by the data, and whether even simpler model assumptions would still be compatible with the experimental observations, we fitted all the parameters of the model to the data of figures 2(B) and (C) using Maximum Likelihood. We assumed Gaussian experimental errors, which we estimated from the pooled error over all donors. We compared models

with various assumptions and levels of simplicity (see supplementary material): a bottleneck model such as described above; a model without a bottleneck, where the LPS, TNF α and IL-10 signals are all integrated into a single regulation function; a model with just LPS and TNF α activation; and a linear model of activation. To compare the models of different complexities, we used the Akaike Information Criterion, which penalizes the likelihood score of a model with the number of its parameters. The bottleneck model was the best fitting model (table S1), indicating that the bottleneck is a necessary ingredient to explain the data. The model

prediction for the levels of cytokines as a function of dose (figure 2(A)) resulting from the fitting procedure are shown in figure S6.

We evaluated the robustness of the parameter fit by sampling from the posterior distribution obtained by Bayes' rule with a flat prior, using a Monte-Carlo algorithm (see supplementary material). The standard errors and confidence intervals for each parameter, reported in table S2, show that all the parameters are constrained by the data within an order of magnitude of their optimal value. This analysis also estimates the effect of varying the parameters on the accuracy of the model: for instance, changing K_C by 50% would make the prediction fall significantly outside the error bars, while changing K_I or K_T by the same amount would have little effect on the output, as these parameters are less constrained by the data.

2.4. Paracrine signalling predominantly controls DC maturation

DC in our experiment, as in the organism, are not isolated and signal integration depends on the diffusion of cytokines: a cytokine produced by a given cell could be picked up by a receptor on the surface of this same cell (autocrine loop) or by a neighboring cell (paracrine loop). Since we cannot directly measure inter-cellular communication with single molecule resolution, we designed and performed cell dilution experiments to get insight into DC communication at a larger spatial scale. At high cellular concentrations, cells can sense signals from nearby cells (figure 5(A)), and at large dilutions, only from themselves (figure 5(C)). Large dilution conditions correspond to pure autocrine signaling. This experiment is based on the assumption that the effect of a purely paracrine loop will decrease as cells are diluted, while a purely autocrine loop will not be sensitive to dilution of the population density. Since the effect of the TNF α feedback loop was observed at low LPS concentrations, whereas the IL-10 feedback was active at high LPS concentrations, we performed dilution experiments at two distinct LPS doses.

To predict the behavior of the DC response in the dilution experiments we combined our phenomenological bottleneck model (figure 3) with diffusion-based estimates for the probabilities of autocrine and paracrine absorption in an effective heterogeneous medium [35] (see supplementary material for details). The model ignores cross-talk across cytokines. Using previously measured kinetic and geometric parameters (see table S3), the theoretical calculation predicts that a large fraction of the signaling is paracrine in nature. In figures 5(E) and (G) we plot the predictions for the mean log CD86 expression at a low and high LPS concentration as a function of the cell concentration. If most of the signaling is paracrine in nature, as we see that at high LPS concentrations (figure 5(G)), with increasing cell dilutions all the blocking conditions converge to nearly the same activation levels,

equal to the levels predicted in the case when all the loops are non-functional (orange curve in figures 5(B) and (G)). For very low cell density we expect the paracrine feedback loops to have no effect on CD86 expression and all feedback takes place by autocrine loops. Measurements of ligand affinity of TNF α and IL-10 to their respective membrane receptors [36–38] show that TNF α has a greater affinity for its receptor than IL-10 does. We thus predict that TNF α autocrine fraction should be greater than IL-10. Since the effect of the TNF α feedback is observed at low LPS concentrations, and the IL-10 feedback at high LPS concentrations, we expect the convergence of the curves corresponding to different conditions at low LPS concentrations to be less pronounced than at high concentrations. Our model predicts (see figure 5(E)) that the curves corresponding to blocking the TNF α loop do not converge to those where the TNF α is active at high dilutions for low LPS concentration.

To experimentally assess the effect of dilutions on the loops we activated DC with either low (1 ng ml^{-1}) or high (100 ng ml^{-1}) LPS in different cell dilutions with the initial culture concentration being $10^6 \text{ cells.ml}^{-1}$ (figures 5(F) and (H)). In agreement with our model we could observe that at both low and high LPS doses all conditions were converging to the same amount of activation. Because of the saturation effect we could not observe a slower convergence for the case of a blocked TNF α loop for high LPS dose, however it was observable for low LPS dose (figure 5(F)). In the case of the lower LPS dose, in which the TNF α loop plays a more specific role, we observed that despite serial dilution, the effect of blocking the loop was maintained, at least to some extent, suggesting the existence of an autocrine signaling. Interestingly, in the higher dose of LPS, the effect of IL-10 loop was rather sensitive to dilutions, suggesting that in a context of high microbial load IL-10 acts in a paracrine manner.

3. Discussion

Innate immune recognition is key to promote an efficient anti-microbial immune response, but also needs to be controlled, in order to avoid immunopathology. It is known that immune activating and immune dampening signals are both rapidly produced and co-exist within any inflamed tissue [2]. However, the interplay between exogenous microbial signals, and endogenous pro- and anti-inflammatory signals has not been formalized in an integrated manner. This is critical to the decision making of the immune response, as it is driven by multiple dynamic signals, conveying different types of information to innate immune cells. By combining experiments with modeling, we showed that the final response of the DC population relies on integrating the initial signal with the induced pro- and anti-inflammatory responses using feedback loops. The integration is based on two steps: first the pro-inflammatory signals are integrated

through a bottleneck and then the amplitude of the result is further modulated by the anti-inflammatory signal. The key element of this integration occurs at the signal bottleneck, which controls the effective concentration range (EC50) of the response to LPS and limits the maximum pro-inflammatory response. The anti-inflammatory regulation that follows is mostly paracrine, as opposed to the bottleneck integration that has an autocrine component, suggesting that the final response is modulated based on the population level response.

Bottleneck signal integration in molecular systems have mostly been proposed for the integration of two positive signals. They were suggested as a means for TNF α activation [39]. Here we propose that a bottleneck is the essential component in making the decision to the response in the presence of two opposing signals: IL-10 and TNF α . Since the negative regulation by IL-10 acts after the bottleneck, it regulates the maximum level of activation, while the positive TNF α acts before the bottleneck thereby affecting the activation threshold. The two opposing signals thus control distinct aspects of the dose response. This feature is independent of the fact that the two signals have opposing effects: the possibility of additional pre- or post-bottleneck regulation would have the same effect on two positive signals.

The modulated bottleneck model is purely phenomenological and aims at describing the observed integration in an effective way, by contrast to more detailed mechanistic models such as proposed for TNF α IL-10 interplay in macrophages [40] and microglia [41]. We do not propose a detailed explanation of how the two cytokines are integrated mechanistically. Further experiments are needed to explore this question in more detail, as well as the possible integration of detailed knowledge about signaling mechanisms. The model proposes an integration mode that seems to be dominant in the experimental system we looked at. Of course, real cells function in many environments and other integration modules with behaviors not predicted by the modulated bottleneck could be present in DC. In general, the modulated bottleneck model is consistent with all experimental observations and known forms of interactions. Simple alternatives to the bottleneck hypothesis cannot explain the data. For example, a model with negative feedback acting on any of the signals would give a plateau that would be either sensitive to the activation signals, or insensitive to IL-10 inhibition. Future experiments that block other DC maturation factors with similar regulatory profiles will give more insight into the role of the bottleneck integrator, or whether other integration models should be favored.

A natural candidate for this bottleneck integrator is the widely studied [42] nuclear factor NF κ B: several studies demonstrated how LPS and TNF α trigger NF κ B nuclear translocation [32], and how IL-10 inhibits NF κ B or its target genes in certain cell types

[43]. Additionally the saturation effect observed in our data was also seen when looking at NF κ B nuclear translocation due to the limited and constant amount of NF κ B [10]. It is also known that, while IL-10 is known to signal through Jak-STAT pathway, IL-10 also inhibits NF κ B [33, 34] giving experimental support for the modulation interaction. Future experiments that block other DC maturation factors with similar regulatory profiles will give more insight into the role of the bottleneck integrator.

Additionally to the main modes of signal integration based on the bottleneck and IL-10 repression, TNF α activates IL-10 expression, while IL-10 represses TNF α . These secondary interactions do not change the basic flow of signal integration, but are predicted by the model to produce a maximum in the CD86 at intermediate LPS concentrations (figure 4(A)). Since LPS activates both IL-10 and TNF α , repression of TNF α slightly shifts the EC50 of the response to larger LPS concentrations, while activation of IL-10 results in a larger moderation of the response than in the absence of TNF α for high LPS concentrations.

The presented results are population averages over multiple independent measurements. The fluorescence distributions plotted in figure S2 show a large heterogeneity in the population, indicating that particular cells can have very different responses. The error bars indicate the standard error of the mean over multiple experiments. The measurement noise is impossible to distinguish from the natural heterogeneity of the response in the population. Given this heterogeneity, the mean CD86 response in the double blocked mutant is consistent with the theoretical prediction.

Dendritic cells often are surrounded by other dendritic cells and, through secreting signaling molecules, communicate with each other to make a decision at the population level. This collective decision making process can help make the right readout in a noisy environment thus reducing response variability as for wound healing [44]. By sharing their response, cells in a population can confirm initial measurements by sensing the signals that their neighbors secrete. Alternatively, cells could simply use the feedback loops to amplify their own initial signal to accelerate their response.

Previous experiments have highlighted the difference between population and single cell measurements in TNF α responses [32]. The nature of the signal (paracrine or autocrine) controls the spatial range of the responding cells and determines the lengthscale on which the decision is made. Feedback loops are necessary elements for integrating population-level signals. The signalling range controls whether there is population level averaging, or whether each cell only listens to itself. Here, by using a combination of dilution and fluorescence experiments with modelling, we show that the anti-inflammatory IL-10 signal is paracrine and long range, as opposed to the autocrine and short range pro-inflammatory TNF α signal. Cells rely

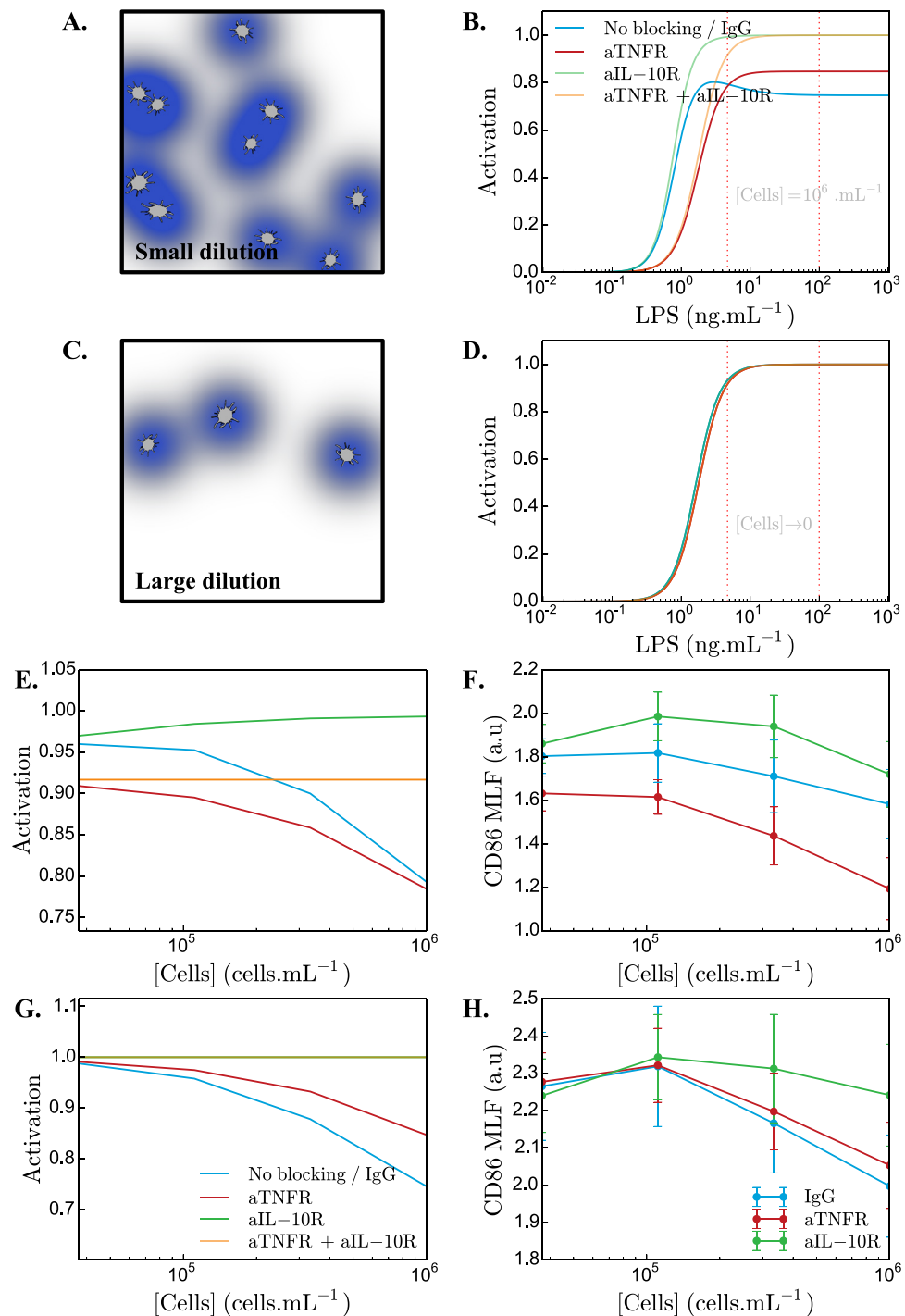


Figure 5. Discriminating autocrine from paracrine loops using dilutions. (A.) and (B.) Cartoon and prediction of our steady state model with diffusion for high cell concentration (the cell concentrations in the cartoons are illustrative and not quantitative). (C.) and (D.) Cartoon and prediction of our steady state model with diffusion for very low cell concentration. (E.) Prediction of our steady state model with diffusion on DC activation for a weak LPS stimuli. Computing the expected activation for a range of cell concentrations gives us a qualitative prediction for serial dilutions experiments. (F.) Corresponding dilution experiment with low dose of LPS (1 ng.mL^{-1}). (G.) Model prediction for high dose of LPS. (H.) Corresponding dilution experiment with high dose of LPS (100 ng.mL^{-1}). LPS concentration values used for the model predictions in (E.) and (G.) are shown with red dashed lines in (B.) and (D.). The parameters of the model are set to the values summarized in table S3.

on local signals to detect bacterial signals, but integrate anti-inflammatory signals from anywhere in the population to modulate their response.

Such a localized pro-inflammatory response can be useful in the case of an infection: cells that are further away from the source of the signal do not need to respond. In view of their signalling ranges, autocrine

or paracrine feedback loops have different roles: autocrine signaling modifies the strength of response to LPS of the cell itself, while paracrine signaling is used to transmit information to neighboring cells that may not have been exposed to LPS directly. Such a combination of local, excitatory feedback with global, inhibitory regulation has been suggested as a general way

to sense differences in spatial concentration profiles, and has been proposed as a mechanism for detecting spatial concentration gradients in the slime mold *Dictyostelium* [45–47], or more recently for wound healing [44] and in the context of morphogenesis of mammary epithelial cells in response to a gradient of the epidermal growth factor [48]. Our results extend this concept to the immune system following innate microbial sensing.

In summary, in this study we quantified how a cell makes decisions about the appropriate response to a given concentration of the bacterial signal LPS in the environment, and as a result whether to initiate an inflammatory response or not. More broadly, the mechanisms described give a way to integrate information and make decisions in the presence of conflicting signals. Furthermore we show how simple biophysical models give us insights into cell-cell communication in cell density regimes that are inaccessible by single-cell microscopy [14, 15].

Acknowledgments

This work was supported by MCCIG grant no. 303561, by the Agence Nationale pour la Recherche (ANR), by the Fondation pour la Recherche Medicale (FRM), by the European Research Council (ERC Starting Grant 306312 and ERC Consolidator Grant 281987), by ANR-10-IDEX-0001-02 PSL, ANR-11-LABX-0043, CIC IGR-Curie 1428, and by EMBO and Institut Curie post-doctoral fellowships to ICL.

ORCID iDs

Thierry Mora  <https://orcid.org/0000-0002-5456-9361>

Aleksandra M Walczak  <https://orcid.org/0000-0002-2686-5702>

References

- [1] Hu X, Chakravarty S D and Ivashkiv L B 2008 Regulation of interferon and toll-like receptor signaling during macrophage activation by opposing feedforward and feedback inhibition mechanisms *Immunol. Rev.* **226** 41–56
- [2] Tamayo E *et al* 2011 Pro- and anti-inflammatory responses are regulated simultaneously from the first moments of septic shock *Eur. Cytokine Netw.* **22** 82–7
- [3] Cappuccio A *et al* 2015 Combinatorial code governing cellular responses to complex stimuli *Nat. Commun.* **6** 6847
- [4] Long E O, Kim H S, Liu D, Peterson M E and Rajagopalan S 2013 Controlling *nk* cell responses: integration of signals for activation and inhibition *Annu. Rev. Immunol.* **31** 227–58
- [5] Krummel M F and Allison J P 1995 CD28 and CTLA-4 have opposing effects on the response of T cells to stimulation *J. Exp. Med.* **182** 459–65
- [6] McKeithan T W 1995 Kinetic proofreading in T-cell receptor signal transduction *Proc. Natl Acad. Sci.* **92** 5042–6
- [7] François P, Voisin G, Siggia E D, Altan-Bonnet G and Vergassola M 2013 Phenotypic model for early T-cell activation displaying sensitivity, specificity, and antagonism *Proc. Natl Acad. Sci. USA* **110** E888–97
- [8] Dushek O and van der Merwe P A 2014 An induced rebinding model of antigen discrimination *Trends Immunol.* **35** 153–8
- [9] Hoffmann A, Levchenko A and Scott M L 2002 The I B NF- B signaling module: temporal control 425 and selective gene activation *Science* **298** 1241–5
- [10] Tay S *et al* 2010 Single-cell NF-kappaB dynamics reveal digital activation and analogue information processing *Nature* **466** 267–71
- [11] Freeman M 2000 Feedback control of intercellular signalling in development *Nature* **408** 313–9
- [12] Pyle D 2005 The multiple feedback loop hypothesis of chronic diseases *Med. Hypotheses* **64** 408–13
- [13] Guan H, Holland K, Qwarnstrom E, Dower S K and Kiss-Toth E 2006 Feedback loops in intracellular signal processing and their potential for identifying novel signalling proteins *Cell. Immunol.* **244** 158–61
- [14] Youk H and Wa L 2014 Sending mixed messages for cell population control *Cell* **158** 973–5
- [15] Youk H and Wa L 2014 Secreting and sensing the same molecule allows cells to achieve versatile social behaviors *Science* **343** 1242782
- [16] Pasare C and Medzhitov R 2005 *Mechanisms of Lymphocyte Activation and Immune Regulation X* (Berlin: Springer) pp 11–8
- [17] de Jong E C, Smits H H and Kapsenberg M L 2005 *Dendritic Cell-Mediated T Cell Polarization* vol 26 (Berlin: Springer) pp 289–307
- [18] Moore K W, de Waal Malefyt R, Coffman R L and O'Garra A 2001 Interleukin-10 and the interleukin-10 receptor *Annu. Rev. Immunol.* **19** 683–765
- [19] Blanco P, Palucka A K, Pascual V and Banchereau J 2008 Dendritic cells and cytokines in human inflammatory and autoimmune diseases *Cytokine Growth Factor Rev.* **19** 41–52
- [20] Verhasselt V *et al* 1997 Bacterial lipopolysaccharide stimulates the production of cytokines and the expression of costimulatory molecules by human peripheral blood dendritic cells: evidence for a soluble CD14-dependent pathway *J. Immunol.* **158** 2919–25
- [21] Dearman R J, Cumberbatch M, Maxwell G, Basketter D A and Kimber I 2009 Toll-like receptor ligand activation of murine bone marrow-derived dendritic cells *Immunology* **126** 475–84
- [22] Corinti S, Albanesi C, La Sala A, Pastore S and Girolomoni G 2001 Regulatory activity of autocrine IL-10 on dendritic cell functions *J. Immunol.* **166** 4312–8
- [23] Gately M K *et al* 1998 The interleukin-12/interleukin-12-receptor system: role in normal and pathologic immune responses *Annu. Rev. Immunol.* **16** 495–521
- [24] Hopp A K, Rupp A and Lukacs-Kornek V 2014 Self-antigen presentation by dendritic cells in autoimmunity *Frontiers Immunol.* **5** 55
- [25] Van Amersfoort E S, Van Berkel T J and Kuiper J 2003 Receptors, mediators, and mechanisms involved in bacterial sepsis and septic shock *Clin. Microbiol. Rev.* **16** 379–414
- [26] Pasare C and Medzhitov R 2003 Toll pathway-dependent blockade of CD4+CD25+ T cell-mediated suppression by dendritic cells *Science* **299** 1033–6
- [27] van Beelen A J *et al* 2007 Stimulation of the intracellular bacterial sensor NOD2 programs dendritic cells to promote interleukin-17 production in human memory T cells *Immunity* **27** 660–9
- [28] Huang Q 2001 The plasticity of dendritic cell responses to pathogens and their components *Science* **294** 870–5
- [29] Platzer C, Meisel C, Vogt K, Platzer M and Volk H D 1995 Up-regulation of monocytic IL-10 by tumor necrosis factor- α and camp elevating drugs *Int. Immunol.* **7** 517–23
- [30] Rossato M *et al* 2012 IL-10-induced microRNA-187 negatively regulates *tnf- α* , IL-6, and IL-12p40 production in *tlr4*-stimulated monocytes *Proc. Natl Acad. Sci.* **109** E3101–10
- [31] Shin D I *et al* 1999 Interleukin 10 inhibits *tnf- α* production in human monocytes independently of interleukin 12 and interleukin 1 beta *Immunol. Investigations* **28** 165–75

- [32] Lee T K *et al* 2009 A noisy paracrine signal determines the cellular $\text{nf-}\kappa\text{b}$ response to lipopolysaccharide *Sci. Signal.* **2** ra65
- [33] Driessler F, Venstrom K, Sabat R, Asadullah K and Schottelius A J 2004 Molecular mechanisms of interleukin-10-mediated inhibition of NF-kappaB activity: a role for p50 *Clin. Exp. Immunol.* **135** 64–73
- [34] Wang P, Wu P, Siegel M I, Egan R W and Billah M M 1995 Interleukin (IL)-10 inhibits nuclear factor κB (NF κB) activation in human monocytes. IL-10 and IL-4 suppress cytokine synthesis by different mechanisms *J. Biol. Chem.* **270** 9558–63
- [35] Coppey M, Berezhkovskii A M, Sealfon S C and Shvartsman S Y 2007 Time and length scales of autocrine signals in three dimensions *Biophys. J.* **93** 1917–22
- [36] Grell M, Wajant H, Zimmermann G and Scheurich P 1998 The type 1 receptor (CD120A) is the high-affinity receptor for soluble tumor necrosis factor *Proc. Natl Acad. Sci.* **95** 570–5
- [37] Tan J C, Indelicato S R, Narula S K, Zavodny P J and Chou C 1993 Characterization of interleukin-10 receptors on human and mouse cells *J. Biol. Chem.* **268** 21053–9
- [38] Liu Y, Wei S, Ho A, de Waal Malefyt R and Moore K W 1994 Expression cloning and characterization of a human IL-10 receptor *J. Immunol.* **152** 1821–9
- [39] Cheong R, Rhee A, Wang C J, Nemenman I and Levchenko A 2011 Information transduction capacity of noisy biochemical signaling networks *Science* **334** 354–8
- [40] Maiti S, Dai W, Alaniz R, Hahn J and Jayaraman A 2014 Mathematical modeling of pro- and anti-inflammatory signaling in macrophages *Processes* **3** 1–18
- [41] Anderson W D *et al* 2015 Computational modeling of cytokine signaling in microglia *Mol. Biosyst.* **11** 3332–46
- [42] Basak S, Behar M and Hoffmann A 2012 Lessons from mathematically modeling the $\text{nf-}\kappa\text{b}$ pathway *Immunol. Rev.* **246** 221–38
- [43] Hutchins A P, Takahashi Y and Miranda-Saavedra D 2015 Genomic analysis of LPS-stimulated myeloid cells identifies a common pro-inflammatory response but divergent IL-10 anti-inflammatory responses *Sci. Rep.* **5** 1–12
- [44] Handly L N, Pilko A and Wollman R 2015 Paracrine communication maximizes cellular response fidelity in wound signaling *eLife* **4** e09652
- [45] Jilkine A and Edelstein-Keshet L 2011 A comparison of mathematical models for polarization of single eukaryotic cells in response to guided cues *PLoS Comput. Biol.* **7** e1001121
- [46] Iglesias P A and Levchenko A 2002 Modeling the cells guidance system *Sci. Stke* **2002** re12
- [47] Levchenko A and Iglesias P A 2002 Models of eukaryotic gradient sensing: application to chemotaxis of amoebae and neutrophils *Biophys. J.* **82** 50–63
- [48] Ellison D *et al* 2016 Cell–cell communication enhances the capacity of cell ensembles to sense shallow gradients during morphogenesis *Proc. Natl Acad. Sci.* **113** E679–88

3. Appendix 3

TLR1/2 orchestrate human plasmacytoid pre-dendritic cell response to Gram+ bacteria

Salvatore Raieli, Coline Trichot, Sarantis Korniotis, Lucia Pattarini, and Vassili Soumelis

PLoS Biol. 2019 Apr 24;17(4):e3000209

SHORT REPORTS

TLR1/2 orchestrate human plasmacytoid predendritic cell response to gram+ bacteria

Salvatore Raieli^{1,2}, Coline Trichot^{1,2}, Sarantis Korniotis^{1,2}, Lucia Pattarini^{1,2}, Vassili Soumelis^{1,2*}

1 Institut Curie, Centre de Recherche, PSL Research University, Paris, France, **2** INSERM U932, Immunity and Cancer, Paris, France

* vassili.soumelis@curie.fr



OPEN ACCESS

Citation: Raieli S, Trichot C, Korniotis S, Pattarini L, Soumelis V (2019) TLR1/2 orchestrate human plasmacytoid predendritic cell response to gram+ bacteria. *PLoS Biol* 17(4): e3000209. <https://doi.org/10.1371/journal.pbio.3000209>

Academic Editor: Ken Cadwell, New York University School of Medicine, UNITED STATES

Received: August 22, 2018

Accepted: March 19, 2019

Published: April 24, 2019

Copyright: © 2019 Raieli et al. This is an open access article distributed under the terms of the [Creative Commons Attribution License](https://creativecommons.org/licenses/by/4.0/), which permits unrestricted use, distribution, and reproduction in any medium, provided the original author and source are credited.

Data Availability Statement: All relevant data are within the paper and its Supporting Information files.

Funding: This work was supported by funding from INSERM (BIO2014-08) (www.inserm.fr), Agence nationale de la recherche (<http://www.agence-nationale-recherche.fr>) ANR-13-BSV1-0024-02, ANR-10-IDEX-0001-02 PSL* and ANR-11-LABX-0043, ERC (erc.europa.eu) (IT-DC 281987 and HEALTH 2011-261366) and CIC IGR-Curie 1428 (www.curie.fr). S.R. was supported by MESR - Ministry of Higher Education and Research

Abstract

Gram+ infections are worldwide life-threatening diseases in which the pathological role of type I interferon (IFN) has been highlighted. Plasmacytoid predendritic cells (pDCs) produce high amounts of type I IFN following viral sensing. Despite studies suggesting that pDCs respond to bacteria, the mechanisms underlying bacterial sensing in pDCs are unknown. We show here that human primary pDCs express toll-like receptor 1 (TLR1) and 2 (TLR2) and respond to bacterial lipoproteins. We demonstrated that pDCs differentially respond to gram+ bacteria through the TLR1/2 pathway. Notably, up-regulation of costimulatory molecules and pro-inflammatory cytokines was TLR1 dependent, whereas type I IFN secretion was TLR2 dependent. Mechanistically, we demonstrated that these differences relied on diverse signaling pathways activated by TLR1/2. MAPK and NF-κB pathways were engaged by TLR1, whereas the Phosphoinositide 3-kinase (PI3K) pathway was activated by TLR2. This dichotomy was reflected in a different role of TLR2 and TLR1 in pDC priming of naïve cluster of differentiation 4⁺ (CD4⁺) T cells, and T helper (Th) cell differentiation. This work provides the rationale to explore and target pDCs in bacterial infection.

Introduction

Tuberculosis (TB) and multidrug-resistant bacteria are a major concern for worldwide health [1]. In TB and gram+ infection, type I interferon (IFN) has been shown to play a pathological role [2,3]. Plasmacytoid pre-dendritic cells (pDCs) are known to produce high amounts of type I IFN in response to viral sensing [4]. It is reported that pDCs are able to respond to gram+ bacteria [5], can be recruited at the site of the infection, and are enriched in TB lymph nodes [6].

Gram+ bacteria express lipoproteins on their surface membrane, which play an important role in their survival and pathogenicity [7]. Bacterial lipoproteins are recognized by toll-like receptor (TLR)1/2 and induce activation and maturation in dendritic cells (DCs) [8]. TLR2 knockout mice are more susceptible to mycobacterial infection, but *Mycobacterium tuberculosis* is able to hijack TLR2 signaling to enhance its survival in the host [9]. TLR1 and TLR2

of France, MESR fellowship (<http://www.enseignementsup-recherche.gouv.fr/>). The funders had no role in study design, data collection and analysis, decision to publish, or preparation of the manuscript.

Competing interests: The authors have declared that no competing interests exist.

Abbreviations: AKT, AKT serine/threonine kinase; AS-DC, AXL⁺SIGLEC6⁺; AU, arbitrary unit; AXL, AXL receptor tyrosine kinase; BCL-6, B-cell lymphoma 6; CD, cluster of differentiation; CFSE, carboxyfluorescein diacetate succinimidyl ester; Cp, crossing point; DAPI, 4,6-diamidino-2-phenylindole; DC, dendritic cell; DHX, DEAH box protein; FACS, fluorescence-activated cell sorting; FLU, influenza virus; FOXP3, forkhead box P3; GATA3, GATA binding protein 3; GM-CSF, granulocyte-macrophage colony-stimulating factor; GZMB, Granzyme B; ICOSL, inducible T cell costimulator ligand; IFN, interferon; IL, interleukin; IP-10, Interferon gamma-induced protein 10; IRF7, interferon regulatory factor 7; LPS, lipopolysaccharide; MAPK, Mitogen-activated protein kinases; NF- κ B, nuclear factor kappa-light-chain-enhancer of activated B cells; PAM3, PAM3CSK4; PBMC, peripheral blood mononuclear cell; pDC, plasmacytoid dendritic cell; PDL1, programmed cell death ligand 1; PI3K, Phosphoinositide 3-kinase; TB, tuberculosis; Tbet, T-box transcription factor TBX21; Tfh, T-follicular helper; Th, T helper; TLR, toll-like receptor; TNF, tumor necrosis factor; Treg, T regulatory cell.

expression in human pDCs has not been reported [10], leading to the conclusion that TLR 1 and 2 do not have a functional role in pDCs.

Human pDCs express mainly TLR7 and TLR9, localized in the endosomes and capable of sensing nucleic acids [10–12]. pDCs also express a range of cytosolic sensors, either at steady state, such as the helicases DEAH box protein 9 (DHX9) and DHX36 [13], or following innate activation, such as retinoic acid inducible gene 1 (RIG-I) [14]. However, how pDCs sense gram⁺ bacteria is still debated, and their role in gram⁺ infections is still poorly investigated [15].

Here, using human primary cells, we provide definite evidence that pDCs sense gram⁺ bacteria through TLR1 and TLR2.

Results

Human pDCs respond to bacterial lipoproteins through TLR1 and TLR2

In order to investigate how pDCs sense gram⁺ bacteria, we screened steady-state blood pDCs for TLR mRNA expression. In addition to the known expression of TLR7 and TLR9, we detected low levels of TLR1, TLR2, TLR6, and TLR10 (S1A Fig). Among the TLRs expressed by pDCs, TLR1 and TLR2 mediate bacterial sensing by binding lipoproteins [8].

We measured pDC TLR1 and TLR2 mRNA expression on freshly isolated blood pDC and following stimulation with PAM3CSK4 (PAM3), a bacterial lipoprotein used as a prototypical TLR1/2 ligand. HeLa cells were used as negative control and CD11c⁺ DCs as positive control for the expression of TLR1/2. pDCs maintained a stable TLR1 mRNA expression following stimulation. PAM3 activation increased TLR2 expression as compared with ex vivo pDCs (Fig 1A).

We further investigated whether pDCs express TLR1 and TLR2 at the protein level. Using flow cytometry, we confirmed in freshly isolated peripheral blood mononuclear cells (PBMCs) that pDCs expressed TLR1 and TLR2 at their surface, as compared to isotype control (Fig 1B and quantification in S1B Fig).

To address the functionality of TLR1 and 2 on pDC, we investigated pDC response to PAM3 after 24 hours of stimulation. We observed up-regulation of costimulatory molecules (CD86, inducible T cell costimulator ligand (ICOSL), CD83, CD80, CD40 and programmed cell death ligand 1 (PDL1)) and MHC-II expression (HLA-DR) on the surface (Fig 1C, S1C and S1D Fig), as compared to untreated pDCs and lipopolysaccharide (LPS)-treated pDCs. As expected, pDCs activated by influenza virus (FLU) or granulocyte-macrophage colony-stimulating factor (GM-CSF) expressed CD86, ICOSL, CD83, CD80, CD40, and PDL1 (Fig 1C) [16]. pDCs stimulation with PAM3 induced a higher CD40, CD86, ICOSL, and CD83 expression in comparison with GM-CSF. As expected, FLU induced a stronger expression of checkpoints compared with both PAM3 and GM-CSF (Fig 1C).

A feature of pDCs is high type I IFN secretion. The ability of PAM3 to induce type I IFN secretion in human pDCs has been questioned [17,18]. Here, highly pure (99%) pDCs responded to 1 and 10 μ g/ml of PAM3 by secreting type I IFN (Fig 1D). In addition, PAM3 induced the secretion of pro-inflammatory cytokines (interleukin [IL]-6, tumor necrosis factor [TNF]- α), and chemokines (IL-8, IP-10), although to a lower extent than with FLU (Fig 1D). Furthermore, pDCs secreted Granzyme B (GZMB) in response to bacterial lipoprotein stimulation (Fig 1D). Both 1 and 10 μ g/ml of PAM3-induced pDCs the expression of costimulatory molecules and cytokine secretion at comparable levels (Fig 1C and 1D).

We used PAM3 to stimulate pDCs purified from tonsils, a site of frequent encounter with gram⁺ bacteria. Tonsillar pDCs up-regulated surface costimulatory molecules (CD86, CD80,

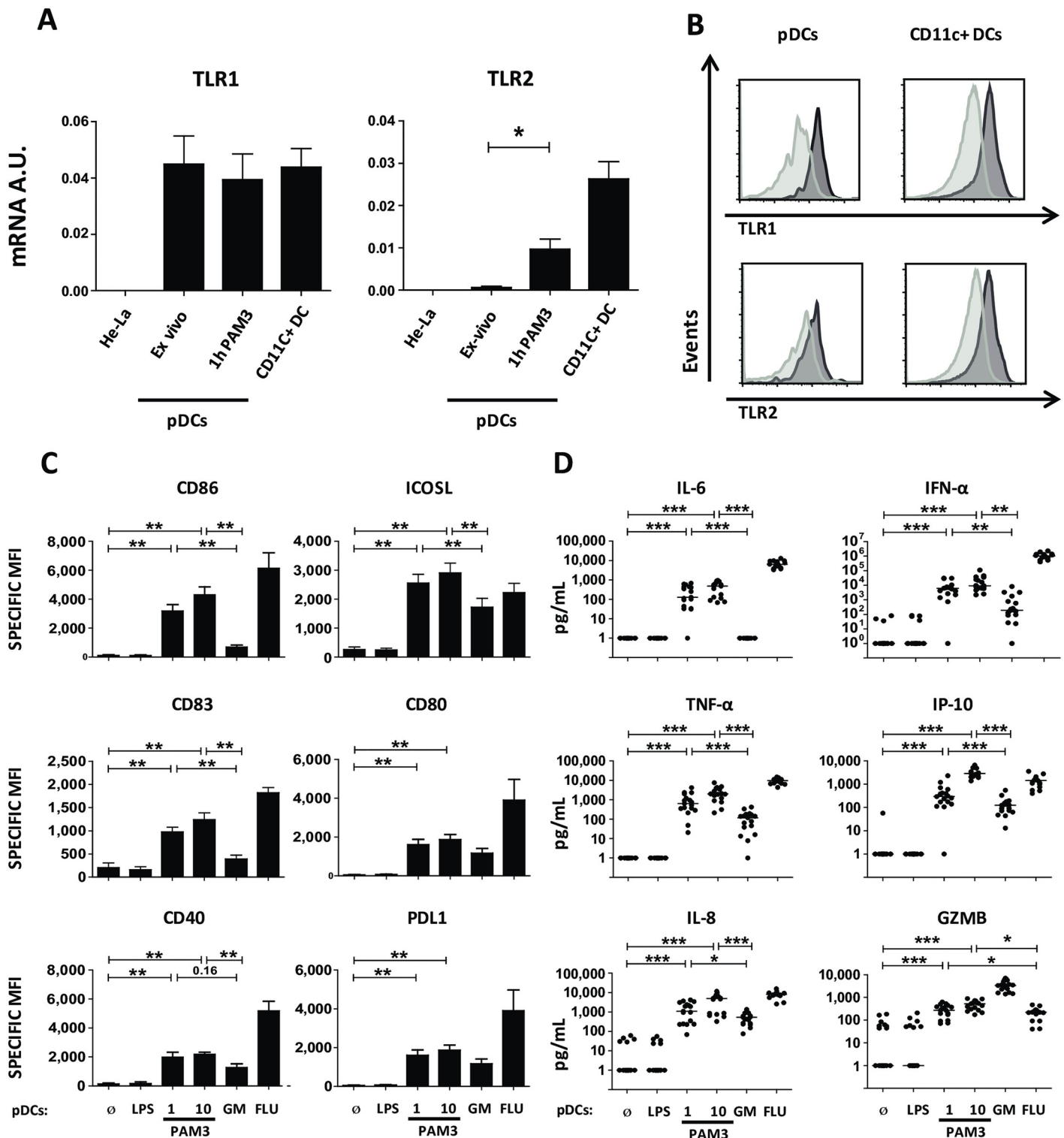


Fig 1. Human pDCs express TLR1/2 and respond to PAM3. (A) RT-PCR quantification of TLR1 and TLR2 expression from total mRNA of sorted human blood pDCs before and after 1-hour activation with PAM3 as compared to CD11c⁺ DCs and HeLa cells. Results were normalized on 3 housekeeping genes. Results include 5 donors. (B) pDCs and CD11c⁺ DCs were stained in freshly isolated PBMCs with anti-TLR1 and anti-TLR2 antibody (dark gray), respective cognate isotype (light gray). (C–D) Sorted human pDCs were cultured during 24 hours with medium (∅), 0.1 μg/mL LPS, 1 and 10 μg/mL PAM3, 100 ng/mL GM, or 82 HA/ml FLU. (C) Specific MFI for surface expression of costimulatory or coinhibitory molecules from activated pDCs by FACS. Results include the mean of 9 donors. (D) Cytokine secretion by pDCs. Results include the mean of 17 donors. Each dot represents a donor. **p* < 0.05; ***p* < 0.01; ****p* < 0.001 (Wilcoxon test). Underlying data for this

figure can be found in [S1 Data](#). AU, arbitrary unit; CD, cluster of differentiation; DC, dendritic cell; FACS, fluorescence-activated cell sorting; FLU, influenza virus; GM, GM-CSF; Gm-CSF, granulocyte-macrophage colony-stimulating factor; GZMB, Granzyme B; ICOSL, inducible T cell costimulator ligand; HA, hemagglutinin; IFN, interferon; IL, interleukin; IP-10, Interferon gamma-induced protein 10; LPS, lipopolysaccharide; PBMC, peripheral blood mononuclear cell; PAM3, PAM3CSK4; pDC, Plasmacytoid predendritic cell; PDL1, programmed cell death ligand 1; RT, real time; TLR, toll-like receptor; TNF, tumor necrosis factor.

<https://doi.org/10.1371/journal.pbio.3000209.g001>

CD40, and PDL1) ([S1E Fig](#)) and MHC-II complex in line with our data on blood pDCs ([S1D Fig](#)).

These data suggest that pDCs from both blood and from physiological bacterial interfaces functionally respond to bacterial lipoproteins.

TLR1/2 pathway is necessary for pDC response to gram+ bacteria

We next questioned whether, in addition to purified lipoproteins, pDCs could respond to whole gram+ bacteria. Although pDC activation by *Staphylococcus aureus* was reported [5], whether pDCs can respond to *M. tuberculosis* is still debated [6]. Sorted blood pDCs were stimulated with 3 different heat-killed gram+ bacteria relevant to human infections: *M. tuberculosis*, *S. aureus*, and *Listeria monocytogenes*. We observed up-regulation of CD80 and CD86 following pDC culture with heat-killed bacteria ([Fig 2A](#)). To establish the role of TLR1/2, we took advantage of a chemical antagonist for both TLR1 and 2, CU-CPT22 [19]. CU-CPT22 did not affect unstimulated pDCs, nor did it impact costimulatory molecule expression (CD80, CD86) or type I IFN secretion in FLU-activated pDCs ([S2A–S2C Fig](#)). On the contrary, CU-CPT22 treatment strongly decreased bacteria-induced CD80 and CD86 expression by pDCs ([Fig 2A](#) and [S2D Fig](#)). Furthermore, gram+-stimulated pDCs secrete high amount of type I IFN ([Fig 2B](#)) thus indicating full activation of pDCs by bacteria ([Fig 2B](#)). TLR1/2 blocking by CU-CPT22 almost completely abrogated type I IFN production ([Fig 2B](#)). Therefore, pDCs responded to whole gram+ bacteria in a TLR1/2-dependent manner.

T-cell priming is an important adaptive function of activated pDCs [20]. We investigated whether gram+-stimulated pDCs control T-cell priming. pDCs primed with gram+ bacteria, or FLU as a positive control, were cultured with allogeneic naive CD4⁺ T cells for 6 days. Bacteria-primed pDCs induced CD4⁺ T-cell expansion ([Fig 2C](#)) and proliferation ([Fig 2D](#)) comparable to FLU-activated pDCs ([Fig 2C and 2D](#)). After 6 days of coculture, T cells were polyclonally restimulated to measure T helper (Th) cytokine production. Gram+ bacteria-activated pDCs induced secretion of IL-4, IFN- γ , and TNF- α from CD4 T cells ([Fig 2E](#)). Additionally, we detected IL-10 ([Fig 2E](#)). Overall, these cytokines suggest a diversity of Th cell cytokine patterns induced by bacterial-activated pDCs: Th1 (IFN- γ), Th2 (IL-4), and T regulatory (Treg) (IL-10).

CD11c⁺ DCs are known to express TLR1/2 and to be able to induce Th cell differentiation. We investigated the differences in naive CD4⁺ T-cell priming by PAM3-activated CD11c⁺ DCs and pDCs ([S2E Fig](#)). T cells primed with PAM3-activated CD11c⁺ DC or pDCs showed a comparable state of activation. However, pDCs induced a prominent Th2-like profile compared with CD11c⁺ DCs (higher secretion of IL-4, IL-5, and IL-10), suggesting different contributions to immune regulation in the context of bacterial infection ([S2E Fig](#)).

To establish whether TLR1/2-activated pDCs were able to induce cytokine production by memory T cells, we cultured PAM3-activated pDCs with allogeneic memory CD4⁺ T cells from healthy donor peripheral blood. Memory CD4⁺ T cells secreted significant amounts of IFN- γ , IL-10, IL-3, IL-4, and IL-9 when cocultured with PAM3-activated pDCs compared with memory CD4 T cells cocultured with untreated pDCs ([S3A Fig](#)). The amounts of these cytokines were comparable to FLU condition and much higher than the negative control LPS. Moreover, PAM3-activated pDCs were the only ones capable of inducing the production of both IL-17A

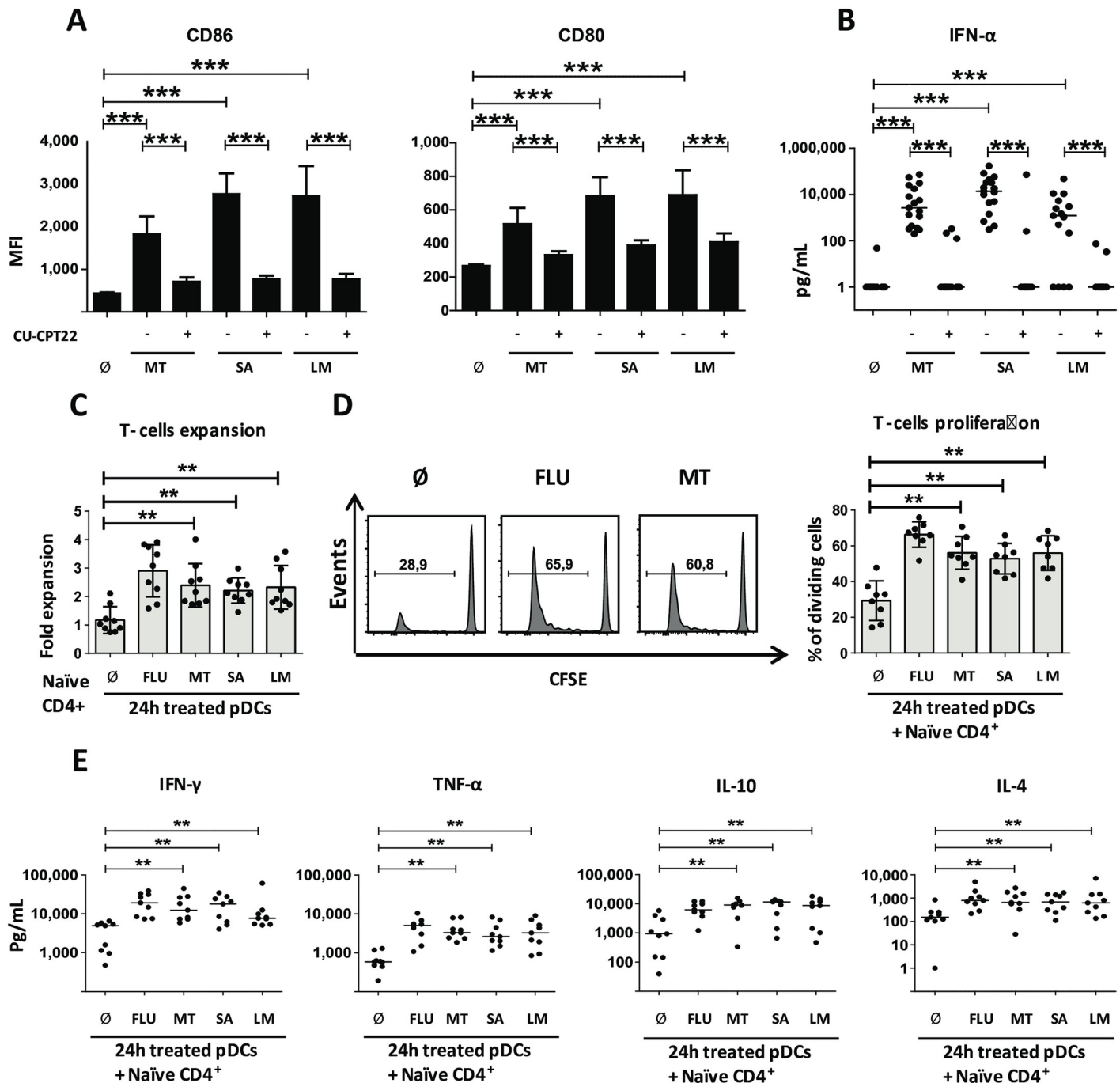


Fig 2. pDCs sense different gram+ bacteria through TLR1/2 pathway. (A–B) Sorted human blood pDCs were cultured during 24 hours with medium either without (\emptyset) or with: heat-killed MT, heat-killed SA, or heat-killed LM and in presence (+) or absence (-) of CU-CPT22. (A) MFI for surface expression of costimulatory molecules from activated pDCs. Results include the mean of 27 independent donors. (B) Cytokine secretion by pDCs. Results include 17 independent donors. (C–D) Allogeneic CD4⁺ naive expansion and percentage of dividing living cells after 6 days of coculture with 24-hours gram⁺-stimulated pDCs. FLU activated pDCs were used as a control. Results include the mean of 9 donors. (E) Th cytokine pattern from gram⁺ pDCs activated T-cell coculture. Cytokines were measured after 24 hours polyclonal restimulation of the T cells. Results include the mean of 9 independent donors. Each dot represents a donor. * $p < 0.05$; ** $p < 0.01$; *** $p < 0.001$ (Wilcoxon test). Underlying data for this figure can be found in [S1 Data](#). CD, cluster of differentiation; FLU, influenza virus; LM, *Listeria monocytogenes*; MT, *Mycobacterium tuberculosis*; pDC, Plasmacytoid dendritic cell; SA, *Staphylococcus aureus*; Th, T helper; TLR, toll-like receptor.

<https://doi.org/10.1371/journal.pbio.3000209.g002>

and IL-17F from memory CD4⁺ T cells as compared with untreated pDCs and FLU-pDCs. This shows that PAM3-activated pDCs are capable of inducing effector cytokine production by memory CD4⁺ T cells, including IL-17A and F, important in epithelial immunity.

Recent results demonstrated the existence of a rare DC subset defined as DC5 or AXL⁺SI-GLEC6⁺ (AS-DC) [21]. This subset is characterized by the expression of the surface markers CD2, CD5, and AXL receptor tyrosine kinase (AXL) but also shares some markers with pDCs, leading to potential contamination of the pDC population. In order to determine whether pure pDCs (DC5-depleted pDCs) were able to induce T-cell expansion and Th polarization to the same extent as LIN⁻CD4⁺CD11c⁻ pDCs, we cell sorted pure pDCs following the presented gating strategy (S3B Fig). CD2⁻CD5⁻AXL⁻ pDCs were activated for 24-hours with PAM3, FLU, LPS, or GM-CSF and cocultured with allogeneic naïve CD4⁺ T cells from healthy peripheral blood. We found that TLR1-activated pure pDCs were capable of inducing CD4 T-cell expansion and Th cell differentiation (S3C Fig), with increased production of IFN- γ , IL-10, IL-3, IL-4, IL-9, and GM-CSF as compared with nontreated pDCs. These results show that CD4⁺ T-cell expansion and Th cell differentiation induced by TLR1-activated pDCs is not due to contamination with DC5.

TLR1 and TLR2 play a differential role in the pDCs response to bacterial lipoproteins

In order to investigate the differential contribution of TLR1 and TLR2 in mediating pDC response to bacterial lipoproteins, we separately blocked the 2 receptors with specific antibodies, as compared with matched isotype controls [22,23]. TLR1 functional blocking significantly reduced costimulatory molecule expression (CD80, CD86, and ICOSL), whereas TLR2 blockade did not (Fig 3A and S4A Fig). TLR1 blocking almost completely abolished secretion of the pro-inflammatory cytokines IL-6 and TNF- α (Fig 3B). Conversely, TLR2 blocking inhibited type I IFN secretion, which was not impacted by TLR1 blocking (Fig 3B). Combined TLR1 and TLR2 blockade, as well as the TLR1/2 competitive antagonist CU-CPT22, inhibited both costimulatory molecule expression and cytokine release (Fig 3A and 3B). These results suggest a differential control of pDC functions by TLR1 and TLR2.

Next, we performed coculture experiments with PAM3-treated pDCs and naïve CD4⁺ T cells, with and without TLR1 or TLR2 blocking antibodies. TLR1 blocking during PAM3 activation reduced T-cell expansion and proliferation (S4B and S4C Fig). Following polyclonal restimulation, we did not detect any difference in the Th1 prototypical cytokine IFN- γ (Fig 3C and S4E Fig). However, TLR1 blocking in pDCs decreased prototypical Th2 cytokines (IL-13, IL-4, IL-5) (Fig 3C and S4E Fig). TLR1 blocking also diminished IL-10 production by Th cells, suggesting a decrease in Treg generation (Fig 3C). We found that TLR1 blocking reduced IL-9 secretion by Th cells (Fig 3C). After 4 days of pDCs-T cell coculture, we performed intracellular staining for Th master regulator transcription factors to better characterize the Th subsets induced. TLR1/TLR2 blocking did not reduce Tbet induction (Fig 3D and S4D Fig), in line with our observation on IFN- γ production. However, TLR1 blocking diminished GATA3 and FOXP3 expression (Fig 3D and S4D Fig), in line with its impact on Th2 and Treg polarization. TLR1 blocking also reduced BCL-6 expression (Fig 3D and S4D Fig), involved in T-follicular helper (Tfh) generation [24].

TLR1 and TLR2 activate different signaling pathways in response to bacterial lipoproteins

In pDCs, MAPK and NF- κ B pathway activation leads to costimulatory expression and pro-inflammatory cytokine release, whereas PI3K signaling controls Type I IFN induction [25]. In

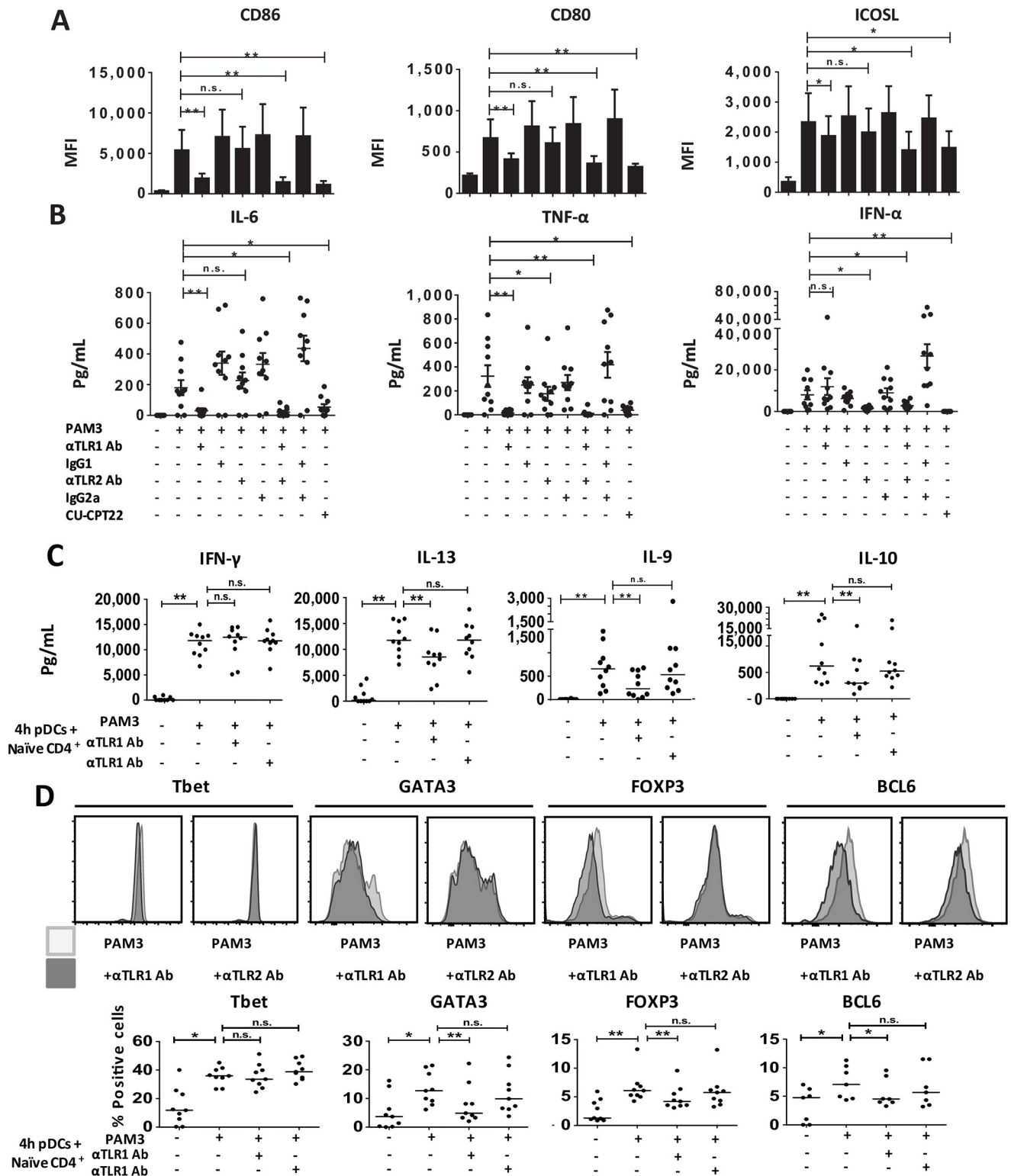


Fig 3. TLR1 and TLR2 functional blocking has a differential impact on pDC innate and adaptive functions. (A–B) Sorted human pDCs were cultured during 24 hours with medium or PAM3 in the presence or not of TLR1 neutralizing antibody (α TLR1 Ab), TLR2 neutralizing antibody (α TLR2 Ab), or IgG1 isotype control antibody (IgG1); or IgA2 Isotype Control (IgG2a), double blocking (TLR1 Ab + α TLR2 Ab), double control isotype (IgG1 + IgG2a), or CU-CPT22. (A) MFI for surface expression of costimulatory molecules. Results include the mean of 9 independent donors. (B) Cytokine secretion by pDCs. Results include the mean of 10 independent donors. Each dot is an independent donor. (C–D) The 24-hour-stimulated pDCs were cocultured with

allogeneic CD4⁺ naive T cells during 6 days. (C) Th cytokine quantification. Cytokines were measured after 24-hour polyclonal restimulation of the T cells. Each dot is an independent donor, $n = 10$. (D) Percentage of Th master regulator expression. Intracellular FACS was performed after 4 days of coculture. Results include the mean of 9 independent donors for Tbet, GATA3, and FOXP3. Results show the mean of 7 independent donors for BCL-6. Each dot represents a donor. * $p < 0.05$; ** $p < 0.01$; *** $p < 0.001$ (Wilcoxon test). Underlying data for this figure can be found in [S1 Data](#). Ab, antibody; BCL-6, B-cell lymphoma 6; CD, cluster of differentiation; CU-CPT22; FACS, fluorescence-activated cell sorting; FOXP3, forkhead box P3; GATA3, GATA binding protein 3; ICOSL, inducible T cell costimulator ligand; IFN, interferon; IgG, Immunoglobulin G; IL, interleukin; MFI, mean fluorescence intensity; n.s., not significant; PAM3, PAM3CSK4; pDC, Plasmacytoid pre-dendritic cell; Tbet, T-box transcription factor TBX21; Th, T helper; TLR, toll-like receptor; TNF, tumor necrosis factor.

<https://doi.org/10.1371/journal.pbio.3000209.g003>

the case of TLR7 and TLR9, these 2 signaling pathways are activated in early and late endosomes, respectively [26]. We performed phospho-fluorescence-activated cell sorting (phospho-FACS) to investigate which pathways were activated by bacterial lipoproteins in pDCs. Stimulation with PAM3 (1 and 10 $\mu\text{g}/\text{mL}$) led to p38, p65, and AKT serine/threonine kinase AKT phosphorylation as compared with untreated pDCs (Fig 4A). pDC stimulation with FLU virus was used as positive control (Fig 4A). These results suggested that MAPK, NF- κ B, and PI3K were activated following bacterial lipoproteins activation.

Next, we tested how TLR1/2 blocking affected intracellular signaling cascades. TLR1, but not TLR2, blocking reduced p38 and p65 phosphorylation in pDCs activated with PAM3 (Fig 4B). On the contrary, TLR2 blocking diminished AKT phosphorylation in comparison with PAM3-treated pDCs whereas TLR1 blocking did not show an effect (Fig 4B). We observed this inhibition after 2, 3, and 4-hours of PAM3 activation (Fig 4B).

These data suggest that the mechanism behind the differences observed in pDCs innate versus adaptive responses following TLR1 and TLR2 blocking is related to different signaling pathways controlled by the 2 receptors.

Discussion

pDCs are known to express a narrow TLR pattern that is restricted to TLR7 and TLR9 [10]. Accordingly, TLR1 and TLR2 expression was considered a prototypical feature of myeloid cells and absent from pDCs [10]. The low expression level of TLR1/2 on pDCs as compared with TLR7 and 9 may have previously suggested that it is not functionally relevant. However, peripheral blood pDCs are considered the major source of type I IFN following *S. aureus* stimulation [15]. We found that pDCs express TLR1 at steady state and TLR2 in a stimulation-dependent manner, and that those 2 TLRs are functional for PAM3 sensing.

Commensal bacteria have an immunomodulatory impact in the gut. Some of them, such as *Bacteroides fragilis* and Clostridia, are gram+ [27,28]. Here, we show that pDCs respond to the lipoprotein characteristic of gram+ bacteria and that lipoprotein-activated pDCs induced IL-10 and FOXP3 expression in CD4⁺ T cells. pDCs are present in the human gut at steady state [29]. However, other groups report that pDCs can participate in sustaining inflammation in acute colitis [30]. Our study suggests that pDCs, following bacterial sensing, could instruct CD4⁺ T cells in the gut and promote a mixed Th cell cytokine profile—including a regulatory phenotype—but also cytokines prototypical of Th1, Th2, and Th17 inflammation. Therefore, a detailed investigation of pDC role in the gut is warranted. Our results provide a strong basis for a functional link between pDCs and gram+ bacteria in various physiopathological contexts.

Our data show that GZMB can be induced by bacterial lipoproteins. It has been shown that pDCs in TB patients' lymph nodes produce GZMB [6]. Our data suggest that bacterial sensing through TLR1/2 could induce GZMB in pathological conditions, such as TB infection.

It has been proposed that bacterial nucleic acids can activate pDCs through such intracellular sensors as TLR7 and TLR9, but this requires phagocytosis [15]. However, pDCs are poorly phagocytic cells [5], suggesting the possible implication of putative extracellular sensors. Our

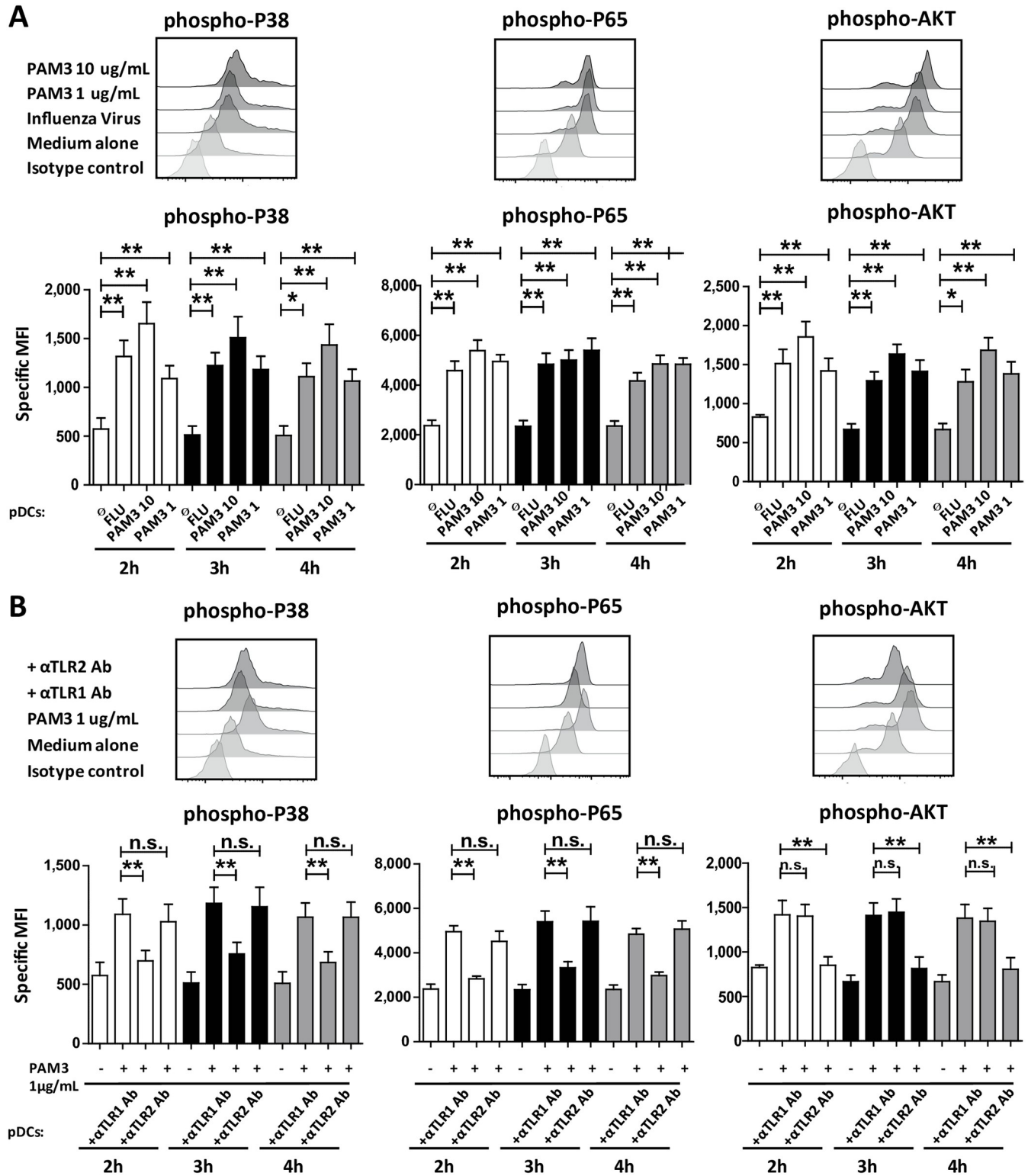


Fig 4. TLR1 and TLR2 exploit distinct pathways following PAM3 stimulation. (A–B) Sorted human blood pDCs were cultured during 4-hours with only medium (\emptyset) and with or without PAM3 in the presence or not of TLR1 neutralizing antibody (α TLR1 Ab), TLR2 neutralizing antibody (α TLR2 Ab), IgG1. FLU was used as control. (A–B) p38 MAPK (first panel), p65 NF- κ B (second panel), AKT PI3K (third panel) at 3-hours. p38 MAPK (first panel), p65 NF- κ B (second panel), AKT PI3K (third panel) at 3-hours. p38 MAPK (first panel), p65 NF- κ B (second panel), AKT PI3K (third panel) at 3-hours. p38 MAPK (first panel), p65 NF- κ B (second panel), AKT PI3K (third panel) at 3-hours. Results include the mean of 8 independent donors. * $p < 0.05$; ** $p < 0.01$; *** $p < 0.001$ (Wilcoxon test). Underlying data for this figure can be found in [S1 Data](#). Ab, antibody; AKT, AKT serine/threonine kinase; FLU, influenza virus;

IgG, Immunoglobulin G; MAPK, Mitogen-activated protein kinases; MFI, mean fluorescence intensity; NF- κ B, nuclear factor kappa-light-chain-enhancer of activated B cells; PAM3, PAM3CSK4; pDC, Plasmacytoid predendritic cell; PI3K, Phosphoinositide 3-kinase; TLR, toll-like receptor.

<https://doi.org/10.1371/journal.pbio.3000209.g004>

results provide the first evidence that TLR1/2 surface receptors are necessary for pDC response to gram+ bacteria.

In TB, a diversity of Th responses has been observed [31]. It has been proposed that Th1 is the protective response in TB and in many gram+ bacterial infections, whereas Th2 and Treg have been shown to promote the disease [31–34]. In atopic dermatitis, in which there is a strong link between disease flare and *S. aureus* skin infection [35], it has been shown that both Th1 and Th2 responses coexist [36]. In vitro, we showed that gram+ stimulation of pDCs induced a mixed Th1, Th2, and Treg cytokine profile, suggesting that they could contribute to the in vivo–observed Th diversity.

Our results showed that TLR1 and TLR2 play a different and complimentary role in the pDC response to bacterial lipoproteins. Although it is reported that TLR2 in inflammatory monocytes can be endocytosed and activate IRF7 in response to a viral ligand [37], our results are the first to link a type I IFN response and the TLR2 pathway in response to a bacterial ligand.

Furthermore, we observed that TLR1 and TLR2 blocking on pDCs had differential effects on Th cytokine secretion. TLR1 blocking on pDCs decreased T-cell polarization toward Th2, Treg, and Tfh but not Th1 cells. Conversely, TLR2 blocking showed a specific inhibition of Type I IFN secretion without impacting T-cell polarization. These data show that TLR1 activation could promote an adaptive response (costimulatory molecule expression, pro-inflammatory cytokine secretion, Th proliferation and polarization), whereas TLR2 activation induced type I IFN, which broadly functions in innate immunity. Our data suggest that the innate and/or adaptive response of pDCs could be differentially targeted.

These data suggest that the mechanism behind the differences observed in pDCs' innate versus adaptive responses following TLR1 and TLR2 blocking is related to different signaling pathways controlled by the 2 receptors.

Our findings open broad perspectives on the possible role of pDCs in gram+ bacterial diseases. Here, we showed that *M. tuberculosis*, *S. aureus*, and *L. monocytogenes* induced high levels of type I IFN production by pDC and that this is abrogated by TLR1/2 antagonist (CU-CPT22). Type I IFN is highly expressed in TB, in which it has been proposed to dampen immune response [38]. Therefore, our data establish pDCs as a possible source of type I IFN in TB-infected tissues. Furthermore, TLR1 polymorphisms are associated with TB susceptibility [39,40]. Future studies are required to establish whether pDCs could represent a pharmacological target in TB. In the past few years, different attempts to develop a vaccine direct against of *S. aureus* have failed [41]. Subsequently, lipoproteins have been considered promising candidates [7]. Besides, vaccines in combination with TLR7 ligand show a boost in the protective immunity [42]. Our results suggest the possible role of pDCs in vaccine efficacy considering their capacity to respond to lipoproteins, high TLR7 expression, and capacity to prime T cells in response to gram+ bacteria.

Materials and methods

Ethic statement

Blood buffy coats from healthy donors were obtained from the French blood bank (Etablissement Français du Sang) through an approved convention (N° 18/EFS/033). Tonsils from patients undergoing tonsillectomy for obstructive sleep apnea were obtained from Hôpital

Necker (Paris, France) as surgical residues, according to the French legislation (public health law, art L 1121-1-1, art L 1121-1-2).

Blood samples and cell isolation

PBMCs were isolated by Ficoll density gradient centrifugation (Ficoll-Paque, GE Healthcare, Chicago, IL). pDCs and CD11c⁺ DCs were isolated by a first step of total DC enrichment (EasySep human Pan-DC Enrichment kit, Stemcell, Canada) followed by FACS sorting as Lineage⁻CD11c⁻CD4⁺ to a 99% purity [20]. Tonsil pDCs were isolated using the following protocol by Durand and Segura [43]. DC5⁻ pDCs was isolated by a first step of total DC enrichment (EasySep human Pan-DC Enrichment kit, Stemcell, Canada) followed by FACS sorting as Lineage⁻CD11c⁻CD4⁺CD2⁻CD5⁻AXL⁻ to 99% purity. Human naive CD4⁺ T cells were isolated from PBMCs by negative selection (naïve CD4 T-cell isolation kit, Miltenyi, Germany) to a >98% purity. Total Memory CD4⁺ T cells were isolated from PBMCs by negative selection (Memory CD4⁺ T Cell isolation Kit and LS columns, Miltenyi, Germany).

Flow cytometry

PBMCs were stained with FITC anti-CD3 (BD, Franklin Lakes, NJ), FITC anti-CD14 (BD, Franklin Lakes, NJ), FITC anti-CD16 (BD, Franklin Lakes, NJ), FITC anti-CD19 (Miltenyi, Germany), PEcy7 anti-CD11c (BD, Franklin Lakes, NJ), VioGreen anti-CD4 (Miltenyi, Germany), PE anti-TLR1 (eBioscience (Thermo Fisher Scientific), Waltham, Ma), and Alexa-Fluor700 anti-TLR2 (eBioscience (Thermo Fisher Scientific), Waltham, Ma). After culture, cells were stained with 4,6-diamidino-2-phenylindole (DAPI; Sigma-Aldrich, Saint Louis, MO) that was added before acquisition to exclude dead cells. pDCs were stained with the following antibodies: AF700 anti-HLA-DR (Biolegend, San Diego, Ca), APC anti-ICOSL (R&D, Minneapolis, MN), PE anti-CD86 (BD, Franklin Lakes, NJ), FITC anti-CD80 (BD, Franklin Lakes, NJ), FITC anti-CD40 (BD, Franklin Lakes, NJ), Percp5.5 anti-CD83 (eBioscience (Thermo Fisher Scientific), Waltham, Ma), and Percp5.5 anti PD-L1 (eBioscience (Thermo Fisher Scientific), Waltham, Ma). Tonsil pDCs were stained with the following antibodies: isotype-matched antibodies Percp5.5 anti PD-L1 (eBioscience (Thermo Fisher Scientific), Waltham, Ma), PE anti-CD80 (BD, Franklin Lakes, NJ), FITC anti-CD40 (BD, Franklin Lakes, NJ), Brilliant violet 650 anti-CD86 (Biolegend, San Diego, Ca), and AF780 anti-HLA-DR (eBioscience (Thermo Fisher Scientific), Waltham, Ma). For intracellular staining, CD4 naive T cells were cultured for 4 days with allogeneic activated pDCs (PAM3 in combination with anti-TLRs antibody). T cells were stained with ZombieNir fixable kit (Biolegend, San Diego, Ca) before surface staining, fixation, and permeabilization (FOXP3 Fix/Perm buffers; eBioscience (Thermo Fisher Scientific), Waltham, Ma). Cells were then stained with APC anti BCL-6 (BD, Franklin Lakes, NJ), PercP55 anti Tbet (BD, Franklin Lakes, NJ), Pcy7 anti GATA3 (eBioscience (Thermo Fisher Scientific), Waltham, Ma), and APC anti FoxP3 (eBioscience (Thermo Fisher Scientific), Waltham, Ma). Isotype-matched antibodies were used as control. For phosphoFACS, pDCs were treated for 4 hours with medium, PAM3 (in combination with neutralizing antibody as described before), and FLU. Cells were fixed with Fix Buffer I (BD, Franklin Lakes, NJ) and permeabilized with Perm Buffer III (BD, Franklin Lakes, NJ). Cells were stained with PE anti-p-AKT (BD, Franklin Lakes, NJ), PEcy7 anti-p-p65 (BD, Franklin Lakes, NJ), and PE anti-p-p38 (Cell signaling, Danvers, Ma). Isotype-matched antibodies were used as control. Cells were analyzed on a flow cytometer (blood pDCs on BD LSRII, tonsil pDCs and T cells on BD Fortessa), and data were processed using FlowJo software (FlowJo LLC, Ashland, OR.).

pDC culture

pDCs were cultured in RPMI 1640 Medium, GlutaMAX (Life Technologies (Thermo Fisher Scientific), Waltham, Ma) containing 10% Fetal Calf Serum (Hyclone (Thermo Fisher Scientific), Waltham, Ma), 100 U/ml Penicillin/Streptomycin (GIBCO (Thermo Fisher Scientific), Waltham, Ma), MEM Non Essential Amino Acids (GIBCO (Thermo Fisher Scientific), Waltham, Ma), and 1mM NA pyruvate (GIBCO (Thermo Fisher Scientific), Waltham, Ma). Cells (1,000,000/mL) were cultured for 24 hours in 96-well flat-bottom plates in the presence of Influenza A/PR/8/34 (H1N1) 82 HA/ml (Charles River Laboratories, Wilmington, MA), PAM3 1 µg/ml and 10 µg/ml (Invivogen, San Diego, CA), 10 ng/mL GM-CSF, 0.1 µg/mL LPS (Invivogen, San Diego, CA), 100 µg/mL heat-killed *M. tuberculosis* (Invivogen), MOI 1 heat-killed *S. aureus* (Invivogen, San Diego, CA), and MOI 10 heat-killed *L. monocytogenes* (Invivogen, San Diego, CA). Blocking experiments were performed by pretreating pDCs 1 hour before stimulation with 1 µM CU-CPT22 (Merck-Millipore, Germany), Human TLR1 Neutralizing antibody—Monoclonal Mouse IgG1 (Invivogen, San Diego, CA), Human TLR2 Detection and Neutralizing antibody—Monoclonal Human IgA2 (Invivogen, San Diego, CA), Mouse IgG1 isotype control antibody (Invivogen, San Diego, CA), Human IgA2 Isotype Control (Invivogen, San Diego, CA). Supernatants were collected after 24-hours of stimulation and frozen until used.

Cytokine quantification

Supernatants were collected after 24-hours of stimulation. Cytokine measurement was performed by Cytometric Bead Array Flex Set (BD Biosciences, Franklin Lakes, NJ). The following cytokines were measured in pDC supernatant: IL-6, IL-8, IFN- α , TNF- α , IP-10, and GZM-B, and for T cells: IL-2, IL-3, IL-4, IL-5, IL-6, IL-9, IL-10, IL-13, IL-17A, IL-17F, GM-CSF, TNF- α , and IFN- γ . Acquisition was performed on a flow cytometer (BD LSR II), and data were analyzed using Fcap array (BD).

Real time quantitative RT-PCR

Total RNA was extracted from freshly isolated, 1-hour PAM3-activated pDCs, freshly isolated CD11c⁺ DCs, and HeLa cells using RNeasy Micro kit (Qiagen, Netherlands) and processed as described by Volpe and colleagues [44]. The following probes (Life Technology (Thermo Fisher Scientific), Waltham, Ma) were used: TLR1 (Hs00413978_m1), TLR2 (Hs00152932_m1), TLR3 (Hs01551078_m1), TLR4 (Hs01060206_m1), TLR5 (Hs01019558_m1), TLR6 (Hs01039989_s1), TLR7 (Hs01933259_s1), TLR8 (Hs00152972_m1), TLR9 (Hs00370913_s1), TLR10 (Hs01935337_s1), B2M (Hs99999907_m1), GAPDH (Hs99999905_m1), and RPL34 (Hs00241560_m1). Crossing points (Cps) from each analyte were calculated using the second derivative maximum method, and the transcripts were quantified as fold changes in comparison to the mean of the 3 housekeeping genes (B2M, GAPDH, and RPL34).

pDC–T cell cocultures

CD4⁺ naive T cells were stained with 5-(and 6)-Carboxyfluorescein diacetate succinimidyl ester (CFSE) (eBioscience (Thermo Fisher Scientific), Waltham, Ma). CD4⁺ naive T cells were cultured for 6 days with allogeneic activated pDCs stimulated (FLU, gram+ bacteria treated, PAM3 in combination with anti-TLRs antibody), with CD11c⁺ DCs stimulated (FLU, PAM3) or with pDC DC5⁻ stimulated (LPS, FLU, PAM3, and 10 µg/mL GM-CSF) at a 5:1 ratio as previously described by Rissoan and colleagues [45]. CD4⁺ memory T cells were cultured for 6

days with allogeneic activated pDCs stimulated (FLU, gram+ bacteria treated, PAM3, and 10 µg/mL LPS, GM-CSF) at a 5:1 ratio as previously described by Rissoan and colleagues [45]. After coculture, T-cell expansion was determined by cell counting, and the percentage of dividing cells was determined by flow cytometer (BD LSR II). Supernatants were collected after 24 hours of polyclonal restimulation with anti-CD3/CD28 microbeads (LifeTech (Thermo Fisher Scientific), Waltham, Ma) and frozen until used.

Statistical analysis

Statistical analyses were performed to compare the different conditions by Wilcoxon paired test using Prism (GraphPad Software, San Diego, Ca). Statistical significance was considered $p < 0.05$.

Supporting information

S1 Fig. pDCs from human tonsils respond to PAM3. Referring to Fig 1. (A) RT-PCR from total mRNA from sorted human pDCs. Results were normalized on 3 housekeeping genes. Results include 5 donors. (B) pDCs and CD11c⁺ DCs were stained in freshly isolated PBMCs with anti-TLR1 (left panel) and anti-TLR2 antibodies (right panel), respective cognate isotype. (C–D) Sorted human pDCs were cultured during 24-hours with medium (Ø), 0.1 µg/mL LPS, 1 and 10 µg/mL PAM3, 100 ng/mL GM, or 82 HA/ml FLU. (D) Surface expression of MHC-II complex from activated pDCs. Results include the mean of 9 donors. (E) Sorted tonsil pDCs were stimulated during 24 hours with only medium (Ø), 1 µg/mL PAM3, and 82 HA/ml FLU. Results include the mean of 4 donors. Surface expression of costimulatory or coinhibitory molecules from activated pDCs by FACS. * $p < 0.05$; ** $p < 0.01$; *** $p < 0.001$ (Wilcoxon test). Underlying data for this figure can be found in S1 Data. CD, cluster of differentiation; FACS, fluorescence-activated cell sorting; FLU, influenza virus; GM, GM-CSF; GM-CSF, HA, hemagglutinin; granulocyte-macrophage colony-stimulating factor; LPS, lipopolysaccharide; PAM3, PAM3CSK4; pDC, Plasmacytoid dendritic cell; RT-PCR, real time PCR; TLR, toll-like receptor. (TIF)

S2 Fig. pDCs sense different gram+ bacteria through TLR1/2 pathway. Referring to Fig 2. (A–C) Sorted human pDCs were culture during 24 hours with only medium (Ø), DMSO, CU-CPT22, and FLU (in combination with DMSO and CU-CPT22). (A) Cell viability as percentage of cells DAPI negative. Results include the mean of 4 independent donors. (B) Surface expression of CD80 and CD86 from treated pDCs. Results include the mean of 4 independent donors. (C) Cytokine secretion by treated pDCs. Each dot represents an independent donor ($n = 4$). (D) Sorted human pDCs were cultured for 24 hours with only medium (Ø), heat-killed MT, heat-killed SA, heat-killed LM in the presence (+) or absence (–) of CU-CPT22. Surface expression of costimulatory molecules from activated pDCs. (E) The 24-hour stimulated pDCs and CD11c⁺ DCs (untreated, FLU, or 10 µg/mL PAM3) were cocultured with allogeneic CD4⁺ naive T cells for 6 days. Cytokines were measured after 24-hour polyclonal restimulation of the T cells. Results show 6 independent donors. Each dot represents a donor. * $p < 0.05$; ** $p < 0.01$; *** $p < 0.001$ (Wilcoxon test). Underlying data for this figure can be found in S1 Data. CD, cluster of differentiation; CU-CPT22, DC, dendritic cell; FLU, influenza virus; LM, *Listeria monocytogenes*; MT, *Mycobacterium tuberculosis*; PAM3, PAM3CSK4; pDC, Plasmacytoid dendritic cell; SA, *Staphylococcus aureus*; TLR, toll-like receptor. (TIF)

S3 Fig. PAM3-activated pDCs induce cytokine secretion from memory CD4⁺ T cells.

Referring to Fig 2. (A) Memory CD4⁺ T cells were cultured with pDCs activated for 24 hours with only medium (NT), 100 ng/mL LPS, 1 μg/mL or 10 μg/mL PAM3, 10 ng/mL GM, or 82 HA/mL Influenza A/PR/8/34 (H1N1). Cytokines were measured in the supernatants by CBA after 6 days of coculture and 24 hours of restimulation with anti-CD3/CD28 beads. Mean ± SD from 6 independent donors. **p* < 0.05 by paired Wilcoxon test. (B) Sort gating strategy of pure pDCs as LIN⁻CD4⁺CD11c⁻CD2⁻CD5⁻AXL⁻ (C) Quantification by CBA of cytokines produced by naive CD4 T cells cocultured with primary human pDCs activated for 24 hours with only medium (NT), 100 ng/mL LPS, 1 μg/mL or 10 μg/mL PAM3, 10 ng/mL GM, or 82 HA/mL Influenza A/PR/8/34 (H1N1). Cytokines were measured by CBA after 6 days of coculture and 24 hours of restimulation with anti-CD3/CD28 beads. Mean ± SD from 6 independent donors. **p* < 0.05 by paired Wilcoxon test. Underlying data for this figure can be found in S1 Data. AXL, AXL receptor tyrosine kinase; CBA, cytokine bead array; CD, cluster of differentiation; FLU, influenza virus; GM, GM-CSF; LIN, lineage; LPS, lipopolysaccharide; NT, medium; PAM3, PAM3CSK4; pDC, Plasmacytoid predendritic cell.

(TIF)

S4 Fig. TLR1/2 functional blocking differentially modifies CD4 T-cell activation.

Referring to Fig 3. (A) Sorted human pDCs were cultured during 24 hours with only medium (∅) and PAM3 in combination with TLR1 neutralizing antibody (αTLR1 Ab), TLR2 neutralizing antibody (αTLR2 Ab). Surface expression of costimulatory molecules from activated pDCs. (B–C) Allogeneic naïve CD4⁺ T-cell fold expansion and percentage of dividing cells after 6 days' coculture with 24 hours PAM3 pDCs (in presence or absence of blocking antibodies). Results include the mean of 9 independent donors. Each dot is an individual donor. (D) Specific MFI of Th master regulator expression from PAM3 pDCs (in the presence or absence of neutralizing antibodies) T-cell coculture. Intracellular FACS was performed after 4 days of coculture. Results include the mean of 9 independent donors for Tbet, GATA3, and FOXP3. Results include the mean of 7 independent donors for BCL-6. (E) Th cytokine pattern from PAM3 (in combination with neutralizing antibody) activated T-cells coculture. Cytokines were measured after 24-hour polyclonal restimulation of the T cells. Results include the mean of 9 independent donors. **p* < 0.05; ***p* < 0.01; ****p* < 0.001 (Wilcoxon test). Underlying data for this figure can be found in S1 Data. Ab, antibody; CD, cluster of differentiation; BCL-6, B-cell lymphoma 6; FACS, fluorescence-activated cell sorting; FOXP3, forkhead box P3; GATA3, GATA binding protein 3; MFI, mean fluorescence intensity; PAM3, PAM3CSK4; pDC, Plasmacytoid predendritic cell; Tbet, T-box transcription factor TBX21; Th, T helper; TLR, toll-like receptor.

(TIF)

S1 Data. Numerical data used in this study. Numeric data shown in separate Excel spreadsheets (Microsoft, Redmond, WA).

(XLSX)

Acknowledgments

We thank Nicolas Manel and Maude Delost for discussions and critical reading of the manuscript. We thank Elodie Segura for critical discussions and suggestions about tonsil pDC isolation. We thank Annick Viguier and Zofia Maciorowski from the Cytometry Core facility of Institut Curie for cell sorting.

Author Contributions

Conceptualization: Salvatore Raieli, Vassili Soumelis.

Data curation: Salvatore Raieli, Coline Trichot.

Formal analysis: Salvatore Raieli.

Funding acquisition: Vassili Soumelis.

Investigation: Salvatore Raieli, Coline Trichot, Sarantis Korniotis.

Methodology: Salvatore Raieli.

Project administration: Vassili Soumelis.

Supervision: Vassili Soumelis.

Validation: Salvatore Raieli, Coline Trichot, Sarantis Korniotis.

Visualization: Salvatore Raieli, Coline Trichot.

Writing – original draft: Salvatore Raieli, Lucia Pattarini, Vassili Soumelis.

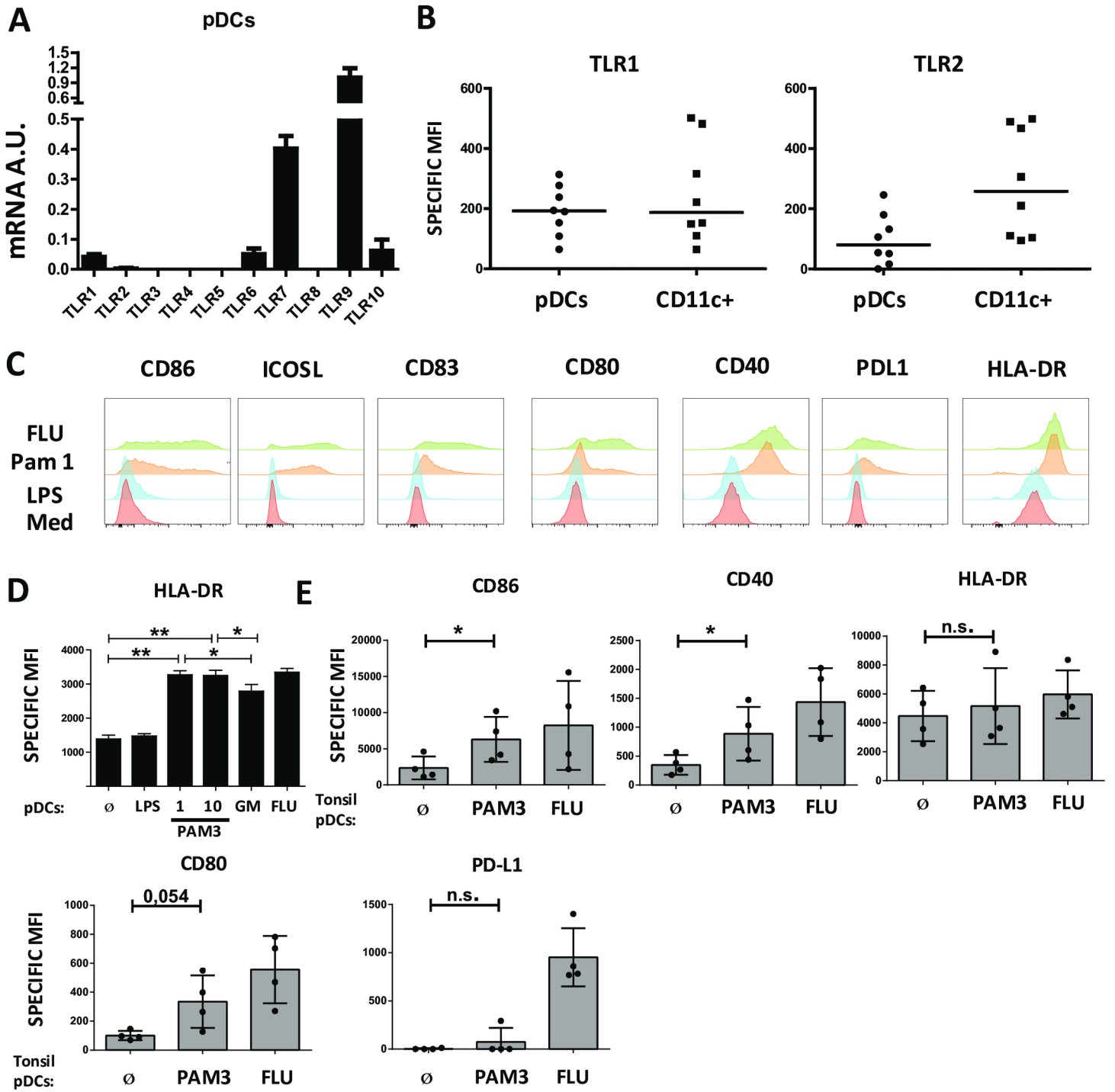
Writing – review & editing: Salvatore Raieli, Coline Trichot, Vassili Soumelis.

References

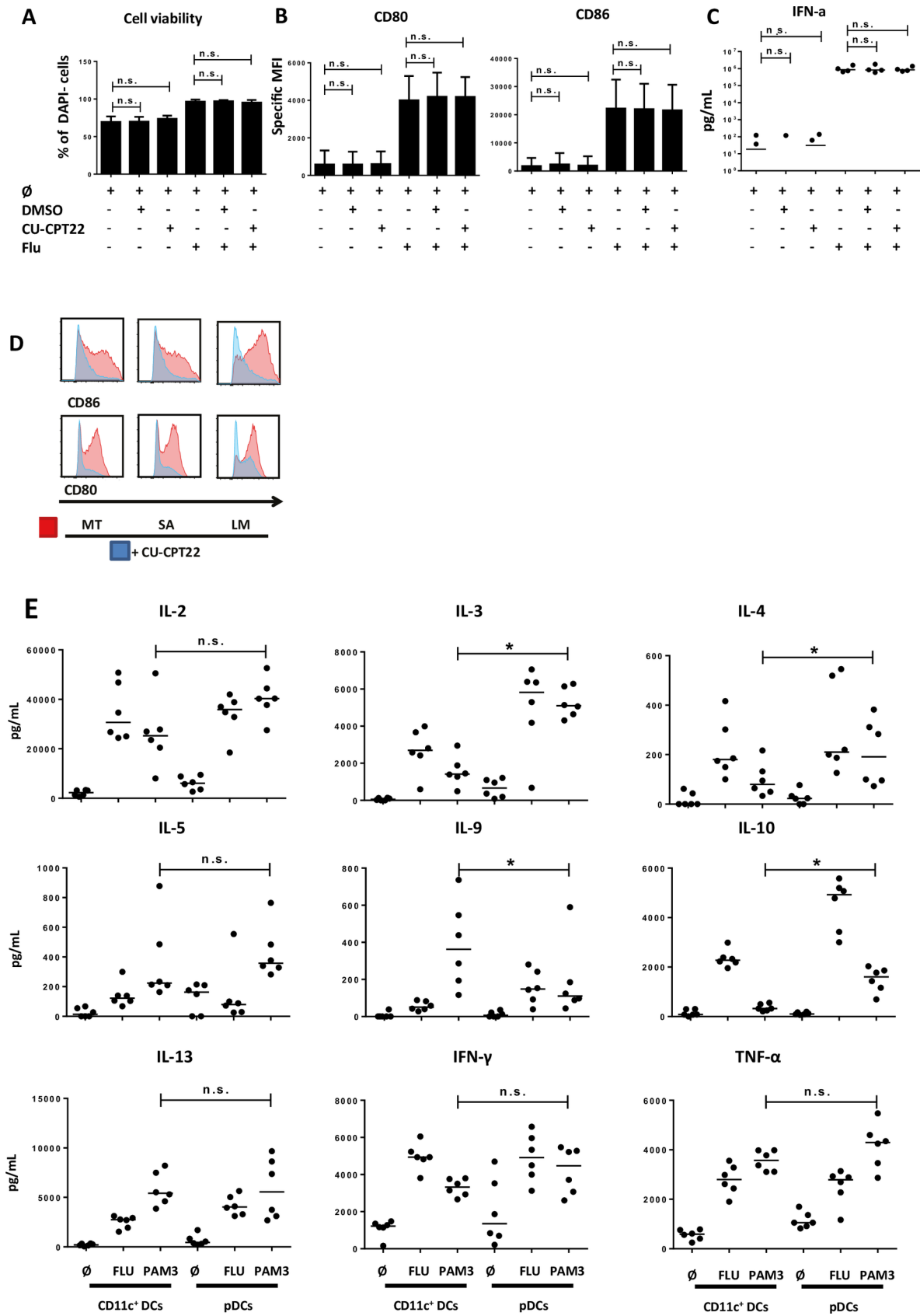
1. Raviglione M, Sulis G. Tuberculosis 2015: Burden, Challenges and Strategy for Control and Elimination. *Infect Dis Rep.* 2016; 8. <https://doi.org/10.4081/idr.2016.6570> PMID: 27403269
2. Berry MPR, Graham CM, McNab FW, Xu Z, Bloch SAA, Oni T, et al. An Interferon-Inducible Neutrophil-Driven Blood Transcriptional Signature in Human Tuberculosis. *Nature.* 2010; 466: 973–977. <https://doi.org/10.1038/nature09247> PMID: 20725040
3. Teles RMB, Graeber TG, Krutzik SR, Montoya D, Schenk M, Lee DJ, et al. Type I Interferon Suppresses Type II Interferon–Triggered Human Anti-Mycobacterial Responses. *Science.* 2013; 339: 1448–1453. <https://doi.org/10.1126/science.1233665>
4. Swiecki M, Colonna M. The multifaceted biology of plasmacytoid dendritic cells. *Nat Rev Immunol.* 2015; 15: 471–485. <https://doi.org/10.1038/nri3865> PMID: 26160613
5. Michea P, Vargas P, Donnadieu M-H, Roseblatt M, Bono MR, Duménil G, et al. Epithelial control of the human pDC response to extracellular bacteria. *Eur J Immunol.* 2013; 43: 1264–1273. <https://doi.org/10.1002/eji.201242990> PMID: 23436642
6. Lozza L, Farinacci M, Bechtel M, Stäber M, Zedler U, Baiocchi A, et al. Communication between Human Dendritic Cell Subsets in Tuberculosis: Requirements for Naive CD4+ T Cell Stimulation. *Front Immunol.* 2014; 5. <https://doi.org/10.3389/fimmu.2014.00324> PMID: 25071784
7. Nguyen MT, Götz F. Lipoproteins of Gram-Positive Bacteria: Key Players in the Immune Response and Virulence. *Microbiol Mol Biol Rev MMBR.* 2016; 80: 891–903. <https://doi.org/10.1128/MMBR.00028-16> PMID: 27512100
8. Jin MS, Kim SE, Heo JY, Lee ME, Kim HM, Paik S-G, et al. Crystal Structure of the TLR1-TLR2 Heterodimer Induced by Binding of a Tri-Acylated Lipopeptide. *Cell.* 2007; 130: 1071–1082. <https://doi.org/10.1016/j.cell.2007.09.008> PMID: 17889651
9. Yu X, Zeng J, Xie J. Navigating through the maze of TLR2 mediated signaling network for better mycobacterium infection control. *Biochimie.* 2014; 102: 1–8. <https://doi.org/10.1016/j.biochi.2014.02.012> PMID: 24594065
10. Kadowaki N, Ho S, Antonenko S, de Waal Malefyt R, Kastelein RA, Bazan F, et al. Subsets of Human Dendritic Cell Precursors Express Different Toll-like Receptors and Respond to Different Microbial Antigens. *J Exp Med.* 2001; 194: 863–870. PMID: 11561001
11. Diebold SS, Kaisho T, Hemmi H, Akira S, Sousa CR. Innate Antiviral Responses by Means of TLR7-Mediated Recognition of Single-Stranded RNA. *Science.* 2004; 303: 1529–1531. <https://doi.org/10.1126/science.1093616> PMID: 14976261
12. Hemmi H, Takeuchi O, Kawai T, Kaisho T, Sato S, Sanjo H, et al. A Toll-like receptor recognizes bacterial DNA. *Nature.* 2000; 408: 740–745. <https://doi.org/10.1038/35047123> PMID: 11130078

13. Kim T, Pazhoor S, Bao M, Zhang Z, Hanabuchi S, Facchinetti V, et al. Aspartate-glutamate-alanine-histidine box motif (DEAH)/RNA helicase A helicases sense microbial DNA in human plasmacytoid dendritic cells. *Proc Natl Acad Sci U S A*. 2010; 107: 15181–15186. <https://doi.org/10.1073/pnas.1006539107> PMID: 20696886
14. Szabo A, Magyarics Z, Pazmandi K, Gopcsa L, Rajnavolgyi E, Bacsai A. TLR ligands upregulate RIG-I expression in human plasmacytoid dendritic cells in a type I IFN-independent manner. *Immunol Cell Biol*. 2014; 92: 671–678. <https://doi.org/10.1038/icc.2014.38> PMID: 24839978
15. Bekeredjian-Ding I, Greil J, Ammann S, Parcina M. Plasmacytoid Dendritic Cells: Neglected Regulators of the Immune Response to *Staphylococcus aureus*. *Front Immunol*. 2014; 5. <https://doi.org/10.3389/fimmu.2014.00238> PMID: 24904586
16. Ghirelli C, Reyat F, Jeanmougin M, Zollinger R, Sirven P, Michea P, et al. Breast Cancer Cell–Derived GM-CSF Licenses Regulatory Th2 Induction by Plasmacytoid Predendritic Cells in Aggressive Disease Subtypes. *Cancer Res*. 2015; 75: 2775–2787. <https://doi.org/10.1158/0008-5472.CAN-14-2386>
17. Parcina M, Wendt C, Goetz F, Zawatzky R, Zähringer U, Heeg K, et al. *Staphylococcus aureus*-Induced Plasmacytoid Dendritic Cell Activation Is Based on an IgG-Mediated Memory Response. *J Immunol*. 2008; 181: 3823–3833. <https://doi.org/10.4049/jimmunol.181.6.3823> PMID: 18768836
18. Piccioli D, Sammiceli C, Tavarini S, Nuti S, Frigimelica E, Manetti AGO, et al. Human plasmacytoid dendritic cells are unresponsive to bacterial stimulation and require a novel type of cooperation with myeloid dendritic cells for maturation. *Blood*. 2009; 113: 4232–4239. <https://doi.org/10.1182/blood-2008-10-186890> PMID: 19176317
19. Cheng K, Wang X, Zhang S, Yin H. Discovery of small molecule inhibitors of the TLR1-TLR2 complex. *Angew Chem Int Ed Engl*. 2012; 51: 12246–12249. <https://doi.org/10.1002/anie.201204910> PMID: 22969053
20. Kadowaki N, Antonenko S, Lau JY-N, Liu Y-J. Natural Interferon α/β -Producing Cells Link Innate and Adaptive Immunity. *J Exp Med*. 2000; 192: 219–226.
21. Villani A-C, Satija R, Reynolds G, Sarkizova S, Shekhar K, Fletcher J, et al. Single-cell RNA-seq reveals new types of human blood dendritic cells, monocytes and progenitors. *Science*. 2017; 356. <https://doi.org/10.1126/science.aah4573> PMID: 28428369
22. Deng Y, Chu J, Ren Y, Fan Z, Ji X, Mundy B, et al. The Natural Product Phyllanthusmin C Enhances IFN- γ Production by Human Natural Killer Cells through Upregulation of TLR-Mediated NF- κ B Signaling. *J Immunol Baltim Md 1950*. 2014; 193: 2994–3002. <https://doi.org/10.4049/jimmunol.1302600>
23. Lebeer S, Claes I, Tytgat HLP, Verhoeven TLA, Marien E, von Ossowski I, et al. Functional Analysis of *Lactobacillus rhamnosus* GG Pili in Relation to Adhesion and Immunomodulatory Interactions with Intestinal Epithelial Cells. *Appl Environ Microbiol*. 2012; 78: 185–193. <https://doi.org/10.1128/AEM.06192-11> PMID: 22020518
24. Yu D, Rao S, Tsai LM, Lee SK, He Y, Sutcliffe EL, et al. The Transcriptional Repressor Bcl-6 Directs T Follicular Helper Cell Lineage Commitment. *Immunity*. 2009; 31: 457–468. <https://doi.org/10.1016/j.immuni.2009.07.002> PMID: 19631565
25. Guiducci C, Ghirelli C, Marloie-Provost M-A, Matray T, Coffman RL, Liu Y-J, et al. PI3K is critical for the nuclear translocation of IRF-7 and type I IFN production by human plasmacytoid predendritic cells in response to TLR activation. *J Exp Med*. 2008; 205: 315–322. <https://doi.org/10.1084/jem.20070763> PMID: 18227218
26. Lande R, Gilliet M. Plasmacytoid dendritic cells: key players in the initiation and regulation of immune responses. *Ann N Y Acad Sci*. 2010; 1183: 89–103. <https://doi.org/10.1111/j.1749-6632.2009.05152.x> PMID: 20146710
27. Atarashi K, Tanoue T, Shima T, Imaoka A, Kuwahara T, Momose Y, et al. Induction of Colonic Regulatory T Cells by Indigenous Clostridium Species. *Science*. 2011; 331: 337–341. <https://doi.org/10.1126/science.1198469> PMID: 21205640
28. Furusawa Y, Obata Y, Hase K. Commensal microbiota regulates T cell fate decision in the gut. *Semin Immunopathol*. 2015; 37: 17–25. <https://doi.org/10.1007/s00281-014-0455-3> PMID: 25315350
29. Lombardi VC, Khaiboullina SF. Plasmacytoid dendritic cells of the gut: Relevance to immunity and pathology. *Clin Immunol Orlando Fla*. 2014; 153: 165–177. <https://doi.org/10.1016/j.clim.2014.04.007> PMID: 24769378
30. Arimura K, Takagi H, Uto T, Fukaya T, Nakamura T, Chojiookhuu N, et al. Crucial role of plasmacytoid dendritic cells in the development of acute colitis through the regulation of intestinal inflammation. *Mucosal Immunol*. 2017; 10: 957–970. <https://doi.org/10.1038/mi.2016.96> PMID: 27848952
31. Jasenosky LD, Scriba TJ, Hanekom WA, Goldfeld AE. T cells and adaptive immunity to *Mycobacterium tuberculosis* in humans. *Immunol Rev*. 2015; 264: 74–87. <https://doi.org/10.1111/imr.12274> PMID: 25703553

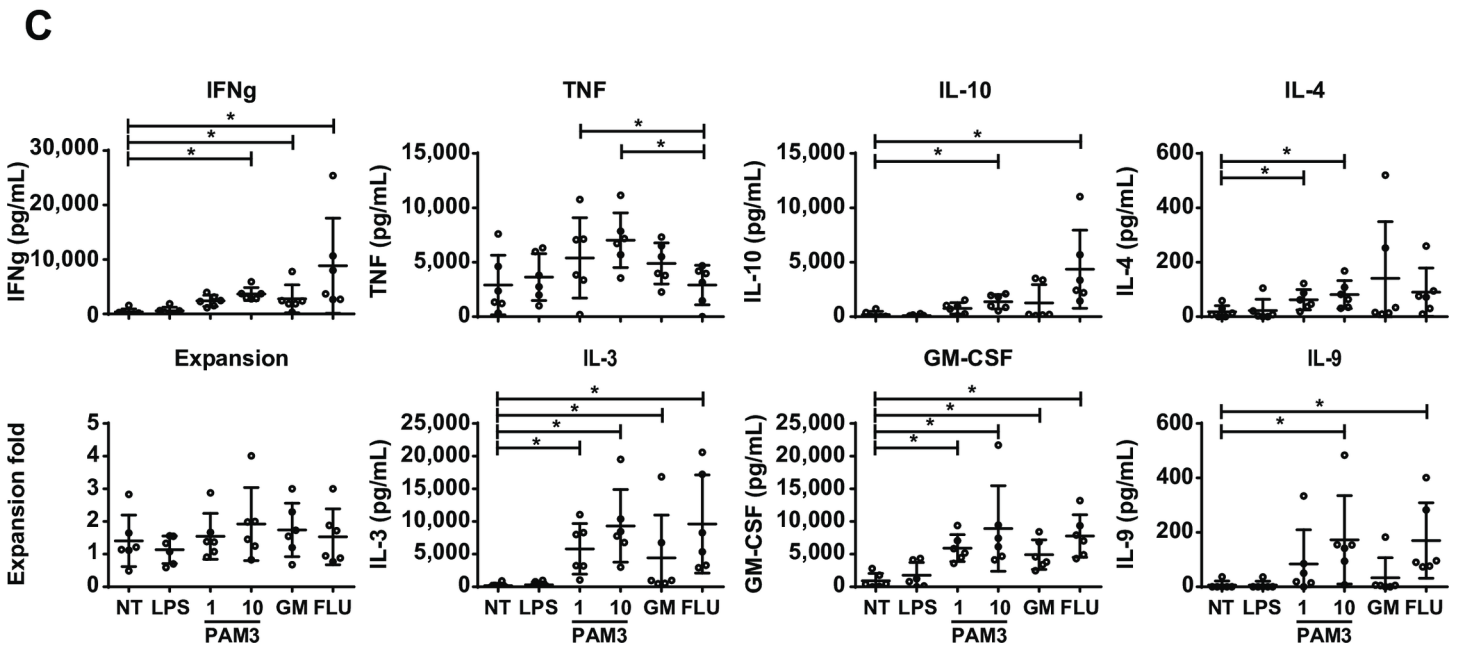
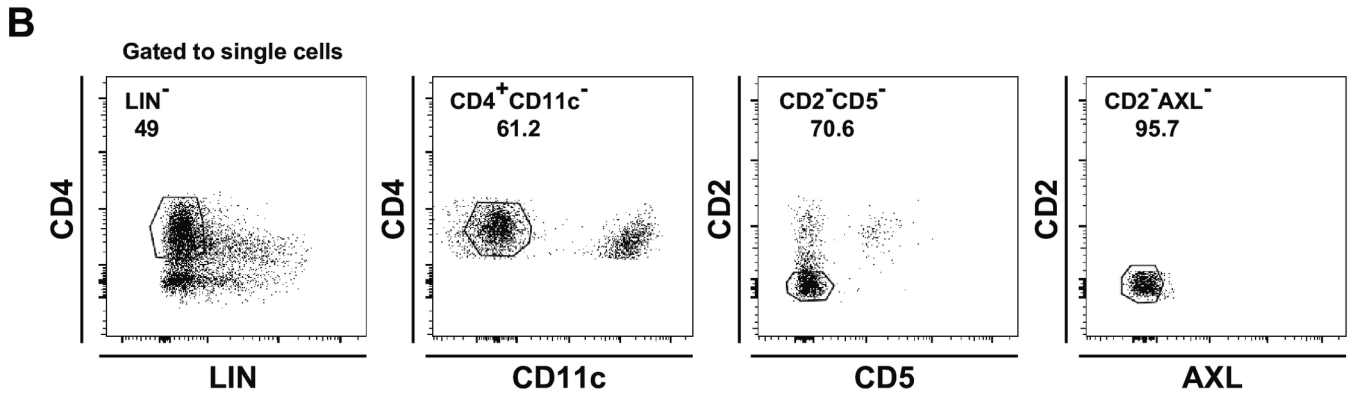
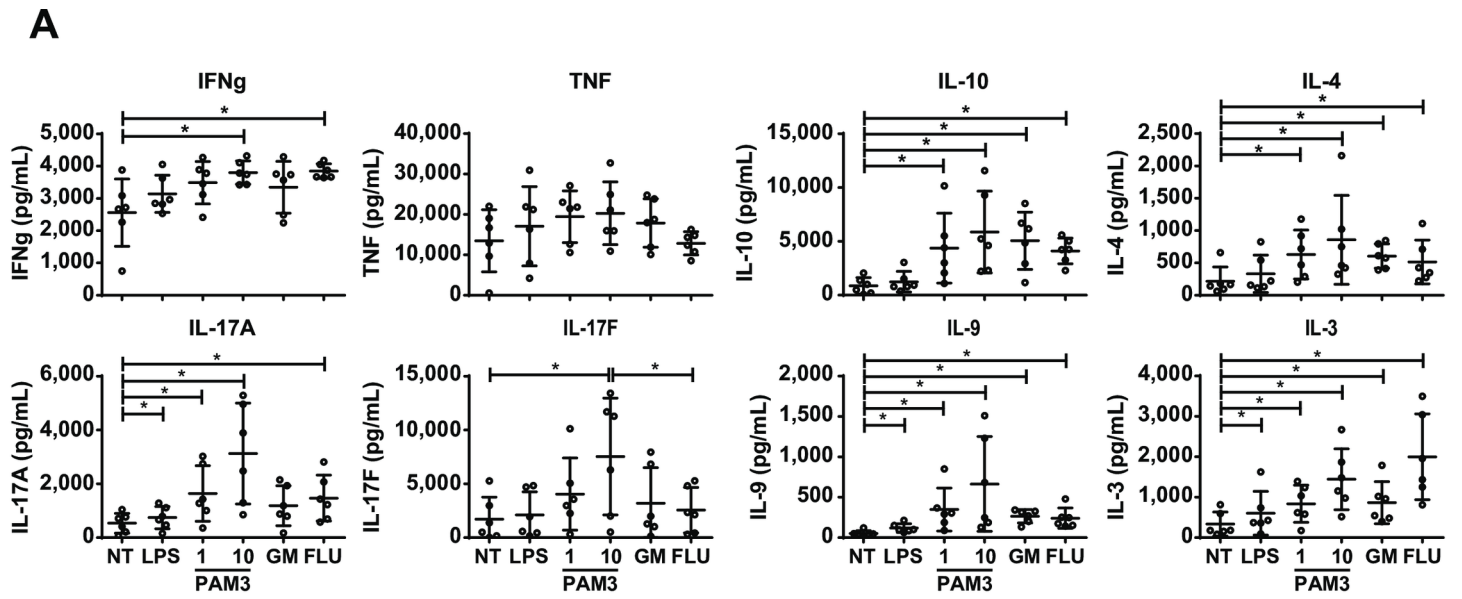
32. Orme IM, Robinson RT, Cooper AM. The balance between protective and pathogenic immune responses in the TB-infected lung. *Nat Immunol.* 2015; 16: 57–63. <https://doi.org/10.1038/ni.3048> PMID: 25521685
33. Parkash O, Agrawal S, Madhan Kumar M. T regulatory cells: Achilles' heel of Mycobacterium tuberculosis infection? *Immunol Res.* 2015; 62: 386–398. <https://doi.org/10.1007/s12026-015-8654-0>
34. Rook GAW. Th2 Cytokines in Susceptibility to Tuberculosis. In: *Current Molecular Medicine* [Internet]. 1 May 2007. <http://www.eurekaselect.com/59099/article>. [cited 20 Jan 2019].
35. Hepburn L, Hijnen DJ, Sellman BR, Mustelin T, Sleeman MA, May RD, et al. The complex biology and contribution of Staphylococcus aureus in atopic dermatitis, current and future therapies. *Br J Dermatol.* 2017; 177: 63–71. <https://doi.org/10.1111/bjd.15139> PMID: 27779765
36. Mu Z, Zhao Y, Liu X, Chang C, Zhang J. Molecular Biology of Atopic Dermatitis. *Clin Rev Allergy Immunol.* 2014; 47: 193–218. <https://doi.org/10.1007/s12016-014-8415-1> PMID: 24715253
37. Barbalat R, Lau L, Locksley RM, Barton GM. Toll-like receptor 2 on inflammatory monocytes induces type I interferon in response to viral but not bacterial ligands. *Nat Immunol.* 2009; 10: 1200–1207. <https://doi.org/10.1038/ni.1792> PMID: 19801985
38. Mayer-Barber KD, Andrade BB, Oland SD, Amaral EP, Barber DL, Gonzales J, et al. Host-directed therapy of tuberculosis based on interleukin-1 and type I interferon crosstalk. *Nature.* 2014; 511: 99–103. <https://doi.org/10.1038/nature13489> PMID: 24990750
39. Randhawa AK, Shey MS, Keyser A, Peixoto B, Wells RD, de Kock M, et al. Association of Human TLR1 and TLR6 Deficiency with Altered Immune Responses to BCG Vaccination in South African Infants. *PLoS Pathog.* 2011; 7(8). <https://doi.org/10.1371/journal.ppat.1002174> PMID: 21852947
40. Uciechowski P, Imhoff H, Lange C, Meyer CG, Browne EN, Kirsten DK, et al. Susceptibility to tuberculosis is associated with TLR1 polymorphisms resulting in a lack of TLR1 cell surface expression. *J Leukoc Biol.* 2011; 90: 377–388. <https://doi.org/10.1189/jlb.0409233> PMID: 21642391
41. Bagnoli F, Bertholet S, Grandi G. Inferring Reasons for the Failure of Staphylococcus aureus Vaccines in Clinical Trials. *Front Cell Infect Microbiol.* 2012; 2. <https://doi.org/10.3389/fcimb.2012.00016> PMID: 22919608
42. Bagnoli F, Fontana MR, Soldaini E, Mishra RPN, Fiaschi L, Cartocci E, et al. Vaccine composition formulated with a novel TLR7-dependent adjuvant induces high and broad protection against Staphylococcus aureus. *Proc Natl Acad Sci U S A.* 2015; 112: 3680–3685. <https://doi.org/10.1073/pnas.1424924112> PMID: 25775551
43. Durand M, Segura E. Dendritic Cell Subset Purification from Human Tonsils and Lymph Nodes. In: Segura E, Onai N, editors. *Dendritic Cell Protocols*. New York, NY: Springer New York; 2016. pp. 89–99. https://doi.org/10.1007/978-1-4939-3606-9_6 PMID: 27142010
44. Volpe E, Servant N, Zollinger R, Bogiatzi SI, Hupé P, Barillot E, et al. A critical function for transforming growth factor- β , interleukin 23 and proinflammatory cytokines in driving and modulating human T_H-17 responses. *Nat Immunol.* 2008; 9: 650–657. <https://doi.org/10.1038/ni.1613>
45. Rissoan M-C, Soumelis V, Kadowaki N, Grouard G, Briere F, Malefyt R de W, et al. Reciprocal Control of T Helper Cell and Dendritic Cell Differentiation. *Science.* 1999; 283: 1183–1186. <https://doi.org/10.1126/science.283.5405.1183> PMID: 10024247



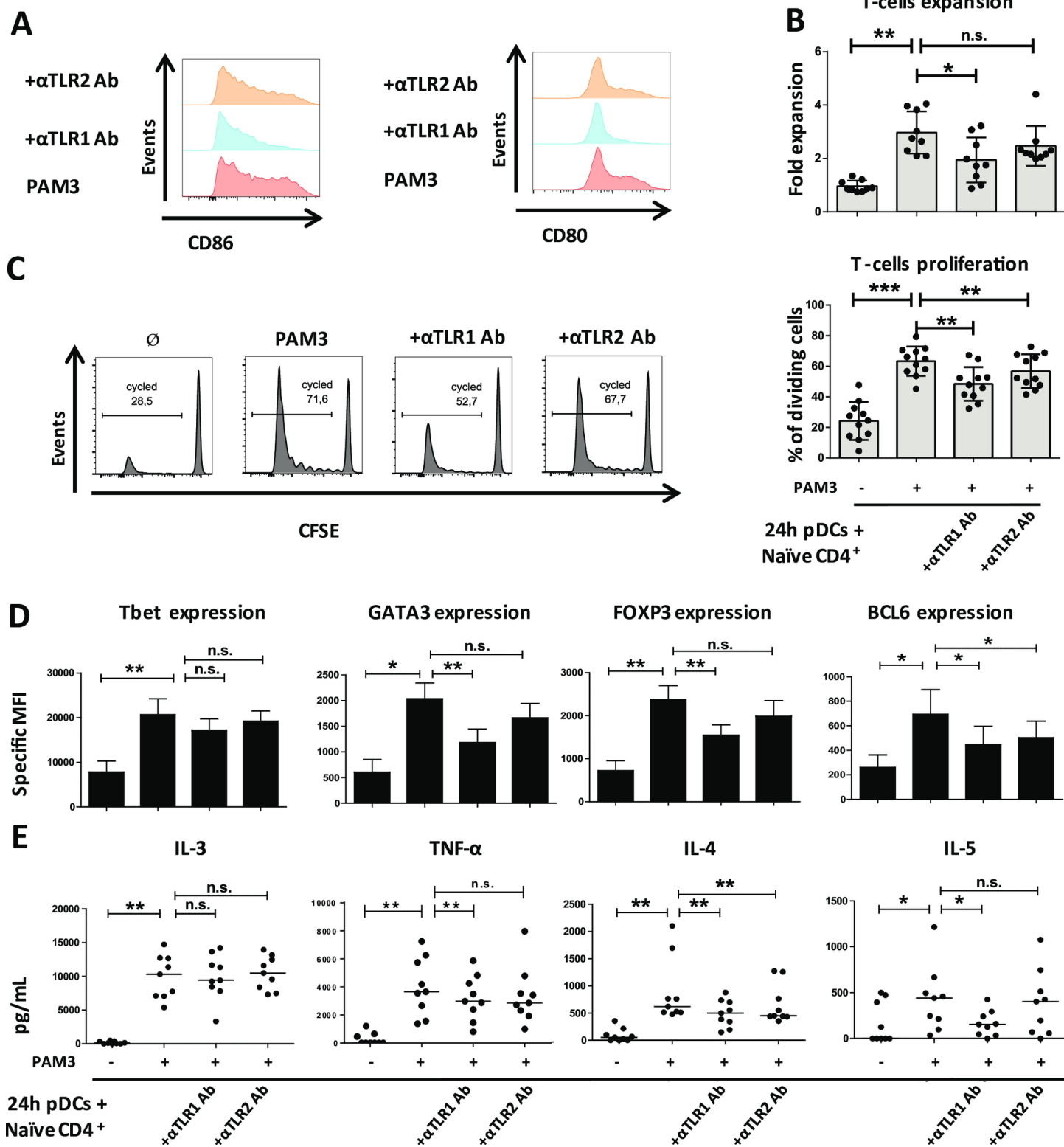
S1 Fig. pDCs from human tonsils respond to PAM3



S2 Fig. pDCs sense different gram+ bacteria through TLR1/2 pathway



S3 Fig. PAM3-activated pDCs induce cytokine secretion from memory CD4⁺ T cells



S4 Fig. TLR1/2 functional blocking differentially modifies CD4 T-cell activation

4. Appendix 4

SYNTHÈSE EN FRANÇAIS DES TRAVAUX DE THÈSE

Régulation de la diversité des sous-populations de lymphocytes T auxiliaires humaines :
des mécanismes in vitro dérivés des cellules dendritiques aux candidats biomarqueurs
dans la dermatite atopique

1. Introduction

a. Les lymphocytes T auxiliaires

Les lymphocytes T auxiliaires (Th) jouent un rôle majeur dans le système immunitaire adaptatif, qui permet la défense de l'hôte contre une grande variété de pathogènes. Via la sécrétion d'ensemble de cytokines spécifiques, les lymphocytes Th instruisent les autres types cellulaires afin qu'ils engagent une réponse immunitaire appropriée à la menace rencontrée, permettant son élimination.

La découverte des lymphocytes Th a commencé par l'identification de deux clones dérivés in vitro : Th1 et Th2, obtenus après l'immunisation de souris [1]. L'étude plus précise de ces deux clones a permis leur caractérisation complète, en termes de cytokines sécrétées, de facteurs de transcription, leurs marqueurs de surface mais aussi leurs fonctions.

Les lymphocytes Th1 sont caractérisés par la production d'IL-2, IFN- γ , TNF- α et TNF- β [2], les facteurs de transcription T-bet, STAT1, STAT4 [4], les récepteurs aux chémokines CCR5 et CXCR3 [9, 10] et ils permettent l'élimination des virus et bactéries intracellulaires [13].

Les lymphocytes Th2 quant à eux, produisent les cytokines IL-4, IL-5, IL-6 et IL-13 [2], sous le contrôle des facteurs de transcription GATA3, STAT5 et STAT6 [5], ils expriment les récepteurs aux chémokines CCR3, CCR5 et CCR8 [10, 11] ainsi que le marqueur CRTH2, un récepteur à la prostaglandine D₂ [12] et sont impliqués dans le contrôle des parasites extracellulaires.

De nombreuses autres sous-populations de lymphocytes Th ont ensuite été identifiées.

Tout d'abord les lymphocytes Th17 ont été caractérisés par la production des cytokines IL-17A, IL-17F, IL-21, IL-22 et IL-26, ainsi que les chémokines CCL20 et CXCL8, les facteurs de transcription ROR γ T, ROR α et STAT3, le marqueur de surface CD161 et le récepteur aux chémokines CCR6 [17].

Ensuite, les lymphocytes Th22, identifiés pour leur production d'IL-22, sans co-production d'IL-17, ont été décrits comme exprimant le facteur de transcription AHR [21], les récepteurs aux chémokines CCR6, CCR4 et CCR10 [22], ils sont impliqués dans les processus d'inflammation cutanée.

De façon similaire, les lymphocytes Th9 ont été décrits pour leur production d'IL-9 sans co-production des autres cytokines Th2. Ils expriment le facteur de transcription PU.1 ainsi que GATA3 et STAT6 [25], le marqueur CLA suggérant leur rôle dans l'immunité cutanée et la défense contre les pathogènes extracellulaires [26].

En parallèle, une population de lymphocytes Th particuliers a été décrite : les lymphocytes T régulateurs (Treg) capables d'inhiber l'activation et la prolifération des lymphocytes T et B reconnaissant des antigènes du soi et ainsi de prévenir les maladies auto-immunes [29]. Ils sont caractérisés par la production d'IL-10 et TGF- β , l'expression des marqueurs CD25, GITR, CTLA4 et du facteur de transcription FoxP3 [27, 28].

Plus récemment, les lymphocytes T folliculaires (Tfh) ont été identifiés tout d'abord dans les centres germinatifs des organes lymphoïdes secondaires. Ils se caractérisent par l'expression des marqueurs CXCR5, ICOS, CD40L, OX40L, PD1, BTLA, de la protéine adaptatrice SAP, du facteur de transcription Bcl-6 [34] et par la production d'IL-21 et CXCL13 [33]. Ils sont indispensables pour apporter de l'aide aux lymphocytes B afin de permettre leur différenciation et leur commutation isotypique [35].

Des lymphocytes T folliculaires régulateurs se développent également en parallèle afin de contrôler la mise en place des centres germinatifs en inhibant lymphocytes Tfh et lymphocytes B. Ils expriment à la fois des marqueurs de Tfh : CXCR5, PD1, ICOS, Bcl-6, et des marqueurs de Treg : FoxP3, CD25, CTLA4, GITR [39] et produisent de grandes quantités de cytokines inhibitrices IL-10 et TGF- β .

Les lymphocytes Tfh ont également été identifiés dans le sang périphérique [32]. De plus, des sous-populations de lymphocytes Tfh ont été décrites dans le sang, faisant un miroir partiel avec les populations Th. On y trouve ainsi des lymphocytes Tfh1, Tfh2 et Tfh17 caractérisés par les marqueurs Tfh accompagnés des marqueurs de la population Th correspondante [45].

Néanmoins cette classification des sous-populations de lymphocytes Th a été largement remise en cause par de nombreuses études montrant non seulement une importante plasticité des différentes sous-populations, capables de passer d'un phénotype à un autre, mais en plus une capacité à adopter un phénotype intermédiaire avec les caractéristiques de deux populations Th à la fois. De plus, de nouvelles technologies telles que la cytométrie de masse, permettant l'analyse de nombreux paramètres à la fois, a montré qu'une très grande diversité et complexité existaient au sein des populations de lymphocytes Th.

b. Les cellules dendritiques

Les cellules dendritiques (DC) sont responsables de l'initiation des réponses immunitaires. En effet, les DC sont des cellules présentatrices d'antigènes professionnelles, grâce à leur forte expression de molécules du complexe majeur d'histocompatibilité. En temps normal, les DC sont au repos dans les tissus périphériques et s'activent dans le cas d'une infection qu'elles détectent via de nombreux récepteurs qui leur permettent de détecter les pathogènes autour d'elles. Les DC capturent les antigènes présents dans leur microenvironnement, les dégradent sous forme de peptides afin de les présenter sur leurs molécules du complexe majeur d'histocompatibilité de classe II. Une fois activées, les DC vont migrer vers les organes lymphoïdes secondaires afin d'activer les lymphocytes T CD4 naïfs spécifiques de l'antigène qu'elles présentent. Si un lymphocyte T reconnaît son antigène, il s'active et prolifère afin de mettre en place la réponse immunitaire appropriée [66-68].

Les cellules dendritiques sont présentes dans de nombreux tissus et peuvent être divisées en plusieurs populations. Les cellules dendritiques plasmacytoïdes (pDC), identifiables par l'expression des marqueurs de surface BDCA-2, BDCA-4, CD123 et leur importante production d'IFN- α , peuvent être identifiés dans le sang et les organes lymphoïdes [71].

Dans la peau, le sang, les organes lymphoïdes et les tissus périphériques, deux sous-types peuvent être trouvés : 1) les cDC1 caractérisées par les marqueurs de surface CD141, CLEC9A et XCR1 et 2) les cDC2 exprimant CD1c et CD11b [73].

Une population supplémentaire est présente dans le sang : les DC CD16⁺ exprimant également CD11c, CD11b et CD1c [80].

Dans la peau une population spécifique a été identifiée au niveau de l'épiderme : les cellules de Langerhans caractérisées par l'expression de CD1a, EpCAM et la Langerin [74]. Plus récemment, une population nommée AS-DC a été identifiée, caractérisée par le marqueur AXL et partageant des marqueurs phénotypiques avec les pDC et les cDC2 [81]. En plus de ces populations provenant d'un progéniteur commun dans la moelle osseuse [70], une population de DC dérivées des monocytes (MoDC) a été décrites tout d'abord dans des contextes inflammatoires puis chez des donneurs sains [78].

Les DC expriment un grand nombre de récepteurs leur permettant de reconnaître des signaux endogènes et exogènes en provenance de leur microenvironnement. Chaque sous-population se caractérise par un ensemble de récepteurs spécifiques, lui permettant de

reconnaitre des pathogènes particuliers. De nombreuses équipes ont montrés qu'une même population de DC, suivant le signal d'activation qu'elle recevait, pouvait induire différentes réponses lymphocytaires Th.

L'activation des lymphocytes Th par les DC nécessitent trois signaux. Tout d'abord la combinaison de l'antigène avec la molécule du complexe majeur d'histocompatibilité de classe II doit entrer en contact avec le récepteur des lymphocytes T. Une fois les DC activées, elles se mettent à exprimer des molécules de costimulation : CD80 et CD86, qui interagissent avec CD28 exprimés à la surface des lymphocytes Th, ceci représente le second signal. Enfin, suivant le signal de danger ayant activé la DC, celle-ci va produire des cytokines spécifiques ou exprimer des molécules de surface particulières, permettant d'induire la réponse lymphocytaire Th appropriée. C'est ce dernier signal qui détermine réellement la réponse Th [139].

Ainsi, de nombreuses molécules ont été identifiées comme étant responsables de réponses Th précises. Néanmoins, comme les DC peuvent exprimer un très grand nombre de molécules de communication (molécules de surface et cytokines), un nombre presque infini de combinaisons peut exister. Ces molécules de communication vont donc agir de manière collective sur les lymphocytes T et une molécule spécifique n'aura pas le même effet suivant les autres molécules coexprimées.

c. Les pathologies liées aux lymphocytes Th, exemple de la dermatite atopique

Les lymphocytes Th ont été décrits dans de très nombreuses pathologies. Nous nous sommes intéressés en particulier à la dermatite atopique (AD), car le modèle expérimental de DC activées par la TSLP que nous utilisons, est particulièrement relevant à l'AD.

L'AD est une maladie chronique inflammatoire de la peau, caractérisée par des lésions rouges qui démangent. L'AD est décrite comme une sensibilisation aux allergènes environnants, due non seulement à des dysfonctions de la barrière épithéliale mais aussi à une dérégulation immune [161]. La sévérité de la maladie est mesurée par différents scores cliniques : EASI, SCORAD, IGA, DLQI [162].

L'AD se compose de deux phases : une phase aiguë dominée par une réponse Th2 et Th22 et une phase chronique dans laquelle apparaît une réponse Th1 en parallèle [163].

Lorsque la barrière cutanée est lésée, elle laisse pénétrer des allergènes et des bactéries, ce qui va induire la sécrétion de cytokines pro-inflammatoires et pro-Th2 par les kératinocytes. Les DC présentes dans la peau vont capter les antigènes étrangers et s'activer en réponse aux cytokines, migrer vers les organes lymphoïdes secondaires où elles vont induire la polarisation des lymphocytes T CD4 naïfs en lymphocytes Th2 [160, 165]. Les molécules Th2 vont agir à plusieurs niveaux et conduire à la dégradation de la barrière cutanée mais aussi inhiber la production de peptides antimicrobiens, conduisant à une aggravation de l'inflammation cutanée [163].

Même si initialement décrite comme une pathologie Th2, l'AD est également caractérisée par l'émergence d'une réponse Th22, Th1 et Th17.

Suivant la sévérité de l'AD, les traitements non-pharmacologiques comme l'application d'émollients ou de thérapies topiques comme des corticostéroïdes peuvent suffire. Dans les cas d'AD modérée à sévère, des traitements immunosuppresseurs sont nécessaires. Mais ceux-ci présentent de nombreux effets secondaires, ce qui limite leur utilisation [171, 172]. Pourtant l'AD représente un vrai fardeau pour les malades et impacte largement leur qualité de vie. Dans ce contexte, un traitement plus efficace et plus sûr était nécessaire pour le traitement des patients atteints d'AD modérée à sévère.

De nombreuses compagnies pharmaceutiques se sont lancées dans le développement d'immunothérapie ciblant différentes molécules des voies de signalisation Th et en particulier la voie Th2 qui joue un rôle majeur dans la pathogénèse de l'AD.

Le Dupilumab, développé par Regeneron et Sanofi, est la première immunothérapie pour le traitement de l'AD modérée à sévère des patients adultes, approuvée à la fois par l'administration américaine des denrées alimentaires et des médicaments (FDA) et par l'agence européenne des médicaments. Récemment il a également été approuvé par la FDA pour le traitement des adolescents.

Le Dupilumab est un anticorps monoclonal entièrement humain antagoniste de la sous-unité alpha du récepteur à l'IL-4. Il inhibe la signalisation de l'IL-4 et de l'IL-13 et ainsi les réponses Th2 aberrantes [182]. De nombreuses études cliniques impliquant un grand nombre de patients ont prouvés l'efficacité et la sûreté du Dupilumab. De façon consistante, le Dupilumab a été prouvé plus efficace qu'un placebo avec de rares effets secondaires [191, 192].

L'efficacité et la sûreté à long terme doivent être évaluées, mais le Dupilumab semble être un traitement puissant pour les patients atteints d'AD sévère à modérée qui ne répondent pas aux traitements classiques.

2. Objectifs

Dans l'introduction j'ai présenté la diversité des lymphocytes T auxiliaires actuellement connue, en commençant par la découverte des lymphocytes Th1 et Th2, puis toutes les autres sous-populations : Th17, Treg, Th9, Th22 et plus récemment les lymphocytes Tfh avec leurs propres sous-populations : Tfh1, Tfh2, Tfh17 et Tfr. Ensuite j'ai décrit les différentes sous-populations de cellules dendritiques et les caractéristiques responsables de l'induction de la diversité des lymphocytes Th. Enfin j'ai décrit l'exemple de la dermatite atopique, où une dérégulation de la réponse Th2 est responsable du développement de la maladie. J'ai également montré que les voies de régulation Th peuvent servir de cible pour de nouveaux traitements par immunothérapie, comme dans le cas du Dupilumab.

Mon travail de thèse a visé à :

1. Comprendre le rôle des DC activées par la TSLP dans la génération de lymphocytes Tfh,
2. Examiner le lien entre la combinaison de molécules de communication exprimée à la surface des DC et la diversité de profils Th induits en réponse,
3. Étudier la modulation des populations Th et Tfh chez les patients atteints de dermatite atopique traités par Dupilumab.

3. Résultats

Publication n°1 : Les cellules dendritiques activées par la lymphopoïétine stromale thymique (TSLP) induisent la différenciation de lymphocytes T folliculaires via OX40L

J Exp Med. 2017 May 1; 214(5): 1529–1546

Dans cette étude, le but était de comprendre si et comment les DC activées par la TSLP étaient capables de polariser des lymphocytes T CD4 naïfs en lymphocytes Tfh capables

d'aider les lymphocytes B. Les DC activées par la TSLP sont connues pour induire une polarisation Th2 [134] et les Tfh ont déjà été décrits dans des environnements dominés par les Th2, comme l'allergie [196]. Cependant, l'IL-4, qui est la cytokine Th2 prototypique, a été démontrée comme inhibant la polarisation des lymphocytes Tfh [145]. De plus, OX40L a été montré comme un signal clé induisant la production d'IL-21 par les lymphocytes T CD4 [141]. Il a été bien décrit que OX40L est fortement exprimé sur les DC activées par la TSLP [135]. En conséquence, il était important d'étudier si la polarisation de lymphocytes Tfh était possible dans ce contexte TSLP, qui est également relevant à la dermatite atopique.

Pour cette étude, nous avons utilisé un modèle de coculture allogénique entre cellules dendritiques et lymphocytes T CD4. Nous avons trié des DC CD11c⁺ primaires à partir de sang périphérique, nous les avons activées pendant 24 heures avec de la TSLP, puis nous les avons co-cultivées avec des lymphocytes T CD4 humains primaires allogéniques. Après 6 jours de coculture, nous avons analysé toutes les caractéristiques des lymphocytes Th polarisés : les cytokines, les molécules de surface et les facteurs de transcription. Nous avons pu observer que les DC activées par la TSLP induisaient la polarisation de cellules présentant toutes les caractéristiques de lymphocytes Tfh : l'expression des marqueurs de surface CXCR5, ICOS, PD1, du facteur de transcription Bcl-6 et la production d'IL-4, IL-21 et CXCL13.

Afin de déterminer de façon définitive si ces cellules étaient des lymphocytes Tfh et possédaient la fonction principale des lymphocytes Tfh, c'est-à-dire la faculté d'aider les lymphocytes B, nous les avons triés et co-cultivées avec des lymphocytes B autologues. Après 14 jours de coculture nous avons mesurés dans les surnageants de culture les différentes immunoglobulines produites. Nous avons observé une induction de la commutation isotypique vers IgE lorsque les lymphocytes Tfh CXCR5⁺PD1⁺ induits par les DC activées par la TSLP étaient en coculture avec des lymphocytes B mémoires. Ceci a permis de confirmer que ces cellules étaient des lymphocytes Tfh fonctionnels.

Afin de comprendre si la polarisation lymphocytaire Th conduite par les DC activées par la TSLP se faisait via OX40L, nous avons utilisé un anticorps bloquant dirigé contre OX40L pendant la coculture entre DC activées par la TSLP et lymphocytes T. Nous avons observé que la polarisation des lymphocytes T CD4 naïfs, ainsi que l'activation des lymphocytes Tfh mémoires par les DC activées par la TSLP se faisaient via OX40L.

Enfin, dans le but d'évaluer la relevance de la polarisation Tfh par les DC activées par la TSLP dans les pathologies humaines, nous avons analysé la présence de lymphocytes Tfh dans des échantillons de sang périphérique provenant de patients atteints de dermatite atopique et les avons comparés à des échantillons provenant de donneurs sains. Nous

avons pu détecter que la population de lymphocytes Tfh2, décrite comme produisant de l'IL-21 en combinaison avec de l'IL-4 [45], était présente en plus grande proportion chez les patients atteints de dermatite atopique que chez les donneurs sains. Ceci suggérait que TSLP et lymphocytes Tfh pourraient être impliqués dans la dermatite atopique.

Publication n°2 : Un modèle quantitatif multivarié de la communication entre cellules dendritiques et lymphocytes T auxiliaires humains

Cell. 2019 Oct 3;179(2):432-447.e21.

La combinatoire de la diversité de molécules de communication que peuvent exprimer les DC à leur surface et pouvant moduler la polarisation des lymphocytes Th est virtuellement illimitée. Jusqu'à présent la plupart des études se sont concentrées sur l'étude du rôle d'une molécule de communication des DC ou d'un petit ensemble, ce qui limite la compréhension des interactions entre molécules. Il y avait donc un besoin d'une étude plus systématique, prenant en compte un plus grand nombre de molécules et étudiant leurs impacts combinés sur la polarisation des lymphocytes Th. Capturer cette complexité de signaux ne pouvait être réalisé qu'à l'aide d'un modèle mathématique.

Pour ce projet, j'ai surtout été impliquée au niveau de la validation expérimentale. En utilisant le même système de coculture entre DC et lymphocytes T CD4 naïfs que celui de la précédente étude, Maximilien Grandclaudon, le responsable de ce projet, a mesuré en parallèle 36 paramètres sur les DC (7 cytokines et 29 molécules de surface) avant coculture, ainsi que 18 paramètres (17 cytokines et l'expansion cellulaire) sur les lymphocytes Th à la fin de la coculture. Ceci a permis de générer un total de 428 observations couplées sur les DC et sur les lymphocytes Th. À partir de ces données, et avec l'aide de Marie Perrot-Dockès, biostatisticienne, ils ont généré un modèle statistique innovant capable de prédire le comportement des 18 paramètres des lymphocytes Th en réponse aux 36 signaux dérivés des DC.

Ce modèle a tout d'abord été largement validé mathématiquement. Il a également été confronté aux connaissances de la littérature, permettant de lui donner un score de validation de 70%. Enfin, il a été validé expérimentalement. Tout d'abord à l'aide d'un anticorps bloquant la molécule CD28 dans des cocultures entre MoDC et lymphocytes T CD4, nous avons pu démontrer que le modèle prédisait correctement 11 fois sur 15 les paramètres Th en fonction des signaux des DC. Ensuite, en utilisant un modèle de polarisation des lymphocytes Th en l'absence de DC, nous avons pu valider 7/10

prédictions concernant l'IL-1, 10/16 pour ICOSL et 13/15 pour IL-12p70. Au final, grâce à ces validations expérimentales, nous avons pu déterminer que le modèle était capable de prédire avec succès en moyenne 73.2% des relations entre paramètres DC et paramètres des lymphocytes Th.

En plus de ces validations systématiques, nous avons également pu valider des prédictions pour des mécanismes entièrement nouveaux et encore inconnus de la littérature. Tout d'abord, nous avons démontré, en utilisant un anticorps agoniste de CD2 dans une expérience de polarisation lymphocytaire Th sans DC et dans un contexte Th17, que CD2 induisait la production d'IL-17A et IL-17F. En allant plus loin dans la caractérisation d'IL-12p70, jusqu'ici associé à la production d'IFN- γ et à la polarisation Th1 [140], nous avons établi qu'IL-12p70 combiné avec IL-1 β (ou IL-1 α) est capable d'induire de hauts niveaux d'IL-17F sans co-production d'IL-17A. À l'opposé, ajouter IL-12p70 à un contexte IL-23+IL-1 β induisait la production d'IL-17A, avec des niveaux similaires d'IL-17F comparé à IL-12p70+IL-1 β seuls. Tous ces nouveaux mécanismes n'avaient jamais été décrits auparavant, mais avaient été prédits par une version avancée du modèle prenant en compte des variables de dépendance de contexte.

Ce modèle de communication entre DC et lymphocytes Th a le potentiel pour être une importante ressource pour la communauté scientifique, afin de fournir des hypothèses non seulement sur l'impact de molécules seules sur les paramètres des lymphocytes Th, mais aussi sur les associations dépendantes du contexte. Au-delà du système DC/lymphocytes Th, cette stratégie peut avoir des applications plus larges dans n'importe quel système de communication impliquant des signaux d'entrée et de sortie.

Publication n°3 : La diminution des lymphocytes Th17 corrélait avec l'amélioration du score EASI chez les patients atteints de dermatite atopique durant le traitement par Dupilumab

Manuscrit en préparation

Dans la publication n°1, nous avons observé une plus grande proportion de lymphocytes Tfh2 chez les patients atteints de dermatite atopique, comparé aux donneurs sains [142]. Nous voulions aller plus loin dans l'analyse des différentes populations de lymphocytes Th et Tfh dans la dermatite atopique.

Récemment, une nouvelle immunothérapie a été développée par Regeneron/Sanofi pour le traitement de la dermatite atopique, appelée Dupilumab. Dupilumab est un anticorps monoclonal entièrement humain d'isotype IgG4 antagoniste pour la sous-unité alpha du

récepteur à l'IL-4, qui a la capacité d'interagir soit avec la chaîne γ commune pour former le récepteur à l'IL-4 ou avec la chaîne $\alpha 1$ du récepteur à l'IL-13 pour former le récepteur à l'IL-13. En conséquence, Dupilumab inhibe la transduction du signal provenant de l'IL-4 mais aussi de l'IL-13 et ainsi les réponses Th2 aberrantes [182]. Nous étions par conséquent intéressés par étudier l'évolution des différentes populations Th et Tfh en réponse à ce traitement.

Grâce à l'aide précieuse du Professeur Jean-David Bouaziz et de son équipe, nous avons reçu des échantillons de sang périphérique provenant de 29 patients atteints de dermatite atopique modérée à sévère traités avec Dupilumab à différents moments au cours de leur traitement.

Nous avons pu mesurer par cytométrie en flux huit sous-populations Th et Tfh (Th1, Th2, Th17, Th1/17, Tfh1, Tfh2, Tfh17 and Tfh1/17) et ces mesures étaient associées aux scores cliniques (SCORAD, IGA, EASI, DLQI) contrôlés par les cliniciens à chaque prélèvement. La plus forte variation mesurée au cours du traitement par Dupilumab était la diminution significative du pourcentage de lymphocytes Th2. De façon surprenante, lorsque nous avons cherché de potentielles associations entre l'évolution des pourcentages des différentes populations de lymphocytes Th et Tfh et l'amélioration du score EASI au cours du traitement, nous avons observé une corrélation entre la diminution du pourcentage de lymphocytes Th17 et l'amélioration du score clinique EASI.

4. Discussion et Perspectives

Les lymphocytes Th représentent un composant très important du système immunitaire. Via les combinaisons de cytokines qu'ils produisent, les lymphocytes Th sont capables d'ordonner la réponse immunitaire appropriée face au pathogène qui envahi l'hôte. Les ensembles de cytokines qu'ils produisent, en fonction de la sous-population, leur permettent d'attirer et/ou activer spécifiquement différents autres types cellulaires au niveau du site d'inflammation, dans le but d'éliminer le pathogène. Cependant, si le processus de polarisation des lymphocytes Th n'est pas régulé correctement, ils peuvent devenir pathogéniques. En effet, les lymphocytes Th ont été décrits dans un grand nombre de maladies. Ici j'ai présenté trois projets étudiant différents aspects de la polarisation Th : 1) la polarisation de lymphocytes Tfh induite par les DC activées par la TSLP, 2) l'étude approfondie de la polarisation Th en réponse à la combinatoire de molécules de communication DC et 3) l'évolution des populations de lymphocytes Th et Tfh comme biomarqueurs supposés de la réponse au traitement de l'AD.

Nos travaux sur la polarisation de lymphocytes Tfh par les DC activées par la TSLP apporte des connaissances nouvelles pour la compréhension de l'émergence de lymphocytes Tfh dans des environnements Th2, tels que l'allergie [196]. Il a été montré que la polarisation de lymphocytes Tfh était induite par l'IL-12 [197], mais aussi par l'IL-23 et le TGF- β [145]. De plus, l'IL-4, cytokine prototypique des lymphocytes Th2, est connue pour inhiber la polarisation des lymphocytes Tfh [145]. Il est donc assez surprenant que des lymphocytes Tfh puissent se différencier dans des conditions Th2 en présence d'IL-4, et il était donc inattendu d'identifier des lymphocytes Tfh aux côtés des lymphocytes Th2 induits par les DC activées par la TSLP. Cette étude permet donc la compréhension de la présence de lymphocytes Tfh dans les environnements Th2 mais apporte aussi un mécanisme responsable de la polarisation des lymphocytes Tfh, via OX40L.

Notre modèle statistique capable de prédire les réponses Th en fonction des molécules DC apparaît comme un outil puissant pour prédire l'impact des molécules de communication DC sur les réponses lymphocytaires Th. Il permet non seulement de prédire l'influence d'une molécule DC seule, mais aussi d'une molécule DC dans différents contextes. Il apparaît donc comme une ressource importante pour la communauté scientifique non seulement pour étudier la communication entre DC et lymphocytes Th mais aussi de manière plus générale la communication entre deux cellules quelles qu'elles soient. On pourrait également imaginer utiliser cette stratégie pour prédire l'impact d'immunothérapies ciblant une ou plusieurs molécules au niveau des DC sur la réponse lymphocytaire Th et ainsi choisir la meilleure combinaison de molécules à évaluer dans différentes pathologies.

Notre étude sur la cohorte de patients AD traités par Dupilumab montre qu'il est possible de suivre l'évolution des populations Th dans le sang périphérique. En effet, grâce à un marquage de surface simple de cinq marqueurs nous avons pu suivre par cytométrie en flux huit populations de lymphocytes Th et Tfh chez ces patients traités par Dupilumab et ainsi mesurer leurs variations au cours du traitement. Nous avons également pu montrer que la diminution du pourcentage de lymphocytes Th17 mesurées au cours du traitement par Dupilumab corrélait avec une diminution du score clinique EASI. Ce travail suggère que les sous-populations de lymphocytes Th pourraient être utilisées comme biomarqueurs de la réponse au traitement par immunothérapie chez les patients atteints d'AD.

REFERENCES

1. Mosmann, T.R., H. Cherwinski, M.W. Bond, M.A. Giedlin, and R.L. Coffman, *Two types of murine helper T cell clone. I. Definition according to profiles of lymphokine activities and secreted proteins*. J Immunol, 1986. **136**(7): p. 2348-57.
2. Mosmann, T.R. and R.L. Coffman, *Heterogeneity of cytokine secretion patterns and functions of helper T cells*. Adv Immunol, 1989. **46**: p. 111-47.
3. Szabo, S.J., S.T. Kim, G.L. Costa, X. Zhang, C.G. Fathman, and L.H. Glimcher, *Pillars article: A novel transcription factor, T-bet, directs Th1 lineage commitment*. Cell. 2000. **100**: 655-669. J Immunol, 2015. **194**(7): p. 2961-75.
4. Szabo, S.J., B.M. Sullivan, S.L. Peng, and L.H. Glimcher, *Molecular mechanisms regulating Th1 immune responses*. Annu Rev Immunol, 2003. **21**: p. 713-58.
5. Zhu, J., *T helper 2 (Th2) cell differentiation, type 2 innate lymphoid cell (ILC2) development and regulation of interleukin-4 (IL-4) and IL-13 production*. Cytokine, 2015. **75**(1): p. 14-24.
6. Usui, T., R. Nishikomori, A. Kitani, and W. Strober, *GATA-3 suppresses Th1 development by downregulation of Stat4 and not through effects on IL-12Rbeta2 chain or T-bet*. Immunity, 2003. **18**(3): p. 415-28.
7. Usui, T., J.C. Preiss, Y. Kanno, Z.J. Yao, J.H. Bream, J.J. O'Shea, and W. Strober, *T-bet regulates Th1 responses through essential effects on GATA-3 function rather than on IFNG gene acetylation and transcription*. J Exp Med, 2006. **203**(3): p. 755-66.
8. Djuretic, I.M., D. Levanon, V. Negreanu, Y. Groner, A. Rao, and K.M. Ansel, *Transcription factors T-bet and Runx3 cooperate to activate Ifng and silence Il4 in T helper type 1 cells*. Nat Immunol, 2007. **8**(2): p. 145-53.
9. Zhang, Y., Y. Zhang, W. Gu, and B. Sun, *TH1/TH2 cell differentiation and molecular signals*. Adv Exp Med Biol, 2014. **841**: p. 15-44.
10. Sallusto, F., D. Lenig, C.R. Mackay, and A. Lanzavecchia, *Flexible programs of chemokine receptor expression on human polarized T helper 1 and 2 lymphocytes*. J Exp Med, 1998. **187**(6): p. 875-83.
11. O'Garra, A., L.M. McEvoy, and A. Zlotnik, *T-cell subsets: chemokine receptors guide the way*. Curr Biol, 1998. **8**(18): p. R646-9.
12. Cosmi, L., F. Annunziato, M.I.G. Galli, R.M.E. Maggi, K. Nagata, and S. Romagnani, *CRTH2 is the most reliable marker for the detection of circulating human type 2 Th and type 2 T cytotoxic cells in health and disease*. Eur J Immunol, 2000. **30**(10): p. 2972-9.
13. Hohl, T.M., *6 - Cell-Mediated Defense against Infection*. Mandell, Douglas, and Bennett's Principles and Practice of Infectious Diseases (Eighth Edition),. 2015.
14. Gordon, S., *Alternative activation of macrophages*. Nat Rev Immunol, 2003. **3**(1): p. 23-35.
15. Coffman, R.L., B.W. Seymour, S. Hudak, J. Jackson, and D. Rennick, *Antibody to interleukin-5 inhibits helminth-induced eosinophilia in mice*. Science, 1989. **245**(4915): p. 308-10.
16. Harrington, L.E., R.D. Hatton, P.R. Mangan, H. Turner, T.L. Murphy, K.M. Murphy, and C.T. Weaver, *Interleukin 17-producing CD4+ effector T cells develop via a lineage distinct from the T helper type 1 and 2 lineages*. Nat Immunol, 2005. **6**(11): p. 1123-32.
17. Annunziato, F., L. Cosmi, F. Liotta, E. Maggi, and S. Romagnani, *Defining the human T helper 17 cell phenotype*. Trends Immunol, 2012. **33**(10): p. 505-12.
18. Wacleche, V.S., A. Landay, J.P. Routy, and P. Ancuta, *The Th17 Lineage: From Barrier Surfaces Homeostasis to Autoimmunity, Cancer, and HIV-1 Pathogenesis*. Viruses, 2017. **9**(10).

19. Song, X., H. Gao, and Y. Qian, *Th17 differentiation and their pro-inflammation function*. Adv Exp Med Biol, 2014. **841**: p. 99-151.
20. Duhon, T., R. Geiger, D. Jarrossay, A. Lanzavecchia, and F. Sallusto, *Production of interleukin 22 but not interleukin 17 by a subset of human skin-homing memory T cells*. Nat Immunol, 2009. **10**(8): p. 857-63.
21. Trifari, S., C.D. Kaplan, E.H. Tran, N.K. Crellin, and H. Spits, *Identification of a human helper T cell population that has abundant production of interleukin 22 and is distinct from T(H)-17, T(H)1 and T(H)2 cells*. Nat Immunol, 2009. **10**(8): p. 864-71.
22. Jia, L. and C. Wu, *The biology and functions of Th22 cells*. Adv Exp Med Biol, 2014. **841**: p. 209-30.
23. Schmitt, E., R. Van Brandwijk, H.G. Fischer, and E. Rude, *Establishment of different T cell sublines using either interleukin 2 or interleukin 4 as growth factors*. Eur J Immunol, 1990. **20**(8): p. 1709-15.
24. Angkasekwina, P., S.H. Chang, M. Thapa, H. Watarai, and C. Dong, *Regulation of IL-9 expression by IL-25 signaling*. Nat Immunol, 2010. **11**(3): p. 250-6.
25. Li, J., S. Chen, X. Xiao, Y. Zhao, W. Ding, and X.C. Li, *IL-9 and Th9 cells in health and diseases-From tolerance to immunopathology*. Cytokine Growth Factor Rev, 2017. **37**: p. 47-55.
26. Clark, R.A. and C. Schlapbach, *TH9 cells in skin disorders*. Semin Immunopathol, 2017. **39**(1): p. 47-54.
27. Piccioni, M., Z. Chen, A. Tsun, and B. Li, *Regulatory T-cell differentiation and their function in immune regulation*. Adv Exp Med Biol, 2014. **841**: p. 67-97.
28. Bilate, A.M. and J.J. Lafaille, *Induced CD4+Foxp3+ regulatory T cells in immune tolerance*. Annu Rev Immunol, 2012. **30**: p. 733-58.
29. Mohr, A., M. Atif, R. Balderas, G. Gorochoy, and M. Miyara, *The role of FOXP3(+) regulatory T cells in human autoimmune and inflammatory diseases*. Clin Exp Immunol, 2019. **197**(1): p. 24-35.
30. Schaerli, P., K. Willmann, A.B. Lang, M. Lipp, P. Loetscher, and B. Moser, *CXC chemokine receptor 5 expression defines follicular homing T cells with B cell helper function*. J Exp Med, 2000. **192**(11): p. 1553-62.
31. Kim, C.H., L.S. Rott, I. Clark-Lewis, D.J. Campbell, L. Wu, and E.C. Butcher, *Subspecialization of CXCR5+ T cells: B helper activity is focused in a germinal center-localized subset of CXCR5+ T cells*. J Exp Med, 2001. **193**(12): p. 1373-81.
32. Breitfeld, D., L. Ohl, E. Kremmer, J. Ellwart, F. Sallusto, M. Lipp, and R. Forster, *Follicular B helper T cells express CXC chemokine receptor 5, localize to B cell follicles, and support immunoglobulin production*. J Exp Med, 2000. **192**(11): p. 1545-52.
33. Ma, C.S., E.K. Deenick, M. Batten, and S.G. Tangye, *The origins, function, and regulation of T follicular helper cells*. J Exp Med, 2012. **209**(7): p. 1241-53.
34. Crotty, S., R.J. Johnston, and S.P. Schoenberger, *Effectors and memories: Bcl-6 and Blimp-1 in T and B lymphocyte differentiation*. Nat Immunol, 2010. **11**(2): p. 114-20.
35. Crotty, S., *Follicular helper CD4 T cells (TFH)*. Annu Rev Immunol, 2011. **29**: p. 621-63.
36. Schmitt, N. and H. Ueno, *Human T follicular helper cells: development and subsets*. Adv Exp Med Biol, 2013. **785**: p. 87-94.
37. Vinuesa, C.G., M.A. Linterman, D. Yu, and I.C. MacLennan, *Follicular Helper T Cells*. Annu Rev Immunol, 2016. **34**: p. 335-68.

38. Ueno, H., J. Banchereau, and C.G. Vinuesa, *Pathophysiology of T follicular helper cells in humans and mice*. Nat Immunol, 2015. **16**(2): p. 142-52.
39. Sage, P.T. and A.H. Sharpe, *T follicular regulatory cells in the regulation of B cell responses*. Trends Immunol, 2015. **36**(7): p. 410-8.
40. Zhu, Y., L. Zou, and Y.C. Liu, *T follicular helper cells, T follicular regulatory cells and autoimmunity*. Int Immunol, 2016. **28**(4): p. 173-9.
41. King, I.L. and M. Mohrs, *IL-4-producing CD4+ T cells in reactive lymph nodes during helminth infection are T follicular helper cells*. J Exp Med, 2009. **206**(5): p. 1001-7.
42. Reinhardt, R.L., H.E. Liang, and R.M. Locksley, *Cytokine-secreting follicular T cells shape the antibody repertoire*. Nat Immunol, 2009. **10**(4): p. 385-93.
43. Glatman Zaretsky, A., J.J. Taylor, I.L. King, F.A. Marshall, M. Mohrs, and E.J. Pearce, *T follicular helper cells differentiate from Th2 cells in response to helminth antigens*. J Exp Med, 2009. **206**(5): p. 991-9.
44. Bauquet, A.T., H. Jin, A.M. Paterson, M. Mitsdoerffer, I.C. Ho, A.H. Sharpe, and V.K. Kuchroo, *The costimulatory molecule ICOS regulates the expression of c-Maf and IL-21 in the development of follicular T helper cells and TH-17 cells*. Nat Immunol, 2009. **10**(2): p. 167-75.
45. Morita, R., N. Schmitt, S.E. Bentebibel, R. Ranganathan, L. Bourdery, G. Zurawski, E. Foucat, M. Dullaers, S. Oh, N. Sabzghabaei, E.M. Lavecchio, M. Punaro, V. Pascual, J. Banchereau, and H. Ueno, *Human blood CXCR5(+)CD4(+) T cells are counterparts of T follicular cells and contain specific subsets that differentially support antibody secretion*. Immunity, 2011. **34**(1): p. 108-21.
46. Schmitt, N. and H. Ueno, *Blood Tfh cells come with colors*. Immunity, 2013. **39**(4): p. 629-30.
47. He, J., L.M. Tsai, Y.A. Leong, X. Hu, C.S. Ma, N. Chevalier, X. Sun, K. Vandenberg, S. Rockman, Y. Ding, L. Zhu, W. Wei, C. Wang, A. Karnowski, G.T. Belz, J.R. Ghali, M.C. Cook, D.S. Riminton, A. Veillette, P.L. Schwartzberg, F. Mackay, R. Brink, S.G. Tangye, C.G. Vinuesa, C.R. Mackay, Z. Li, and D. Yu, *Circulating precursor CCR7(lo)PD-1(hi) CXCR5(+) CD4(+) T cells indicate Tfh cell activity and promote antibody responses upon antigen reexposure*. Immunity, 2013. **39**(4): p. 770-81.
48. Locci, M., C. Havenar-Daughton, E. Landais, J. Wu, M.A. Kroenke, C.L. Arlehamn, L.F. Su, R. Cubas, M.M. Davis, A. Sette, E.K. Haddad, A.V.I.P.C.P.I. International, P. Poignard, and S. Crotty, *Human circulating PD-1+CXCR3-CXCR5+ memory Tfh cells are highly functional and correlate with broadly neutralizing HIV antibody responses*. Immunity, 2013. **39**(4): p. 758-69.
49. Schmitt, N., S.E. Bentebibel, and H. Ueno, *Phenotype and functions of memory Tfh cells in human blood*. Trends Immunol, 2014. **35**(9): p. 436-42.
50. Rao, D.A., M.F. Gurish, J.L. Marshall, K. Slowikowski, C.Y. Fonseka, Y. Liu, L.T. Donlin, L.A. Henderson, K. Wei, F. Mizoguchi, N.C. Teslovich, M.E. Weinblatt, E.M. Massarotti, J.S. Coblyn, S.M. Helfgott, Y.C. Lee, D.J. Todd, V.P. Bykerk, S.M. Goodman, A.B. Pernis, L.B. Ivashkiv, E.W. Karlson, P.A. Nigrovic, A. Filer, C.D. Buckley, J.A. Lederer, S. Raychaudhuri, and M.B. Brenner, *Pathologically expanded peripheral T helper cell subset drives B cells in rheumatoid arthritis*. Nature, 2017. **542**(7639): p. 110-114.
51. Caielli, S., D.T. Veiga, P. Balasubramanian, S. Athale, B. Domic, E. Murat, R. Banchereau, Z. Xu, M. Chandra, C.H. Chung, L. Walters, J. Baisch, T. Wright, M. Punaro, L. Nassi, K. Stewart, J. Fuller, D. Ucar, H. Ueno, J. Zhou, J. Banchereau, and V. Pascual, *A CD4(+) T cell population expanded in lupus blood provides B cell help through interleukin-10 and succinate*. Nat Med, 2019. **25**(1): p. 75-81.

52. Annunziato, F., L. Cosmi, V. Santarlasci, L. Maggi, F. Liotta, B. Mazzinghi, E. Parente, L. Fili, S. Ferri, F. Frosali, F. Giudici, P. Romagnani, P. Parronchi, F. Tonelli, E. Maggi, and S. Romagnani, *Phenotypic and functional features of human Th17 cells*. J Exp Med, 2007. **204**(8): p. 1849-61.
53. Cosmi, L., R. Cimaz, L. Maggi, V. Santarlasci, M. Capone, F. Borriello, F. Frosali, V. Querci, G. Simonini, G. Barra, M.P. Piccinni, F. Liotta, R. De Palma, E. Maggi, S. Romagnani, and F. Annunziato, *Evidence of the transient nature of the Th17 phenotype of CD4+CD161+ T cells in the synovial fluid of patients with juvenile idiopathic arthritis*. Arthritis Rheum, 2011. **63**(8): p. 2504-15.
54. Maggi, L., V. Santarlasci, M. Capone, M.C. Rossi, V. Querci, A. Mazzoni, R. Cimaz, R. De Palma, F. Liotta, E. Maggi, S. Romagnani, L. Cosmi, and F. Annunziato, *Distinctive features of classic and nonclassic (Th17 derived) human Th1 cells*. Eur J Immunol, 2012. **42**(12): p. 3180-8.
55. Cosmi, L., L. Maggi, V. Santarlasci, M. Capone, E. Cardilicchia, F. Frosali, V. Querci, R. Angeli, A. Matucci, M. Fambrini, F. Liotta, P. Parronchi, E. Maggi, S. Romagnani, and F. Annunziato, *Identification of a novel subset of human circulating memory CD4(+) T cells that produce both IL-17A and IL-4*. J Allergy Clin Immunol, 2010. **125**(1): p. 222-30 e1-4.
56. Beriou, G., E.M. Bradshaw, E. Lozano, C.M. Costantino, W.D. Hastings, T. Orban, W. Elyaman, S.J. Khoury, V.K. Kuchroo, C. Baecher-Allan, and D.A. Hafler, *TGF-beta induces IL-9 production from human Th17 cells*. J Immunol, 2010. **185**(1): p. 46-54.
57. Geginat, J., M. Paroni, S. Maglie, J.S. Alfen, I. Kastirr, P. Gruarin, M. De Simone, M. Pagani, and S. Abrignani, *Plasticity of human CD4 T cell subsets*. Front Immunol, 2014. **5**: p. 630.
58. Wang, Y.H., K.S. Voo, B. Liu, C.Y. Chen, B. Uygungil, W. Spoede, J.A. Bernstein, D.P. Huston, and Y.J. Liu, *A novel subset of CD4(+) T(H)2 memory/effector cells that produce inflammatory IL-17 cytokine and promote the exacerbation of chronic allergic asthma*. J Exp Med, 2010. **207**(11): p. 2479-91.
59. Hegazy, A.N., M. Peine, C. Helmstetter, I. Panse, A. Frohlich, A. Bergthaler, L. Flatz, D.D. Pinschewer, A. Radbruch, and M. Lohning, *Interferons direct Th2 cell reprogramming to generate a stable GATA-3(+)T-bet(+) cell subset with combined Th2 and Th1 cell functions*. Immunity, 2010. **32**(1): p. 116-28.
60. Ballesteros-Tato, A., T.D. Randall, F.E. Lund, R. Spolski, W.J. Leonard, and B. Leon, *T Follicular Helper Cell Plasticity Shapes Pathogenic T Helper 2 Cell-Mediated Immunity to Inhaled House Dust Mite*. Immunity, 2016. **44**(2): p. 259-73.
61. Duhon, T., R. Duhon, A. Lanzavecchia, F. Sallusto, and D.J. Campbell, *Functionally distinct subsets of human FOXP3+ Treg cells that phenotypically mirror effector Th cells*. Blood, 2012. **119**(19): p. 4430-40.
62. Mason, G.M., K. Lowe, R. Melchiotti, R. Ellis, E. de Rinaldis, M. Peakman, S. Heck, G. Lombardi, and T.I. Tree, *Phenotypic Complexity of the Human Regulatory T Cell Compartment Revealed by Mass Cytometry*. J Immunol, 2015. **195**(5): p. 2030-7.
63. Kunicki, M.A., L.C. Amaya Hernandez, K.L. Davis, R. Bacchetta, and M.G. Roncarolo, *Identity and Diversity of Human Peripheral Th and T Regulatory Cells Defined by Single-Cell Mass Cytometry*. J Immunol, 2018. **200**(1): p. 336-346.
64. Barcenilla, H., L. Akerman, M. Pihl, J. Ludvigsson, and R. Casas, *Mass Cytometry Identifies Distinct Subsets of Regulatory T Cells and Natural Killer Cells Associated With High Risk for Type 1 Diabetes*. Front Immunol, 2019. **10**: p. 982.
65. Wong, M.T., D.E. Ong, F.S. Lim, K.W. Teng, N. McGovern, S. Narayanan, W.Q. Ho, D. Cerny, H.K. Tan, R. Anicete, B.K. Tan, T.K. Lim, C.Y. Chan, P.C. Cheow, S.Y. Lee, A. Takano, E.H. Tan, J.K. Tam, E.Y. Tan, J.K. Chan, K. Fink, A. Bertoletti, F. Ginhoux, M.A. Curotto de Lafaille, and E.W. Newell,

- A High-Dimensional Atlas of Human T Cell Diversity Reveals Tissue-Specific Trafficking and Cytokine Signatures.* *Immunity*, 2016. **45**(2): p. 442-56.
66. Banchereau, J. and R.M. Steinman, *Dendritic cells and the control of immunity.* *Nature*, 1998. **392**(6673): p. 245-52.
 67. Cella, M., F. Sallusto, and A. Lanzavecchia, *Origin, maturation and antigen presenting function of dendritic cells.* *Curr Opin Immunol*, 1997. **9**(1): p. 10-6.
 68. Steinman, R.M., *The dendritic cell system and its role in immunogenicity.* *Annu Rev Immunol*, 1991. **9**: p. 271-96.
 69. Summers deLuca, L. and J.L. Gommerman, *Fine-tuning of dendritic cell biology by the TNF superfamily.* *Nat Rev Immunol*, 2012. **12**(5): p. 339-51.
 70. See, P., C.A. Dutertre, J. Chen, P. Gunther, N. McGovern, S.E. Irac, M. Gunawan, M. Beyer, K. Handler, K. Duan, H.R.B. Sumatoh, N. Ruffin, M. Jouve, E. Gea-Mallorqui, R.C.M. Hennekam, T. Lim, C.C. Yip, M. Wen, B. Malleret, I. Low, N.B. Shadan, C.F.S. Fen, A. Tay, J. Lum, F. Zolezzi, A. Larbi, M. Poidinger, J.K.Y. Chan, Q. Chen, L. Renia, M. Haniffa, P. Benaroch, A. Schlitzer, J.L. Schultze, E.W. Newell, and F. Ginhoux, *Mapping the human DC lineage through the integration of high-dimensional techniques.* *Science*, 2017. **356**(6342).
 71. Boltjes, A. and F. van Wijk, *Human dendritic cell functional specialization in steady-state and inflammation.* *Front Immunol*, 2014. **5**: p. 131.
 72. Dutertre, C.A., E. Becht, S.E. Irac, A. Khalilnezhad, V. Narang, S. Khalilnezhad, P.Y. Ng, L.L. van den Hoogen, J.Y. Leong, B. Lee, M. Chevrier, X.M. Zhang, P.J.A. Yong, G. Koh, J. Lum, S.W. Howland, E. Mok, J. Chen, A. Larbi, H.K.K. Tan, T.K.H. Lim, P. Karagianni, A.G. Tzioufas, B. Malleret, J. Brody, S. Albani, J. van Roon, T. Radstake, E.W. Newell, and F. Ginhoux, *Single-Cell Analysis of Human Mononuclear Phagocytes Reveals Subset-Defining Markers and Identifies Circulating Inflammatory Dendritic Cells.* *Immunity*, 2019.
 73. Schlitzer, A. and F. Ginhoux, *Organization of the mouse and human DC network.* *Curr Opin Immunol*, 2014. **26**: p. 90-9.
 74. Haniffa, M., M. Collin, and F. Ginhoux, *Ontogeny and functional specialization of dendritic cells in human and mouse.* *Adv Immunol*, 2013. **120**: p. 1-49.
 75. Wollenberg, A., S. Kraft, D. Hanau, and T. Bieber, *Immunomorphological and ultrastructural characterization of Langerhans cells and a novel, inflammatory dendritic epidermal cell (IDEC) population in lesional skin of atopic eczema.* *J Invest Dermatol*, 1996. **106**(3): p. 446-53.
 76. Leon, B., M. Lopez-Bravo, and C. Ardavin, *Monocyte-derived dendritic cells formed at the infection site control the induction of protective T helper 1 responses against Leishmania.* *Immunity*, 2007. **26**(4): p. 519-31.
 77. Segura, E., M. Touzot, A. Bohineust, A. Cappuccio, G. Chiocchia, A. Hosmalin, M. Dalod, V. Soumelis, and S. Amigorena, *Human inflammatory dendritic cells induce Th17 cell differentiation.* *Immunity*, 2013. **38**(2): p. 336-48.
 78. Tang-Huau, T.L. and E. Segura, *Human in vivo-differentiated monocyte-derived dendritic cells.* *Semin Cell Dev Biol*, 2019. **86**: p. 44-49.
 79. Sallusto, F. and A. Lanzavecchia, *Efficient presentation of soluble antigen by cultured human dendritic cells is maintained by granulocyte/macrophage colony-stimulating factor plus interleukin 4 and downregulated by tumor necrosis factor alpha.* *J Exp Med*, 1994. **179**(4): p. 1109-18.
 80. MacDonald, K.P., D.J. Munster, G.J. Clark, A. Dzionek, J. Schmitz, and D.N. Hart, *Characterization of human blood dendritic cell subsets.* *Blood*, 2002. **100**(13): p. 4512-20.

81. Villani, A.C., R. Satija, G. Reynolds, S. Sarkizova, K. Shekhar, J. Fletcher, M. Griesbeck, A. Butler, S. Zheng, S. Lazo, L. Jardine, D. Dixon, E. Stephenson, E. Nilsson, I. Grundberg, D. McDonald, A. Filby, W. Li, P.L. De Jager, O. Rozenblatt-Rosen, A.A. Lane, M. Haniffa, A. Regev, and N. Hacohen, *Single-cell RNA-seq reveals new types of human blood dendritic cells, monocytes, and progenitors*. *Science*, 2017. **356**(6335).
82. Yin, X., H. Yu, X. Jin, J. Li, H. Guo, Q. Shi, Z. Yin, Y. Xu, X. Wang, R. Liu, S. Wang, and L. Zhang, *Human Blood CD1c+ Dendritic Cells Encompass CD5high and CD5low Subsets That Differ Significantly in Phenotype, Gene Expression, and Functions*. *J Immunol*, 2017. **198**(4): p. 1553-1564.
83. Alcantara-Hernandez, M., R. Leylek, L.E. Wagar, E.G. Engleman, T. Keler, M.P. Marinkovich, M.M. Davis, G.P. Nolan, and J. Idoyaga, *High-Dimensional Phenotypic Mapping of Human Dendritic Cells Reveals Interindividual Variation and Tissue Specialization*. *Immunity*, 2017. **47**(6): p. 1037-1050 e6.
84. Klechevsky, E., R. Morita, M. Liu, Y. Cao, S. Coquery, L. Thompson-Snipes, F. Briere, D. Chaussabel, G. Zurawski, A.K. Palucka, Y. Reiter, J. Banchereau, and H. Ueno, *Functional specializations of human epidermal Langerhans cells and CD14+ dermal dendritic cells*. *Immunity*, 2008. **29**(3): p. 497-510.
85. Furio, L., I. Briotet, A. Journeaux, H. Billard, and J. Peguet-Navarro, *Human langerhans cells are more efficient than CD14(-)CD1c(+) dermal dendritic cells at priming naive CD4(+) T cells*. *J Invest Dermatol*, 2010. **130**(5): p. 1345-54.
86. Fujita, H., K.E. Nograles, T. Kikuchi, J. Gonzalez, J.A. Carucci, and J.G. Krueger, *Human Langerhans cells induce distinct IL-22-producing CD4+ T cells lacking IL-17 production*. *Proc Natl Acad Sci U S A*, 2009. **106**(51): p. 21795-800.
87. Penel-Sotirakis, K., E. Simonazzi, J. Peguet-Navarro, and A. Rozieres, *Differential capacity of human skin dendritic cells to polarize CD4+ T cells into IL-17, IL-21 and IL-22 producing cells*. *PLoS One*, 2012. **7**(11): p. e45680.
88. Segura, E., J. Valladeau-Guilemond, M.H. Donnadieu, X. Sastre-Garau, V. Soumelis, and S. Amigorena, *Characterization of resident and migratory dendritic cells in human lymph nodes*. *J Exp Med*, 2012. **209**(4): p. 653-60.
89. Durand, M., T. Walter, T. Pirnay, T. Naessens, P. Gueguen, C. Goudot, S. Lameiras, Q. Chang, N. Talaei, O. Ornatsky, T. Vassilevskaia, S. Baulande, S. Amigorena, and E. Segura, *Human lymphoid organ cDC2 and macrophages play complementary roles in T follicular helper responses*. *J Exp Med*, 2019.
90. Yu, C.I., C. Becker, P. Metang, F. Marches, Y. Wang, H. Toshiyuki, J. Banchereau, M. Merad, and A.K. Palucka, *Human CD141+ dendritic cells induce CD4+ T cells to produce type 2 cytokines*. *J Immunol*, 2014. **193**(9): p. 4335-43.
91. Diebold, S.S., *Activation of dendritic cells by toll-like receptors and C-type lectins*. *Handb Exp Pharmacol*, 2009(188): p. 3-30.
92. Roh, J.S. and D.H. Sohn, *Damage-Associated Molecular Patterns in Inflammatory Diseases*. *Immune Netw*, 2018. **18**(4): p. e27.
93. Takeda, K. and S. Akira, *Toll-like receptors*. *Curr Protoc Immunol*, 2015. **109**: p. 14 12 1-10.
94. Geijtenbeek, T.B. and S.I. Gringhuis, *C-type lectin receptors in the control of T helper cell differentiation*. *Nat Rev Immunol*, 2016. **16**(7): p. 433-48.
95. Shiokawa, M., S. Yamasaki, and S. Saijo, *C-type lectin receptors in anti-fungal immunity*. *Curr Opin Microbiol*, 2017. **40**: p. 123-130.

96. Szabo, A. and E. Rajnavolgyi, *Collaboration of Toll-like and RIG-I-like receptors in human dendritic cells: tRIGgering antiviral innate immune responses*. Am J Clin Exp Immunol, 2013. **2**(3): p. 195-207.
97. Loo, Y.M. and M. Gale, Jr., *Immune signaling by RIG-I-like receptors*. Immunity, 2011. **34**(5): p. 680-92.
98. Krishnaswamy, J.K., T. Chu, and S.C. Eisenbarth, *Beyond pattern recognition: NOD-like receptors in dendritic cells*. Trends Immunol, 2013. **34**(5): p. 224-33.
99. Ferreira, I., J. Liberal, J.D. Martins, A. Silva, B.M. Neves, and M.T. Cruz, *Inflammasome in Dendritic Cells Immunobiology: Implications to Diseases and Therapeutic Strategies*. Curr Drug Targets, 2017. **18**(9): p. 1003-1018.
100. Latz, E., T.S. Xiao, and A. Stutz, *Activation and regulation of the inflammasomes*. Nat Rev Immunol, 2013. **13**(6): p. 397-411.
101. Nakaya, Y., J. Lilue, S. Stavrou, E.A. Moran, and S.R. Ross, *AIM2-Like Receptors Positively and Negatively Regulate the Interferon Response Induced by Cytosolic DNA*. MBio, 2017. **8**(4).
102. Sorrentino, R., M. Terlizzi, V.G. Di Crescenzo, A. Popolo, M. Pecoraro, G. Perillo, A. Galderisi, and A. Pinto, *Human lung cancer-derived immunosuppressive plasmacytoid dendritic cells release IL-1alpha in an AIM2 inflammasome-dependent manner*. Am J Pathol, 2015. **185**(11): p. 3115-24.
103. Eichholz, K., T. Bru, T.T. Tran, P. Fernandes, H. Welles, F.J. Mennechet, N. Manel, P. Alves, M. Perreau, and E.J. Kremer, *Immune-Complexed Adenovirus Induce AIM2-Mediated Pyroptosis in Human Dendritic Cells*. PLoS Pathog, 2016. **12**(9): p. e1005871.
104. Chen, K., Z. Bao, W. Gong, P. Tang, T. Yoshimura, and J.M. Wang, *Regulation of inflammation by members of the formyl-peptide receptor family*. J Autoimmun, 2017. **85**: p. 64-77.
105. Karlsson, A., E. Nygren, J. Karlsson, I. Nordstrom, C. Dahlgren, and K. Eriksson, *Ability of monocyte-derived dendritic cells to secrete oxygen radicals in response to formyl peptide receptor family agonists compared to that of myeloid and plasmacytoid dendritic cells*. Clin Vaccine Immunol, 2007. **14**(3): p. 328-30.
106. Hemont, C., A. Neel, M. Heslan, C. Braudeau, and R. Josien, *Human blood mDC subsets exhibit distinct TLR repertoire and responsiveness*. J Leukoc Biol, 2013. **93**(4): p. 599-609.
107. Krug, A., A. Towarowski, S. Britsch, S. Rothenfusser, V. Hornung, R. Bals, T. Giese, H. Engelmann, S. Endres, A.M. Krieg, and G. Hartmann, *Toll-like receptor expression reveals CpG DNA as a unique microbial stimulus for plasmacytoid dendritic cells which synergizes with CD40 ligand to induce high amounts of IL-12*. Eur J Immunol, 2001. **31**(10): p. 3026-37.
108. Flacher, V., M. Bouschbacher, E. Verronese, C. Massacrier, V. Sisirak, O. Berthier-Vergnes, B. de Saint-Vis, C. Caux, C. Dezutter-Dambuyant, S. Lebecque, and J. Valladeau, *Human Langerhans cells express a specific TLR profile and differentially respond to viruses and Gram-positive bacteria*. J Immunol, 2006. **177**(11): p. 7959-67.
109. Kadowaki, N., S. Ho, S. Antonenko, R.W. Malefyt, R.A. Kastelein, F. Bazan, and Y.J. Liu, *Subsets of human dendritic cell precursors express different toll-like receptors and respond to different microbial antigens*. J Exp Med, 2001. **194**(6): p. 863-9.
110. Raieli, S., C. Trichot, S. Korniotis, L. Pattarini, and V. Soumelis, *TLR1/2 orchestrate human plasmacytoid predendritic cell response to gram+ bacteria*. PLoS Biol, 2019. **17**(4): p. e3000209.
111. Muzio, M., D. Bosisio, N. Polentarutti, G. D'Amico, A. Stoppacciaro, R. Mancinelli, C. van't Veer, G. Penton-Rol, L.P. Ruco, P. Allavena, and A. Mantovani, *Differential expression and regulation of toll-like receptors (TLR) in human leukocytes: selective expression of TLR3 in dendritic cells*. J Immunol, 2000. **164**(11): p. 5998-6004.

112. Means, T.K., F. Hayashi, K.D. Smith, A. Aderem, and A.D. Luster, *The Toll-like receptor 5 stimulus bacterial flagellin induces maturation and chemokine production in human dendritic cells*. J Immunol, 2003. **170**(10): p. 5165-75.
113. Renn, C.N., D.J. Sanchez, M.T. Ochoa, A.J. Legaspi, C.K. Oh, P.T. Liu, S.R. Krutzik, P.A. Sieling, G. Cheng, and R.L. Modlin, *TLR activation of Langerhans cell-like dendritic cells triggers an antiviral immune response*. J Immunol, 2006. **177**(1): p. 298-305.
114. Lindstedt, M., K. Lundberg, and C.A. Borrebaeck, *Gene family clustering identifies functionally associated subsets of human in vivo blood and tonsillar dendritic cells*. J Immunol, 2005. **175**(8): p. 4839-46.
115. Matsumoto, M., K. Funami, M. Tanabe, H. Oshiumi, M. Shingai, Y. Seto, A. Yamamoto, and T. Seya, *Subcellular localization of Toll-like receptor 3 in human dendritic cells*. J Immunol, 2003. **171**(6): p. 3154-62.
116. Ito, T., R. Amakawa, T. Kaisho, H. Hemmi, K. Tajima, K. Uehira, Y. Ozaki, H. Tomizawa, S. Akira, and S. Fukuhara, *Interferon-alpha and interleukin-12 are induced differentially by Toll-like receptor 7 ligands in human blood dendritic cell subsets*. J Exp Med, 2002. **195**(11): p. 1507-12.
117. Lundberg, K., F. Rydnert, L. Greiff, and M. Lindstedt, *Human blood dendritic cell subsets exhibit discriminative pattern recognition receptor profiles*. Immunology, 2014. **142**(2): p. 279-88.
118. Hefter, M., J. Lothar, E. Weiss, A.L. Schmitt, M. Fliesser, H. Einsele, and J. Loeffler, *Human primary myeloid dendritic cells interact with the opportunistic fungal pathogen *Aspergillus fumigatus* via the C-type lectin receptor Dectin-1*. Med Mycol, 2017. **55**(5): p. 573-578.
119. van Haren, S.D., D.J. Dowling, W. Foppen, D. Christensen, P. Andersen, S.G. Reed, R.M. Hershberg, L.R. Baden, and O. Levy, *Age-Specific Adjuvant Synergy: Dual TLR7/8 and Mincle Activation of Human Newborn Dendritic Cells Enables Th1 Polarization*. J Immunol, 2016. **197**(11): p. 4413-4424.
120. Hole, C.R., C.M. Leopold Wager, A.S. Mendiola, K.L. Wozniak, A. Campuzano, X. Lin, and F.L. Wormley, Jr., *Antifungal Activity of Plasmacytoid Dendritic Cells against *Cryptococcus neoformans* In Vitro Requires Expression of Dectin-3 (CLEC4D) and Reactive Oxygen Species*. Infect Immun, 2016. **84**(9): p. 2493-504.
121. Dzionek, A., A. Fuchs, P. Schmidt, S. Cremer, M. Zysk, S. Miltenyi, D.W. Buck, and J. Schmitz, *BDCA-2, BDCA-3, and BDCA-4: three markers for distinct subsets of dendritic cells in human peripheral blood*. J Immunol, 2000. **165**(11): p. 6037-46.
122. van Dalen, R., J.S. De La Cruz Diaz, M. Rumpret, F.F. Fuchsberger, N.H. van Teijlingen, J. Hanske, C. Rademacher, T.B.H. Geijtenbeek, J.A.G. van Strijp, C. Weidenmaier, A. Peschel, D.H. Kaplan, and N.M. van Sorge, *Langerhans Cells Sense *Staphylococcus aureus* Wall Teichoic Acid through Langerin To Induce Inflammatory Responses*. MBio, 2019. **10**(3).
123. Heger, L., S. Balk, J.J. Luhr, G.F. Heidkamp, C.H.K. Lehmann, L. Hatscher, A. Purbojo, A. Hartmann, F. Garcia-Martin, S.I. Nishimura, R. Cesnjevar, F. Nimmerjahn, and D. Dudziak, *CLEC10A Is a Specific Marker for Human CD1c(+) Dendritic Cells and Enhances Their Toll-Like Receptor 7/8-Induced Cytokine Secretion*. Front Immunol, 2018. **9**: p. 744.
124. Hutten, T.J., S. Thordardottir, H. Fredrix, L. Janssen, R. Woestenenk, J. Tel, B. Joosten, A. Cambi, M.H. Heemskerk, G.M. Franssen, O.C. Boerman, L.B. Bakker, J.H. Jansen, N. Schaap, H. Dolstra, and W. Hobo, *CLEC12A-Mediated Antigen Uptake and Cross-Presentation by Human Dendritic Cell Subsets Efficiently Boost Tumor-Reactive T Cell Responses*. J Immunol, 2016. **197**(7): p. 2715-25.
125. Perrot, I., F. Deauvieu, C. Massacrier, N. Hughes, P. Garrone, I. Durand, O. Demaria, N. Viaud, L. Gauthier, M. Blery, N. Bonnefoy-Berard, Y. Morel, J. Tschopp, L. Alexopoulou, G. Trinchieri, C.

- Paturel, and C. Caux, *TLR3 and Rig-like receptor on myeloid dendritic cells and Rig-like receptor on human NK cells are both mandatory for production of IFN-gamma in response to double-stranded RNA*. *J Immunol*, 2010. **185**(4): p. 2080-8.
126. Fekete, T., D. Bencze, A. Szabo, E. Csoma, T. Biro, A. Bacsi, and K. Pazmandi, *Regulatory NLRs Control the RLR-Mediated Type I Interferon and Inflammatory Responses in Human Dendritic Cells*. *Front Immunol*, 2018. **9**: p. 2314.
127. Szabo, A., Z. Magyarics, K. Pazmandi, L. Gopcsa, E. Rajnavolgyi, and A. Bacsi, *TLR ligands upregulate RIG-I expression in human plasmacytoid dendritic cells in a type I IFN-independent manner*. *Immunol Cell Biol*, 2014. **92**(8): p. 671-8.
128. Fekete, T., M.I. Suto, D. Bencze, A. Mazlo, A. Szabo, T. Biro, A. Bacsi, and K. Pazmandi, *Human Plasmacytoid and Monocyte-Derived Dendritic Cells Display Distinct Metabolic Profile Upon RIG-I Activation*. *Front Immunol*, 2018. **9**: p. 3070.
129. Szabo, A., K. Bene, P. Gogolak, B. Rethi, A. Lanyi, I. Jankovich, B. Dezso, and E. Rajnavolgyi, *RLR-mediated production of interferon-beta by a human dendritic cell subset and its role in virus-specific immunity*. *J Leukoc Biol*, 2012. **92**(1): p. 159-69.
130. Kalinski, P. and M. Moser, *Consensual immunity: success-driven development of T-helper-1 and T-helper-2 responses*. *Nat Rev Immunol*, 2005. **5**(3): p. 251-60.
131. Agrawal, S., A. Agrawal, B. Doughty, A. Gerwitz, J. Blenis, T. Van Dyke, and B. Pulendran, *Cutting edge: different Toll-like receptor agonists instruct dendritic cells to induce distinct Th responses via differential modulation of extracellular signal-regulated kinase-mitogen-activated protein kinase and c-Fos*. *J Immunol*, 2003. **171**(10): p. 4984-9.
132. Agrawal, S., S. Gupta, and A. Agrawal, *Human dendritic cells activated via dectin-1 are efficient at priming Th17, cytotoxic CD8 T and B cell responses*. *PLoS One*, 2010. **5**(10): p. e13418.
133. Reche, P.A., V. Soumelis, D.M. Gorman, T. Clifford, M. Liu, M. Travis, S.M. Zurawski, J. Johnston, Y.J. Liu, H. Spits, R. de Waal Malefyt, R.A. Kastelein, and J.F. Bazan, *Human thymic stromal lymphopoietin preferentially stimulates myeloid cells*. *J Immunol*, 2001. **167**(1): p. 336-43.
134. Soumelis, V., P.A. Reche, H. Kanzler, W. Yuan, G. Edward, B. Homey, M. Gilliet, S. Ho, S. Antonenko, A. Lauerma, K. Smith, D. Gorman, S. Zurawski, J. Abrams, S. Menon, T. McClanahan, R. de Waal-Malefyt, F. Bazan, R.A. Kastelein, and Y.J. Liu, *Human epithelial cells trigger dendritic cell mediated allergic inflammation by producing TSLP*. *Nat Immunol*, 2002. **3**(7): p. 673-80.
135. Ito, T., Y.H. Wang, O. Duramad, T. Hori, G.J. Delespesse, N. Watanabe, F.X. Qin, Z. Yao, W. Cao, and Y.J. Liu, *TSLP-activated dendritic cells induce an inflammatory T helper type 2 cell response through OX40 ligand*. *J Exp Med*, 2005. **202**(9): p. 1213-23.
136. Furio, L., H. Billard, J. Valladeau, J. Peguet-Navarro, and O. Berthier-Vergnes, *Poly(I:C)-Treated human langerhans cells promote the differentiation of CD4+ T cells producing IFN-gamma and IL-10*. *J Invest Dermatol*, 2009. **129**(8): p. 1963-71.
137. Moseman, E.A., X. Liang, A.J. Dawson, A. Panoskaltsis-Mortari, A.M. Krieg, Y.J. Liu, B.R. Blazar, and W. Chen, *Human plasmacytoid dendritic cells activated by CpG oligodeoxynucleotides induce the generation of CD4+CD25+ regulatory T cells*. *J Immunol*, 2004. **173**(7): p. 4433-42.
138. Joo, H., K. Upchurch, W. Zhang, L. Ni, D. Li, Y. Xue, X.H. Li, T. Hori, S. Zurawski, Y.J. Liu, G. Zurawski, and S. Oh, *Opposing Roles of Dectin-1 Expressed on Human Plasmacytoid Dendritic Cells and Myeloid Dendritic Cells in Th2 Polarization*. *J Immunol*, 2015. **195**(4): p. 1723-31.
139. Kapsenberg, M.L., *Dendritic-cell control of pathogen-driven T-cell polarization*. *Nat Rev Immunol*, 2003. **3**(12): p. 984-93.

140. Trinchieri, G., *Interleukin-12 and the regulation of innate resistance and adaptive immunity*. Nat Rev Immunol, 2003. **3**(2): p. 133-46.
141. Jacquemin, C., N. Schmitt, C. Contin-Bordes, Y. Liu, P. Narayanan, J. Seneschal, T. Maurouard, D. Dougall, E.S. Davizon, H. Dumortier, I. Douchet, L. Raffray, C. Richez, E. Lazaro, P. Duffau, M.E. Truchetet, L. Khoryati, P. Mercie, L. Couzi, P. Merville, T. Schaefferbeke, J.F. Viillard, J.L. Pellegrin, J.F. Moreau, S. Muller, S. Zurawski, R.L. Coffman, V. Pascual, H. Ueno, and P. Blanco, *OX40 Ligand Contributes to Human Lupus Pathogenesis by Promoting T Follicular Helper Response*. Immunity, 2015. **42**(6): p. 1159-70.
142. Pattarini, L., C. Trichot, S. Bogiatzi, M. Grandclaoudon, S. Meller, Z. Keuylian, M. Durand, E. Volpe, S. Madonna, A. Cavani, A. Chiricozzi, M. Romanelli, T. Hori, A. Hovnanian, B. Homey, and V. Soumelis, *TSLP-activated dendritic cells induce human T follicular helper cell differentiation through OX40-ligand*. J Exp Med, 2017. **214**(5): p. 1529-1546.
143. Ito, T., M. Yang, Y.H. Wang, R. Lande, J. Gregorio, O.A. Perng, X.F. Qin, Y.J. Liu, and M. Gilliet, *Plasmacytoid dendritic cells prime IL-10-producing T regulatory cells by inducible costimulator ligand*. J Exp Med, 2007. **204**(1): p. 105-15.
144. Volpe, E., N. Servant, R. Zollinger, S.I. Bogiatzi, P. Hupe, E. Barillot, and V. Soumelis, *A critical function for transforming growth factor-beta, interleukin 23 and proinflammatory cytokines in driving and modulating human T(H)-17 responses*. Nat Immunol, 2008. **9**(6): p. 650-7.
145. Schmitt, N., Y. Liu, S.E. Bentebibel, I. Munagala, L. Bourdery, K. Venuprasad, J. Banchereau, and H. Ueno, *The cytokine TGF-beta co-opts signaling via STAT3-STAT4 to promote the differentiation of human TFH cells*. Nat Immunol, 2014. **15**(9): p. 856-65.
146. Eizenberg-Magar, I., J. Rimer, I. Zaretsky, D. Lara-Astiaso, S. Reich-Zeliger, and N. Friedman, *Diverse continuum of CD4(+) T-cell states is determined by hierarchical additive integration of cytokine signals*. Proc Natl Acad Sci U S A, 2017. **114**(31): p. E6447-E6456.
147. Singh, V.K., S. Mehrotra, and S.S. Agarwal, *The paradigm of Th1 and Th2 cytokines: its relevance to autoimmunity and allergy*. Immunol Res, 1999. **20**(2): p. 147-61.
148. Crane, I.J. and J.V. Forrester, *Th1 and Th2 lymphocytes in autoimmune disease*. Crit Rev Immunol, 2005. **25**(2): p. 75-102.
149. Nakayama, T., K. Hirahara, A. Onodera, Y. Endo, H. Hosokawa, K. Shinoda, D.J. Tumes, and Y. Okamoto, *Th2 Cells in Health and Disease*. Annu Rev Immunol, 2017. **35**: p. 53-84.
150. Kubo, M., *T follicular helper and TH2 cells in allergic responses*. Allergol Int, 2017. **66**(3): p. 377-381.
151. Hawkes, J.E., T.C. Chan, and J.G. Krueger, *Psoriasis pathogenesis and the development of novel targeted immune therapies*. J Allergy Clin Immunol, 2017. **140**(3): p. 645-653.
152. Fragoulis, G.E., S. Siebert, and I.B. McInnes, *Therapeutic Targeting of IL-17 and IL-23 Cytokines in Immune-Mediated Diseases*. Annu Rev Med, 2016. **67**: p. 337-53.
153. Dolff, S., O. Witzke, and B. Wilde, *Th17 cells in renal inflammation and autoimmunity*. Autoimmun Rev, 2019. **18**(2): p. 129-136.
154. Kaskow, B.J. and C. Baecher-Allan, *Effector T Cells in Multiple Sclerosis*. Cold Spring Harb Perspect Med, 2018. **8**(4).
155. Giuffrida, P., G.R. Corazza, and A. Di Sabatino, *Old and New Lymphocyte Players in Inflammatory Bowel Disease*. Dig Dis Sci, 2018. **63**(2): p. 277-288.
156. Abdel-Moneim, A., H.H. Bakery, and G. Allam, *The potential pathogenic role of IL-17/Th17 cells in both type 1 and type 2 diabetes mellitus*. Biomed Pharmacother, 2018. **101**: p. 287-292.

157. Jia, L. and C. Wu, *Differentiation, regulation and function of Th9 cells*. Adv Exp Med Biol, 2014. **841**: p. 181-207.
158. Eivazi, S., S. Bagheri, M.S. Hashemzadeh, M. Ghalavand, E.S. Qamsari, R. Dorostkar, and M. Yasemi, *Development of T follicular helper cells and their role in disease and immune system*. Biomed Pharmacother, 2016. **84**: p. 1668-1678.
159. Jeger-Madiot, R., M. Heredia, and S. Graff-Dubois, *Germinal centers B-cell reaction and T follicular helper cells in response to HIV-1 infection*. Curr Opin HIV AIDS, 2019. **14**(4): p. 246-252.
160. Ziegler, S.F. and D. Artis, *Sensing the outside world: TSLP regulates barrier immunity*. Nat Immunol, 2010. **11**(4): p. 289-93.
161. Fortson, E.A., B. Li, and M. Bhayana, *Introduction*. Adv Exp Med Biol, 2017. **1027**: p. 1-10.
162. Laird, M. and K. Lo Sicco, *Defining and Measuring the Scope of Atopic Dermatitis*. Adv Exp Med Biol, 2017. **1027**: p. 93-104.
163. Brunner, P.M., E. Guttman-Yassky, and D.Y. Leung, *The immunology of atopic dermatitis and its reversibility with broad-spectrum and targeted therapies*. J Allergy Clin Immunol, 2017. **139**(4S): p. S65-S76.
164. Sidbury, R. and K. Khorsand, *Evolving Concepts in Atopic Dermatitis*. Curr Allergy Asthma Rep, 2017. **17**(7): p. 42.
165. Oyoshi, M.K., R. He, L. Kumar, J. Yoon, and R.S. Geha, *Cellular and molecular mechanisms in atopic dermatitis*. Adv Immunol, 2009. **102**: p. 135-226.
166. Furue, M., T. Chiba, G. Tsuji, D. Ulzii, M. Kido-Nakahara, T. Nakahara, and T. Kadono, *Atopic dermatitis: immune deviation, barrier dysfunction, IgE autoreactivity and new therapies*. Allergol Int, 2017. **66**(3): p. 398-403.
167. Brandt, E.B. and U. Sivaprasad, *Th2 Cytokines and Atopic Dermatitis*. J Clin Cell Immunol, 2011. **2**(3).
168. Gooderham, M.J., H.C. Hong, P. Eshtiaghi, and K.A. Papp, *Dupilumab: A review of its use in the treatment of atopic dermatitis*. J Am Acad Dermatol, 2018. **78**(3 Suppl 1): p. S28-S36.
169. Leung, D.Y., M. Boguniewicz, M.D. Howell, I. Nomura, and Q.A. Hamid, *New insights into atopic dermatitis*. J Clin Invest, 2004. **113**(5): p. 651-7.
170. Szabo, K., K. Gaspar, Z. Dajnoki, G. Papp, B. Fabos, A. Szegedi, and M. Zeher, *Expansion of circulating follicular T helper cells associates with disease severity in childhood atopic dermatitis*. Immunol Lett, 2017. **189**: p. 101-108.
171. Kusari, A., A.M. Han, D. Schairer, and L.F. Eichenfield, *Atopic Dermatitis: New Developments*. Dermatol Clin, 2019. **37**(1): p. 11-20.
172. Ackerson, B., R. Thorpe, and W.N. M, *Prescription Treatment Options*. Adv Exp Med Biol, 2017. **1027**: p. 105-120.
173. Simpson, E.L., C. Flohr, L.F. Eichenfield, T. Bieber, H. Sofen, A. Taieb, R. Owen, W. Putnam, M. Castro, K. DeBusk, C.Y. Lin, A. Voulgari, K. Yen, and T.A. Omachi, *Efficacy and safety of lebrikizumab (an anti-IL-13 monoclonal antibody) in adults with moderate-to-severe atopic dermatitis inadequately controlled by topical corticosteroids: A randomized, placebo-controlled phase II trial (TREBLE)*. J Am Acad Dermatol, 2018. **78**(5): p. 863-871 e11.
174. Oldhoff, J.M., U. Darsow, T. Werfel, K. Katzer, A. Wulf, J. Laifaoui, D.J. Hijnen, S. Plotz, E.F. Knol, A. Kapp, C.A. Bruijnzeel-Koomen, J. Ring, and M.S. de Bruin-Weller, *Anti-IL-5 recombinant humanized monoclonal antibody (mepolizumab) for the treatment of atopic dermatitis*. Allergy, 2005. **60**(5): p. 693-6.

175. Kabashima, K., M. Furue, J.M. Hanifin, G. Pulka, A. Wollenberg, R. Galus, T. Etoh, R. Mihara, M. Nakano, and T. Ruzicka, *Nemolizumab in patients with moderate-to-severe atopic dermatitis: Randomized, phase II, long-term extension study*. *J Allergy Clin Immunol*, 2018. **142**(4): p. 1121-1130 e7.
176. Simpson, E.L., J.R. Parnes, D. She, S. Crouch, W. Rees, M. Mo, and R. van der Merwe, *Tezepelumab, an anti-thymic stromal lymphopoietin monoclonal antibody, in the treatment of moderate to severe atopic dermatitis: A randomized phase 2a clinical trial*. *J Am Acad Dermatol*, 2019. **80**(4): p. 1013-1021.
177. Wang, H.H., Y.C. Li, and Y.C. Huang, *Efficacy of omalizumab in patients with atopic dermatitis: A systematic review and meta-analysis*. *J Allergy Clin Immunol*, 2016. **138**(6): p. 1719-1722 e1.
178. Sheldon, E., M. Schwickart, J. Li, K. Kim, S. Crouch, S. Parveen, C. Kell, and C. Birrell, *Pharmacokinetics, Pharmacodynamics, and Safety of MEDI4212, an Anti-IgE Monoclonal Antibody, in Subjects with Atopy: A Phase I Study*. *Adv Ther*, 2016. **33**(2): p. 225-51.
179. Guttman-Yassky, E., P.M. Brunner, A.U. Neumann, S. Khattri, A.B. Pavel, K. Malik, G.K. Singer, D. Baum, P. Gilleaudeau, M. Sullivan-Whalen, S. Rose, S. Jim On, X. Li, J. Fuentes-Duculan, Y. Estrada, S. Garcet, C. Traidl-Hoffmann, J.G. Krueger, and M.G. Lebwohl, *Efficacy and safety of fezakinumab (an IL-22 monoclonal antibody) in adults with moderate-to-severe atopic dermatitis inadequately controlled by conventional treatments: A randomized, double-blind, phase 2a trial*. *J Am Acad Dermatol*, 2018. **78**(5): p. 872-881 e6.
180. Saeki, H., K. Kabashima, Y. Tokura, Y. Murata, A. Shiraiishi, R. Tamamura, B. Randazzo, and K. Imanaka, *Efficacy and safety of ustekinumab in Japanese patients with severe atopic dermatitis: a randomized, double-blind, placebo-controlled, phase II study*. *Br J Dermatol*, 2017. **177**(2): p. 419-427.
181. Khattri, S., P.M. Brunner, S. Garcet, R. Finney, S.R. Cohen, M. Oliva, R. Dutt, J. Fuentes-Duculan, X. Zheng, X. Li, K.M. Bonifacio, N. Kunjrvia, I. Coats, I. Cueto, P. Gilleaudeau, M. Sullivan-Whalen, M. Suarez-Farinas, J.G. Krueger, and E. Guttman-Yassky, *Efficacy and safety of ustekinumab treatment in adults with moderate-to-severe atopic dermatitis*. *Exp Dermatol*, 2017. **26**(1): p. 28-35.
182. Renert-Yuval, Y. and E. Guttman-Yassky, *Monoclonal antibodies for the treatment of atopic dermatitis*. *Curr Opin Allergy Clin Immunol*, 2018. **18**(4): p. 356-364.
183. Navarini, A.A., L.E. French, and G.F. Hofbauer, *Interrupting IL-6-receptor signaling improves atopic dermatitis but associates with bacterial superinfection*. *J Allergy Clin Immunol*, 2011. **128**(5): p. 1128-30.
184. Jaspers, S.R.R., Mark W; Dillon, Stacey R; Ramsdell, Frederick J; Krejsa, Cecile M; Yi, Eugene C, *Anti-human IL-21 monoclonal antibodies*. 2010, Zymogenetics Inc; Jaspers, Stephen R; Rixon, Mark W; Dillon, Stacey R; Ramsdell, Frederick J; Krejsa, Cecile M; Yi, Eugene C.
185. Moll, T.S., Terry; Zheng, Xin Xiao, *Antagonists of IL-21 and modulation of IL-21-mediated T cell responses*. 2003, Beth Israel Deaconess Medical Center; Moll, Thomas; Strom, Terry; Zheng, Xin Xiao.
186. Young, D.A.W., Matthew J; Valge-Archer, Viia; Collins, Mary; Williams, Andrew James; Witek, Joanne, *Antibodies Against Human IL-21 Receptor and Uses Therefor*. 2004, Wyeth Corp; Young, Deborah A; Whitters, Matthew J; Valge-Archer, Viia; Collins, Mary; Williams, Andrew James; Witek, Joanne.
187. Werfel, T., G. Layton, M. Yeadon, L. Whitlock, I. Osterloh, P. Jimenez, W. Liu, V. Lynch, A. Asher, A. Tsianakas, and L. Purkins, *Efficacy and safety of the histamine H4 receptor antagonist ZPL-*

- 3893787 in patients with atopic dermatitis. *J Allergy Clin Immunol*, 2019. **143**(5): p. 1830-1837 e4.
188. Ramachandran, V., A. Cline, S.R. Feldman, and L.C. Strowd, *Evaluating crisaborole as a treatment option for atopic dermatitis*. *Expert Opin Pharmacother*, 2019. **20**(9): p. 1057-1063.
 189. Seegraber, M., J. Srour, A. Walter, M. Knop, and A. Wollenberg, *Dupilumab for treatment of atopic dermatitis*. *Expert Rev Clin Pharmacol*, 2018. **11**(5): p. 467-474.
 190. Connelly, D., *Atopic dermatitis: emerging and current treatments*. *The Pharmaceutical Journal*, 2017. **298**(7898).
 191. Han, Y., Y. Chen, X. Liu, J. Zhang, H. Su, H. Wen, W. Li, and X. Yao, *Efficacy and safety of dupilumab for the treatment of adult atopic dermatitis: A meta-analysis of randomized clinical trials*. *J Allergy Clin Immunol*, 2017. **140**(3): p. 888-891 e6.
 192. Simpson, E.L., T. Bieber, E. Guttman-Yassky, L.A. Beck, A. Blauvelt, M.J. Cork, J.I. Silverberg, M. Deleuran, Y. Kataoka, J.P. Lacour, K. Kingo, M. Worm, Y. Poulin, A. Wollenberg, Y. Soo, N.M. Graham, G. Pirozzi, B. Akinlade, H. Staudinger, V. Mastey, L. Eckert, A. Gadkari, N. Stahl, G.D. Yancopoulos, M. Ardeleanu, Solo, and S. Investigators, *Two Phase 3 Trials of Dupilumab versus Placebo in Atopic Dermatitis*. *N Engl J Med*, 2016. **375**(24): p. 2335-2348.
 193. Beck, L.A., D. Thaci, J.D. Hamilton, N.M. Graham, T. Bieber, R. Rocklin, J.E. Ming, H. Ren, R. Kao, E. Simpson, M. Ardeleanu, S.P. Weinstein, G. Pirozzi, E. Guttman-Yassky, M. Suarez-Farinas, M.D. Hager, N. Stahl, G.D. Yancopoulos, and A.R. Radin, *Dupilumab treatment in adults with moderate-to-severe atopic dermatitis*. *N Engl J Med*, 2014. **371**(2): p. 130-9.
 194. Hamilton, J.D., M. Suarez-Farinas, N. Dhingra, I. Cardinale, X. Li, A. Kostic, J.E. Ming, A.R. Radin, J.G. Krueger, N. Graham, G.D. Yancopoulos, G. Pirozzi, and E. Guttman-Yassky, *Dupilumab improves the molecular signature in skin of patients with moderate-to-severe atopic dermatitis*. *J Allergy Clin Immunol*, 2014. **134**(6): p. 1293-1300.
 195. Faiz, S., J. Giovannelli, C. Podevin, M. Jachiet, J.D. Bouaziz, Z. Reguijai, A. Nosbaum, A. Lasek, M.C. Ferrier le Bouedec, A. Du Thanh, N. Raison-Peyron, F. Tetart, A.B. Duval-Modeste, L. Misery, F. Aubin, A. Dompmartin, C. Morice, C. Droitcourt, A. Soria, J.P. Arnault, J. Delaunay, E. Mahe, M.A. Richard, A. Schoeffler, J.P. Lacour, E. Begon, A. Walter-Lepage, A.S. Dillies, S. Rappelle-Duruy, S. Barete, N. Bellon, N. Beneton, A. Valois, S. Barbarot, J. Senechal, D. Staumont-Salle, and F. Groupe de Recherche sur l'Eczema aTopique, *Effectiveness and safety of dupilumab for the treatment of atopic dermatitis in a real-life French multicenter adult cohort*. *J Am Acad Dermatol*, 2019. **81**(1): p. 143-151.
 196. Kemeny, D.M., *The role of the T follicular helper cells in allergic disease*. *Cell Mol Immunol*, 2012. **9**(5): p. 386-9.
 197. Schmitt, N., R. Morita, L. Bourdery, S.E. Bentebibel, S.M. Zurawski, J. Banchereau, and H. Ueno, *Human dendritic cells induce the differentiation of interleukin-21-producing T follicular helper-like cells through interleukin-12*. *Immunity*, 2009. **31**(1): p. 158-69.
 198. Divekar, R. and H. Kita, *Recent advances in epithelium-derived cytokines (IL-33, IL-25, and thymic stromal lymphopoietin) and allergic inflammation*. *Curr Opin Allergy Clin Immunol*, 2015. **15**(1): p. 98-103.
 199. Choi, Y.S., R. Kageyama, D. Eto, T.C. Escobar, R.J. Johnston, L. Monticelli, C. Lao, and S. Crotty, *ICOS receptor instructs T follicular helper cell versus effector cell differentiation via induction of the transcriptional repressor Bcl6*. *Immunity*, 2011. **34**(6): p. 932-46.
 200. Hoeve, M.A., N.D. Savage, T. de Boer, D.M. Langenberg, R. de Waal Malefyt, T.H. Ottenhoff, and F.A. Verreck, *Divergent effects of IL-12 and IL-23 on the production of IL-17 by human T cells*. *Eur J Immunol*, 2006. **36**(3): p. 661-70.

201. Gomez-Rodriguez, J., N. Sahu, R. Handon, T.S. Davidson, S.M. Anderson, M.R. Kirby, A. August, and P.L. Schwartzberg, *Differential expression of interleukin-17A and -17F is coupled to T cell receptor signaling via inducible T cell kinase*. *Immunity*, 2009. **31**(4): p. 587-97.
202. Adamik, J., M. Henkel, A. Ray, P.E. Auron, R. Duerr, and A. Barrie, *The IL17A and IL17F loci have divergent histone modifications and are differentially regulated by prostaglandin E2 in Th17 cells*. *Cytokine*, 2013. **64**(1): p. 404-12.
203. Esaki, H., T. Czarnowicki, J. Gonzalez, M. Oliva, S. Talasila, I. Haugh, G. Rodriguez, L. Becker, J.G. Krueger, E. Guttman-Yassky, and A.S. Paller, *Accelerated T-cell activation and differentiation of polar subsets characterizes early atopic dermatitis development*. *J Allergy Clin Immunol*, 2016. **138**(5): p. 1473-1477 e5.
204. Esaki, H., P.M. Brunner, Y. Renert-Yuval, T. Czarnowicki, T. Huynh, G. Tran, S. Lyon, G. Rodriguez, S. Immaneni, D.B. Johnson, B. Bauer, J. Fuentes-Duculan, X. Zheng, X. Peng, Y.D. Estrada, H. Xu, C. de Guzman Strong, M. Suarez-Farinas, J.G. Krueger, A.S. Paller, and E. Guttman-Yassky, *Early-onset pediatric atopic dermatitis is TH2 but also TH17 polarized in skin*. *J Allergy Clin Immunol*, 2016. **138**(6): p. 1639-1651.
205. Antunez, C., M.J. Torres, C. Mayorga, J.A. Cornejo-Garcia, L.F. Santamaria-Babi, and M. Blanca, *Different cytokine production and activation marker profiles in circulating cutaneous-lymphocyte-associated antigen T cells from patients with acute or chronic atopic dermatitis*. *Clin Exp Allergy*, 2004. **34**(4): p. 559-66.
206. Teraki, Y., A. Sakurai, and S. Izaki, *IL-13/IL-22-coproducing T cells, a novel subset, are increased in atopic dermatitis*. *J Allergy Clin Immunol*, 2013. **132**(4): p. 971-4.
207. Czarnowicki, T., H. Esaki, J. Gonzalez, D. Malajian, A. Shemer, S. Noda, S. Talasila, A. Berry, J. Gray, L. Becker, Y. Estrada, H. Xu, X. Zheng, M. Suarez-Farinas, J.G. Krueger, A.S. Paller, and E. Guttman-Yassky, *Early pediatric atopic dermatitis shows only a cutaneous lymphocyte antigen (CLA)(+) TH2/TH1 cell imbalance, whereas adults acquire CLA(+) TH22/TC22 cell subsets*. *J Allergy Clin Immunol*, 2015. **136**(4): p. 941-951 e3.
208. Inagaki-Katashiba, N., T. Ito, M. Inaba, Y. Azuma, A. Tanaka, V. Phan, K. Kibata, A. Satake, and S. Nomura, *Statins can suppress DC-mediated Th2 responses through the repression of OX40-ligand and CCL17 expression*. *Eur J Immunol*, 2019.
209. Zhou, M. and W. Ouyang, *The function role of GATA-3 in Th1 and Th2 differentiation*. *Immunol Res*, 2003. **28**(1): p. 25-37.

Titre : Régulation de la diversité des sous-populations de lymphocytes T auxiliaires humaines : des mécanismes in vitro dérivés des cellules dendritiques aux candidats biomarqueurs dans la dermatite atopique

Mots clés : Lymphocytes T auxiliaires, lymphocytes T folliculaires, cellules dendritiques, lymphopoïétine stromale thymique (TSLP), dermatite atopique

Résumé : L'immunité humaine est principalement commandée par les cellules dendritiques et les lymphocytes T auxiliaires. Lorsque les cellules dendritiques détectent un danger, elles vont instruire les lymphocytes T auxiliaires afin qu'ils adoptent le phénotype approprié à la menace rencontrée. Les lymphocytes T auxiliaires sont divisés en plusieurs sous-populations en fonction des cytokines qu'ils produisent. Chacune possède des fonctions propres et est impliquée dans l'élimination de pathogènes distincts. Si les réponses des lymphocytes T auxiliaires ne sont pas finement régulées, ils peuvent devenir pathogéniques, et dans ce cas, servir de cibles potentielles pour des thérapies. Dans ce contexte, j'ai concentré mon travail de doctorat sur l'étude de la diversité des sous-populations de lymphocytes T auxiliaires et de leur régulation. Premièrement, j'ai démontré que les cellules dendritiques

activées par la TSLP sont capables d'induire la polarisation de lymphocytes T folliculaires. Ensuite, j'ai participé à la construction d'un modèle mathématique capable de prédire la réponse des lymphocytes T auxiliaires en fonction de signaux dérivés des cellules dendritiques. Ce modèle nous a permis d'identifier un rôle spécifique de l'IL-12p70, dans un contexte IL-1, dans l'induction d'IL-17F sans IL-17A. Enfin, j'ai monitoré huit populations de lymphocytes T auxiliaires et folliculaires dans le sang périphérique de patients atteints de dermatite atopique traités par Dupilumab (immunothérapie ciblant le récepteur alpha à l'IL-4) et j'ai pu montrer que la diminution du pourcentage de lymphocytes Th17 corrélait avec l'amélioration du score clinique EASI. Globalement, mon travail sur la diversité de phénotypes T apporte une ressource mécanistique importante, avec une potentielle application en immunothérapie.

Title: Regulation of human T helper cell diversity: from in vitro dendritic cell-based mechanisms to candidate biomarkers in atopic dermatitis

Keywords: T helper cells, T follicular helper cells, dendritic cells, Thymic Stromal Lymphopoietin (TSLP), Atopic dermatitis

Abstract: Human immunity is essentially driven by dendritic cells and T helper cells. When dendritic cells detect a danger, they will instruct T helper cells to adopt the appropriate phenotype for the specific threat encountered. T helper cells are subdivided in multiple subsets, characterized by particular sets of cytokines. Each T helper subset has specific functions and is involved in the clearance of distinct pathogens. If T helper responses are not precisely regulated, they can become pathogenic, in this case T helper pathways can become potential targets for therapy. In this context, I focused my PhD work on studying T helper cell subset diversity and regulation. First, I demonstrated the ability of TSLP-activated

dendritic cell to induce T follicular helper cell polarization. Then I participated in building a mathematical model capable of predicting T helper cell response to dendritic-cell derived signals. This model allowed us to identify a new role of IL-12p70, in an IL-1 context, to induce IL-17F without IL-17A. Finally, I monitored eight T helper and T follicular helper cell populations in peripheral blood from atopic dermatitis patients treated with Dupilumab (anti-IL-4 receptor alpha immunotherapy) and was able to show a correlation between decrease of Th17 cell percentage and improvement of EASI clinical score. Overall, my work on T helper diversity provides key mechanistic insight with potential application in immunotherapy.